Recovery and functionalization of cellulosic fibers from pulp and paper mill waste streams

by

Liezl Carien van der Watt

Thesis presented in partial fulfilment
of the requirements for the Degree

of

MASTER OF ENGINEERING
(CHEMICAL ENGINEERING)

in the Faculty of Engineering
at Stellenbosch University

Supervisor

Prof A.F.A. Chimphango

April 2022

DECLARATION

By submitting this thesis electronically, I declare that the entirety of the work contained therein is my own, original work, that I am the sole author thereof (save to the extent explicitly otherwise stated), that reproduction and publication thereof by Stellenbosch University will not infringe any third party rights and that I have not previously in its entirety or in part submitted it for obtaining any qualification.

Date: *April 2022*

ABSTRACT

Pulp and paper mills lose between 1 to 3% of their production to waste effluent. The effluent contains cellulosic fibre which is normally discarded as sludge to landfills or is incinerated. This is a waste of valuable resources. The objectives of the current project were: (i) identify waste streams in Kraft pulp and paper mills, (ii) develop and validate a method to recover these fibres and (iii) to develop and validate a method to functionalize the recovered fibres to nanocellulose. The recovery method was developed based on fibre size distribution and validated based on flotation efficiency (> 55%) while the functionalization method was based on forming nanocellulose gel-like suspensions within 5 min of mechanical treatment. The waste sources were categorized into continuous and batch losses. The largest source of continuous waste is from the paper machine whitewater not treated by save-all devices (a unit installed to recover fiber internally) whereas, the greatest batch losses occur during grade changes. Sludge samples were collected from various sampling points in the Kraft mill bleaching plant as well as from paper machine broke systems and paper machine cut-offs or trimmings. The fibres from these locations are normally sprayed into paper machine, alkaline and acid effluent drains. Fibres from the effluent streams were recovered by flotation with colloidal gas aphrons (CGAs) generated using two types of non-ionic surfactants (synthetic and green-based). The average size of fibres collected were 93 ± 3.1, 72 ± 3.9 and 93 ± 5.3 μm for paper machine, alkaline and acid effluent streams. The synthetic surfactant used was Triton X-100 and the alternative, green-based surfactant tested was N-Dodecyl β-D-maltoside (DDM). The average recovery efficiencies achieved by both surfactants were between 50 and 78%. DDM is a promising alternative to Triton X-100 and achieved similar efficiencies. Functionalization of nanocellulose fibres was achieved by phosphorylation pre-treatment using ammonium dihydrogen orthophosphate and urea in the ratio 1:1.2:19.6, which gave nanocellulose gel-like suspensions within 5 min of blending using a high speed blender (900 W nutribullet). The suspensions obtained were highly heterogeneous by being both in the microscale (1.0 to 2.0 μm) and nanoscale ranges (50 to 800 nm). Alcohol insoluble (95% ethanol) films were made from these recovered fibres. The results obtained after validating the fibre recovery and functionalization methods formed a basis for evaluating the feasibility of using soft sensors to predict the quality of nanocellulose produced. The properties of the fibres collected along the different stages in the bleaching sequence produced nanocellulose materials with varying quality as determined by particle size distribution and other measured properties of the recovered fibres like zeta potential (between -31 and -58 mV) and crystallinity indices (between 13 to 27%). By using index quality models combined with near-infrared spectroscopy results a soft sensor can be developed that can accurately predicted the quality of the nanocellulose material produced. Based on the results of this study it was concluded that all effluent streams can be combined into a single waste source from which fibres can be recovered and functionalized to high-value products like nanocellulose.

OPSOMMING

Pulp-en-papiermeule verloor tussen 1 en 3 % van hul produksie aan afvaluitvloeisel. Die uitvloeisel bevat sellulosiese vesel wat normaalweg weggegooi word as slyk in vullishope, of verbrand word. Hierdie is ’n mors van waardevolle hulpbronne. Die doel van hierdie projek was om (i) afvalstrome in Kraft pulp-en-papiermeule te identifiseer, (ii) ’n metode te ontwikkel en dan valideer om hierdie vesels te herwin en (iii) om ’n metode te ontwikkel en te valideer wat hierdie vesels funksionaliseer tot nanosellulose. Die geïdentifiseerde afvalbronne is gekategoriseer as kontinue of lotverlieste. Die grootste bron van kontinue afval is van papiermasjienwitwater wat nie behandel is deur red-alles-toestelle nie, waarteenoor die grootste lotverlieste gedurende graadveranderinge plaasvind. Slykmonsters is versamel van verskeie proefpunte in die Kraft meul se blykaanleg sowel as van papiermasjienbreeksisteme en papiermasjiene se afsnydings of afwerkings. Die vesels van hierdie bronne word normaalweg in papiermasjien-, alkali- en suuruitvloeiseldreine gesproei. Vesels van die uitvloeiselstrome is herwin deur flotasie met kolloïdale gas skuim (CGAs) gegenereer deur twee tipes nie-ioniese surfaktante (sinteties en groen-gebaseerd) te gebruik. Die gemiddelde grootte vesels versamel was 93±3.1, 72±3.9 en 93±5.3 µm vir papiermasjien-, alkali- en suuruitvloeiselstrome. Die sintetiese surfaktant wat gebruik is was Triton X-100 en die alternatiewe, groen-gebaseerde surfaktant wat getoets is, was N-Dodecyl β-D-maltosied (DDM). Die gemiddelde herwinningdoeltreffendheid bereik was tussen 50 en 78%. DDM is ’n belowende alternatief vir Triton X-100 en bereik soortgelyke doeltreffendheid. Vesels is gefunksionaliseer tot nanosellulose, eers deur voorbehandeling van vesels deur fosforilasie deur ammonium-diwaterstof-ortofosfaat en ureum in die verhouding 1:1.2:19.6 te gebruik. Deur hierdie verhouding te gebruik was dit moontlik om jelagtige nanosellulosesuspensies te verkry na net 5 minute van vermenging met ’n 900 W nutribullet. Die suspensies verkry uit die fosforilasieproses was hoogs heterogeen met verskeie fraksies van vesels wat in die mikroskaal (tussen 1.0 en 2.0 µm) en nanoskaal (tussen 50 en 800 nm) gestrek het. Termies stabiele en alkoholies onoplosbare (95% etanol) films is gemaak van hierdie vesels. Die resultate verkry na die validasie van die veselherwinning en funksionaliseringsmetodes het ’n basis gevorm vir die evaluasie van die uitvoerbaarheid van die gebruik van sagtesensors om die kwaliteit van nanosellulose geproduseer, te voorspel. Die eienskappe van die vesels versamel in die verskillende stadia van die blyk volgorde het nanosellulose met verskillende kwaliteit geproduseer soos bepaal deur partikelgrootteverspreiding en ander gemete eienskappe van die herwinde vesels soos zeta potensiaal (tussen -31 en -58 mV) en kristalliniteitindekse (tussen 13 en 27%). Deur indekskwaliteitmodelle gekombineer met naby-infrarooispektroskopieresultate te gebruik, kan ’n sagtesensor ontwikkel word wat die kwaliteit van die nanosellulosemateriaal geproduseer, akkuraat kan voorspel. Gebaseer op die resultate van hierdie studie is dit bevind dat alle uitvloeiselstrome in een afvalbron gekombineer kan word waaruit die vesels herwin en gefunksionaliseer kan word tot hoë-waarde produkte soos nanosellulose.

NOMENCLATURE

Acronyms	
AGU	Anhydroglucose Unit
ANOVA	Analyses of Variance
AFM	Atomic Force Microscopy
BNC	Bacterial nanocellulose. Also known as microbial cellulose and biocellulose.
CAGR	Compound Annual Growth Rate
CCD	Central Composite Design
CI	Crystallinity Index
CMC	Critical micelle concentration
CTMP	Chemical thermo-mechanical pulping
DAF	Dissolved air flotation
DP	Degree of Polymerization
DS	Degrees of Substitution
FTIR	Fourier Transform Infrared Spectroscopy
HLB	Hydrophilic-lipophilic balance
HPLC	High Performance Liquid
NFC	Microfibrillated cellulose. Also known as nanofibrillated cellulose, nanofibrils and microfibrils.
MIMO	Multiple Input Multiple Output
NCC	Nanocrystalline Cellulose
NFC	Nanofibrillated Cellulose
NIR	Near-infrared Spectroscopy
PPM	Pulp and Paper mill
RSM	Response Surface Methodology
SEM	Scanning Electron Microscopy
TAPPI	Technical Association of the Pulp and Paper Industry
TEM	Transmission Electron Microscopy
TEMPO	2, 2, 6, 6- tertramethylpiperidinyl-1-oxyl
TGA	Thermogravimetric Analysis
TMP	Thermo-mechanical pulping
WCA	Water Contact Angle
WWTP	Wastewater treatment plant
XRD	X-ray Diffraction

Glossary	
Bleaching	Chemical treatment process by which pulped wood particles are whitened, purified, and stabilized. Normally carried out in several stages.
Breaks	Paper sheets that break while passing through the paper machine.
Brightness	The percentage of blue light, measured at a specific wavelength of 457 nm, reflected from the surface of pulp or paper product.
Broke	Refers to partial or fully manufactured product on a paper machine that has been discarded. Can also refer to paper trimmings or damaged paper due to breaks on paper machine. Represents a loss in money, time, and effort.
Broke pit	A pit or well situated below a paper machine into which broke is disposed from the machine floor.
Colloidal gas aphrons	Colloidal gas aphrons are microbubbles stabilized by surfactant layers which are created by stirring surfactant solutions at high speed.
Cooking	Process of reacting fibre with suitable chemicals, usually under high pressure and temperature, in order to convert fibrous material like wood chips into pulp.
Defibrillation	Term for separating fibres in water by mechanical action.
Digester	A large vessel used to chemically treat wood chips under elevated pressure and temperature in order to separate fibres and produce pulp.
Drainage	Formation of paper on the paper machine wire by removing water at the wet end of the paper machine.
Dry end	Last part of the paper machine where sheet moisture is removed by evaporation. Consists of several drying sections.
Effluent	Liquid waste and rejects from which fibre is recovered in wastewater treatment plants prior to discharge from the mill.
Fillers	Inorganic, non-fibrous material added to the pulp prior papermaking to improve the characteristics of the finished paper.
Fines	Fraction of fibre that escapes through a mesh screen having a hole diameter of 76 μm.
Grade change	Refers to changes in process variables of a paper machine. Includes variables like speed, steam pressure, and stock flow. Transition needs to occur as fast as possible and normally takes between a few minutes to a half an hour to be completed depending on the size of the change. The paper made during the grade change is normally off-spec and becomes waste.
Head box	Part of a paper machine. Responsible for applying and distributing low consistency stock into the forming section of the paper machine in a uniform manner.
Hydrapulper	A tank that is fitted with an agitator rotor to disintegrate pulp and broke in water.

Nanocellulose	A biodegradable and biocompatible material derived from natural sources that plays a large role in nanotechnology research for the development of advanced and novel materials.
Refining	The mechanical treatment and modification of fibre to impart certain characteristics such as increased capacity to absorb water and improved sheet formation.
Rejects	Refers to material that has been removed and discarded during the cleaning of pulp.
Save-all device	A unit, such as a disk filter for example, that is used to recover fibre from the white water stream. The filtrate from the device is treated further to provide water that is clean and free of suspended and/or dissolved solids so that it can be reused in the process.
Slurry	A semi-liquid mixture consisting of solid material including suspended fibres, fillers and coating pigments.
Stock	Fibrous material to be made into paper. May consist of one or more types of pulp, with or without suitable filler, additives, and other chemicals.
Wet-end	First part of the paper machine up to the dry end section. In this section the paper sheet is formed from the stock furnish and most water is removed before the drying stage. Includes the head box, wire and wet press sections.
White water	The water drained from wet pulp stock is called white water, regardless of its colour or what stage of the process it comes from.

TABLE OF CONTENTS

LIST OF FIGURES

LIST OF TABLES

1 INTRODUCTION AND PROJECT MOTIVATION

1.1 Background and problem statement

Contrary to popular belief, the pulp and paper industry has been growing since the beginning of the digital age, although this is happening at a slower pace since 2015. Noteworthy, digitalisation has resulted in the graphic-paper market (which includes newsprint as well as printing and writing paper) declining significantly with a compound annual growth rate (CAGR) from 2010 to 2018 of -7.6%. This gap in the market has been filled by other market products including packaging material, tissue and new novel products such as nanocellulose derivatives which add up to a CAGR from 2010 to 2018 of 9.1%. (Berg and Lingqvist, 2019)

To remain competitive however, pulp and paper mills (PPMs) face a series of challenges that will require substantial changes to their long-established modus operandi. These challenges range from pressure placed on the industry by the government and public to reduce their environmental impact, to shifts in the availability and quality of raw materials (Bousios and Worrell, 2017). In South Africa legislation is currently being implemented to address these concerns including a Carbon Tax Act and Scheduled landfill restrictions (GreenCape, 2020). Key challenges to reduce environmental impact include water saving initiatives as well as valorisation of side streams which often have a negative impact on the environment if not disposed of properly. There have been many proposed solutions to address the challenges mentioned including striving toward an effluent-free mill (Hamm and Schabel, 2007), the biorefinery concept (Kamm et al., 2015) and a fairly new concept called the Multiple Input Multiple Output (MIMO) Paper Mill (Bousios and Worrell, 2017).

Striving toward an effluent-free mill involves systematically closing white water loops (the water drained from wet pulp stock) by implementing different process water treatment plants as kidneys. This is referred to as “kidney technology”. A disadvantage of closing white water loops is the accumulation of rejected and lost fibres. The presence of these fibres contributes toward the chemical oxygen demand (COD), conductivity and bad smell of effluent (Hamm and Schabel, 2007). Methods to remove these fibres include aerobic and anaerobic treatment. The sludge produced by these processes is usually disposed of by one of two ways: incineration or land disposal (Bird and Talberth, 2008). Disposal by these methods entails significant cost. According to Eikelboom *et al.* (2018) the cost of landfill disposal and incineration is 309 and between 332 and 441 US$ per ton of Kraft pulp sludge produced respectively. For landfill disposal the cost includes labour, vehicle fuel, electricity, landfill tax and gate fees whereas for incineration the calculated cost includes labour, transport to site and quality control. These fibres can potentially be recovered and functionalised into high value products e.g., nanocellulose, building materials or biofuel thereby reducing disposal costs and potentially even result in a side revenue.

The amount and source(s) of fibre loss during pulping depends on the processing method. Pulp from virgin fibre is produced by either mechanical or chemical pulping technologies. Chemical pulping methods have much lower yields of between 45 and 65% compared to yields of above 95% for

mechanical pulps (Riley, 2012). Yield is defined as the percentage by oven dry weight of pulp obtained from the original wood weight (Briggs, 1994). The yield loss in chemical pulping is mainly due to alkaline hydrolysis during the cooking stage which leads to almost complete dissolution of lignin and hemicelluloses and partial dissolution of cellulose (Brännvall, 2018).

After the cooking stage pulp undergoes washing and screening to separate fibres from the cooking chemicals and waste products which is referred to as black liquor. The black liquor is subjected to a recovery process to regenerate the cooking chemicals which is referred to as white liquor. Shortly, the process consists of evaporation and combustion stages to increase the solids contents. During combustion black liquor is burned to produce various dissolved salts including sulphides, sulphates, carbonates as well as sodium and potassium chlorides (Simão *et al.*, 2018). The process is however not discussed in detail in this document as it falls outside the scope of this project.

Other factors that contribute to yield loss and specifically fibre loss includes paper machine white water that is left untreated by paper machine save-all devices (a piece of equipment installed to recover fibers from white water) as well as screening and washing stages where some of the fibre will unintentionally be removed along with the chemicals. Fibre loss contributing to yield loss has been reported from hot stock screeners, brownstock washers and bleach plant washers (Brogdon, 2015). Save-all devices, usually disc filters, are installed to recover fibres with the objective of clarifying paper machine white water so that the water is suitable for reuse in the process (Savage and Koch, 1950). This source of fibre loss is relevant in any papermaking process irrespective of the pulping process (mechanical or chemical). Depending on the desired product, screening, and washing stages are not always necessary. Bleached chemical pulps however, which is the interest of this project, involve a multi-stage bleaching sequence with washing steps between each stage.

Another major source of fibre loss occurs during grade changes. A grade change refers to a quality change on a paper machine and includes changing variables such as refiner loads, stock flows, headbox settings, machine speed, steam pressures, coating settings and lineal pressures in wet processing (Yeo *et al.*, 2005). The stock that is discarded during a grade change is referred to as “broke” and the system that processes the stock the “broke system” (Vector Solutions, 2021b). A broke pit or well is situated below the paper machine into which broke is disposed from the machine floor. From a financial as well as operational perspective it is important to salvage and reprocess as much of this valuable fiber resource as possible as this resource of fibre usually amounts to around 5% of a machine’s total production (Vector Solutions, 2021b).

Recovery and functionalisation of fibres from these waste sources instead of disposal by landfill or incineration could be advantageous for PPMs. Such a technology can also be viewed as a kidney technology as it can be added to existing wastewater treatment technologies that are already in place and will help prevent the accumulation of fibres in closed water circuits. Not only does such a solution promote the closing of water circuits but it also addresses the biorefinery- and MIMO concept. By functionalizing recovered fibres to nanocellulose multiple inputs and outputs can be considered, as nanomaterials can be produced from many different raw materials.

This study focused on only one raw material which is hardwood fibre from *Eucalyptus globulus* which was processed to pulp via the Kraft pulping method. The Kraft process is the most widely used chemical route making the results of this study relevant to most pulping mills (Simão *et al.*, 2018). The relevant waste streams contributing to fibre loss from such a mill include paper machine white water left untreated by the save-all device, grade changes as well as screening and washing steps after the cooking and bleaching stages. Samples were collected from various locations in the mill to determine if there is a major difference in composition and functional groups that influence their recovery and functionalization to nanocellulose. Depending on these properties, the nanomaterial produced can have varying properties and thus multiple outputs can potentially be considered ranging from products such as films, aerogels, coating agents, wound dressings etc. Based on these findings, the feasibility of combining different waste streams will be discussed.

1.2 Project aims and objectives

1.2.1 Aims

The aim of this study was to identify effective methods for recovering and modifying the properties of cellulosic fibres recovered from Kraft PPM waste streams. Recovered fibres were functionalised to nanocellulose which can be used as a raw material for various applications including the production of biocomposites, oil spillage cleaning, bioremediation etc.

1.2.2 Key research questions

The following are key questions of the project that will guide the investigation:

1. What is an effective method for recovering cellulosic fibres from different waste streams?
2. What are the properties of the cellulosic fibres that influence their recovery?
3. Can the properties of the cellulosic fibres be predicted based on the upstream processes?
4. How do the physical and functional properties of the cellulosic fibres influence their functionalization and performance in films?

1.2.3 Objectives

The specific objectives are as follows:

1. Identify which waste streams in the Kraft pulp and paper mill are the most relevant for recovering rejected fibres and investigate why the fibres have been rejected. The composition of wastewater containing the fibres, and the potential advantage of combining some of these identified waste streams as sources of fibre for recovery are discussed under this objective.
2. Evaluate methods from literature for recovering and functionalising fibres recovered from the Kraft pulp and paper mill waste streams identified in objective 1. The methods will be evaluated based on their economic feasibility, ease of industrialisation, and environmental sustainability. Evaluations for all three criteria are based on literature information. A method was chosen using a decision-making tree which was created as an analytical tool for the purpose of sorting through potential methods (**Figure 1**).

3. Propose and develop a feasible method for recovering and functionalizing fibres from Kraft pulp and paper mill waste streams based on the evaluations of the second objective.
4. Determine the character and estimate the amount of waste discharged. Recovered and functionalized fibres are characterized in terms of physical and functional properties.
5. Assess the potential of using collected data from objective 4 for soft sensor development.

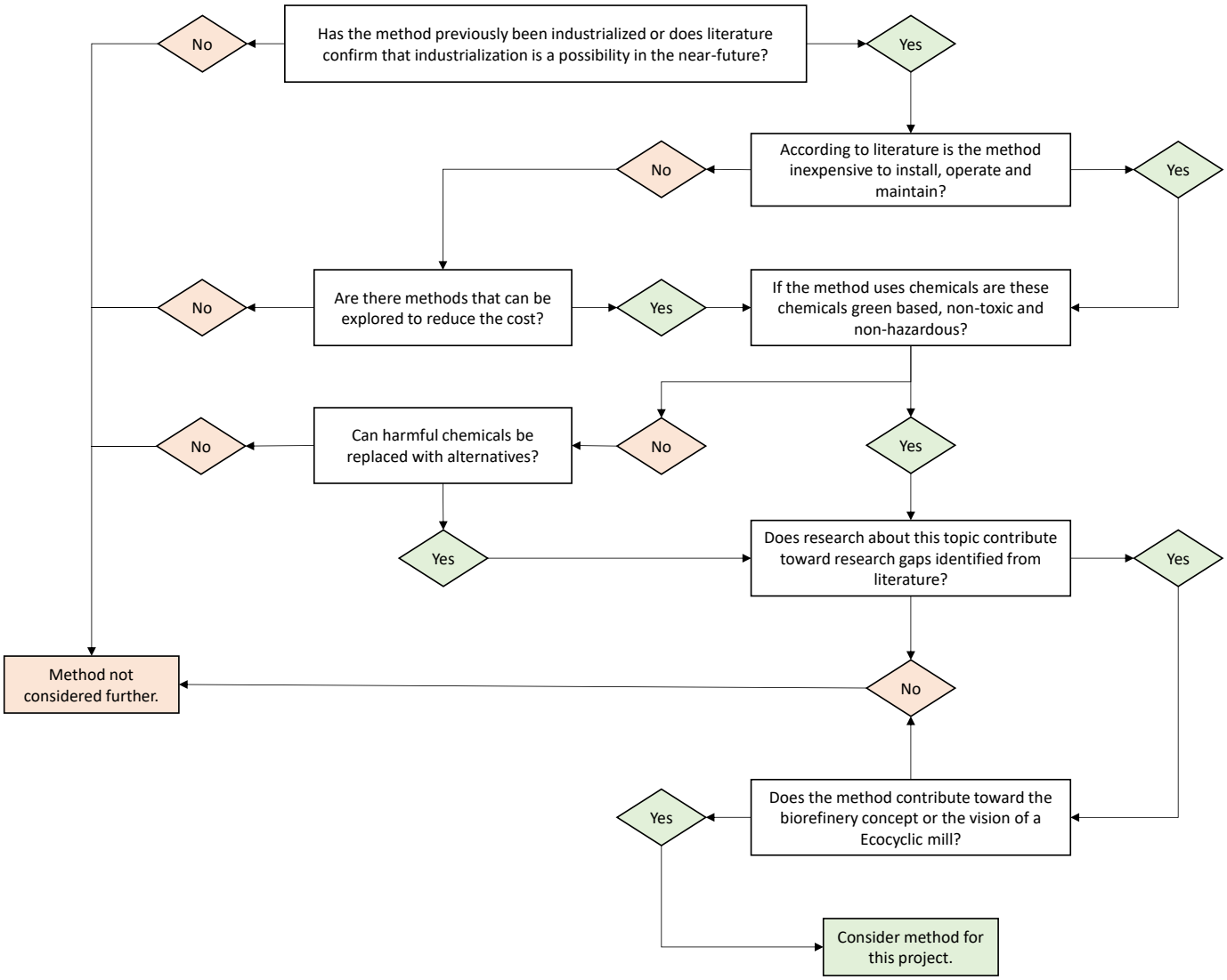

Figure 1: Decision-making tree to determine which recovery and functionalization methods are best based on economic feasibility, ease of industrialisation, and environmental sustainability.

1.3 Project scope and limitations

This project scope was narrowed by only focusing on the Kraft pulping process. The project was further limited to pulp mills processing hardwood, specifically *Eucalyptus globulus*, as the feedstock. To complete the objective of identifying waste sources in a Kraft mill it was necessary to collect certain mill data including an accurate process flow diagram, details about their modus operandi and specific equipment etc. Samples from these waste sources were collected to develop and validate methods

for recovering and functionalizing fibres. The mill from which the data and samples were acquired is referred to as “Kraft pulp and paper mill” or “Kraft PPM” in this document.

The mill studied has the capacity to produce more than 720 000 tons per annum (total paper output excluding waste streams). It produces two key products: a premier grade bleached hardwood pulp made purely from *Eucalyptus globulus* fibre, and a white top Kraft linerboard. The linerboard is made partly of unbleached softwood pulp and partly from the bleached hardwood pulp for the “white top” of the linerboard. The processes to produce the softwood and hardwood pulp are separate and thus, it was possible to study only the hardwood line. The processing of hardwood includes the continuous cooking of hardwood fibres, followed by the washing, bleaching and paper machine stages.

2 LITERATURE REVIEW

2.1 The waste situation in pulp and paper mills today

In the 1960s the pulp and paper industry was one of the main industries responsible for a series of serious environmental problems, from smoking chimneys spreading dust and sulfur dioxide, unpleasant smells and soot settling in nearby areas as well as severely affecting watercourses in the area. Back then concepts like chemical recovery, internal fibre recovery and sedimentation ponds were not employed within this industry. Consequently, fibre banks started to spread over large areas and, due to lack of oxygen as well as malodorous hydrogen sulfide present in water bodies, fish populations decreased. (Ek, Gellerstedt and Henriksson, 2009)

This has changed in the past 20 years with huge investments made by the forest industry to work on ways to prevent or limit emissions. This includes finding greener alternatives to chlorine bleaching, eliminating fibre emissions, COD emissions and odors. A list of the main problems and the current situation in industry is given in **Table 1**. The vision is for mills is to become totally “closed” and “emission-free”. This is not completely realistic as there will always be water and carbon dioxide emissions to some extent. A more accurate definition of an ecocyclic mill is one that creates no environmentally hazardous emissions (Ek, Gellerstedt and Henriksson, 2009). All substances leaving the process are to be treated or re-used so that it does no harm when being released to the environment.

Even though many problems have been solved, there is still room for much improvement to further adapt the Kraft mill. One challenge remaining is closure of process water loops as pulp production is a highly water intensive process which subsequently generates a substantial amount of effluent that contains fibres which escape through the fine mesh wire on which paper is formed (Hamm and Schabel, 2007). Although mills are equipped with save-all devices (usually disc filters as mentioned in Section 1.1) to recover as much of these fibres as possible, these devices are unable to operate at 100% efficiency and subsequently there will be an accumulation of fibre in the effluent stream.

Table 1: The emission situation in 2009 regarding Kraft pulping. (Backlund, 2009)

Problem	**Status in 2009**
Fibre emission	Solved
BOD emissions (deoxygenated water)	Solved
Sulfur dioxide emissions	Almost solved
Odors (sulfur compounds)	Unsolved but greatly improved
Oil consumption	Not completely eliminated
COD emissions (organic substances)	Almost solved
Emissions of organically bound chlorine	Almost solved
Chlorate emissions	Solved
Nitrogen oxide emissions	Low emissions
Nutrient salt emissions (nitrogen and phosphorous)	Unsolved
Metal emissions	Uncertain whether this is a problem
Chemical additives	Situation unclear, research underway

There are seven main risks associated with closure of water loops including corrosion, increased slime formation, reduced retention, formation of deposits, emission of odorous compounds, reduced product quality and increased complexity of the papermaking process (Hamm and Schabel, 2007). These challenges can be overcome by installation of "kidney technologies" which can also be described as intermediate treatment stages. A disc filter installed as a save-all device to specifically recover fiber or an intermediate clarifier installed specifically for the recovery of lime can be seen as examples of kidney technologies. Some problems, like COD emissions and chlorate emissions, are easier to address than others, including odors and oil consumption, but it is possible to overcome these problems and operate an "effluent-free" mill that only needs freshwater consumption of around 1.5 m^3/ton paper (Hamm and Schabel, 2007). This is needed to replace the volume of water lost by evaporation in the paper machine dryer section as well as water lost via the solids not recovered by the save-all device if not re-used in the stock preparation.

Some benefits to consider when closing water loops include no wastewater discharge fee owed to authorities and that a mill operating with zero-effluent is no longer limited to be placed in an area with sufficient receiving water flow. Reduced freshwater consumption also increases the mill's white-water temperature which improves water drainage at the paper machine forming section and gives a higher solids concentration after the press section (Ek, Gellerstedt and Henriksson, 2009). This leads to a reduction in the amount of energy required in the drying section. Many mills have managed to close process water loops significantly. In the beginning of industrial papermaking, paper was produced with high freshwater consumption rates of around 500 m^3/ton of paper (Hamm and Schabel, 2007). In the past 40 years industry has succeeded in reducing this to an average of

50 m^3/ton and according to Hamm and Schabel (2007) some mills have even managed to further decrease the amount to 13 m^3/ton.

According to the author Backlund (2009) fibre emission problems have been solved. This is true as most mills treat mill effluent in wastewater treatment plants (WWTPs) to produce sludge that is normally either incinerated or landfilled (Lekha *et al.*, 2017). Sludge in this context is defined as the residual solid product obtained after treatment of effluent from a PPM in wastewater treatment plant (WWTP). This solution to dispose of fibre however comes with its own set of environmental and financial problems. Landfilling leads to emission of greenhouse gases (GHG) and leeching of toxic substances into surrounding ground and water systems. Incineration leads to emission of gaseous NO_x and SO_2 which are major precursors of acid rain. The remaining ash after incineration also needs to be landfilled and contains various toxic metals resulting in ground water contamination.

From an economic aspect there is Capex investments for large mills to consider and transport fees for smaller mills to landfill sites. Large mills will usually acquire land for landfill which incur huge Capex costs for maintenance and improvement of this fixed asset. Except for environmental and economic considerations, it is also a waste of valuable fibres that can be used in various alternative products like biofuels, biopolymers, nanocellulose, fish feed (converted to a glucose rich hydrolysate) and building materials (Lekha *et al.*, 2017). According to Lekha *et al.* (2017) sludge from recycled fibre is an especially suitable feedstock for biofuel production and even though poly lactic acids (PLA) in biopolymers have traditionally been produced from corn or potato starches, cellulosic fibres from PPM waste streams have proved technically feasible.

2.2 Fibre loss and recovery in pulp and paper mills

As mentioned in Section 1.1, three sources of fibre loss were identified from literature including (1) the portion of white water left untreated by the paper machine save-all device, (2) grade changes and (3) screening and washing stages. These losses will occur in the bleaching plant and paper machine stages as shown in the simplified process flow diagram of a Kraft pulp mill in **Figure 2**. From the digester (Figure 2) there will be a loss of mass due to alkaline hydrolysis which leads to the dissolution of lignin and hemicelluloses and partial dissolution of cellulose as stated in Section 1.1. A more detailed overview of the Kraft process is given in Section 2.3.3. A mass balance was conducted to quantify the amount of fibre lost during these stages of Kraft pulping. The results are given and discussed in Section 4.4. Fibre losses associated with the paper machine save-all devices as well as screening stages are universally relevant for mechanical as well as chemical pulps whereas screening and washing stages are mostly relevant to chemical pulping. To understand these losses better, the details of the equipment involved in these losses were investigated.

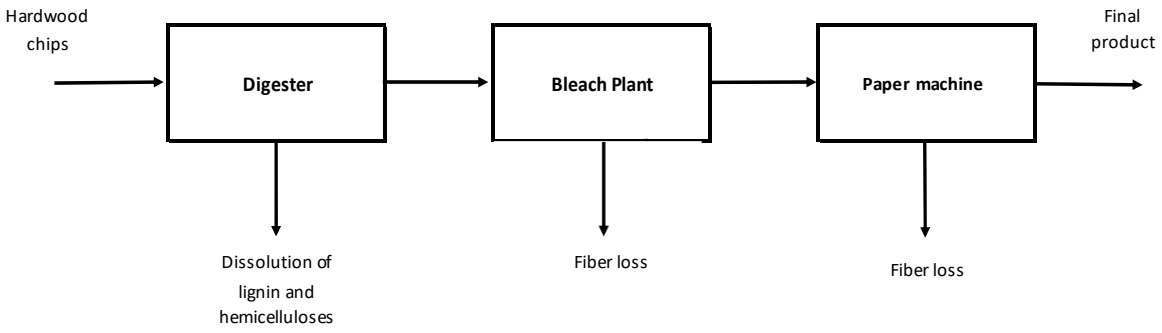

Figure 2: Simplified process flow diagram of a Kraft pulp and paper mill showing the stages from which cellulosic fiber is lost.

Modern paper machines consist of a headbox, wire section, wet pressing, drying and sometimes coating units. This process to produce paper is identical for all pulp types and processes, irrespective of the method used to obtain the pulp for papermaking (Bajpai, 2015). Pulp stock is diluted to a consistency of between 0.3 and 1% with white water before being fed to the paper machine headbox (Yeo *et al.*, 2005). The headbox spreads the stock flow across the width of the paper machine which then moves across the wire section where the paper web is formed. The final steps are all used to remove the water and dry pulp. Wet pressing is used to press most water from the pulp and is then followed by steam-heated cylinders to obtain the paper product.

As stock flows over the wire section some fibres escape through the fine mesh. Save-all devices are installed to recover these fibres and clarify white water for re-use in the process. These devices are normally disc filters or in some cases flotation type devices (CNBM Anyang Machinery, no date; Savage and Koch, 1950). The efficiency of disc filters are usually between 33 to 90% (Khan, Rehman and Nasir Jamal, 2017). A disc filter consists of several steel fan discs covered in cloth. Fibre is collected on either side of the cloth forming a sludge cake. A section of the disc is submerged in a trough filled with white water. The discs are mounted about 30 cm apart along a shaft which is driven by a motor that rotates the discs clockwise (Wills and Finch, 2016). As the disc rotates, the solid cake is lifted above the height of white water in the trough. At this point the cake is suction dried and removed using a scraper.

Regarding grade changes on a paper machine, the type of loss can be divided into two categories namely (1) continuous and (2) event related broke (Vector Solutions, 2021a). The former is generated as winder trim, wet edge trim, cull rolls and dressing from reels. The latter comes from sheet breaks as well as machine startups and shutdowns. Broke is fed back into the system in a controlled manner. The fibers behave differently from virgin fibers due to fibers being able to hold less water and thus dry more easily (Vector Solutions, 2021b). According to Vector Solutions (2021b) this phenomenon negatively affects sheet quality and machine runnability which is why the amount in the system needs to be carefully controlled.

Pulp washing is a complex and dynamic process. In textbooks of chemical engineering the operation of washing pulp is described as a solid-liquid extraction process (Ek, Gellerstedt and Henriksson, 2009). The pulp web forms a porous bed in which part of the liquid phase is closely associated with the fibres as a stagnant liquid while the other part of liquid phase is considered free moving. The displacement of liquid out of a pulp web is thus considered a special case of flow through a porous media. Unbleached pulps produced by mechanical as well as chemical methods will require one or two washing stages before further treatment. Bleached pulps however consist of multi-stage bleaching sequences which require further extensive washing between each stage as mentioned in Section 1.1. Common equipment used for pulp washing includes horizontal belt washers, vacuum filters, pressure filters, pressurized diffusers, displacement or wash presses and drum displacement washers (Ek, Gellerstedt and Henriksson, 2009).

2.2.1 Methods to recover fibres from dilute waste streams

The fibre losses discussed in Section 2.2 are sent to WWTPs where fibres are normally recovered by sedimentation (Andreoli et al., 2007). The clarified wastewater is followed by biological treatment. These processes produce primary and secondary sludge respectively. The two types of sludge have different characteristics although both contain organic matter, nitrogen and phosphorous which can be used as macronutrients in fertilizer products (Simão *et al.*, 2018). In most cases, both secondary and primary sludge are mixed to facilitate handling. According to Simão *et al.* (2018), primary sludge consists mainly of cellulose fibres, fillers (like kaolintic clay or calcium carbonate) and low amounts of potassium, magnesium, sodium and possibly several toxic metals. In some cases, the sludge may also contain ash and inert materials. Secondary sludge has a much higher nutrient content (Simão *et al.*, 2018).

In the past 10 years there has been increasing awareness that there is a need to reduce the amount of solid waste sludge that is produced during the pulp and papermaking process. A study by Mladenov and Pelovski (2010) and Ince, Cetecioglu and Ince (2011) revealed that from a total solid waste generation of 238 771 thousand ton produced by the Bulgarian Industry in 2006, the pulp and paper industry largely contributed to this figure with around 186 thousand ton being generated annually. Also, according to Mahmood and Elliott (2006) 60% of the costs involved in WWTPs are related to the disposal of produced sludge. For economic as well as environmental purposes it is thus important to explore methods to remove fibres in effluent streams prior to being treated in WWTPs, thereby reducing the amount of effluent that needs to be treated and reducing the volume of sludge that needs to be disposed. Methods that have been explored and reported in literature focus on screening devices and flotation technology.

2.2.1.1 Screening technology

One of the main hindrances with recovering fibre from waste streams has always been finding an efficient and economically feasible way to do so. Many early attempted separation methods were unsuccessful in producing a suitable yield of cellulosic product with a low ash content (Gardner, 1965). Some of the earliest recovery methods involved a mechanical screening technology. Patents for such

inventions include vibrating screens (Gardner, 1965), sieve bend screens and cyclones (Boniface and Redding, 1974), curved wire washers, rotating drums or disk filters combined with centrifugal cleaning (Wolfer *et al.*, 1997) as well as bending and stretching screens (McDonald, 2003).

The recovery methods as patented by Boniface and Redding (1974) and Wolfer et al. (1997) use stationary screens with small openings to separate fibres from the aqueous suspension. These small openings have a significant tendency to plug or "blind over" due to build-up of material. Accordingly, such systems do not function properly or require maintenance on a regular basis to keep the screen opening from plugging. Stationary screens therefore have a major disadvantage when compared to vibrating or flexible and pliable screens such as the inventions patented by Gardner (1965) and McDonald (2003). Screening and centrifuging techniques such as the one proposed by Wolfer et al. (1997) have also never been commercialized because of the high cost involved and poor-quality product obtained.

The vibrating screen invented by Gardner (1965) consists of a screen with openings or apertures of a size sufficiently large that when stationary retains neither fibres nor non-fibrous material. The screen moves in a gyratory pattern, i.e. simultaneously in several directions about a multitude of axes, which results in fibres forming agglomerates. These fibre agglomerates, which leave through an outlet on the same level as the screen, are essentially retained by the particular motion imparted on the screen while at the same time non-fibrous material and water flow through the screen onto a dome-shaped bottom and finally through a separate outlet (Gardner, 1965). Underneath the dome-shape is the motor that controls the gyratory motion of the screen. This separation device has a claimed recovery of at least 55% and often 75% of the fibres. Two such screens in series would increase the yield to between 90 and 95%. The screen has openings of between 0.4 to 0.8 mm depending on the average fibre length of the raw material used in the process.

The system invented by McDonald (2003) consist of a flexible and pliable screen that is suspended from a frame. The screen has a truncated cone shape. Incoming white water strikes the screen at various locations which results in the bending and flexing of the screen. This method of varying the position at which white water strikes the screen helps to rotate the screen and consequently reduce the risk of clogging as the screen openings are self-cleaned. The screen is designed to direct usable fibre toward a discharge opening located at the lower end of the truncated cone shape screen while wastewater will pass through the screen to be collected in a tank situated below. Usable fibres in this case are defined as fibres within a certain size class as defined by the producer. The screen can also be suspended horizontally in a trough form to have an open discharge end.

2.2.1.2 Flotation

Flotation methods are preferred for recovery of particles in a thin suspension – the energy demand for mechanical methods increases greatly with a decrease in concentration (Wille et al., 2020). Since the solid content in effluent streams is between 0.1 to 1%, which according to Gardner (1965), flotation would be a better method to consider. Flotation methods can easily be adapted and adjusted for multiple different inputs compared to for example the vibrating screen patented by Gardner

(1965), which has a screen aperture based on the average fibre length based on the raw material used. It is also a well understood and universal concept that has been successfully industrialised by many industries including the pulp and paper industry (Edzwald, 2010).

Flotation is a collective term for multiple processes called "adsorptive bubble techniques" (Lmlich, 1972). It is a liquid-solid separation process by which particles in a suspension are recovered by their attachment to gas bubbles which are normally made of air. These attached solid particles, called bubble-particle aggregates, have a lower density than the suspension itself which causes the aggregates to drift to the surface where it can easily be removed. The process most effectively removes particles between 10 to 200 μm (Wakeman, 2011).

Conventionally flotation methods are placed into two categories: foaming and non-foaming. The difference between these is that foaming methods use the addition of surfactants to create a relatively stable froth. The froth (or foam) acts as a carrier fluid during particle removal. The additional cost of surfactants is a disadvantage when compared to non-foaming techniques that only use air. Recycling of the surfactant could minimize the cost. (Wakeman, 2011)

According to Wakeman (2011), the three most important properties to ensure successful flotation are: bubble particle size ratio, solid hydrophobicity, and the extent of turbulence in the fluid. For particles to attach to gas bubbles in an aqueous medium, the particles need to be hydrophobic. Most inorganic and many organic particles however have hydrophilic surfaces (Howe *et al.*, 2012). Fibres and fibre-fines are in fact hydrophilic (Rol *et al.*, 2019). To ensure removal of these particles by surfactants, also known as collectors, is required to displace the water film from their surfaces thereby rendering the particle surface hydrophobic.

The source of bubbles in flotation systems can be natural or aided. Natural bubbles are released by the process of fermentation, causing a scum layer at the surface of the liquid. Aided bubbles are blown into a suspension by one of two main techniques. The first type is known as mechanical or froth flotation which uses an agitator to generate bubbles with the aid of surfactant solutions. The froth or foam is then pumped to the base of a flotation column with an air injection system. By this method bubbles with dimensions between 0.2 to 2 mm are normally generated (Wakeman, 2011). The second type is known as gas nucleation whereby air is dissolved in water under high pressure. The saturated solution is pumped to the base of a flotation column and then released at atmospheric pressure through a nozzle to produce bubbles with dimensions between 10 to 100 μm (Ghasemi Naghdi and Schenk, 2016).

Another type of flotation, which also produces bubble by agitation in a similar manner to froth flotation, is the generation of colloidal gas aphrons (CGAs). CGAs were first described by Sebba (1971) as microfoams with colloidal properties. In a successive study by Sebba (1987) CGAs are described as being microbubbles created by intense stirring, between 5000 to 10 000 rpm, of a surfactant solution. The surfactant is responsible for converting the entrained air created during intense stirring into highly stabilized aphron structures.

Three of the mentioned flotation techniques have been used to either recover cellulosic fibres or treat PPM waste effluents including DAF (Miranda *et al.*, 2013), flotation aided by CGAs (Mukherjee *et al.*, 2015), and froth flotation (Redlinger-Pohn *et al.*, 2016). The study by Miranda et al. (2013) investigated the efficiency of using chitosans for the treatment of PPM process water by dissolved air flotation. Two native chitosans and two quaternary derivatives of chitosan were evaluated. Mukherjee et al. (2015) investigated the optimization of pulp fibre removal by flotation using CGAs generated from a natural surfactant. The results were compared to those of three synthetic surfactants. Redlinger-Pohn et al. (2016) investigated separation of cellulose fibres from a pulp suspension by froth flotation fractionation with tall oil saponified with sodium hydroxide.

2.2.2 Surfactants

A surfactant molecule is amphiphilic and has two distinct parts namely (1) the moiety that interacts strongly with the solvent, known as the lyophilic part, and (2) the other moiety, the lyophobic part. The lyophobic part has a very weak attraction with the solvent and instead interacts with other molecules with similar properties. Surfactant molecules can also be described as having a hydrophilic head and hydrophobic tail as shown in **Figure 3a**. This duplexity is what makes it possible for the surfactant to attach to molecules and change its surface properties, as shown in **Figure 3b**. (Nakama, 2017)

The hydrophilic head of the surfactant has a strong affinity for water because it is made up of polar groups. Examples of such polar groups include, among others, carboxylic-, hydroxyl-, and sulphate-, groups. The hydrophobic tail consists of hydrocarbon chains and can have a variety of unique structures including linear, branched and even aromatic chains, depending on the number of carbon atoms the molecule contains. When these molecules are dissolved in a liquid, they are adsorbed at the interface which leads to reduced interfacial tension. (PCC Group, no date)

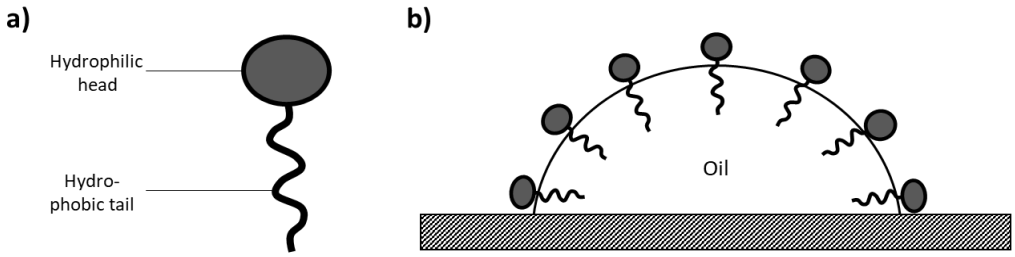

Figure 3. a) Structure of a surfactant molecule and b) Surfactant molecules orientated around a drop of oil.

2.2.2.1 Surfactant properties

2.2.2.1.1 Surface tension

The amphiphilic nature of surfactants as described in Section 2.2.2 allow the molecules to adsorb at air-water or oil-water interfaces. At the interface they align their hydrophilic head to the inside of the liquid and their hydrophobic tail toward air in an air-water environment or oil in an oil-water

environment **Figure 3b**. As surfactants adsorb to either of these interfaces the surface tension decreases. To explain why this phenomenon occurs consider an air-water interface. Initially, before adding a surfactant to the solution, the cohesive forces between water molecules in solution are strong which results in high surface tension. When surfactants are present in the solution, they break these interactions and since the intermolecular forces between surfactants and water molecules are much lower the surface tension will decrease. (Lauren, 2018)

The surface tension can be decreased further by increasing the surfactant concentration up to the point where the critical micelle concentration (CMC) is reached. In a solution the surfactant molecules will initially be randomly dispersed in the liquid volume until the CMC is reached. Once this concentration is reached molecules will start organizing themselves into spherical forms called micelles. Once the CMC point is reached the surface tension will remain constant irrespective of further increases in surfactant concentration. Non-ionic surfactants are known to reduce surface tension most effectively. (PCC Group, no date)

2.2.2.1.2 Foamability

As can be presumed from the name, foaming properties are the ability of surfactant to form foam. The property results from a surfactants ability to coordinate micelle structures and stabilize air bubbles. Surfactants accomplish this by encasing gas bubbles with a thin layered film at the interface which results in formation of foam. Foaming is an undesired phenomenon in certain applications, like mineral flotation, and can be reduced by the addition of anti-foaming chemicals. The foaming capacity of surfactants can also be controlled by modifying the molecules' structure. For example, introduction of ethylene oxide increases a surfactant molecules foaming capacity whereas addition of a polyoxypropylene moiety reduces foaming. (PCC Group, no date)

2.2.2.1.3 Solubility in water

Due to the amphiphilic structure, surfactants are dissolvable in many solvents. The degree of solubility is however dependent on the structure of the hydrocarbon chain of the hydrophobic part with longer and less molecules being less soluble in water branched. It is possible to control the solubility of surfactant molecules by modifying their structure for e.g., by introducing a polyoxyethylene moiety which increases a surfactants solubility in water. Solubility can also be increased by crossing what is known as the Krafft point which is the temperature above which micelles form and thereby increase the solubility. The solubility of a surfactant can be decreased by introducing propylene oxide moieties into its structure. (PCC Group, no date)

2.2.2.2 Types of surfactants

Surfactants can be categorized according to the charge of their hydrophilic moiety. There are three types namely ionic, non-ionic and zwitterionic surfactants. Ionic surfactants can be further divided into anionic and cationic surfactants. Anionic and cationic surfactants have a negatively and a positively charged hydrophilic group respectively. The headgroups in non-ionic surfactants do not carry any

electrical charge. Zwitterionic surfactants have headgroups with both positive and negative charges in equal numbers which like non-ionic surfactants results in a zero net charge.

An alternative way to classify surfactants is to categorize them according to their hydrophilic-lipophilic balance (HLB). The HBL can have a value between 0 to 20 and describes the percentage of hydrophilic groups in the total mass of surfactant. Lower HLB values mean the surfactant has better solubility properties in oils and other hydrophobic compounds. In contrast, higher HLB values mean the surfactant is more hydrophilic and consequently its solubility in water increases while solubility in oil decreases. According to this method of characterization surfactants can be divided into 7 groups namely detergents (HLB value: 12-15), foaming agents (HLB value: 14-18), anti-foaming agents (HLB value: 0-2), W/O emulsifiers (HLB value: 3-6), O/W emulsifiers (HLB value: 8-15), wetting agents (HLB value: 7-9), and solubilizers (HLB value: 12-18). (Nakama, 2017)

2.2.2.3 Synthetic surfactants versus biosurfactants

There is a great demand in current markets for bio-based surfactants due to health as well as environmental concerns. This is also true for pulp and paper industries especially for mills that use recycled fibres. Recycled fibre feedstock is prepared for re-use in a de-inking process by flotation. The most common non-ionic surfactants used in this process are alcohol ethoxylates, consisting of an ethylene oxide (EO) hydrophilic part and propylene oxide (PO) hydrophobic part (Jiang and Ma, 2000). The EO part of this copolymer is a petroleum derived product meaning that the production cost of these chemicals, as well as most other hydrophobic components, rely on the highly volatile price of petroleum (Xiang *et al.*, 2019). This further motivates the search for alternative, greener surfactants.

Sugar-based surfactants are an attractive alternative to consider. Sucrose fatty acid esters, like sucrose dodecanoate, are popular biosurfactants widely used for food, cosmetic and medicine applications (Iwasawa, Oyama and Kunieda, 2001). Other typical hydrophilic sugar components include maltose, pyranoside and glucose. Example surfactant products derived from these sugars include n-Dodecyl-β-maltoside, n-octyl-β-D-thioglucopyranoside, octyl glucoside, lauryl glucoside and decyl glucoside. The foam properties of n-Dodecyl-β-maltoside are especially promising for flotation application and applications involving diverse harsh conditions (Zhao *et al.*, 2018).

Sugars from hemicellulosic biomass can also be considered to produce surfactants. Of all the different hemicellulose sugars, xylan specifically has earned much attention as a possible raw material for this application. Xylan-based surfactants, otherwise known as alkyl xylosides, have exceptional biodegradation properties and good surface activity that make them a great option in that respect. Finding greener processes for the extraction of xylan and synthesis of xylan-based surfactants with higher yields is critical for its market growth. Toward achieving this goal, a study by Faryar (2019) used enzymatic methods to produce these types of surfactants, specifically n-octyl xylobioside and n-octyl xylotrioside. Another study by Sekine et al., (2013) aimed to produce alkyl glycosides by Fischer's mechanism under mild conditions. Octanol was chosen as the alcohol because it is a renewable resource and because octyl xylosides are known to be highly biodegradable surfactants (Matsumura *et al.*, 1998). The study showed that a direct conversion of xylan to alkyl glycosides under mild

conditions is possible by using 1-*n*-butyl-3-methylimidazolium chloride as ionic liquid and 10-camphorsulfonic acid (CSA) as catalyst.

2.2.3 Colloidal gas aphrons (CGAs)

As mentioned in Section 2.2.1.2 CGAs were first described by Sebba (1971) as microfoams with colloidal properties. The bubbles were reported having diameters of between 10 to 100 μm which is the reason for the term colloidal being used. Sebba later described them as being microbubbles created by intense stirring. Another definition is given by Longe (1989) which states that CGAs are a collection of spherical, micron-sized gas bubbles dispersed in an aqueous surfactant solution with a volumetric gas fraction of at most 0.74 and 95% of bubbles having diameters not exceeding 100 microns. The volumetric gas fraction of 0.74, also referred to as CGA quality, is the highest possible packing density of uniformly sized spheres. Bubbles with diameter of more than 100 micron are non-spherical.

Some authors in literature deem that CGAs are not truly in the colloidal range which is between 1 nm and 1 μm according to Shaw (1992). Opposingly, sources such Eastoe (2010) state that the colloidal domain is traditionally defined as having a range from a few nanometers to a few tens of micrometers. Within this range a constant set of physical laws can be used to effectively describe the behavior of the colloidal materials (Hughes, 2010). According to Hughes (2010), for materials having a length of a few nanometers, the molecular and atomic properties are most significant. At the boundaries of the colloidal range these laws become less meaningful and instead kinematics as well as wetting phenomena become more important.

Colloidal systems comprise of at least two phases where one phase is dispersed in another. The dispersed phase is denoted as β and the second phase as α as illustrated in **Figure 4**. Several examples of colloidal systems are given in **Table 2**. As can be inferred from the definitions, CGAs have a liquid medium (α) and gas bubbles in the dispersed phase (β) which correctly describes the aphrons to be foams as stated in the definition. A CGA system is also a multicomponent system with at least one component in the gas phase and at least two components (water and a surfactant) in the liquid phase.

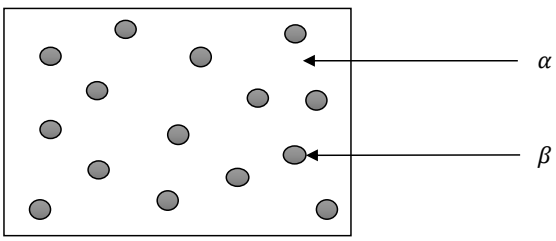

Figure 4: Schematic representation of a colloidal system representing the dispersed phase β and the second phase α. (Hughes, 2010)

Table 2: Examples of various phases in the colloidal domain. (Hughes, 2010)

Dispersed phase (β)	**Medium (α)**		
	Gas (fluid)	**Liquid**	**Solid**
Gas (bubbles)	-	Foam	Solid foam
Liquid (droplets)	Liquid aerosol	Liquid emulsion	Solid emulsion
Solid (particles)	Solid aerosol	Sol	Solid Sol

CGAs are known to be more stable systems than conventional foams. It has been postulated by Sebba (1971), although without any direct scientific evidence, that this is due to the structure of a an aphron as illustrated in **Figure 5**. Aphrons have spherical cores, normally made of gas but sometimes liquid, that are encased by a shell of surfactant multilayers. Within the inner layer, surfactants orientate themselves so that the hydrophobic, non-polar ends attach to the core and the hydrophilic, polar ends are faced toward the second layer. The outer layer surfactants form a bilayer to hide their hydrophobic, non-polar ends and expose the hydrophilic, polar ends toward the second (α) phase on one end and the bulk fluid on the other end. The aphron shell is made up of water, an aphron stabilizer, and a thickening agent. Sebba (1971) claims that this structure possibly explains why CGA dispersions show such high stability compared to other foams.

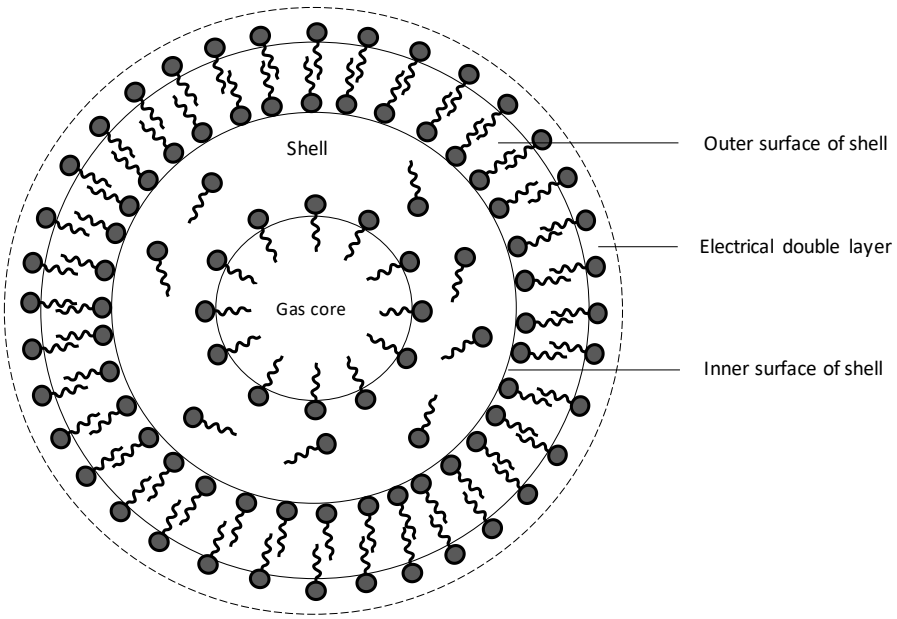

Figure 5: Proposed structure of colloidal gas aphrons. (Molaei and Waters, 2015)

2.2.3.1 Mechanism of CGA formation

The first step in CGA formation is the dispersion of the gas phase into the liquid phase. The gas phase is introduced by any suitable method that creates vortex surface waves. The classic method to achieve this is by using a high-speed stirrer in a baffled beaker. Other methods that have been used in the past include sonication and homogenization (Molaei and Waters, 2015). Once dispersed in the liquid phase, the bubbles breakup into smaller ones through a series of interdependent processes namely hydrodynamic forces, interbubble gas diffusion and interbubble collision. This results in a dispersion

of bubbles ranging from 10 to 100 μm in size. The following section is adapted from Longe (1989) except where otherwise stated.

2.2.3.1.1 Hydrodynamic forces

The turbulence needed to form CGAs implies that hydrodynamic (inertial) forces are a significant factor that leads to initial bubble breakup. The hydrodynamic force resulting from bubbles shear and turbulent forces is counteracted by the bubble's surface force. The ratio of these two forces is known as the Weber number (We) and is given mathematically by equation 1 where ρ is the density of the gas, D is the bubble diameter, v is the bubble velocity and σ is the surface tension.

$$We = \frac{inertial\ forces}{surface\ tension\ forces} = \frac{\rho D v^2}{\sigma} \qquad [1]$$

Where:

$We = Weber\ number$

$\rho = density\ of\ the\ gas$

$D = bubble\ diameter$

$v = bubble\ velocity$

$\sigma = surface\ tension$

According to Hinze (1955),the critical Weber number for dispersion processes in turbulent flow is equal to about 1. When the Weber number exceeds the critical value the bubbles in the system become unstable and breakup may occur. Factors that significantly affect the Weber number include the difference in phase density, presence of a surfactant and the occurrence of other processes such as inter-bubble diffusion.

During the breakup process, the external hydrodynamic pressure is opposed by the internal pressure of the bubble. Since the attraction between molecules in the liquid state is far greater than that between molecules in the gas phase, the result is a net force pulling the surface molecules away from the gas phase. In order to bring the molecules to the interface from the liquid and expand it, work must be done against the free surface energy.

For a spherical bubble of radius r the total surface free energy is equal to $4\pi r^2\sigma$. Increasing the radius by dr would create a change in surface free energy by $8\pi r dr\sigma$. At equilibrium these forces will be balanced by the work against the pressure drop across the interface ΔP. Mathematically this is expressed as in equation 2. Simplifying and rearranging this equation gives an equation for the difference between the internal pressure of the bubble and the ambient pressure of the bulk fluid, as given by equation 3. This equation is also referred to as the Laplace equation. The equation implies that a lower surface tension and larger radius will enhance bubble breakup. Pure water for example has a very high surface tension of 0.0728 at 20 °C which makes bubble breakup tedious without a surfactant.

$$4\pi r^2 dr\Delta P = 8\pi r dr\sigma \qquad [2]$$

$$\Delta P = \frac{2\sigma}{r} \quad [3]$$

Where for equation 2 and 3:

$\Delta P = pressure\ drop\ across\ the\ interface$

$r = spherical\ bubble\ radius$

$\sigma = surface\ tension$

Surfactants not only help to lower the surface tension by displacing water molecules but also create an interfacial film which helps to stabilize the bubble. Without this interfacial film the bubbles will rupture quite easily. Compared to conventional bubbles, the colloidal gas aphrons structure makes it possible to survive a compression of at least 27.3 MPa which is 10 times more than the pressure a conventional bubble can survive (Molaei and Waters, 2015).

For ionic surfactants the lowering of surface tension is often a function of surfactant concentration up to a point where micelles begin to form in the bulk liquid. As mentioned in Section 2.2.2.1.1 this concentration is termed the critical micelle concentration (CMC). Above the CMC the concentration of surfactant molecules at the interface does not change, and excess surfactant molecules would therefore just go into the bulk fluid.

2.2.3.1.2 Interbubble gas diffusion

The process where large bubbles grow at the expense of small bubbles due to pressure differences is known as interbubble gas diffusion. Sebba (1987) described the formation of CGAs as an array of bubbles initially ranging from sub-micron bubbles to those greater than 100 μm in size. As time progresses the big bubbles become smaller while small bubbles with a diameter of less than 25 μm tend to disappear. The tendency for small bubbles to disappear is a due to the greater internal gas pressure. This pressure difference is given by the Laplace and Young equation for a curved interface, as given by equation 4. In this equation σ represents the interfacial area and r_1 and r_2 are the principal radii of curvature. For spherical particles equation 4 reduces to the Laplace equation as given by equation 5.

$$\Delta P = \sigma\left(\frac{1}{r_1} + \frac{1}{r_2}\right) \quad [4]$$

$$\Delta P = 2\frac{\sigma}{r} \quad [5]$$

Where for equation 4 and 5:

$\Delta P = pressure\ drop\ across\ the\ interface$

$\sigma = interfacial\ area$

$r_1 and\ r_2 = principal\ radii\ of\ curvature\ for\ non-spherical\ bubble$

$r = spherical\ bubble\ radius$

According to equation 6 the internal pressure of a bubble exceeds the average hydrodynamic pressure in the surrounding bulk liquid. The equation implies that for a given fluid of known σ the tendency for interbubble gas diffusion to occur increases with decreasing radius. The concept is illustrated by **Figure 6**. In the figure bubble A has a greater radius than bubble B. Consequently, the internal pressure of bubble B (P_B) will be greater than for bubble A (P_A) and thus there exists a driving force for mass transfer in the direction of the larger bubble, known as the gas flux, through the liquid layer separating the two. This driving force is expressed mathematically by equation 6, where r_A and r_B are the radii of the large and small bubbles respectively.

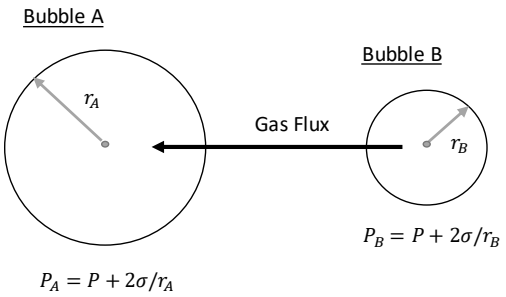

Figure 6: Interbubble gas diffusion. (Stevenson, 2010)

$$\Delta P_{BA} = \Delta P_B - \Delta P_A = 2\sigma\left(\frac{1}{r_B} - \frac{1}{r_A}\right) \quad [6]$$

Where:

$\Delta P_{BA} = gas\ flux\ from\ bubble\ B\ to\ A$

$\Delta P_B = internal\ pressure\ of\ bubble\ B$

$\Delta P_A = internal\ pressure\ of\ bubble\ A$

$\sigma = interfacial\ area$

$r_A = radius\ of\ larger\ bubble\ A$

$r_B = radius\ of\ smaller\ bubble\ B$

As gas diffuses out of the small bubble and it gets smaller in size, the internal area across which the gas molecules are transferred is reduced thereby slowing the diffusion rate. This interbubble gas diffusion rate can be estimated from Fick's law, given by equation 7. In the equation A is the area of the diffusion interface, D is the diffusion coefficient, S the solubility, ΔP the pressure drop across the interface and Δx the thickness of the diffusion barrier. Fick's law can also be expressed as shown in equation 8 where $J = DS/\delta x$ which is a measure of the resistance to mass transfer. The term considers the distance between the two bubbles, packing structure of surfactant molecules at the interface, chemical structure of the surfactants, contact time and presence of other materials at the interface, and viscosity of the medium α.

$$\frac{dn}{dt} = -ADS\frac{\Delta P}{\Delta x} \quad [7]$$

$$\frac{dn}{dt} = JA\Delta P \qquad [8]$$

Where for equation 7 and 8:

$\frac{dn}{dt} = rate\ of\ diffusion$

$dn = change\ in\ concentration\ of\ particle$

$dt = change\ in\ time$

$A = area\ of\ diffusion\ interface$

$D = diffusion\ coefficient$

$S = solubility$

$\Delta P = pressure\ drop\ across\ interface$

$\Delta x = thickness\ of\ diffusion\ barrier$

$J = \frac{DS}{\delta x} =$ measure of resistance to mass transfer

2.2.3.1.3 Interbubble collision

Due to turbulent conditions during CGA generation the bubbles will collide with each other frequently. When this occurs one of three things could possibly happen to the bubbles: they are not affected significantly, or they breakup into smaller pieces or they coalesce into bigger bubbles. Each of these processes appear to take place over a certain range of bubble diameter. Smaller CGA bubbles, between 25 to 50 μm in size, for instance show momentary bulging on contact and then drift apart. In this case the interfacial film resistance is strong enough to prevent coalescence. On the other hand, bubbles in the size range between 150 to 250 μm tend to undergo bubble fission while coalescence occurs primarily with bubbles greater than 350 μm in size.

2.2.3.2 CGA characterization

This section is also based on the study by Longe (1989). According to Longe (1989) stability is the most important characteristic when analyzing CGA performance. It is defined as the CGA bubble's ability to resist change in bubble size, liquid content or degree of dispersion. In other words, a stable CGA system is one where the bubbles maintain an average size and are uniformly distributed through the continuous liquid phase. This definition differs from the literature definition of foam stability which states that stability of foam is related to the intrinsic nature of the films to resist rupture (Longe, 1989).

CGA stability cannot be assessed according to the conventional definition of foam due to the gas bubbles being much smaller and liquid content being higher than for conventional foams. The difference between the properties of these two phases promote instability and as a result CGA systems cannot maintain their integrity without the help of some external hydrodynamic force (hence the addition of surfactants). In this sense, CGAs cannot be regarded a stable system (Longe, 1989).

The stability is influenced by the average size and the size distribution of the bubbles. Microscopic-assisted photographic techniques are the most common methods to determine the size distribution. With these methods the time is crucial because under static conditions the size and morphology of the bubbles change due to coalescence, creaming and diffusion problems. To minimize these problems an alternative technique of freezing and cutting through a plane cross-section to measure the size distribution of bubbles has been proposed by other authors. Another approach is to quickly observe the bubbles in the plane of contact between the foam and a flat glass wall, neglecting the slight degree of distortion of bubbles by the glass wall.

The photographic techniques are analyzed by a suitable image analysis program that provides statistical information on the number of bubbles, the maximum and minimum bubble diameter, average bubble size and the standard deviation from the mean. The data can be used to plot a histogram of the frequency for every size class of bubble diameter. To ensure the results are repeatable, at least three pictures need to be examined for each case.

The study by (Longe, 1989) found that for all types of surfactants (ionic and non-ionic) CGAs of excellent quality are produced at concentrations above 0.1 wt%. The non-ionic surfactant was found to have the smallest bubble sizes at this concentration. Another interesting observation was that as the surfactant concentration decreased the size of the smallest bubbles decreased while the maximum bubble size increased. This phenomenon can be explained by the Laplace equation. According to the equation as the size of bubble increase the internal pressure decreases. The pressure difference between the small and the big bubbles also increase which promotes interbubble diffusion particularly between very small and very big bubbles. The result is the widening of the gap between the two ends of the bubble size range as observed.

2.2.3.2.1 Effect of agitation on CGA stability

CGA stability is controlled by agitation. Without agitation the liquid and gas phases tend to separate due to difference in density. Continuous agitation is a critical factor to preserve the integrity of the CGA. As soon as agitation is stopped or if the hydrodynamic force acting on the CGA bubbles is less than the buoyancy force, the bubbles will rise to the top. Simultaneously, there is a hydrodynamic outflow of liquid from the bubbles which is referred to as creaming. The bubbles cream upwards as the liquid drains downwards. As CGA bubbles rise they expand. At the point where the gas to liquid ratio exceeds 0.74, the bubbles begin to arrange in polyhedral manner separated by thin liquid films, also known as lamellae. Liquid will continue to drain through the lamellae due to capillary pressure and plateau border suction. The liquid film will eventually become sufficiently small ($< 0.1\ \mu m$) in which case the van der Waals repulsive forces of the electrostatic double layer play an important role. In the end, the films ruptures and bubbles coalesce.

The rising velocity of non-interacting bubbles has been found to be significantly affected by the presence of surfactants. According to a study by Levich (1962) the adsorbed surfactant molecules are not uniformly distributed around the surface of an ascending bubble. The surface concentration of the downstream side of the bubble exceeds equilibrium value while the upstream side is less than

equilibrium. This surface concentration disequilibrium leads to the development of a surface tension gradient which causes tangential stress along the bubble interface and consequently lowers the surface tension where the adsorbate concentration is greater. The disequilibrium phenomenon results from the viscous drag of the medium acting on the interface.

Due to the surface tension gradient, interfacial liquid flows from the downstream side to the upstream side of the bubble. This flow opposes the force induced by the shear stress in the outer fluid of the interface which restrains the net flow of the interface. The result is an increase in bubble rigidity and a lowering in bubble rise velocity. If the surface tension gradient is sufficiently large, complete rigidity of the interface will be achieved. Under this condition the gas bubble will behave like a solid sphere of the same density and thus the terminal rise velocity can be described by Stokes law as given by the righthand- side of equation 9 for bubbles of radius r dispersed in a liquid of viscosity μ. Under steady state conditions the gravitational drainage force can be equated to the opposing hydrodynamic force which is why equation 9 is valid and can be rearranged to calculate the bubble rise velocity (U) as shown in equation 10 where $\Delta\rho$ is the density difference between the two phases and g is acceleration due to gravity.

$$\frac{4}{3}\pi r^3 \Delta\rho g = 6\pi\mu r U \qquad [9]$$

$$U = \frac{2gr^2\Delta\rho}{9\mu} \qquad [10]$$

Where for equation 9 and 10:

$r = radius\ of\ bubble$

$\mu = liquid\ viscosity$

$g = accelartion\ due\ to\ gravity$

$U = bubble\ rise\ velocity$

$\Delta\rho = \ density\ difference\ between\ the\ two\ phases$

Equation 10 is only valid for uniform, non-interacting non-deformable spheres. Given that CGA bubble diameters are not uniform a modification of this equation is necessary. In a system with n_i bubbles having an effective mass of $\frac{4}{3}\pi r_i^3 \Delta\rho$, the center of mass will have a velocity as given by equation 11 where V is the total volume of the dispersed phase. Substituting into equation 10 gives the final bubble rise velocity as shown by equation 12.

$$U = \frac{1}{V}\sum\frac{4}{3}\pi r_i^3 n_i U_i \qquad [11]$$

$$U = \frac{8\pi g\Delta\rho}{27\mu V}\sum n_i r_i^5 \qquad [12]$$

Where for equation 11 and 12:

$U = center\ of\ mass\ bubble\ rise\ velocity$

$V = total\ volume\ of\ dispersed\ phase$

$n_i = number\ of\ bubbles\ in\ class\ size\ i$

$r_i = radius\ of\ bubbles\ in\ class\ size\ i$

$U_i = bubble\ rise\ velocity\ of\ bubbles\ in\ class\ size\ i$

$\mu = liquid\ viscosity$

$g = accelartion\ due\ to\ gravity$

$\Delta\rho = density\ difference\ between\ the\ two\ phases$

The stability of a CGA system is often quantitively calculated by the measuring the time needed to drain half of the liquid phase of CGA in a column of given column height h, defined as the half-life τ. The half-life is derived from equation 12 and is written as shown in equation 13. From this equation it is evident that the half-life of CGA is inversely proportional to the fifth power of the bubble radius. Thus, smaller bubbles promote significantly more CGA systems.

$$\tau = \frac{h}{2}\ \frac{27\mu V}{8\pi g\Delta\rho}\ \frac{1}{\sum n_i r_i^5} \qquad [13]$$

Where:

$\tau = half - life\ of\ colloidal\ gas\ aphron\ system$

$h = height\ of\ flotation\ column$

$V = total\ volume\ of\ dispersed\ phase$

$n_i = number\ of\ bubbles\ in\ class\ size\ i$

$r_i = radius\ of\ bubbles\ in\ class\ size\ i$

$\mu = liquid\ viscosity$

$g = accelartion\ due\ to\ gravity$

$\Delta\rho = density\ difference\ between\ the\ two\ phases$

2.2.3.2.2 Effect of temperature on CGA stability

The stability of CGAs are also temperature dependent. Temperatures of below 40 $°C$ need to be maintained to ensure stability of the system. Above this temperature CGA instability increases rather sharply and above 65 $°C$ the system breaks down. This dependence is best examined from development of an equation of state, assuming that the gas phase obeys the ideal gas law as given in equation 14, where P_T is the total pressure acting on the bubble, V is the volume of the bubble, n the number of molecules per bubble and T the temperature.

$$P_T V = nRT \qquad [14]$$

Where:

$P_T = total\ pressure\ acting\ on\ bubble$

$V = volume\ of\ bubble$

$n = number\ of\ molecules\ per\ bubble$

$R = universal\ gas\ constant\ \left(8.314\frac{J}{mol \cdot K}\right)$

$T = temperature$

Equation 14 can be combined with the Laplace equation to give equation 15 which when simplified is given by equation 16 where P is the external pressure ($P_T = P + \Delta P$).The equation was first developed by Ross (1969) for foams. It has been proved to hold for single spheres and assemblages of spheres, whether uniform or non-uniform (Morrison and Ross, 1983). The equation suggests that, under the same hydrodynamic conditions, bubble size is dependent on temperature.

$$PV + \frac{2\sigma}{r}\left(\frac{4}{3}\pi r^3\right) = nRT \quad [15]$$

$$PV + \frac{2}{3}\sigma A = nRT \quad [16]$$

Where for equation 15 and 16:

$P = P_T - \Delta P = external\ pressure\ on\ bubble$

$r = radius\ of\ spherical\ bubble$

$A = surface\ area\ of\ a\ spherical\ bubble$

$V = volume\ of\ bubble$

$n = number\ of\ molecules\ per\ bubble$

$R = universal\ gas\ constant\ \left(8.314\frac{J}{mol \cdot K}\right)$

$T = temperature$

2.3 Properties of pulp produced from wood biomass

As mentioned in Section 2.1, sludge produced from pulp and paper mill effluent comprises of valuable fibre that can be used to produce a range of alternative products like biofuels, biopolymers, nanocellulose, fish feed and building materials. To functionalize recovered fibre from a mill's waste stream to one of these products it is important to first gain an understanding of the composition of the biomass as well as the chemical reactions occurring during the process that influence the physical and functional properties of these fibres.

2.3.1 Composition of lignocellulosic biomass

Wood is one of the major sources for lignocellulosic fibre and the raw material needed for pulp production. It consists of an orderly arrangement of cells surrounded by a cell wall made up of varying amounts of cellulose, hemicelluloses and lignin. Cellulose and hemicellulose combined are interchangeably referred to as polysaccharides or carbohydrates. The broad variety of woody plants is typically divided into two general categories based on their morphology and chemical composition,

namely hardwoods and softwood. The most common hardwoods used for papermaking include eucalyptus, maples, birch and oaks whereas softwoods include pine and spruce.

Of the three elements that make up the cell wall, only cellulose has a highly ordered (around 70 to 80%) crystalline structure (Arthur, 1989). Hemicellulose and lignin on the other hand are amorphous. The macromolecular structure is made up of cellulose chains, held together by hydrogen bonds, forming elemental fibrils with a diameter of about 3.5 nm (Schmitt, Koch and Lehnen, 2013). These elemental fibrils are further joined to form microfibrils which are about 10 times thicker. The microfibrils in turn form layers between which lignin and hemicellulose are present. Irregular hydrogen bonds exist between the hydroxyl groups of polysaccharides and lignin which creates a complex and irregular network of the three compounds. The hydroxyl groups present give fibres their negative charge which can influence the recovery process, especially in flotation with surfactants where the mechanism of flotation is influenced by the type of surfactant and the charge of particles to be recovered (Hiraoki *et al.*, 2015). This is discussed in more detail in Section 2.3.4.

2.3.1.1 Cellulose

A cellulose molecule is built up of unbranched long chains of repeating β-(1,4)-glycosidically bonded D-glucose units with chemical formula $(C_6H_{10}O_5)_n$ where n is the number of repeating sugar units referred to as the degree of polymerization (DP). In native cellulose the DP is between 7000 and 15000 depending on the isolation method (Österberg, 2000; Schmitt, Koch and Lehnen, 2013). However, during pulping and bleaching the chains are shortened due to hydrolysis, oxidation or mechanical wear and the DP value is degraded to between 300 and 2000. These units exist as pyranose rings in the thermodynamically preferred $^4C_1$ confirmation with equatorial hydroxide (OH) and hydroxymethyl (CH_2OH) groups (Schmitt, Koch and Lehnen, 2013).

The hierarchical structure of cellulose exists due to intrachain hydroxyl bonding. These bonds are the reason for cellulose chains being so stiff and highly orientated. The microfibrils as explained in Section 2.3.1 consist of cellulose chains parallel to one another. These chains are stabilized by frequent hydrogen bonding which subsequently interacts by hydrophobic interaction and van der Waals forces to form the highly ordered crystalline domains mentioned in Section 2.3.1.The amorphous region of cellulose (i.e., 20 to 30%) form fibrils which tend to agglomerate either by hydrogen bonding or by grouping from diverged molecules. (Schmitt, Koch and Lehnen, 2013)

The repeating unit of a cellulose chain is known as a cellobiose unit. Two adjacent units are known as an anhydro-glucopyranose unit (AGU). Each unit is linked to another by elimination of a water molecule between the hydroxylic groups at carbon 1 (C1) of the first unit and carbon 4 (C4) of the second unit. Even though hydroxyl (OH) groups are situated at both ends of a cellulose chain, these groups behave differently. The C1-OH is an aldehyde hydrate group whereas the C4-OH is an alcoholic hydroxyl. Thus, the C1-OH has reducing properties whereas the C4-OH displays non-reducing properties. This is shown in **Figure 7**. (Fengel and Wegener, 1989)

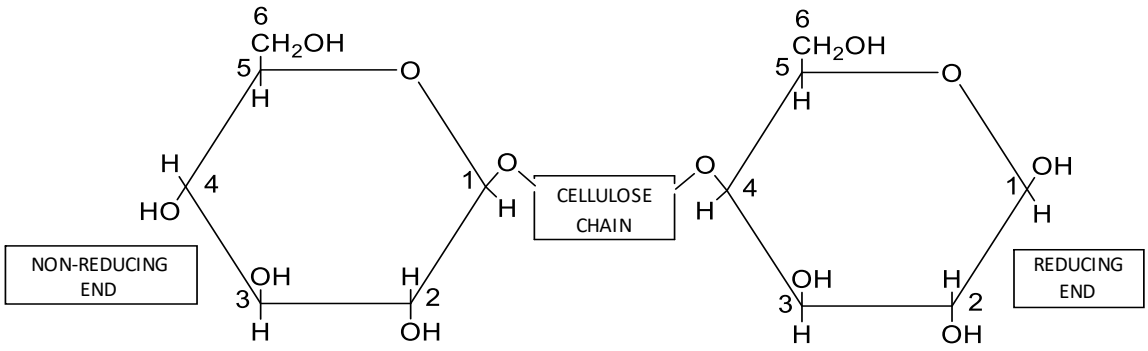

Figure 7: Reducing and non-reducing end group of a cellulose molecule. (Fengel and Wegener, 1989)

Cellulose is not only accompanied by hemicellulose and lignin but is intimately associated with them. Intensive chemical treatment is needed to separate and isolate cellulose. The isolated cellulose remains relatively pure and is known as alpha (α) cellulose (DP > 19). The chemical pulping process produces pulp that is high in alpha (α) cellulose. To acquire 100% pure cellulose from wood, alpha cellulose must undergo further intensive treatment by processes such as dissolution or partial hydrolysis. The resultant product of these treatments is very short molecular chains. This class of cellulose is known as beta (β) cellulose (DP 15 – 90). (Fengel and Wegener, 1989; Paquet, Chang and Rutkowski, 2016)

The rest of the polysaccharides, i.e., hemicelluloses, are divided into a class named gamma (γ) cellulose (DP <19). In Kraft pulping alpha cellulose is separated from these hemicelluloses during the cooking stage with sodium hydroxide and subsequently removed in black liquor along with lignin. Kraft pulp thus contains low concentration of gamma (α) cellulose. The portion of cellulose which is soluble in alkaline medium but can be precipitated from a neutral solution is known as beta (β) cellulose. The portion which remains soluble even in a neutral solution is known as gamma (γ) cellulose. (Fengel and Wegener, 1989; Paquet, Chang and Rutkowski, 2016)

When producing nanocellulose, specifically NFC, the aim is not to intentionally decrease the DP of cellulose as it has been found that higher DP values lead to increasing mechanical strength of nanocellulose films (Fang *et al.*, 2020). Mechanical and chemical pre-treatment will however result in a decrease of DP to some extent. A study by Qing *et al.*, (2013) found that mechanically fibrillating pulp fibres with an original DP of 1000 decreases the DP to 664 when refining the fibres with a SuperMassColloider (MasukoSangyo Co. Ltd, Saitama, Japan) and microfluidizer (Microfluidics, Newton, MA). The study also determined that NFC when pre-treated enzymatically or by TEMPO oxidation followed by mechanical treatment decreased DP values to 287 and 580 respectively. Another term often used in pulp and bleaching is holocellulose. The term was first used by Ritter and Kurth (1933) for the product obtained after the removal of lignin from wood. There are three important criteria for using this term, namely that the product (1) has a low residual lignin content, (2) there is a minimal loss of polysaccharides (i.e., cellulose and hemicellulose) and (3) minimal oxidative and hydrolytic degradation of cellulose.

2.3.1.2 Hemicellulose

Hemicelluloses are closely linked with cellulose in the cell wall where their most important biological function is their interaction with cellulose and lignin to strengthen the cell wall. These molecules have a rather low DP (between 50 and 200) and are mostly branched molecules aside from their linear backbone that is composed of β-(1,4)-linked D-glucose, D-xylose, or D-mannose units (Ekland, 1991). The short side branches of these molecules comprise mainly of xylose, glucose, arabinose or glucuronic acid monomer sugars. The exact composition varies depending on the source, but in most cases hemicelluloses contain between two to six of these sugars. Hemicelluloses often contain some carboxylic groups that introduce some charge to the fibre (Ekland, 1991).

These molecules are characterized based on the main sugar residues in the backbone (Faryar, 2019). Examples include xylan (xylose backbone), mannans (mannose backbone), xyloglucans (glucose backbone with xylose decoration), and β-glucans with mixed linkages (homopolymer of glucose). In hardwood xylan (glucoronoxylan) is the dominant sugar whereas in softwood mannan (glucomannan) is more dominant. Pulp strength is not only related to the amount of cellulose but also the ratio between the amounts of cellulose and hemicellulose presents (Ek, Gellerstedt and Henriksson, 2009). A higher ratio is favourable. It is known that hemicellulose makes beating and refining easier (Page, 1989). It is therefore apparent why it is important to retain as much hemicellulose throughout delignification and bleaching processes.

2.3.1.3 Lignin

Lignin interpenetrates the polysaccharide fibrils (cellulose and hemicellulose), so strengthening the cell wall. It is a complex aromatic polymer that functions as both a matrix between the fibres in microfibrils (Section 2.3.1) and as a component which gives resistance towards decay and attack by microorganisms (Österberg, 2000). The aromatic system is composed of phenylpropane units (C_9) which are bonded by four kinds of carbon-carbon bonds and three types of ether linkages (Schmitt, Koch and Lehnen, 2013). Unlike polysaccharides, lignin does not have a well-defined repeating unit, instead, it has an irregular, crosslinked polymer network formed by random recombination of phenoxy radicals (Schmitt, Koch and Lehnen, 2013). These radicals consist of three main monomers namely coniferyl alcohol, p-hydroxy-cinnamic alcohol and sinapyl alcohol (Ekland, 1991). Native lignin does not contain carboxyl groups, but carboxylic acid groups are formed during alkaline pulping (Österberg, 2000).

The formation of lignin macromolecules from monomeric units can generally be described as a dehydrogenative polymerization (Fengel and Wegener, 1989). The first step of the pathway is enzymatic dehydrogenation of the p-hydroxy-cinnamic alcohols which yields mesomeric ring systems with a loosened proton. From this point five formations of resonance-stabilized phenoxy radicals are possible, although only four are involved in biosynthesis as the fifth is thermodynamically disfavoured. These five structures are shown in **Figure 8**. It is important to understand how lignin monomers form polymers to better understand the chemistry of these molecules during the cooking and bleaching stages in Kraft pulping (Section 2.3.4.2).

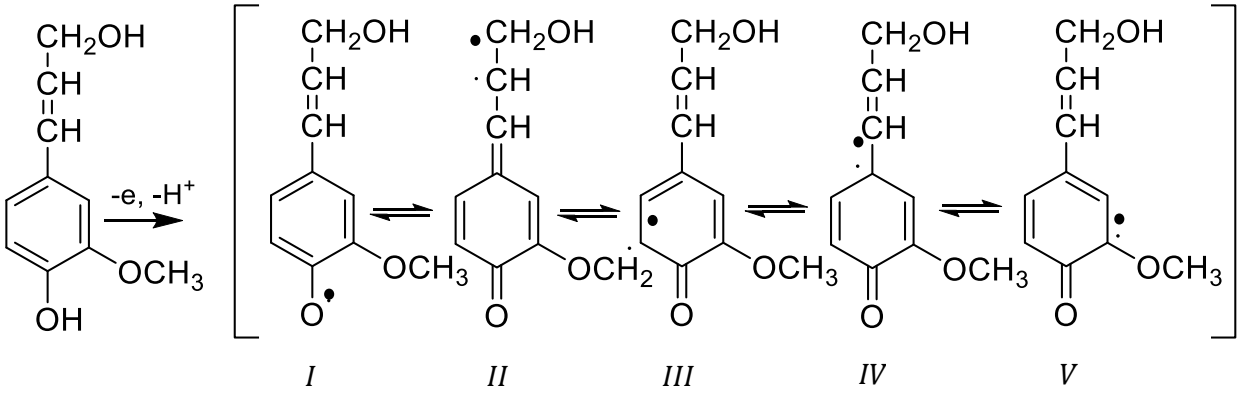

Figure 8: Enzymatic dehydrogenation of coniferyl alcohol yielding phenoxy radicals. (Fengel and Wegener, 1989)

The four thermodynamically favoured phenoxy radicals in **Figure 8** are randomly coupled leading to various linkages as summarized in **Table 3**. Not all of these coupling modes are stable or thermodynamically favourable and it has been found (by quantum mechanical calculations) that phenoxy radicals have the highest π-electron density when placed at the phenolic oxygen atom which leads to the formation of aryl ether linkages. The β-O-4 linkage is the most recurrent type of bond found in both hardwood and softwood lignans. Other possible bonds include β-β, β-5 and 4-O-5. A summary of all possible bonds is given in. (Fengel and Wegener, 1989)

Table 3: Coupling modes of phenoxy radicals from p-hydroxycinnamyl alcohols. (Glasser, 1980)

	I	*II*	*III*	*IV*
I	Unstable peroxide	β-O-4	4-O-5	1-O-4*
II	β-O-4	β-β	β-5	β-1*
III	4-O-5	β-5	5-5	1-5*
IV	1-O-4*	β-1*	1-5*	1-1*

* Other options possible

2.3.1.4 Ionisable groups and fibre charge

The ionisable groups found in Kraft pulp are carboxylic acid ($R-COOH$) and phenolic hydroxyl ($R-OH$) groups. Carboxylic groups are related to polysaccharides and phenolic groups to lignin. The repelling forces between these negatively charged groups create a swelling effect of the fibril network. Each acidic group has a unique pK_a value and not all groups are ionized during pulp production, especially the hydroxyl groups. A rather high pH is required to ionize phenolic hydroxyl groups in

lignin (Sjostrom, 1981). There is a direct correlation between swelling and paper strength, higher degrees of swelling result in stronger paper (Ek, Gellerstedt and Henriksson, 2009).

The charge that fibres carry can be quantified by determining the total charge or the surface charge. The surface charge is important for interaction with other fibres, although it is a smaller portion (7 to 10%) of the total charge (Ek, Gellerstedt and Henriksson, 2009). Total charge can be determined by conductometric titration with sodium hydroxide ($NaOH$) and sodium hydrocarbonate ($NaHCO_3$). Surface charge can be determined by polyelectrolyte titration or Electron Spectroscopy for Chemical Analysis (ECSA) measurements. A study by Horvath, Lindström and Laine (2006) found good agreement between the two techniques.

The amount of charge that these ionisable groups carry is a complex function of the chemical composition of fibres, state of ionization of the acid groups and the nature as well as amount of additional substances present. Charge depends on the pulping and bleaching method used, the pH and concentration of electrolytes in surrounding medium. Never-dried pulp has a surface charge-density of more than 100 $\frac{m^2}{g}$. The tensile strength of paper increases with increase in surface charge density. Charge density of fibres is a major factor in the formulation of hydrogen bonding between fibres. (Antes and Joutsimo, 2015)

During the bleaching stages of chemical pulp, bleaching agents are responsible for oxidising polysaccharide chains and forming aldehydic groups cleavage. Depending on the bleaching conditions these aldehydic groups (at the C1 position of cellulose molecules) either undergo a peeling reaction which is described later in Section 2.3.4.1.1 or forms a stable carboxylic acid. However, even though carboxylic acid groups are created, the overall amount of acidic groups decreases due to dissolution of hemicelluloses and lignin. (Horvath, 2003)

2.3.2 Pulping technologies

There are two main types of pulping processes and two intermediate methods to produce pulp from virgin fibre. The main types are mechanical and chemical production. Intermediate methods are used to lower the cost of fibre production and to improve the properties of the final product (Riley, 2012). Methods to produce intermediate pulp qualities include thermomechanical pulping (TMP) and chemical thermo-mechanical pulping (CTMP). The performance (yield) and quality (% lignin removed) of the different pulping processes are shown in **Table 4**. Chemical pulping removes between 80 to 90% of lignin with a yield of 45 to 65%. Further bleaching of these pulps removes essentially all lignin but at the expense of further yield loss with the highest yield obtained usually being around 55%. The difference between the maximum yields is 10%. Bleaching thus does not contribute as significantly to the yield as cooking with chemicals does. This confirms that the main cause of yield loss in chemical pulping is due to alkaline hydrolysis as stated previously in Section 1.1.

Table 4: Pulp production processes. (Riley, 2012)

Pulp preparation	Lignin removed (%)	Yield (%)	Process
Mechanical	0	95+	Grinding
Chemical	80-90	45-65	Cooking with chemicals
Chemical + Bleaching	100	45-55	Plus bleaching agents
TMP	0	95+	Steam heating + grinding
CTMP	10-80	65-85	Cooking with chemicals + grinding

Recycled fibre is prepared in an isolated process first using what is known as a hyrapulper before being treated further by mechanical, chemical or intermediate processes. This process is also used to combine different sources of pulp, as not all mills produce their own pulp. This is the case for many small and to an extent some large mills. These mills buy pulp and disperse it into water using a hyrapulper. A hyrapulper consists of a large vessel with an agitating blade. Large sheets of paper are dropped into the water and dispersed to concentration of between 0.3 and 3.0% depending on what the intended product is. Lower concentrations are normally used for paper and high concentrations for paperboard. (Riley, 2012)

2.3.2.1 Mechanical pulp production

Mechanically produced pulp is used for low grade paper such as newsprint and as a liner between chemical pulps to produce folding boxboard. This method of production is the fastest and least costly method of obtaining virgin fibres (Riley, 2012). Another main advantage of this method is its high pulp yield which is 95% or more as stated in **Table 4**. Mechanical pulp is sometimes blended with chemical and CTMP produced pulps to cut costs (Riley, 2012).

The fibres are mechanically separated by a grinding process. Before grinding, the wood chips need to be washed to ensure contaminants like soil and stone are removed. Traditionally, logs were grinded directly by using grindstones like those commonly used for grinding flour. Today, ridged metal discs known as refiner plates are used to refine wood chips. This method of refining effectively separates fibres individually but at the cost of breaking them into shorter lengths. Another disadvantage of the process is that it does not remove chromophores associated with lignin or other impurities which results in discolouration of fibres with age and a product with inferior quality compared to chemical pulps, hence its use for low grade paper products. (Riley, 2012)

2.3.2.2 Chemical pulp production

Chemical production is the most costly method for production of fibres for paper and paperboard manufacture (Bajpai, 2018). In Europe, chemically produced pulp can amount to almost twice the cost of mechanically produced pulp (Riley, 2012). This is due to a much lower yield compared to mechanical

pulping (45 to 55% according to **Table 4**) as well as the cost of energy and chemicals that the process requires. Chemical pulping is consequently only used for products which require maximum toughness, whiteness, and purity. Examples include the products like the outside layer of linerboard, packaging for high-value products like cosmetics and liquid packaging cartons for products like milk (Riley, 2012).

In this method, wood chips are placed in a pressure vessel called a digester. During digestion or 'cooking' fibrous material is subjected to heat and chemicals which result in separation of cellulosic fibres from lignin and other impurities. There are three chemical pulping technologies namely the Kraft (or sulphate), soda, and sulphite process. The Kraft and soda process takes place in alkaline medium whereas the sulphite process has a neutral or acidic pH. The end products are referred to as paper grade pulp, bagasse pulp ad dissolving pulp respectively. After chemical treatment by one of these methods, a process known as bleaching is an optional stage. The process is carried out if white fibres are required. Bleaching removes more of the residual lignin left after the digestion process but at the expense of a lower yield.

Sodium hydroxide ($NaOH$) is the primary cooking chemical in the Kraft and soda process. Sodium sulphide (Na_2S) is used as an additional active pulping component in the Kraft process. Both processes receive their names from the regeneration chemicals used to replenish the $NaOH$ concentration (i.e., sodium sulphate and sodium carbonate). The Kraft process is the dominant alkaline pulping process in industry because of the higher yields achieved and superior properties of the pulp product (Fengel and Wegener, 1989).

The sulphite method uses metal or ammonium salts of sulphurous acids in the digestion process. The chemicals used in the sulphite process result in the formation of sulphites or bisulphates which ingest impurities but in doing so also hydrolyse some of the cellulose (due to their acidic nature). This results in the final paper product having inferior strength properties compared to paper products produced by the Kraft process. At present less than 20% of all chemical pulps are produced by the sulphite pulping method (Riley, 2012).

2.3.2.3 Intermediate pulp production

As mentioned in Section 2.3.2, TMP and CTMP are used to lower the cost of fibre production and to improve the properties of the final product. The TMP method uses hot water to soften the fibres and make them more supple (Riley, 2012). This results in less damage during the mechanical process and accordingly superior strength properties are obtained compared to the standard mechanical pulping process. The CTMP, also known as a semi-chemical process, uses a combination of both mechanical and chemical methods to obtain virgin fibres. Wood chips are mechanically grinded for some time and then partially digested by either the sulphite or Kraft process. The method uses far less chemicals than a purely chemical process. This significantly reduces the time taken for digestion and therefore reduces total costs.

2.3.3 Overview of the Kraft process

The focus of this study is the Kraft process which usually follows a relatively uniform process scheme though numerous variations are possible specifically regarding the cooking conditions and unique equipment. The basics of pulping can be described simply as shown in equation 17. A simplified process flow diagram of the Kraft process is presented in **Figure 9**

Figure 9. As mentioned in Section 1.1, the recovery of black liquor to regenerate white liquor is not part of the scope of this project and is thus not discussed in any subsection of this document. The cooking process, i.e. delignification, is discussed in Section 2.3.3.1 followed by common bleaching sequences employed in Kraft pulping in Sections 2.3.3.2 and 2.3.3.3. The final subsection (2.3.3.4) discusses one of the most important measured variables of the process: the Kappa number. This number describes the extent of delignification and is the hallmark of the quality of pulp and paper (Amazouz, Platon and Champagne, 2005).

$$Chemicals + Raw\ Fibre \rightarrow Pulp + Lignin\ Waste\ (black\ liquor) \qquad [17]$$

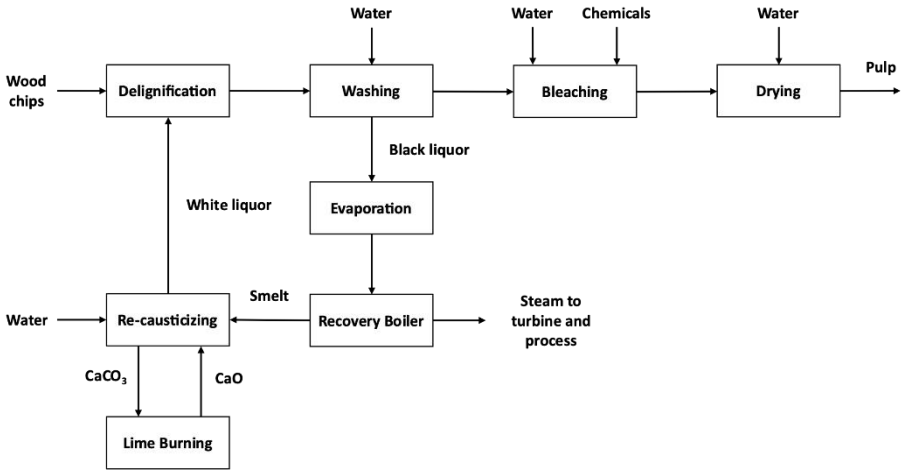

Figure 9: A simplified diagram of the Kraft pulping process. (Bonhivers and Stuart, 2013)

2.3.3.1 Delignification

In any process, the core of the pulping system is the digester. As shown in **Figure 9**, wood in the form of chips is charged to the digester with fresh cooking liquor, referred to as white liquor, from the chemical recovery plant which consist of an evaporation, recovery boiler and re-causticizing sections. The process can run continuously or batch-wise. Continuous technologies have lower energy requirements and better emission control whereas batch technologies offer higher flexibility and lower maintenance costs (Fengel and Wegener, 1989). A continuous process pretreats wood chips with steam in a pre-steaming vessel before being charged to the digester. This is done to remove entrapped air between chips. Typically, digester systems have a three-phase, vertical downflow configuration. The first phase is impregnation where the chips are impregnated with liquor as the chip-

liquor mixture moves downwards, usually in a separate column. In the second phase the hot, liquor-filled chips are pumped to the top of the continuous digester where chips are gradually cooked (turned to pulp) as they move down the column. The cooking temperature is reached by direct steaming or indirectly by heat exchange where liquor circulation between the impregnation column and digester brings the chips to cooking temperature. Conventional cooking time is usually between 4 to 6 hours with a cooking temperature between 160 to 180 °C and a pressure of 7 to 11 bar (Fengel and Wegener, 1989). The lower part of the digester is used for washing, the final phase of digestion.

In traditional cooking methods wood chips and white liquor are charged into a digester simultaneously which results in a very high alkali concentration at the start of the process and a low concentration toward the end. This configuration may cause carbohydrate degradation leading to inefficient delignification rates (Antes and Joutsimo, 2015). Modified cooking conditions have since been developed by the Royal Institute of Technology (KTH) and the Swedish Pulp and Paper Research Institute (STFI) (Carnö and Hartler, 1976; Norden and Teder, 1979; Teder and Olm, 1981; Johansson *et al.*, 1984). New conditions include (1) ensuring alkali concentrations are stabilized, (2) ensuring the initial bulk phase contains a high concentration of hydrogen sulfide ions, (3) lowering the concentration of dissolved lignin and sodium ions toward the end the process and (4) decreasing cooking temperatures. These modifications have led to several new pulping technologies, including the Lo-Solids™ and CompactCooking™ technologies which are presently the two main Kraft pulping methods used for continuous cooking in industry (Antes and Joutsimo, 2015).

The washed raw pulp, called brownstock, leaves the bottom of the digester and is pumped to the top of pressure diffusers which can be considered extensions of the digester wash zone. These diffusion-type washers are fully enclosed and operate under pressure, pushing the pulp through the column without the use of pumps. This type of washing is preferred to atmospheric diffusers, mainly because of higher efficiency and higher blow temperatures are not a problem. Also, since the equipment is completely enclosed, there are no gas emissions or pulp spills. These vertical diffusers also require very small spaces for installation.

Most of the spent liquor from extended delignification, called black liquor, is discharged into a blow tank. The pressure is reduced as black liquor enters a blow tank which has a volume several times more than the volume produced during cooking. Black liquor is a mixture of dissolved organic and inorganic material obtained from the pulp cooking process. Some black liquor is further removed by the pressure diffusers. Recovering the black liquor is an important aspect of Kraft pulping from an economic and environmental perspective. The chemicals used in the process are expensive compared to those used in other pulping process like the sulphite process. It is thus imperative that a very high percentage of cooking chemical be recovered. The liquor is further processed within the recovery line, which is not discussed here as it falls outside the scope of this study.

The brownstock product is pumped through a de-knotting plant which removes large impurities and then through pressure screens which removes bundles of undercooked fibres and other large particles. The screens are usually the first of a few stages to screen and clean the pulp. The pulp is

often washed in a wash filter called a Brown Stock Decker. Brownstock washing is a complex and dynamic process that separates weak black liquor from pulp fibres. Material balancing techniques are a crucial part of the operation and is used to identify how well the system is operating. The cleaned pulp is then stored in holding towers for further processing.

2.3.3.2 Bleaching sequences

The purpose of bleaching is to remove residual lignin products that are present after cooking to obtain either fully-bleached or semi-bleached pulps with brightness levels above 90% or 60 to 70% respectively (Fengel and Wegener, 1989). Industrial scale processes use multi-stage bleaching sequences tailored to the specific pulp type. The bleaching chemicals used can be classified into oxidizing and reducing agents and the most common agents used in industry as well as those less commonly applied are listed in **Table 5**. For environmental purposes, chemicals can also be classified into chlorine-containing and chlorine-free chemicals.

Table 5: Oxidizing and reducing agents used in bleaching of chemical pulp. (Fengel and Wegener, 1989)

	Oxidizing agents		**Reducing agents**	
Industrially important	Chlorine	Cl_2	Sodium dithionite	$Na_2S_2O_4$
	Sodium hypochlorite	$NaOCl$	Zine dithionite	ZnS_2O_4
	Calcium hypochlorite	$Ca(OCl)_2$	Sodium bisulphite	$NaHSO_3$
	Chlorine dioxide	ClO_2		
	Hydrogen peroxide	H_2O_2		
	Sodium peroxide	Na_2O_2		
	Oxygen	O_2		
Less important or not commercially applied	Ozone	O_3	Sulphur dioxide	SO_2
	Sodium chlorite	$NaClO_2$	Sodium borohydride	$NaBH_4$
	Peracetic acid	CH_3CO_3H	Calcium dithionite	CaS_2O_4
	Chlorine monoxide	Cl_2O	Aluminium dithionite	$Al_2(S_2O_4)_3$
	Thioglycolic acid	$CH_2SHCOOH$		
	Hydrogen	H_2		
	Potassium permanganate	$KMnO_4$		

Numerous bleaching stages and sequences exist, a nomenclature list along with some common sequences in the Kraft process is given in **Table B1** and **Table B2** in Appendix B. Essential to all bleaching procedures is the mixing of the pulp with white liquor followed by one or more intensive washing stages afterwards to remove the solubilized reaction products. Modern bleaching processes consist of continuous bleaching processes with bleaching towers in which the pulp-liquid mixture moves uniformly.

As can be seen in **Table B2** in Appendix B, chlorination (C-stage) is the first bleaching stage for most processes. The process is sometimes referred to as a pre-bleaching step. Chlorine is used to convert residual lignin to water- and alkali-soluble degradation products which is why the subsequent

bleaching step is normally an alkaline extraction step with sodium hydroxide (E-stage) to remove these components. Technically this is not a bleaching stage as the main objective is the removal of lignin degradation products and neutralization of the acidic components formed during the chlorination stage. Chlorination is normally carried out at low temperatures of between 20 to 40 $°C$ for 30 to 60 min at a low consistency of between 3% and 4% (Fengel and Wegener, 1989).

Chlorine-containing chemicals cause many environmental problems and earnest efforts have been made to replace these chemicals or at least reduce the amounts used during the bleaching stage. Such attempts include replacing part of chlorine with chlorine dioxide which leads to more oxidated lignin products rather than highly toxic chlorinated fragments (D, C_D, D/C and C + D stages). Another solution is replacing chlorine entirely with peroxide or oxygen bleaching (P, P/E and O stages). This is the best solution as it generates an effluent with far fewer problems regarding environmental protection.

The alkaline extraction stage with sodium hydroxide can be replaced by an alkaline peroxide stage (P or P/E stages) which is advantageous because it combines bleaching and extraction in a single stage resulting in a brightness increase without needing an additional stage and reduces the amount of chlorine bleaching chemicals needed. The main drawback of using peroxide is the high price of the chemical. Extraction with peroxide is usually carried out at a temperature of between 60 to 80 $°C$ for 2 to 4 hours at a medium to high consistency whereas extraction with sodium hydroxide (E-stage) is usually carried out at temperature of between 50 to 60 $°C$ for 30 to 60 min at a medium consistency level of 10% to 18% (Fengel and Wegener, 1989).

2.3.3.3 Oxygen delignification and Ozone

It is standard practice in mill scale beaching these days to remove around half of residual lignin in unbleached pulps by oxygen bleaching (also referred to as oxygen delignification or O-stage) prior to conventional bleaching sequences. Examples, as can be seen in Appendix B, include O – D – E – D and O – C – E – D – E – D. This is one of the most comprehensively investigated processes in the field of pulping and bleaching since 2003 (Hostachy *et al.*, 2012).

Delignification alone cannot be used to bleach pulps to high brightness because oxygen is not a selective lignin-degrading chemical, which is why only about half of the residual lignin is removed by this stage (i.e., to prevent excessive attack on polysaccharides). Main advantages of delignification include oxygen being a cheap oxidizing agent and the practicality that effluents from this step can be processed within a normal Kraft recovery system. The process is in principle a gas-phase reaction performed at pressures between 4 and 8 bar in an alkaline medium, at temperatures of between 90 to 140 $°C$ and usually high consistencies of 20% to 30% (Fengel and Wegener, 1989).

After oxygen delignification, ozone bleaching (Z-stage) has emerged as the latest technology in the field of pulping and bleaching. Ozone is a very effective bleaching agent and is a promising alternative to chlorine dioxide which is reaching its ecological terminus. The first industrial-scale production of ozone pulp was reported 30 years ago, but since then it has taken some time to develop the method and to gain a better understanding of the mechanisms in ozone chemistry. The choice of using ozone

is motivated by ecological constraints as well as economical savings resulting largely from chemical cost. Improvements in modern ozone generators efficiency have improved the energy requirement to produce ozone to a mere 7 to 8 kWh per kg of ozone, making 1 kg of ozone cheaper than 1 kg of chlorine dioxide. (Hostachy *et al.*, 2012; Perrin *et al.*, 2014)

2.3.3.4 The Kappa number

Lignin content is a vital measurement in delignification and bleaching processes to measure as it determines the conditions to be used. This can be determined by direct or indirect methods. The most common direct method is called the *Klason lignin method*, although it is a very time-consuming method and indirect methods are preferred. By far the most common and well-known indirect method is the *Kappa number* determination. To determine the Kappa number of a pulp sample a specific amount of potassium permanganate ($KMnO_4$) and sulphuric acid (H_2SO_4) is added whereupon lignin swiftly reacts with the $KMnO_4$ as manganese is added. The reaction is time is 15 min, after which potassium iodide is added to terminate the reaction. The amount of lignin that reacted is then calculated by back-titration of the free iodine with sodium thiosulphate. (Ek, Gellerstedt and Henriksson, 2009)

When using the *Kappa number*, it needs to be taken into consideration that polysaccharides, or more specifically degradation products from xylan (hexenuronic acids) contribute to the consumption of permanganate. Hexenuronic acids (HexA) have double bonds that consume permanganate which contributes to the Kappa number calculated. Another method to determine lignin content indirectly is reacting samples with chlorine. The lignin content is referred to as the *chlorine* or *Roe number*. The procedure is like the *Kappa number* test where the amount of chlorine that reacted is determined by iodometric titration. Given that chlorine is very hazardous to the environment however, this method is not very common in industry. (Ek, Gellerstedt and Henriksson, 2009)

The Kappa and chlorine numbers can easily be related to the Klason lignin content in pulp. Dependence for both is a straight-line relationship. For the Kappa number, the relationship depends on the wood species and delignification method. According to TAPPI standards the lignin content is determined by multiplying the Kappa number with 0.13. The chlorine number is related in a similar way, multiplying the number with 0.9 gives the percentage of lignin in pulp (Kyrklund and Strandell, 1969). These values give the maker of the pulp as well as the user of the pulp valuable information about the properties of the pulp, particularly regarding the concentration of residual lignin present.

2.3.4 Chemistry of Polysaccharides and Lignin

The following section as well as **Section 2.3.5** is based on literature studies from *Wood: chemistry, ultrastructure, reactions* by Fengel (1989) and *Pulp and Paper Chemistry and Technology – Pulping Chemistry and Technology Volume 2* by Ek, Gellerstedt and Henriksson (2009).

2.3.4.1 Polysaccharide reactions

While intensive chemical treatment is necessary to isolate cellulose, this leads to a large yield loss of polysaccharides no matter the conditions around the process. The vast majority of this yield loss occurs during the early stages of cooking. The predominant reaction, referred to as the peeling reaction, starts instantly when wood chips mix with the pulping white liquor and proceeds quickly even at lower temperatures around 100 °C. At higher temperatures of around 170 °C or more, a random reaction of alkaline hydrolysis (Section 2.3.4.1.2) may also occur to some extent.

2.3.4.1.1 The peeling reaction

The peeling reaction is the mechanism resulting in successive depolymerization of polysaccharides starting from the reducing end group. The reaction is particularly important for cellulose, xylan and glucomannan which contain a substituent in the C4 position. When a polysaccharide chain has been cleaved the shortened chain cannot be repaired. In aqueous environments the reduced end group of a polysaccharides will form an equilibrium between its hemiacetal and open aldehyde form. In an alkali environment a further equilibrium is established between the aldehyde and keto form. A β-elimination reaction can occur from either of these forms. When the keto form undergoes a β-elimination reaction, the C4-substituent of the molecule is cleaved resulting in a shortened polysaccharide chain. The cleaved molecule liberates a new reducing end group that can either go through the same reaction sequence again or react further via a benzilic acid rearrangement to form an isosaccharinic acid which is a stable product. The mechanism for the reaction is shown in **Figure 10**. When the aldehyde form undergoes a β-elimination reaction the result is a stabilized polysaccharide chain.

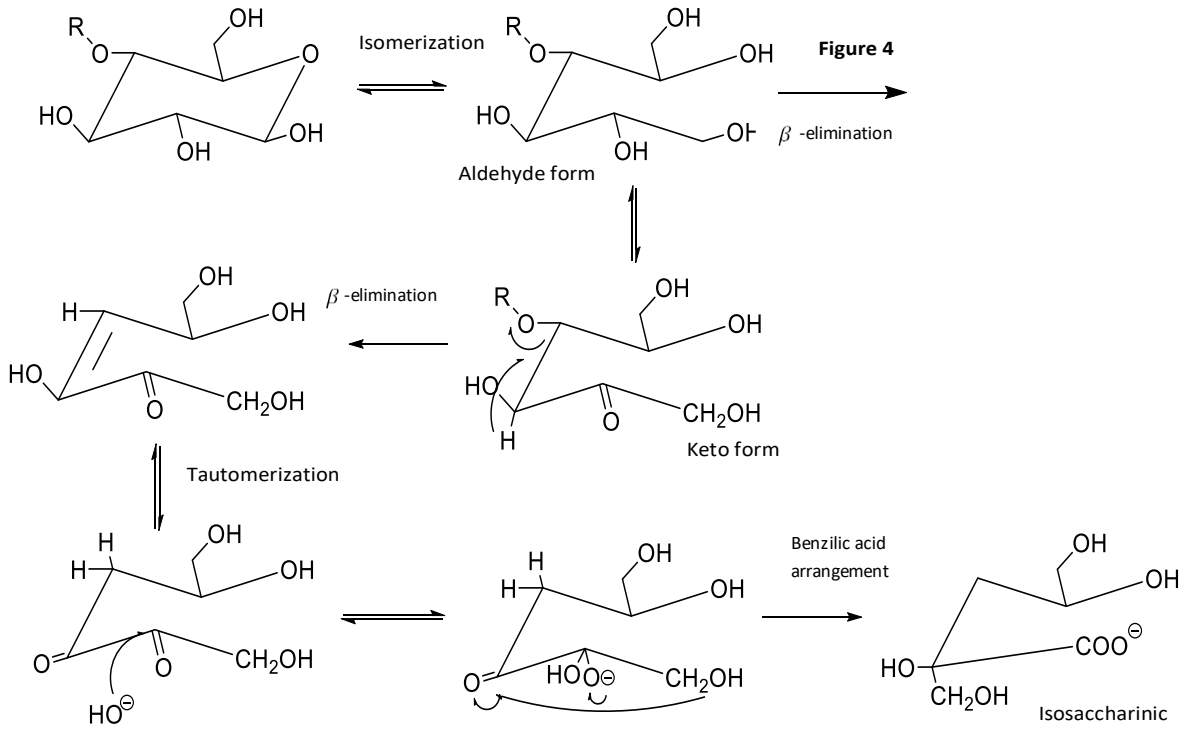

Figure 10: Peeling mechanism of polysaccharides in Kraft pulping. (Ek, Gellerstedt and Henriksson, 2009)

The peeling reaction is a bit different for glucomannan, cellulose and xylan respectively. For glucomannan, which has quite a low DP of around 100 in its native state, the reaction is very efficient irrespective of the alkali charge. This subsequently leads to total degradation and dissolution of glucomannan. For cellulose, which has a much higher DP, the reaction does not lead to a significant degree of dissolution. For xylan the peeling reaction is not efficient due to some of its substituents like 4-O-methylglucuronic acid found in hardwoods. The substituent favors a direct β-elimnation reaction from the open aldehyde form to formation of a metasaccharinic acid, a stable form that prevents further peeling. The mechanism is illustrated in **Figure 11**. This stabilization reaction occurs to some extent for cellulose and is referred to as the "stopping-mechanism". On average a peeling reaction will result in the loss of between 50 to 100 sugar units before the stopping reaction takes place.

Figure 10

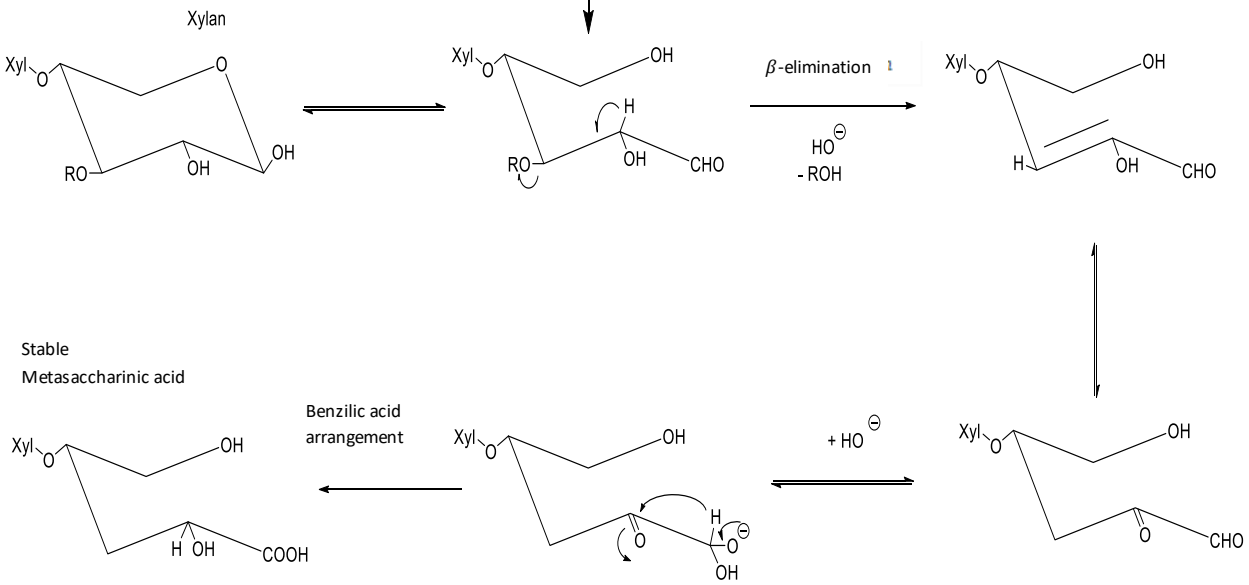

Figure 11: The beta-elimination in polysaccharide end groups known as the stopping mechanism. RO = arabinose unit. (Ek, Gellerstedt and Henriksson, 2009)

Yield loss is clearly a serious drawback and many attempts have been made to find ways to increase yield by minimizing the peeling reaction. This can be accomplished, in theory, by either reductive or oxidative reactions that stabilize the reducing end-groups in polysaccharides. Reducing agents like sodium borohydride have been found to efficiently stabilize polysaccharide peeling reactions by formation of an alditol end-group. However, due to cost the process has never been industrialized. A more successful approach implemented by some mills in the world is catalytic partial oxidation of the hydrosulfide ions present in white liquor to polysulfide which results in the formation of aldonic acid groups. Allegedly, the enediol form of the reducing end-group, which is in equilibrium with the open aldehyde form, is oxidized to a diketo structure and then transformed through a benzilic acid rearrangement to the aldonic acid (Ek, Gellerstedt and Henriksson, 2009).

2.3.4.1.2 Alkaline hydrolysis

At higher temperatures of around 170 °C or more, further loss of cellulose may take place due to alkaline hydrolysis, also known as secondary peeling. The reaction is initiated by the C2-OH group which, if ionized, can attack the C1 carbon atom thereby expelling the attached AGU. This essentially splits the polysaccharide chain forming new reducing end-groups which are also subjected to the end-wise degradation by secondary peeling. The reaction occurs only in the amorphous part of the cellulose microfibrils and results in a total loss of cellulose of around 10%. (Ek, Gellerstedt and Henriksson, 2009)

2.3.4.1.3 Hexenuronic acid

Hexenuronic acid (HexA) can form under the alkaline conditions of Kraft cooking as stipulated in Section 2.3.3.1 when the methoxyl group (4-O-methylglucoronic acid) on xylan is eliminated as methanol. Since HexA is stable in alkaline mediums, the xylan that remains in pulp after cooking will contain a considerable amount of such groups. HexA influences pulp properties and contributes to the bleachability of pulp. Hardwood pulps will contain a significant amount of HexA which need to be taken into consideration when determining the Kappa number. These HexA groups have detrimental effects on pulp qualities such as brightness stability. (Ek, Gellerstedt and Henriksson, 2009)

2.3.4.2 Lignin reactions

2.3.4.2.1 Cleavage of β-O-4 structures

During Kraft cooking each β-O-4 structure that is cleaved will result in a new aromatic end group with a free phenolic hydroxyl group. Hydroxyl groups are ionized in the alkaline pulping environment which results in the dissolution of the lignin fragments. It is known that for lignin to become solubilized a large number of phenolic groups must be formed and it is estimated that the required ratio is 60 hydroxyl groups per 100 phenylpropane units present (Ek, Gellerstedt and Henriksson, 2009).

In the alkaline conditions of Kraft cooking the phenolic benzyl alcohol structure in its β-O-4 structure forms an equilibrium with quinone methide which is formed by loss of an ROH group. Due to the presence of hydrosulfide ions (HS) a further equilibrium is present resulting in a benzyl thioalcohol structure. Following the formation of this structure, a nucleophilic reaction takes place in which the β-carbon atom is attacked to form an episulphide (thiirane) and a new phenolic end-group. The thiirane structure is not a stable structure and consequently an elemental sulfur is expelled to form polysulfide which in alkaline conditions will be further disproportionate to form hydrosulfide and thiosulfate, as shown in equations 18.

$$\begin{gathered} 4nS_o + 4HS^- + 4HO^- \rightarrow 4S_nS^{2-} + 4H_2O \\ 4SnS^{2-} + 4(n-1)HO^- \rightarrow nS_2O_3^{2-} + 2(n+2)HS^- + (n-4)H_2O \\ \hline 4S_o + 4HO^- \rightarrow S_2O_3^{2-} + 2HS^- + H_2O \end{gathered} \qquad [18]$$

Three competing reactions occur simultaneously during the reaction. One possible mechanism is where the quinone methide intermediate loses a γ-hydroxymethyl group which results in the

formation of an enol ether structure without cleavage of the β-linkage. Another possibility is that the quinone methide reacts with other nucleophiles present in the liquor which will result in new stable carbon-carbon linkages. The final alternative reaction is the reduction of the quinone methide intermediate to formation of an α-methylene group. The mechanisms of these reactions are shown in **Figure 12**.

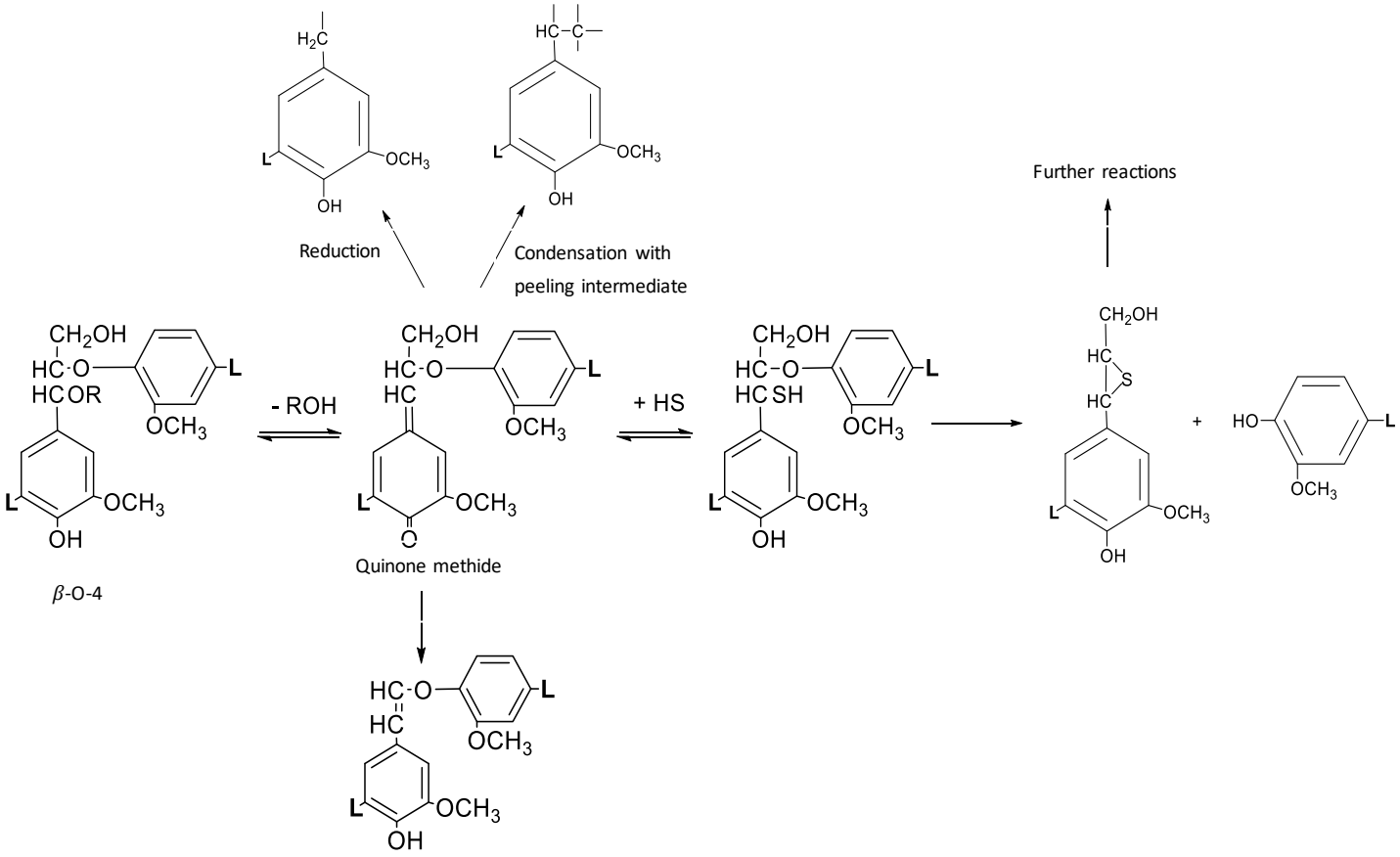

Figure 12: Reaction scheme for the cleavage of phenolic β-O-4 structure in lignin. L denotes lignin residue. (Ek, Gellerstedt and Henriksson, 2009)

It is possible that non-phenolic β-O-4 structures are cleaved as well during Kraft cooking. This mechanism does not involve hydrosulfide ions (HS) like cleavage of phenolic structures does but instead the mechanism requires the presence of an α-hydroxyl or γ-hydroxyl group which can become ionized in the alkaline cooking environment. The mechanism, as shown in **Figure 13**, is similar to that of the phenolic structure (**Figure 12**) where a nucleophilic attack results in cleavage of the β-ether linkage consequently forming an epoxide structure with a new phenolic lignin end-group. The epoxide structure is unstable and will react further with other nucleophiles in the cooking liquor.

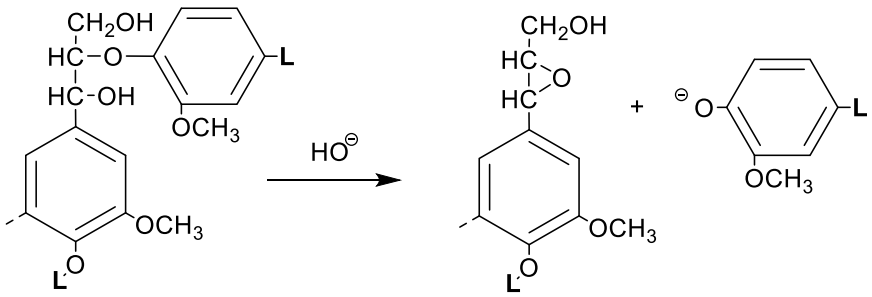

Figure 13: The cleavage of non-phenolic β-O-4 structures in Kraft pulping. (Ek, Gellerstedt and Henriksson, 2009)

2.3.4.2.2 Formation of odorous compounds

The combination of high temperature and presence of strong nucleophiles in the Kraft cooking liquor induces a cleavage of the methyl-aryl ether linkages in lignin. The extent of the reaction is minor, but the products formed are responsible for the smell from Kraft mills and extremely harmful to the environment. The reaction mechanism is shown in **Figure 14**.

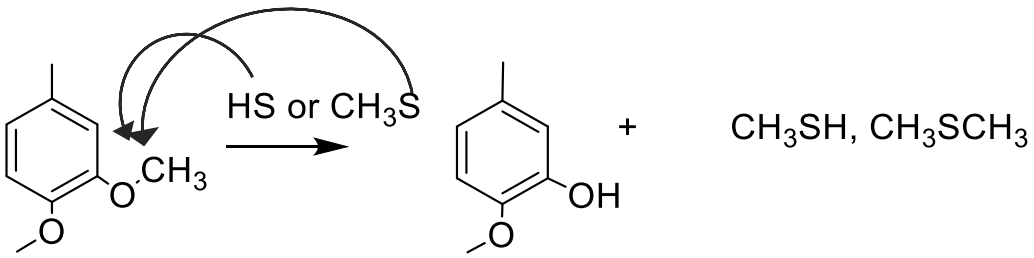

Figure 14: Formation of odorous compounds in Kraft pulping. (Ek, Gellerstedt and Henriksson, 2009)

The principal reaction is an attack of a hydrosulfide ion on the aromatic methyl ether group which forms methyl-mercaptan and a phenolic hydroxyl group. At the same time the methyl-mercaptan group can attack a new methyl group which forms dimethyl-sulfide (DMS). Methyl-mercaptan is extremely toxic and when exposed to oxygen a portion may become oxidized to form dimethyl-disulfide (DMDS), a further odorous and volatile product. During Kraft cooking approximately 1 to 2 % of methoxyl groups are converted into hydroxyl groups.

2.3.5 Chemistry of Bleaching Sequence

As mentioned in **Section 2.3.4,** this section is based on literature studies from *Wood: chemistry, ultrastructure, reactions* by Fengel (1989) and *Pulp and Paper Chemistry and Technology – Pulping Chemistry and Technology Volume 2* by Ek, Gellerstedt and Henriksson (2009).

2.3.5.1 Delignification selectivity

In Kraft pulping lignin reacts with the hydroxide ions in $NaOH$ and the hydrosulfide ions in Na_2S to form sodium lignate products which are water-soluble, causing the fibres to separate (Ek, Gellerstedt and Henriksson, 2009). According to Ek, Gellerstedt and Henriksson (2009) the presence of

hydrosulfide ions ensures that delignification proceeds rapidly and give the Kraft process the advantage of a much more comprehensive delignification versus the soda process which requires extremely long cooking times and even then, leaves a considerable amount of residual lignin in fibres.

The selectivity of dissolution of polysaccharides and lignin during cooking proceed in three distinct phases referred to as the (1) initial phase, (2) bulk phase and (3) the final phase. During the initial phase both polysaccharides and lignin are extracted. After about 20% of both components have gone into solution, the kinetics changes significantly. From this point onward selective lignin dissolution occurs until approximately 90% of all lignin has been dissolved. This is the bulk phase. At this stage cooking is normally interrupted before transition to the final phase can occur where the last of residual lignin can be removed but with considerable difficulty and at the cost of a large polysaccharide loss. (Ek, Gellerstedt and Henriksson, 2009)

According to Ek, Gellerstedt and Henriksson (2009) the dissolution of lignin does not proceed uniformly due to two reasons. The first is the lower accessibility of the middle lamella region in lignin which requires high temperatures (170 $^{\circ}C$ or more) in order to become dissolved. The second is ascribed to the structural differences between lignin molecules depending on their main monomer constituents (coniferyl alcohol, p-hydroxy-cinnamic alcohol or sinapyl alcohol) and final residual product after the cleavage reaction. The rate of delignification is lower for softwood species compared to hardwood species. This is due to the differences in hardwood and softwood morphology and their lignin structure.

2.3.5.2 The structure of residual lignin

It should be noted that the Kappa number does not only include the amount of residual lignin but (as mentioned in Section 2.3.3.4) other oxidizable structures like hexenuronic acid (HexA) are also present in unbleached pulp, and this need to be accounted for when determining the Kappa number. The desired brightness of pulp which is the purpose of bleaching is however, explicitly related to the removal of the lignin component (Fengel & Wegener, 1989). Eucalyptus is known to have high concentrations of hexenuronic acid (Ek, Gellerstedt and Henriksson, 2009).

The residual lignin present in fibres after cooking is known to have a much different structure from native lignin in wood, for example the number of chemical linkages between lignin and the major polysaccharides i.e., cellulose, xylan and glucomannan increases. Most of the residual lignin in a Kraft pulp is chemically linked to hemicellulose. There is also a large decrease in the amount of remaining β-O-4 structures (estimated to be around 10 to 20% of the initial value) and an increase in the amount of free phenolic hydroxyl groups (between 25 to 35 units per 100 phenylpropane units). These changes are expected consequences of pulping. (Ek, Gellerstedt and Henriksson, 2009)

An unexpected change, however, is the presence of a number of new aliphatic methylene groups confirmed by ^{13}C NMR analysis of isolated lignin samples. This indicates a less reactive chemical structure. It is possible that the phenomenon is created by a side reaction during cooking, but a more plausible explanation is that a number of minor lignin structures with reduced sidechains are already

present. Some fatty acids that are chemically incorporated during pulping also contribute to the concentration of methylene groups present. Thus, the most probable explanation for the high concentration of methylene groups in residual lignin is the presence of already reduced sidechain lignin molecules and the fatty acids incorporated in lignin structures during pulping. (Ek, Gellerstedt and Henriksson, 2009)

2.3.5.3 Oxygen delignification (O-stage) chemistry

First generation oxygen bleaching stages (O-stages) allowed for a very limited degree of delignification as the desirable oxidation of lignin was associated with a non-selective oxidative degradation of cellulose as well (Fengel & Wegener, 1989). It was later discovered that addition of magnesium(II) salt helped prevent this, although degradation still takes place but less severely (Ek, Gellerstedt and Henriksson, 2009). Due to this and other improvements the O-stage, according to Ek, Gellerstedt and Henriksson (2009), is used today as an extensive delignification method with the added benefits of being an environmentally friendly method and low in cost.

The most important reaction in the oxygen stage is the oxidation of phenolic end groups in lignin (Ek, Gellerstedt and Henriksson, 2009). The first step in the reaction is an electron transfer from a phenolate anion to oxygen which leads to the formation of one phenoxy and one superoxide radical as shown by equation 19. Neither of the structures are stable and will react further. The first possible reaction is where superoxide radicals react with other superoxide radicals to form hydrogen peroxide and oxygen as shown by equation 20. The second possible reaction is where superoxide radicals react with phenoxy radicals to form a new intermediate which is an organic hydroperoxide. If transition metals are present in the oxidized state, it is also possible for the superoxide to react and form oxygen as shown by equation 21.

$$\text{Phenol-OH} \xrightarrow{HO^{\ominus}} \text{Phenol-O}^{\ominus} \xrightarrow{O_2} \text{Phenol-O}^{\cdot} + O_2^{\cdot\ominus} \qquad [19]$$

$$O_2^{\cdot\ominus} + O_2^{\cdot\ominus} + H_2O \longrightarrow HO_2^{\ominus} + O_2 + HO^{\ominus} \qquad [20]$$

$$M^{\oplus} + O_2^{\cdot\ominus} \longrightarrow M + O_2 \qquad [21]$$

In modern O-stages the peeling reaction of polysaccharides is minimal even though the reaction is carried out in an alkaline medium (Ek, Gellerstedt and Henriksson, 2009). In oxidative conditions, the reducing end group that are present will quickly become oxidized to an aldonic acid group (Section 2.3.4.1.1) thereby stopping endwise degradation by the peeling reaction from occurring. However, even though the peeling reaction is of minor consequence there is still a reduction in DP which is attributed to the oxidation of one or more of the hydroxyl groups positioned along the cellulose chain which leads to a viscosity loss in pulp (Ek, Gellerstedt and Henriksson, 2009). The oxidation reaction creates a carbonyl group and subsequently, because of the alkaline medium, an elimination reaction

takes place which results in the cleavage of the chain to two shorter chains. One of the ends will have a reducing end but as mentioned previously due to oxidative conditions further peeling will not occur.

The initial oxidation mechanism which results in the formation of a carbonyl group is not known (Ek, Gellerstedt and Henriksson, 2009). According to Ek, Gellerstedt and Henriksson (2009), there are two possibilities, the first is that oxygen can advance the final conversion of the carbohydrate radical anion to a carbonyl group. The second possibility is formation of a carbonyl group by addition of a superoxide radical to the carbohydrate radical which is subsequently succeeded by the elimination of hydrogen peroxide. The two possible mechanisms are shown in **Figure 15**.

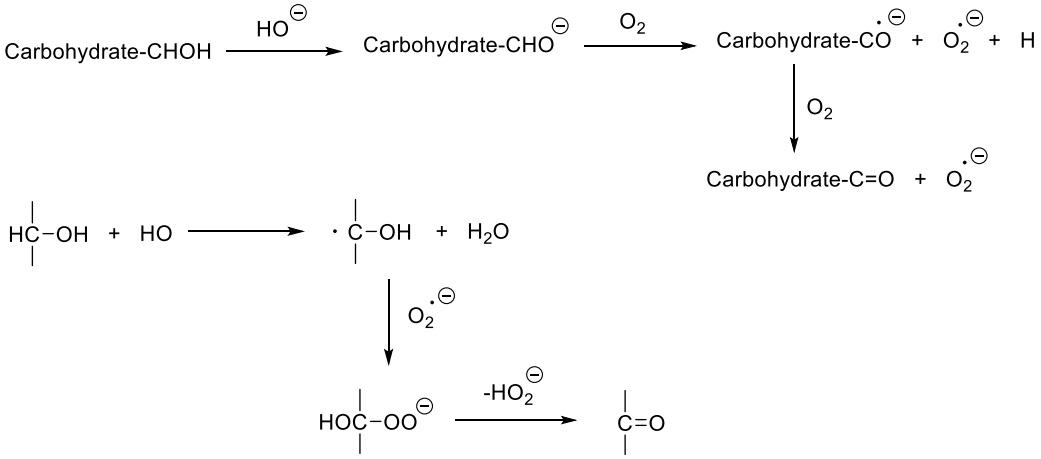

Figure 15: Possible methods of formation of carbonyl groups in polysaccharides on oxidation with oxygen in alkaline environment. (Ek, Gellerstedt and Henriksson, 2009)

The extensive delignification of lignin during oxygen delignification is not complemented by a similar large decrease in the Kappa number, mainly since oxidization has no effect on the amount of HexA units present from Kraft cooking (Ek, Gellerstedt and Henriksson, 2009). The slight decrease in Kappa number that does occur during the O-stage is ascribed to hemicelluloses that form oxidizable structures. The total overall decrease is only in the order of around ~30% for hardwoods (Ek, Gellerstedt and Henriksson, 2009).

Ek, Gellerstedt and Henriksson (2009) state there is great inhomogeneity in the structure of remaining lignin after cooking. Once all of the accessible lignin structures have been removed by oxidation, the remaining parts become structurally more like native lignin with β-O-4 structures being the most prevalent. It also appears that the oxidation of simple guaiacyl end-groups which leads to formation of biphenyl (5-5) structures is favored. Oxygen delignification will also result in residual lignin with an increased amount of carboxyl groups.

It is known, according to Ek, Gellerstedt and Henriksson (2009), that all residual lignin after oxygen delignification is linked to major polysaccharides i.e., cellulose, xylan and glucomannan although the proportion of linkages differs compared to unbleached pulp. The major portion is linked to the major hemicellulose components, xylan and glucomannan, forming a network with lignin where the amount

of lignin present is at least 50% of the total. A successive oxygen delignification stage will increase the value to between 80 to 90%. (Ek, Gellerstedt and Henriksson, 2009)

2.3.5.4 Chlorine and chlorine dioxide bleaching chemistry (C-stage and D-stage)

As mentioned previously (Section 2.3.3.2), the predominant function of chlorine (C) or chlorine dioxide (D) is delignification in a "pre-bleaching" stage followed by an alkaline extraction stage (E-stage) to remove most of the residual lignin present. Chlorine dioxide is however also often used in the final stage(s) in a bleaching sequence as an effective brightening agent as can be seen in Appendix B with sequences like D/C – O – D or O – D – E – D. (Ek, Gellerstedt and Henriksson, 2009)

Replacing chlorine with a more environmentally friendly alternative like chlorine dioxide has the advantage of producing a significantly smaller amount of acidic bleaching liquor and consequently there is less risk of acid hydrolysis occurring in polysaccharides. It has the disadvantage, however, of not being able to remove HexA groups from the pulp as efficiently. This has led to further advancements in bleaching sequences where mills add a hydrolytic stage either as a separate stage or a combined stage with chlorine dioxide (D-stage). The objective of the process is to selectively degrade HexA groups to 5 – formylfuroic acid (FFA) and furoic acid (FA) as shown in **Figure 16**. Hydrolysis is normally carried out with sulphuric acid (H_2SO_4). (Ek, Gellerstedt and Henriksson, 2009)

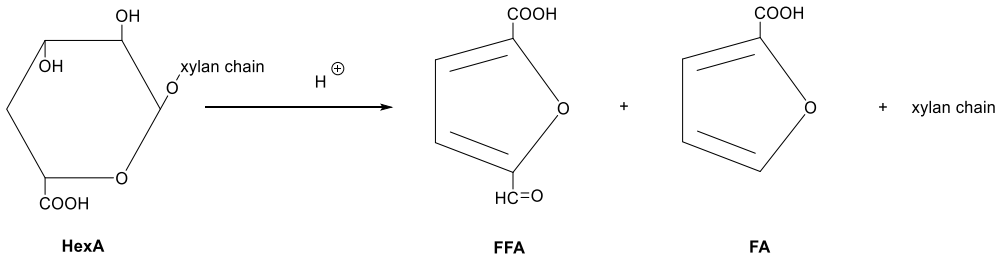

Figure 16: Acidic hydrolysis of HexA resulting in the formation of FFA and FA. (Ek, Gellerstedt and Henriksson, 2009)

The structure of residual lignin at this stage, after either Kraft cooking or the subsequent oxygen delignification stage, remains a polyphenolic macromolecule as discussed in Section 2.3.4.2. When using chlorine dioxide as a pre-bleaching agent, the mechanism for oxidation of lignin differs slightly for phenolic and non-phenolic compounds according to Ek, Gellerstedt and Henriksson (2009). Essentially, for both mechanisms, the first reaction is a one-electron transfer step which forms a phenoxy radical and a radical cation. This reduces chlorine dioxide to a chlorite ion. In the subsequent reaction another molecule of chlorine dioxide is added to the radical species which forms esters of hypochlorous acid. In final reaction these compounds are further hydrolyzed and give rise to either acids of the muconic acid type or quinones depending on the type of leaving group. The reactions described liberate hypochlorous acid and chlorous acid together with methanol.

The pH of the chlorine dioxide process is in the order of 2 to 3 (Ek, Gellerstedt and Henriksson, 2009). Initially chlorine dioxide is consumed very fast, within a few seconds. The formation of chloride, chlorite and chlorate ions occurs simultaneously. The formation of chlorite is useful as these ions can

potentially still participate in the overall reactions, but chlorate is an undesirable product since the ion is inert and thus will not participate in further reactions. It is also a biologically active ion which can cause environmental problems. However, it has been found that adding sulfamic acid during this stage suppresses the formation of chlorate. The charge of chlorine dioxide needed, expressed as "active chlorine", is based on the Kappa number of the incoming pulp. For example, if the incoming pulp has a Kappa number of 15 and needs to bleached to a Kappa factor of 0.2 then 0.2 × 15 = 3% active chlorine or 30/2.63 = 11.4 kg chlorine dioxide per ton of pulp is needed. When using chlorine dioxide as a final bleaching stage, the residual lignin present will have many carboxyl groups and a lower number of uncondensed guaiacyl groups and methoxyl groups. This is due to the first chlorine dioxide stage earlier in the bleaching sequence where guaiacyl end-groups were oxidized to acids of the muconic type. In order to further increase brightness to a value of around 90% ISO and remove most of the residual lignin still present, either two further chlorine dioxide stages are necessary or alternatively a combination of chlorine dioxide and hydrogen peroxide stages. Further delignification reactions are characterized by longer reaction times (about 3 hours), higher temperatures and higher pH, with an end pH of between 3.5 and 4, compared to the pre-bleaching stage. (Ek, Gellerstedt and Henriksson, 2009)

2.3.5.5 Reactions in the extraction stage (E-stage)

According to Ek, Gellerstedt and Henriksson (2009), the most important reaction in an extraction stage (E-stage) is neutralization of carboxyl groups with sodium hydroxide. This greatly increases the water solubility of the oxidized lignin. An additional reaction is the complete removal of organically bound chlorine and the formation of chloride ions instead. Normally, oxidants like oxygen or hydrogen peroxide are added to this stage to increase the extent of lignin removal and to decrease the charge of chlorine dioxide. Presence of the oxidants will result in increased formation of quinones.

From an environmental assessment, the E-stage is highly beneficial (Ek, Gellerstedt and Henriksson, 2009). In bleaching sequences that employ chlorine dioxide instead of chlorine, generation of a small amount of organically bound chlorine in pulp is still unavoidable. However, once the effluent of chlorine dioxide and extraction stages mix organically bound chlorine will efficiently be eliminated and result in the final bleaching effluent having a near-neutral pH.

2.3.5.6 Hydrogen peroxide bleaching chemistry (P-stage)

Two sets of reactions are encountered in the hydrogen peroxide bleaching stage (P-stage) namely (1) the general lignin oxidation reaction and (2) the brightening of pulp through chromophore elimination (Ek, Gellerstedt and Henriksson, 2009). The direct brightening effect on lignin is fast, inclining suddenly, before reaching a plateau. Full brightness cannot be achieved by this stage. The exact structure of chromophore groups present in pulping is unknown although it is generally presumed that quinones are the most reactive portions of these (Ek, Gellerstedt and Henriksson, 2009).

According to Ek, Gellerstedt and Henriksson (2009), technical pulp bleaching it is extremely important that the bleaching agent hydrogen peroxide is preserved to prevent degradation products, oxygen and

water, from forming and resulting in a very inefficient bleaching system. To achieve this, it must be ensured that the pulp at this stage is virtually free of all types of transition metal ions (Ek, Gellerstedt and Henriksson, 2009). Sometimes a pre-treating stage with a chelating agent like EDTA or DTPA is necessary. This will ensure decomposition of hydrogen peroxide is kept to a minimum, although it is not unavoidable and decomposition reactions will lead to the formation of oxygen and water through the intermediate formation of radicals (hydroxyl and superoxide). These radicals are responsible for the oxidation of lignin to an extent and also the oxidation of polysaccharides although to a lesser extent (Ek, Gellerstedt and Henriksson, 2009). The latter reaction will result in a further drop of pulp viscosity and a loss of between 50 to 200 units depending on the bleaching conditions at this stage.

The hydrogen peroxide bleaching stage is usually a few stages after oxygen delignification, the latter being the stage in which lignin "regains" a chemical structure similar to native lignin (Fengel & Wegener, 1989). This facilitates further oxidative degradation during the alkaline P-stage. The high temperature required in the P-stage (~ 100 $°C$) also results in the formation of quinone methide structures from phenolic benzyl alcohol structures (Ek, Gellerstedt and Henriksson, 2009). This makes a nucleophilic addition of a peroxy anion possible which can result in further side chain cleavage and fragmentation of lignin in successive reactions.

Hydrogen peroxide stages, in analogy to oxygen delignification stages, is unable to degrade HexA groups. The dissolved material from the P-stage will contain these HexA groups as well as a significant amount of low molecular weight aliphatic acids such as glycolic acid, formic acid, 3-hydroxypropionic acid and 3,4-dihydroxybutanoic acid. The origin of these aliphatic acids is unknown. The gradual consumption of phenolic lignin structures during the P-stage is linked with the formation carboxyl groups as a product of the reaction. (Ek, Gellerstedt and Henriksson, 2009)

2.4 Functionalization of recovered fibres to nanocellulose

2.4.1 Types of nanocellulose

The production of nanocellulose, a bio-based biodegradable and biocompatible material with very promising barrier and mechanical properties, has gained much attention in the past decade (Rol *et al.*, 2019). According to Rol *et al.* (2019) nanocellulose is currently the second-ranked priority of the European bioeconomy. The nomenclature used to describe different types of nanocelluloses has however not been used in a consistent manner. To clarify, nanocellulose can be divided into three categories. Nanocellulose can be produced from top-down approaches which involve enzymatic, chemical, and physical methodologies for their isolation from wood or bottom-up approaches where nanocellulose is produced from glucose by bacteria.

Two types of nanocellulose are produced from the top-down approach: microfibrillated cellulose (NFC) and nanocrystalline cellulose (NCC). Synonyms for NFC include nanofibrillated cellulose, nanofibrils and microfibrils. NFC is produced by delamination of wood pulp by mechanical treatment and is normally preceded by chemical or enzymatic treatment. The average diameter of NFC is 5 to 60 nm. The length is usually several micrometres. Synonyms for NCC are cellulose nanocrystals,

crystallites, whiskers and rod-like cellulose microcrystals. NCC is produced by acid hydrolysis of cellulose. Its diameter ranges from 5 to 70 nm and has a length of 100 to 250 nm. The third type of nanocellulose produced by bottom-up approach is bacterial nanocellulose. It is also known as microbial cellulose or biocellulose. As the name suggests it is produced by bacterial synthesis from low-molecular-weight sugars and alcohols. Hereon forth the terms NFC, NCC and BNC are used. (Klemm *et al.*, 2011)

Studies in the last few years have focused on ways to upscale NFC production to industrial scales. Of all papers published on nanocellulose, studies on NFC represent nearly 65% of that literature (Rol *et al.*, 2019). NFC is also the focus of the current study. NCC and BNC is not part of the scope of this work. Most recent studies on NFC focus on finding methods that reduce the energy consumption which is a major hindrance preventing commercial success. Traditional methods of producing NFC have energy consumption amounts pf over 25 000 kWh per ton which is attributed to the multiple passes required through homogenizers (Klemm *et al.*, 2011). However, thanks to recent studies aimed at improving energy consumption during mechanical treatment, industrialization has been made a possibility only quite recently. Two methods to reduce energy consumption have been recommended to achieve this, namely chemical pre-treatment and modification methods or using alternative mechanical processing equipment. Most studies focus on the former method.

2.4.2 Mechanical treatment to produce nanocellulose (NFC)

Homogenization of cellulose suspensions was the first method used to isolate NFCs. The manufacture thereof was pioneered by (Turbak, Snyder and Sandberg, 1983). Today there are many other mechanical treatments. The three most common techniques include homogenizers, microfluidizers and grinders. These methods are extremely energy intensive and produce aqueous dispersions of NFC at low solid content (< 5%). Low solid content leads to high transportation cost, storage challenges and limits certain applications. Several passes are needed for each of these methods.

In general, it has been reported that sulphite pulps are easier to delaminate (making it a less energy intensive process) than Kraft pulps and also that a high hemicellulose content as well as charge density facilitates delamination (Page, 1989). Nevertheless, about 27 000 kWh per ton of NFC was still necessary to produce NFC from a sulphite-pulp suspension with a high hemicellulose content as can be seen from **Table 6**. This table also illustrates the strong decrease in energy that can be achieved by introducing charged groups into the pulp fibres by chemical pre-treatment. The following section reviews such methods as reported in literature.

Table 6: Approximate energy requirements for the production of nanocellulose (NFC). (Klemm *et al.*, 2011)

Pre-treatment	Pulp type, bleached	Energy requirement (kWh/t)	Source
none	kraft	12000-70000	31
none	sulphite	27000	32
carboxymethylation	kraft/sulphite	500	28b,32
enzymatic/refining	sulphite	1500	1a,32

2.4.2.1 Homogenization, Microfluidization and Grinding

Besides high energy consumption, another major disadvantage of homogenization is that long fibres often clog the system as mentioned in Section 2.4.1. However, homogenizers can easily be implemented on industrial scale and can be operated continuously which is highly advantageous (Rol *et al.*, 2019). Processing with a microfluidizer instead can reduce the probability of clogging due to no in-line moving parts. Microfluidizers have Z or Y shape chambers with a small channel diameter through which a cellulose suspension is injected using high pressure of around 276 MPa (Rol *et al.*, 2019). The suspension is then expulsed through an orifice with dimensions between 100 to 400 μm. The high pressure along with the impacts against the channel walls create shear force and nanofibrillate the pulp. Even though the likelihood of clogging is small, long fibres cans till ca use fibrils to entangle and subsequently clog the equipment. Industrialization is also a challenge seeing as the chamber needs to be redesigned and altered to improve fibrillation which can be a limiting factor for industrialization of this method.

Grinders, the final commonly used method used to produce NFC has the following working principle: a cellulose suspension passes through a rotary- and static stone. The variable distance between the grinding stones is decreased after each pass. With each pass the fibre size decreases, making it possible to bridge the gaps between the grinding stones without resulting in clogging. Shear force is created between the two disks which delaminates fibres. Several passes are still needed with this method which results in high energy consumption (Rol *et al.*, 2019).

2.4.2.1 Twin-screw extruders, cryocrushing and ball mills

Twin-screw extruders, also known as a screw press, are the only equipment currently able of producing NFC with high solid contents (Nechyporchuk and Belgacem, 2016). Extruders are often used in WWTPs for sludge dewatering (Schaum and Lux, 2010). The equipment cost is however quite high, and not always deemed worth the expense compared to the cost of sludge disposal. In cases where it is already installed it could be a feasible method for recovering partially fibrillated material as a starting material for NFC production.

The cryocrushing method involves freezing suspensions with liquid nitrogen and then submitting it to high shear forces. During this process fibres are crushed as ice crystals break and release cell wall

fragments. Even though this method has been reported to produce good quality NFC, the capital investment and handling costs of cryogenic liquids on industrial scale would most likely exceed the final cost of the product (Balasubramanian, Gupta and Singh, 2012). There are also serious risks involved while handling liquid nitrogen including cryogenic burns, frostbite, hypothermia and asphyxiation.

Ball mills have been used to produce nanocellulose by authors like De Souza *et al.* (2017). In this method cellulose suspensions are agitated in a hollow cylindrical container partially filled with balls. The vessel rotates about its axis and results in high energy collision between the balls causing the delamination of fibres. The ball size and weight ratio compared to that of cellulose influences the NFC quality. The quality and homogeneity however of NFC produced by this method needs to be improved. Compared to other methods, this method currently does not produce competing NFC quality fibres (Rol *et al.*, 2019).

2.4.2.2 Ultrasonication

Ultrasonication has also been proposed as a potential method for NFC production. Ultrasonication can be applied at industrial level and has been successfully industrialized in the food processing industry where it has been reported by Ravikumar (2017) that the method has capability for large commercial scale-up. It has been investigated by Yang et al. (2010) and Chen et al. (2011) using lignocellulosic fibre from wood sources as raw material and by (Santucci *et al.*, 2016) using sugarcane bagasse as raw material. Shear force is created by introducing high power ultrasound into the cellulose suspension. The sound waves that are transferred into the fluid result in alternating high-pressure and low-pressure cycles. The rate of each cycle depends on the frequency. During the low-pressure cycle the high-intensity ultrasonic waves form small voids or vacuum bubbles. These bubbles collapse forcefully during the high-pressure cycle, a phenomenon which occurs due to bubbles reaching a maximum volume after which they cannot absorb energy any longer. This phenomenon is also known as cavitation.

There are two types of sonication treatment: probe-type sonication homogenizer and ultrasonic bath homogenizer. It has been found that in an ultrasonication bath the sonication effect is of low intensity and disproportionately distributed (Hielscher Ultrasonics, 2020). The repeatability and scalability of this process is also not very good or reliable. In contrast probe-type ultrasonication devices have been found to have a high localized intensity and consequently higher efficiency than tank-type ultrasonication. The most important properties of ultrasonication, according to Hielscher Ultrasonics (2020), include the amplitude, pressure, temperature, viscosity, concentration and reactor volume. Ultrasonic probe devices can be operated batch-wise or continuously. In batch mode the probe is used in an open beaker and is generally used for feasibility testing or smaller volumes. The most advanced sonication results are attained by continuous processing because, in a continuous processing environment, the entire volume is subjected to the same ultrasound intensity and the residence time in the reactor chamber can be controlled accurately. (Hielscher Ultrasonics, 2020)

In the study conducted by Chen et al. (2011) the intensity of nanofibrillation with regard to output power was tested. Chemically treated cellulose fibres were placed in a beaker with a probe-type ultrasonic homogenizer. Output power of 400, 800, 1000 and 1200 W was tested respectively. The treatment was carried out in an ice/water bath and replaced throughout the entire duration of the experiment (30 min). By visually inspection of the different samples, the study by Chen et al. (2011) found that there was a clear improvement in dispersion when the output power increased above 800 W. At outputs between 1000 to 1200 W the cellulose nanofibres were homogenously dispersed and converted to highly viscous suspensions. TEM images confirmed this observation, for an output of 400 W about 62 % of nanofibres were shorter than 20 nm. The diameter distribution revealed a diverse range of sizes, ranging from several nanometres to several hundred nanometres. At a power output of 1000 W nearly 100% of the nanofibres were shorter than 20 nm. The size distribution became much more homogenous with most fibres having a diameter between 10 to 15 nm.

2.4.3 Pre-treatment of cellulose fibres for nanocellulose (NFC) production

In a study by Rol et al. (2019) all known chemical pre-treatment methods were ranked according to their quality, possibility of industrialization and novelty of the process. The results are shown in **Figure 17**. The quality of fibres is determined using a 'quality index' method developed by (Desmaisons *et al.*, 2017). The method is described and discussed in the next section. Ease of industrialization was based on the literature review findings and authors experience. The novelty of the process is indicated by the size of the bubble, where largest bubble sizes present the most novel processes. As can be seen from this figure (**Figure 17**) enzymatic treatment is the most promising industrial method with a score of 5 out of 5. This method scores a 6 out of 10 for NFC quality which is just above average. Carboxymethylation and phosphorylation are second to enzymatic treatment concerning the ease of industrializing the method with scores of 4 out of 5. Phosphorylation however has a much higher quality score, 8 out of 10, compared to that of carboxymethylation, 5 out of 10.

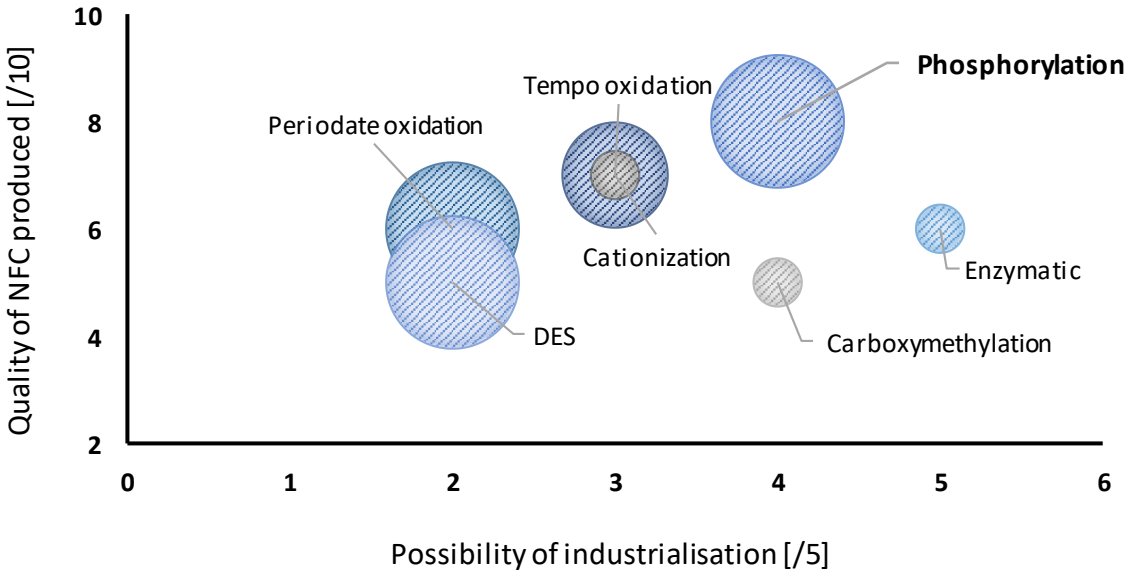

Figure 17: Evaluation of cellulose pre-treatment methods. (Rol *et al.*, 2019)

Carboxymethylation was developed in 1918 and is a well-known process for treatment of cellulose fibres (Rol *et al.*, 2019). Except for the drawback of delivering quite low-quality fibres this method also uses toxic chemicals such as monochloroacetic acid and consists of a rather complex multi-steps procedure. Enzymatic hydrolysis is a green alternative that produces relatively good quality NFC and has been implemented by numerous NFC producers (Rol *et al.*, 2019). NFCs obtained by this method are not functionalized however and require further processing and modifications to broaden their application potential. Phosphorylation is the most recent method suggested to treat cellulose fibres, there are in fact only 4 papers available in literature (Ghanadpour *et al.*, 2015; Noguchi, Homma and Matsubara, 2017; Rol *et al.*, 2020). This method of pre-treatment is easy to implement and non-toxic. An additional benefit of this method is that phosphorylated nanopapers display self-extinguishing behavior during flammability tests (Ghanadpour *et al.*, 2015). This method of pre-treatment appears to be an attractive alternative to TEMPO oxidation and carboxymethylation. Even though it is quite a new process, the potential thereof is evident from the evaluation of the method as presented in **Figure 17**. Thus, phosphorylation was used as a pre-treatment method in the experimental section of this study. Other pre-treatment methods like imidazole, sulfoethylation or ozonation are not included in the evaluation of methods as these pre-treatments are simply new and research is not sufficiently advanced to evaluate the ease of industrialization or quality of NFC produced from these methods (Rol *et al.*, 2019).

2.4.4 Quality and characterization of nanocellulose (NFC)

Technically NFC suspensions are multiscale and complex materials containing fibres of millimeter scale, poorly fibrillated fibres of micrometer scale and nanofibres with diameters of less than 100 nm. The possibilities of NFC quality are further differentiated using different sources and initial fibre properties. These differences in grade and quality are what makes nanocellulose usable for a wide range of applications (Desmaisons *et al.*, 2017). According to Desmaisons *et al.*, (2017) it is necessary to have clear distinctions between different nanocellulose grades to help choose the most appropriate one for each application.

Such a comparison of all nanofibre products is difficult due to the vastly different nomenclature used for these products ranging from “fibril aggregates”, “cellulose microfibrils”, “microfibrillated cellulose” or “cellulose nanofibrils”. By technical definition a nanocellulose suspension is a combination of all of these terms at the same time. Some attempts have been made in the past to standardize the terms needed to adequately describe nanocellulose materials. For example, the Technical Association of the Pulp and Paper Industry (TAPPI) has proposed standard terms TAPPI WI 3021 based on size and aspect ratio.

Other authors such as Kangas et al., (2014) have proposed many different analytical methods based on the amount of nanomaterial, particle size distribution, rheology, morphology, crystallinity, mechanical properties, and surface chemistry. However, many of these methods are expensive, complex, time-consuming, requires expertise and does not allow for comparison. Examples include microscopy techniques such as Scanning Electron Microscopy (SEM), Transmission Electron

Microscopy (TEM), and Atomic Force Microscopy (AFM) which are expensive, time-consuming and require a high level of expertise. Any method that using high-level microscopy tools would be very difficult to implement in a production mill. Also, even though AFM and TEM are some of the most powerful tools for determining nanofiber dimensions, these tools focus only on the nanoscale range and consequently conceal information about the macroscopic dimensions of fibres.

Many other methods have been proposed over time. Some of these include determining the "degree of fibrillation" (Oksman, Mathew and Sain, 2009) or "yield of fibrillation" (Naderi, Lindström and Sundström, 2015) which is determined by isolation of nanoparticles by centrifugation steps. The capacity of NFC to transmit or scatter light has been related to the fibrillation degree, both in suspensions (Saito *et al.*, 2006) and films (Qing *et al.*, 2013). Other studies have focused on suspension comparison by using a multicriteria approach, although these methods still do not provide a clear definition or normalized method. An interesting method proposed by Chinga-Carrasco (2013) is the use of an image scanner that allows for the classification of nanoparticles in the microscale and nanoscale range. A method such as this has great potential for the evaluation of NFC quality in online processes. One disadvantage of the method is that results have a qualitative ranking and ultimately need to be compared test by test.

Desmaisons et al., (2017) proposed an alternative solution: a multi-factor NFC "Quality Index" (Q.I.). The objective of the study was to obtain a unique value combining a number of factors representative of the three scales of NFC material. The index was developed using only simple and standard equipment which makes it possible to use for both lab-scale and industrial scale. The outcome of the study gave a regression model as proposed by equation 22.

A simplified Q.I was also created by using principal component analysis (PCA) which allows for reduction in the number of variables and make information less redundant (Desmaisons et al., 2017). The PCA results were combined with a matrix correlation of 8 parameters (as denoted by x_1 to x_2) to come up with a simplified Q.I. as given by equation 23. Equations such as these present a manner to automatically determine the quality index by just entering the test results.

$$Q.I. = 0.20\,x_1 + (-0.02\,x_2) - 0.035\,x_3^2 + 1.27\,x_3 - 0.16\,x_4 + 1.65\ln(x_5) - 3.59\ln(x_6) - 2.67\ln(x_7) + 0.18\,x_8 + 69.6 \quad [22]$$

$$Q.I. = 0.30\,x_1 + (-0.03\,x_2) - 0.071\,x_3^2 + 2.54\,x_3 - 5.35\ln(x_7) + 59.9 \quad [23]$$

Where for equation 24 and 25:

$x_1 = nanosized\ fraction(\%)$

$x_2 = turbidity\ (NTU)$

$x_3 = Young's\ modulus\ (GPa)$

$x_4 = porosity\ (\%)$

$x_5 = transmittance\ at\ 550\ nm\ (\%)$

$x_6 = tear\ resistance\ (mN)$

$x_7 = macrosized\ fibre\ content\ (\mu m^2)$

$x_8 = macroscopic\ homogeneity\ (\%)$

Quality indices as proposed in equations 24 and 25 can be used to plot Q.I. as a function of the energy consumption, corresponding to different treatment duration for a certain method of NFC production. This was done by Desmaisons et al., (2017) for the super-grinding treatment of kraft pulp from eucalyptus as well as a combination of aspen and maple after enzymatic pre-treatment. For eucalyptus pulp it was found that the Q.I. increases from 68.3 ($\pm$4.5) to 75 ($\pm$5.7) for an increase of 5267 kWh/t. This means that for a 9% increase in quality index, 42% of total energy is consumed. On the same graph of Q.I. versus energy consumption, the effect of hemicellulose content can be plotted.

From the trends plotted by Desmaisons et al., (2017) it was determined that for low hemicellulose content treatments should be stopped after a consumption of 4000 kWh/t instead of running it to 12000 kWh/t for only a slight difference of 10% in Q.I. This would result in a 63% reduction in energy consumption. Plots such as this can be used by producers to compromise between energy efficiency and necessary NFC quality.

Furthermore, Desmaisons et al., (2017) determined the difference between NFC production from dry sheets and from never-dried samples that are left in suspension. It is known that the drying step of pulp causes irreversible changes that influence the defibrillation process (Balea *et al.*, 2017). When fibres are dried, the water being removed brings neighboring microfibrils into close contact which results in the formation of hydrogen bonds between them (Desmaisons et al., 2017). The result is a loss of fibre conformability and swelling capacity which impedes the bonding potential of fibres and diminishes strength properties (Garcia *et al.*, 2002).

The results from Desmaisons et al., (2017) confirms the theory that never-dried samples are easier to fibrillate, as the Q.I. obtained with never-dried pulp at 4000 kWh/t is reached at 12000 kWh/t with dried pulp. The energy consumption is three times more for producing the same quality NFC from dried pulp versus never-dried pulp. Another interesting result from Desmaisons et al., (2017) study was that of all the samples tested, good quality NFC from eucalyptus pulp was the easiest to obtain. This is a promising result as in eucalyptus is a fast-growing species with decent quality fibre and a relatively low market price (Desmaisons *et al.*, 2017).

2.4.4.1 Soft sensor development

A soft sensor is an empirical model that correlates several raw data sources to create a new source of useful information (Amazouz, Platon and Champagne, 2005). Soft sensor technology is a promising tool to replace hardware sensors that are unreliable or unavailable and can help industries to reduce their environmental impact as well as improve final product quality and reduce operating costs. A major problem in the manufacturing industry, including the pulp and paper industry, is the lack of real-

time measurement of the process and product variables (Zarko *et al.*, 2019). This online unavailability of important variables can lead to off-specification production.

The concept is better explained by an example. Consider the determination of the Kappa number in pulp and paper industries. As discussed in Section 2.3.3.4 the Kappa number is closely related to the residual lignin content remaining in pulp and represents the hallmark of the quality of paper produced (Amazouz, Platon and Champagne, 2005). Process samples are taken once per hour, once per 8-hour shift or once per day to a laboratory to determine this number. This infrequent sampling procedure may not be representative of the process and consequently many companies require at least 3 laboratory results before taking action. If, for example, a sample is taken every hour and the laboratory requires 20 min to determine the Kappa number then the PPM could easily produce 3 hours of off-spec product before action can be taken. This leads to increases in energy usage and also has a great impact on the environment because more waste is being generated that needs to be disposed of. Often the material needs to be reprocessed which creates additional energy, chemical consumption and labour costs.

Soft sensors can replace laboratory measurements for monitoring and control purposes by providing online, accurate estimates of variables like the Kappa number thereby eliminating the additional cost linked with off-specification products. In the process industry a soft sensor can be designed to substitute a momentarily or permanently unavailable sensor in a plant. The sensor is designed using sampling and offline laboratory analysis. The concept of a soft sensor connected to a plant is shown in **Figure 18**. It is estimated that the application of soft sensor packages can potentially result in cost reduction of between 75 and 135 million US$ per year if it is 100% successful (Amazouz, Platon and Champagne, 2005). According to Amazouz, Platon and Champagne (2005) the technology has been successfully implemented in several companies in Canada including Tembec Inc. and Abitibi-Consolidated Inc. The soft sensors used include near infrared based soft sensors that were developed to predict the Kappa number and wood moisture content.

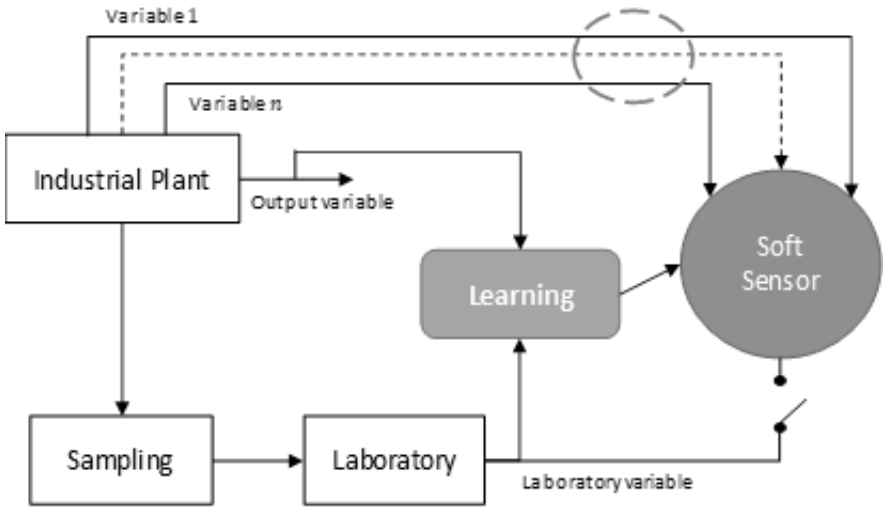

Figure 18: Concept of soft sensor integration in plant. (Soares *et al.*, 2011)

Soft sensors can be divided into two categories namely model-driven and data-driven sensors (Raffaele and Ondruch, 2020). Model-driven sensors are built on first principles which aim to describe the physical boundaries of a process in a detailed manner. First principle models are the least common soft sensors used as it is a very time consuming method and usually a significant amount of parameters are unknown (Fortuna, Graziani and Xibilia, 2005). These models are based on the understanding of the physics of the process and require knowledge about the mathematical relationship between the inputs and outputs of the system or knowledge about the qualitative functions of the various units in a process (Amazouz, Platon and Champagne, 2005). Consequently, even though these models are typically more robust they are problematic to obtain since accurate mathematical models are required.

Data-driven soft sensors are based on models that use data fitting techniques to approximate unknown process variables using historic process data (Raffaele and Ondruch, 2020). Factor-based models normally used for soft sensors include principal component analysis (PCA) and partial least of squares, also known as projection to latent structures (PLS) (Amazouz, Platon and Champagne, 2005). According to Amazouz, Platon and Champagne (2005) these methods work well with industrial datasets. These methods are capable of coping with large data sets including observations and variables, noisy data sets, missing data and correlated variables within the data sets. This method of developing soft sensors has been used by authors like Liu, Li and Yang (2018) to predict the chemical oxygen demand (COD) and suspended solids concentration of pulp and paper mill wastewater.

Another method commonly employed for developing data-driven soft sensors is the "black box method" (Amazouz, Platon and Champagne, 2005). Black box models are normally based on neural networking techniques, also known as artificial neural networks (Fortuna, Graziani and Xibilia, 2005). Artificial neural networks are a type of artificial intelligence technique used to mimic the human brain in its ability to recognize patterns through a similar parallel processing structure (Chiang, Zhang and Zhou, 2006). Like the human neural system, these models learn the intrinsic nature of a pattern or process from historic process data. This method has been applied by authors Edwards *et al.* (1999) to predict paper "curl" properties during the papermaking process which is a quality measure that can only be measured reliably offline after manufacturing. In the study by Edwards *et al.* (1999) the characteristics of the paper machine reel are used to predict whether the level of curl at the end of manufacturing will be acceptable.

2.4.4.2 Effect of fines and lignin content on NFC properties

Fines are defined as the fraction of pulp that can pass through a mesh screen or perforated plate with hole diameters of 76 μm (Odabas *et al.*, 2016). When referring to fines there are two categories: primary fines, also known as mechanical fines and secondary fines (Fischer *et al.*, 2017). Primary fines are produced during the pulping and bleaching stage where they are separated from fibres by harsh chemical and mechanical treatment. Secondary fines are produced during the refining process in which case the mechanical treatment thereof partly fibrillates the cell wall of fibres which results in formation of fibrils with microscale dimensions.

According to Fischer *et al.* (2017) both primary and secondary fines are usually present in paper furnish. They differ in morphology and chemical structure, but these variations are also dependent on the type of pulping process and because of this have different impact on paper quality. Secondary fines have a large aspect ratio, surface area and bonding ability that enhance the mechanical strength of paper. These properties have a negative impact on dewatering in the forming section of a paper machine. Primary fines mostly alter the optical properties of the final product but are also known to have a negative impact on dewatering properties and in some cases the mechanical properties of sheets formed (Luukko, 1999; Tovar *et al.*, 2015). Even though these properties of fines are known, the effect of these properties is difficult to quantify (Bäckström et al., 2008).

Fischer et al., (2017) investigated the structural properties of different types of fines and other cellulosic microparticles (NFC) using unbleached Kraft pulp as the starting material. Fines were isolated from the pulp using a lab scale pressure screen and dissolved air flotation to further concentrate the solid content of the suspension. Hand-sheets were prepared from primary and secondary fines and compared to sheets from NFC. The results of the study concluded that NFC sheets form the densest and smoothest sheets and achieve the highest strength. Hand-sheets from secondary fines exhibited structural and mechanical properties similar to the properties of NFC sheets. The well-known advantages of kraft pulp over sulphite pulp in strength were also seen when comparing the stress-strain curves obtained from mechanical testing. The sheet density was measured according to DIN EN ISO 534:2011 and it was found that fines sheets of mechanical pulp have the lowest apparent density of 500 kg/m^3 compared to unbleached kraft pulps where primary fines sheets have a density of between 700-750 kg/m^3 and secondary fines sheets has a density of 900-950 kg/m^3.

This result differentiates from studies by Bian et al. (2018) which found that higher lignin content resulted in a higher density. According to Bian et al. (2018) this is due to empty spaces or pore among the fibrils in the films being effectively compacted by lignin during ultrafiltration. Approximately the same range of densities was found by (Kumar *et al.*, 2014). The study also found that the stiff nature of fibrils containing lignin resulted in a more uneven surface structure with a higher roughness value. These results align with those in the study by Fischer et al. (2017) but differ from a study by Rojo et al. (2015) which concluded that fibrils with high lignin content formed smoother surfaces with a lower roughness values. The difference can possibly be attributed to different drying techniques. In the study by Rojo et al. (2015) films were dried by hot-pressing at 100 °C for 2 hours where as in the study by Bian et al. (2018) films were dried at room temperature for 2 days. The raised temperature softened the amorphous lignin during pressing which made it easier to fill the voids between the fibrils and consequently resulted in smoother surfaces. Films dried at room temperature were not able to achieve the same smoothness and instead the rigid residual lignin led to uneven surfaces and increased roughness values. All studies concluded that lignin interferes with hydrogen bonding between cellulose nanofibrils which impair mechanical properties of films such as tensile strength and Young's modulus (Bian et al., 2018; Fischer et al., 2017; Kumar et al., 2014; Rojo et al., 2015). Morphologically, films with little to low lignin are clear and flexible showing no cracks or defects upon folding (Bian et al., 2018).

2.4.5 Film fabrication methods

Various film fabrication methods have been reported in literature, but most of them are based on basic methods such as the vacuum filtration method and the casting method (Dai *et al.*, 2019). According to Dai *et al.* (2019) vacuum filtration is a fast, simple and accessible process that produces layered structures of nanocellulose membrane and nanopapers. In this study it was desired to find a simple, fast method to fabricate films and thus vacuum filtration was considered the best method.

During vacuum filtration a sufficient suction force is applied to remove most of the water from the underside of the film. The nanocellulose suspension must be diluted to a low consistency of between 0.1 and 0.5 wt% and dispersed before film formation (Visanko, 2015). Degassing is usually required to remove residual air trapped within the suspension. Unwanted air bubbles may burst leaving cavities in the suspension which consequently reduce barrier and strength properties of the film. Under laboratory conditions a glass filter funnel or similar device is mostly used for vacuum filtration of nanocellulose suspensions. Various filter papers or commercial membranes with a sufficient pore size can be used to trap nanocellulose during the filtration process and ensure the formation of smooth films (Henriksson *et al.*, 2008; Nogi *et al.*, 2009; Chun *et al.*, 2011). Once most of the water has been removed by suction, a wet gel-like hydrogel film is formed. The film is then moved to a suitable drying environment.

According to Visanko (2015), a more time-consuming method to produce films is casting of nanocellulose suspensions on a petri dish or glass plate. Depending on the drying temperature and residual water present, the eventual formation of films takes several days (24 to 72 h). The drying process can be accelerated by oven drying at elevated temperatures, hot pressing or the use of a semi-automatic sheet former. A study by Sehaqui et al., (2010) compared different drying methods and found that semi-automatic sheet formers produce the best mechanical properties due to wrinkle-free formation of films, good in-plane orientation of nanofibrils and rapid moisture removal. The parameters in the drying environment can be adjusted along with using different solvents to alter the formation of the nanonetwork. Depending on the characteristics of this network, films are either ultra-porous or highly compact barrier structures (Visanko, 2015).

2.4.5.1 Technical aspects and considerations of the drying kinetics of thin films

When preparing films, the drying step is a critical process step, and it is important to consider that the drying rate is dependent on the (1) heat transfer, (2) solvent diffusion and (3) mass transfer coefficients of the mass transfer resistance of each film. Two of the most well-known thin film preparation methods in industry are solvent casting and spin-coating (Rodriguez, 2015). Solvent casting is a method where a suspension is poured into a Petri dish or other flat surface and evaporated under specified conditions of humidity, temperature, and pressure to obtain films. The upside to this method is that is a simple technique, but the downside is reproducibility which is difficult to obtain. Spin-coating is a more technical method using centrifugal force to form ultrathin films that are subsequently dried. The method is able to produce films with nanometric thickness.

It is important to understand the relationship between the mass transfer phenomena, i.e., the drying rate, and physical changes to better control the physico-mechanical properties of films as the rate of drying influences the crystallinity of the polymer. A study by Velaga, Nikjoo and Vuddanda (2018) proposes a simple model to explain drying behaviour and the effects on physical form changes in two water-soluble polymers namely hydroxypropyl methylcellulose (HPMC, amorphous) and polyvinyl alcohol (PVA, semicrystalline).

The model by Velaga, Nikjoo and Vuddanda (2018) uses the well-known Hill equation, as given by equation 24, as a simple alternative to complex traditional drying models. The three-parameter equation is extensively used in scenarios when the relationship between x and y variables is nonlinear and where y reaches constant values over time. Drying data can be sigmoidal or hyperbolic which is also why the Hill equation is a better estimation compared to other two-parameter equations.

$$y = \frac{y_{max} x^n}{c^n + x^n} \qquad [24]$$

Where:

$y = reaction\ or\ process\ rate$

$y_{max} = maximum\ reaction\ or\ process\ rate$

$c = half - maximal\ concentration\ constant$

$n = Hill\ coefficient$

$x = substrate\ concentration$

The descriptive traits of the equation provide flexibility and effectiveness which make it applicable to many processes. The probabilistic term $x^n/(c^n + x^n)$ can be used as a cumulative distribution function $F(x)$ with random values provided for x to give an indication of the descriptive aspects of the equation. The probability density function is determined form the first derivative $F(x)$ which is expressed in equation 25.

$$f(x) = F'(x) = \frac{n c^n x^{n-1}}{(c^n + x^n)^2} \qquad [25]$$

Where:

$c = half - maximal\ concentration\ constant$

$n = Hill\ coefficient$

$x = substrate\ concentration$

Equation 22 is valid for $F(x) = P\{X \leq x\} = \frac{x^n}{c^n + x^n}, x \epsilon R^+, c > 0, n > 0$. The model assumes that the effect of thermal diffusion on film drying kinetics is negligible because it occurs much faster than mass diffusion (about one thousand times faster than the maximum value of the mass transfer coefficient). The Hill equation is adapted as shown in equation 26 to explain the drying behavior of films. Thermogravimetric analysis (TGA) is used to determine the values for the equation. In the equation

W_{max} is the maximum weight of film lost during the duration of the dehydration process (t) and τ is the time where 50% of weight loss has occurred. Lastly, n is the Hill coefficient which is reflected in the shape of the graph.

$$W_{loss} = \frac{W_{max} t^n}{\tau^n + t^n} \quad [26]$$

Where:

$W_{loss} = mass\ change/loss$

$W_{max} = maximum\ weight\ of\ film\ lost\ during\ time\ t$

$t = duration\ of\ the\ dehydration\ process$

$\tau = time\ where\ 50\%\ of\ weight\ loss\ has\ occured$

$n = Hill\ coefficient$

The mass change (W_{loss}) affects the distribution function $F(x)$ and consequently the density function $f(x)$. The distribution function $F(x)$ will have a sigmoidal shape in cases when $1 > n > 0$ or $n > 1$ or a hyperbolic shape when $n = 1$. The drying rate, expressed as K_d, can be calculated at any time by determining the first order differential of W_{loss} as given by equation 27.

$$K_d = \left(\frac{dW_{loss}}{dt}\right)_T = \frac{nW_{max}\tau^n t^{n-1}}{(\tau^n + t^n)^2} \quad [27]$$

Where:

$K_d = drying\ rate$

$dW_{loss}/dt\ = change\ in\ mass\ loss\ with\ time$

$W_{max} = maximum\ weight\ of\ film\ lost\ during\ time\ t$

$t = duration\ of\ the\ dehydration\ process$

$\tau = time\ where\ 50\%\ of\ weight\ loss\ has\ occured$

$n = Hill\ coefficient$

The dehydration process can be better understood having knowledge about the actual significance of the parameters in the above equation. Important physical parameters occur at point in the graph where (1) $t \to \infty$ and $W_{loss} = W_{max}$, (2) $t = \tau$ and $W_{loss} = W_{max}/2$ and finally (3) $t \to 0$. The first point (i.e., as $t \to \infty$) stipulates the maximum weight of film lost W_{max} during the stipulated drying period. The second point (i.e., when $t \to \tau$) represents the time it takes for W_{loss} to reach half of W_{max} and the final point (i.e., when $t \to 0$) is where $W_{loss} = \frac{W_{max} t^n}{\tau^n}$ which represents the starting point of the drying process.

Thus, TGA graphs can be used to attain useful information about the initial section of the dehydration curve, the upper limit of weight loss as well as important insights into the mechanism of the drying process as given by τ. In the study by Velaga, Nikjoo and Vuddanda (2018) it was found that before

the characteristic time τ the drying rate increased with an increase in temperature but after τ the rate decreased with an increase in temperature before levelling out. According to the author Velaga, Nikjoo and Vuddanda (2018) this occurrence can be justified by the biphasic diffusion of the solvent. During the initial drying period the drying rate follows Fickian diffusion laws whereas non-Fickian diffusion laws dominate the latter phase. The change in mechanism is attributed to changes in the polymer structure that take place during the drying process.

2.5 Research gaps in literature

Even though great strides have been made in research toward finding alternative ways to utilize pulp and paper mill sludge, most mills in South Africa still dispose of sludge by landfill or incineration. This is most likely because of convenience and the fact that alternatives to these methods are still very new, and most methods still emit some source of waste or pollution that needs to be disposed of outside the normal Kraft effluent treatment system. It is also difficult to predict what the market potential for some of these products will be and whether the cost of implementing new technologies will be worthwhile. What makes finding a suitable alternative particularly difficult is that the composition of sludge differs for each mill depending on the feedstock and mill operation. This makes it impossible to provide a single solution for all different types of mills.

Specifically, regarding functionalization of fibres to nanocellulose, one of the greatest challenges is finding ways to sufficiently lower energy consumption to produce nanocellulose that is of good quality but at the same time does not contribute toward environmental problems. The most widely researched chemical pre-treatment method to address this is TEMPO-oxidization. The method successfully lowers energy requirements, but the chemicals used are not environmentally friendly. Other methods are either too expensive or difficult to industrialize. A very new method recently considered is phosphorylation which is easy to industrialize, uses green chemistry and produces good quality nanocellulose without jeopardizing sustainability. However, up to date only four papers about the topic including a review paper, have been published. More lab-scale data is needed before making production on industrial-scale possible.

3 RESEARCH DESIGN AND METHODOLOGY

3.1 Study approach and thesis layout

Figure 19 illustrates the experimental approach followed in this study. The project was divided into three sections namely (1) identification and categorization of waste sources, (2) developing and validating a recovery method and (3) developing and validating a functionalization method.

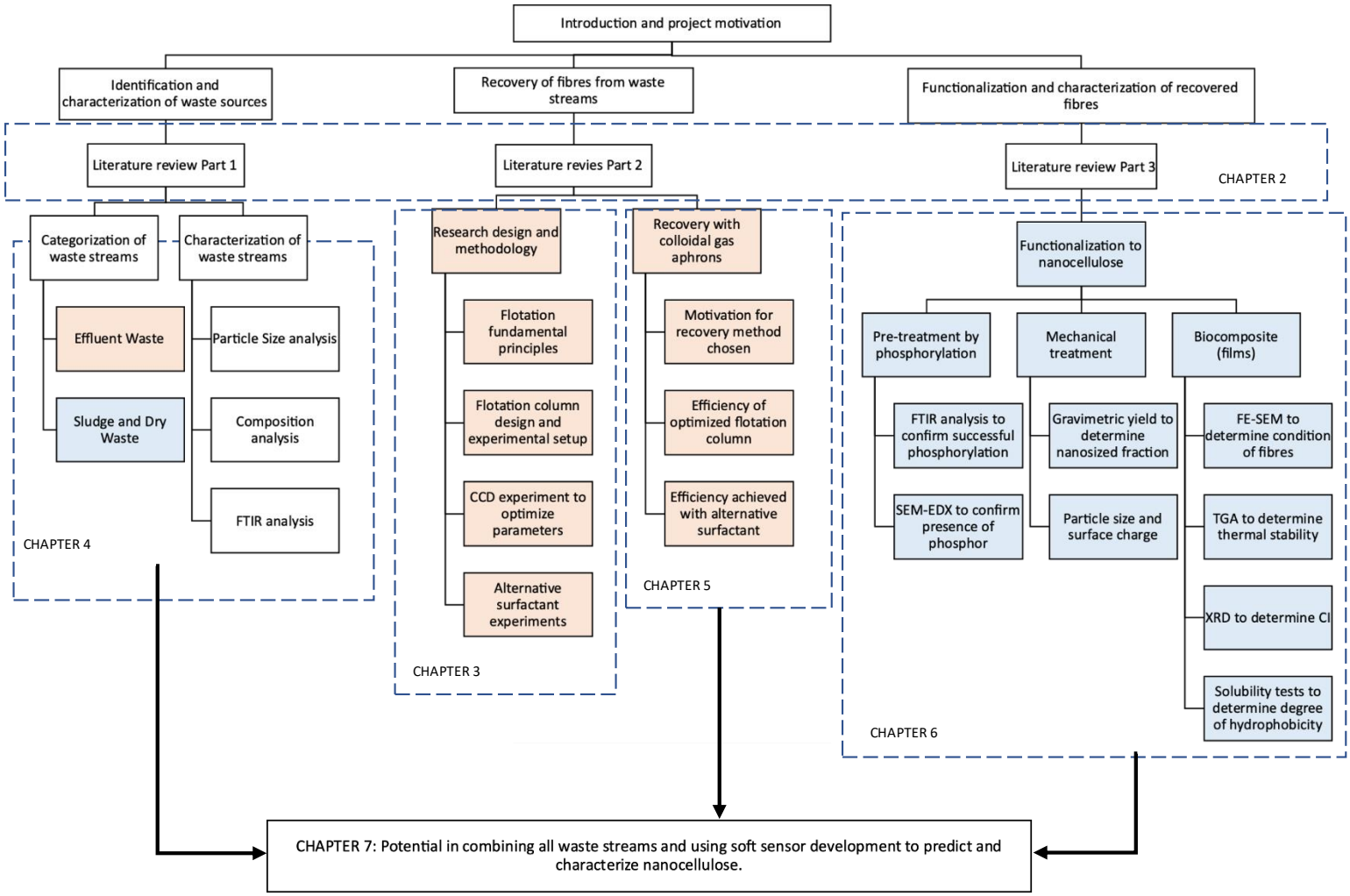

Figure 19: The research approach for recovery and functionalization of lignocellulosic biomass from pulp and paper mill waste streams.

There are five chapters following the literature review which address different aspects of the project. Chapter 3 addresses the research design and methodology of the project. Chapter 4 addresses the methodology to categorize waste streams and includes the results and discussion about biomass characterization. Chapter 5 addresses the technical considerations regarding flotation, the motivation for choosing this method of recovery and the results from lab-scale experiments. Chapter 6 addresses all aspects regarding functionalization of biomass to nanocellulose including motivation for the method chosen and characterization of biocomposites made from gel-like nanocellulose suspensions.

Chapter 7 addresses the possibility of combining all waste streams into a single waste source and the potential in using soft sensor development to characterize and predict nanocellulose quality.

3.2 Recovery by flotation with colloidal gas aphrons (CGAs)

3.2.1 Materials

3.2.1.1 Pulp and paper mill effluent

The three waste streams of interest for recovery included paper machine white water from PM41, Alkaline and Acid Effluent. The location and characterization of these dilute waste streams is discussed in Chapter 4. Samples were sent from Kraft PPM containing some biocide (Busan 1064A supplied from Buckman Laboratories) to preserve the fibers on route. Once the sample were received, they were refrigerated at 4 $°C$ and used within 2 weeks. 1 L of wastewater was used for each run. The samples are removed from the fridge and left overnight to reach room temperature (25 °C) before being used.

3.2.1.2 Surfactants

The use of non-ionic surfactants to generate CGAs were investigated in this project. A synthetic surfactant, Triton X-100, was purchased from Merck for screening and optimization experiments. N-Dodecyl β-D-maltoside (DDM) was investigated as an alternative sugar-based biodegradable surfactant and was supplied from ThermoFisher (LTC Tech South Africa Pty LTD). Surfactants were used at their upper limit critical micelle concentration (CMC) values. The upper CMC limit was chosen as CGAs are more stable (measured in terms of air hold-up and half-life) at these concentrations (Jauregi and Dermiki, 2010). DDM is a sugar based non-ionic surfactant that is usually used as a foam stabilizer. The CMC of Triton X-100 and DDM is 0.2 to 0.9 mM and 0.1 to 0.6 mM respectively (Madden and Safferling, 2007).

3.2.2 Experimental setup

A flotation column with a diameter of 0.05 m and a height of 0.5 m was built for recovery experiments. A schematic of the experimental setup is shown in **Figure 20** and a photo of the actual setup is attached in Appendix C. The setup consisted of the flotation column, a homogenizer, two peristaltic pumps and two magnetic stirrers (**Figure 20**). The homogenizer was used to generate CGAs from a surfactant solution which was kept homogenized using a magnetic stirrer. The CGAs were then pumped to the base of the column by a peristaltic pump. Likewise, wastewater samples were kept agitated using a magnetic stirrer to prevent fibers from settling and then pumped to the column.

The CGAs were generated using a high-speed homogenizer (handheld PRO250, Pro-Scientific, USA). The surfactant solution was homogenized for 10 min at 10 000 rpm. After homogenization, the CGAs were kept in their homogenized state under constant stirring of 1000 rpm using a magnetic stirrer. The CGAs were pumped from this point to the base of a flotation column. Wastewater was pumped to the column from a point 0.3 m from the base of the column. A magnetic stirrer was used to ensure the fibres do not settle, and to keep the mixture as homogenous as possible.

The wastewater and CGAs pass each other in the column in a counter-current flow. The CGA bubbles rise slowly to the top as the fine fibre particles come down from the top. As the bubbles in the froth layer encounter the fibres they were carried upward by entrainment and were removed with the foamate. The wastewater was initially poured into the column until it reached just above the wastewater feed inlet. CGAs were then pumped from the bottom of the column base. Each set of experiments was run for 60 min, with the system requiring 15 min to stabilize. In the end 400 mL of the foamate and 400 mL of the tailing was collected (after being thoroughly mixed using the magnetic stirrer) to determine the amount of TSS in each.

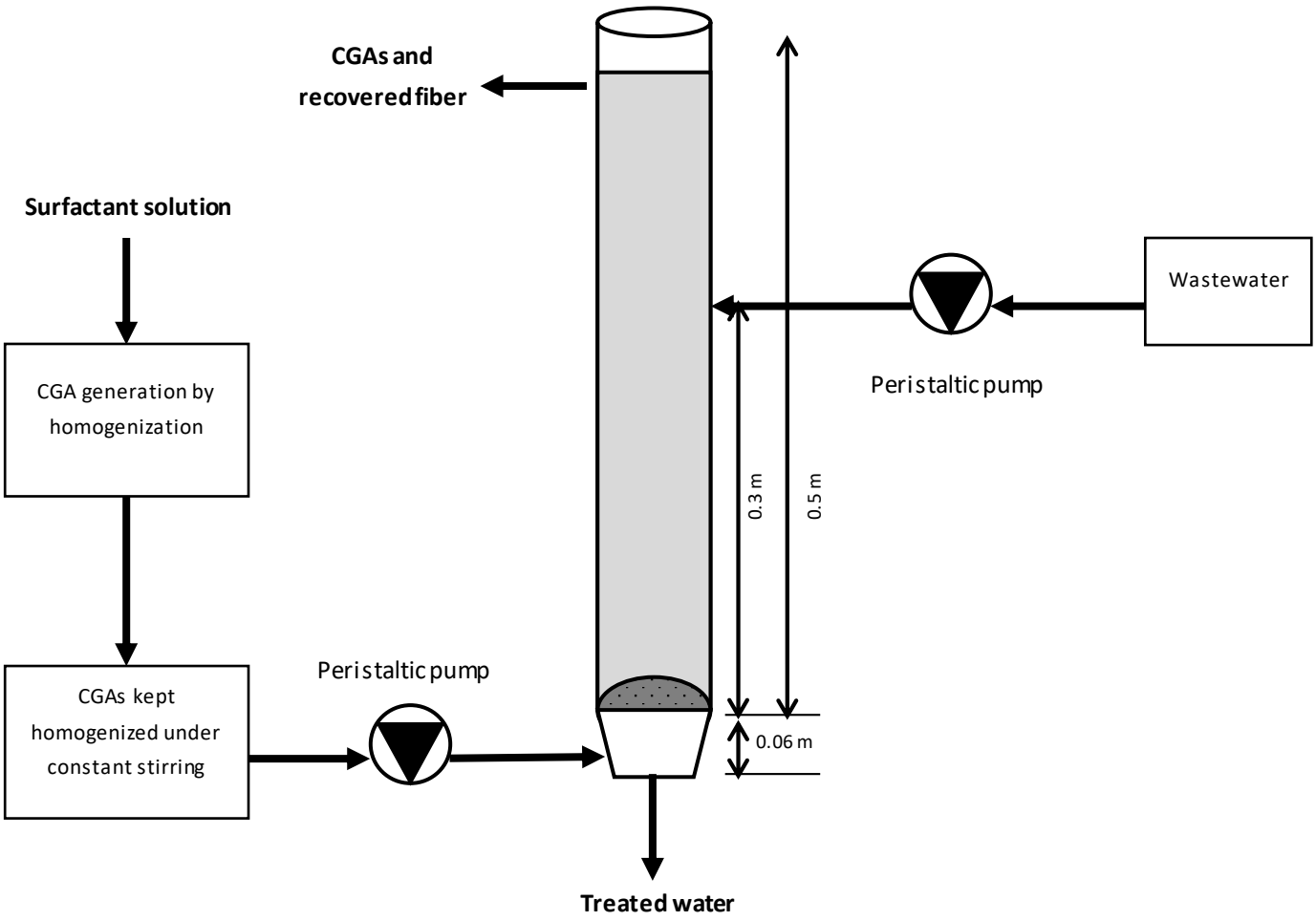

Figure 20: Schematic of experimental setup for recovery of fibres by flotation.

3.2.3 Colloidal gas aphron (CGA) characterization

The quality of CGAs produced were analysed according to the bubbles half-life and air hold-up. Stability of CGAs is the most important characteristic as it describes the bubbles' ability to maintain its structure while being pumped. To determine the air hold-up (ε) the volume of the clear surfactant solution before homogenization (V_{surf}) and the dispersion final volume after stopping stirring time at $t = 0$ of drainage (V_{CGA}) was recorded. The air hold-up is then determined by equation 28.

$$\varepsilon = \frac{V_g}{V_{CGA}} = \frac{V_{CGA} - V_{surf}}{V_{CGA}} \quad [28]$$

Where:

$\varepsilon = air\ hold - up\ of\ colloidal\ gas\ aphrons$

$V_g = volume\ of\ gas$

$V_{CGA} = final\ volume\ of\ dispersion$

$V_{surf} = volume\ of\ solution\ before\ homogenization$

After recording both V_{CGA} at $t = 0$ the CGA suspension was transferred rapidly into a 100 mL graduated cylinder. The volume of the liquid drained was then read as a function of time. An estimated time of 15 min is needed to record this. The half-life (τ) was determined from this function where 50% of the liquid has drained to the bottom, i.e., when $\frac{1}{2}\ V_{surf}$ had been reached. A schematic representation of CGA generation is shown in **Figure 21**. Schematic a) shows the clear surfactant solution before stirring or homogenization, this volume is denoted as V_{surf}. Schematic b) show the aphron dispersion volume, denoted as V_{CGA} after 10 min of stirring. This volume is the sum of the clear surfactant solution volume and the volume of gas incorporated in the mixture V_g. Schematics c) and d) show how the volume of liquid drained is read as a function of time to determine the half-life, $\frac{1}{2}\ V_{surf}$ as shown in schematic d.

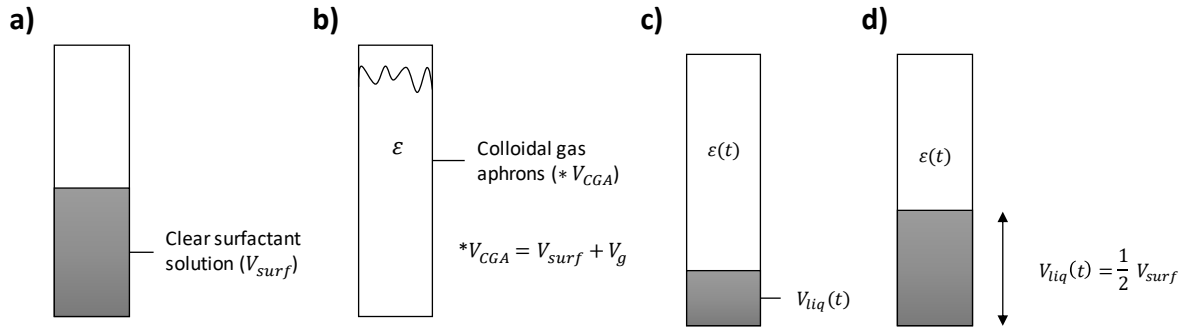

Figure 21: Schematic representation of colloidal gas aphron generation.

3.2.4 Central composite design (CCD) to optimize process parameters

The first objective of the experiment was to find the optimal operating conditions of the flotation setup using synthetic surfactant, Triton X-100. A 2^2 factorial design was considered with the two design factors being the CGA sparging rate and the wastewater flowrate to first confirm if these factors have a significant effect on efficiency. Held-constant factors are the temperature of effluent being pumped to the column, surfactant concentration and homogenization time. The design-, held-constant- and response variable are summarized in **Table 7**.

Table 7: The design-, held-constant- and response variables for flotation experiments.

Design factors	Held constant factors	Response
1. CGA sparging rate 2. Water sparging rate	1. Temperature 2. Run time 3. Surfactant concentration	1. Efficiency (%)

The factorial design was followed by a CCD experiment with 5 levels. The coded and actual values for each level are summarized in **Table 8**. The behavior of the system can be explained by a second-degree polynomial equation as given by equation 29. The regression model described by the equation is a reduced cubic model.

$$y = \beta_o + \sum_{i=1}^{k} \beta_i x_i + \sum_{i=1}^{k} \beta_{ii} x_i^2 + \sum_{i \supseteq j}^{k} \sum_{i=1}^{k} \beta_{ij} x_i x_j \quad [29]$$

Where:

$y = predicted\ response$

$\beta_0 = constant\ term$

$\beta_i = linear\ effect$

$\beta_{ii} = quadratic\ effect$

$\beta_{ij} = interaction\ effect$

Table 8: Actual values for the coded variables of 5-level central composite design (CCD) experiment.

Design factors	**Actual values for coded variables**				
	$-\alpha$	**-1**	**0**	**1**	α
A - CGA sparging rate [mL/s]	0.08	0.47	1.13	1.80	2.22
B - Wastewater flowrate [mL/s]	0.08	0.47	1.13	1.80	2.22

3.2.5 Experiments with alternative surfactant

Using the results from the CCD experiment, flotation experiments were carried out at these conditions with an alternative green surfactant, Dodecyl β-D-maltoside, to see if similar results could be achieved for each of the effluent streams identified. Seeing as the properties of each stream will vary from day to day depending on mill operation conditions, two batches were collected on different days to help explain the variance in results between samples. Experiments were performed in triplicate sets.

3.3 Functionalization of recovered fibres to nanocellulose (NFC)

3.3.1 Materials

3.3.1.1 Paper mill sludge

Sludge samples were obtained from Kraft PPM, also containing some biocide to preserve the fibers on route. Once received, samples were filtered to remove as much excess water as possible before being repackaged and frozen. Samples were then systematically freeze-dried to remove all excess moisture

without changing the morphology or chemistry of fibres. Freeze-drying or lyophilization is a physical change and is a preservation method which involves dehydrating a material at very low temperature.

3.3.1.2 Other chemicals

Ammonium dihydrogen phosphate ($NH_4H_2PO_4$) was purchased from Merck Millipore (ACS reagent grade) and urea from (≥ 98%, analytical grade) from ScienceWorld. De-ionized water was used in all reactions. Other chemicals used include sodium hydroxide pellets (≥ 97%), sodium carbonate and sugar standards (xylose, glucose, and arabinose) from ScienceWorld as well as sulfuric acid (98%) from Kimix Chemicals. All chemicals were of analytical grade.

3.3.2 Methods

3.3.2.1 Pre-treatment by phosphorylation

The method for pre-treatment by phosphorylation was developed from the four published papers available from literature (Ghanadpour *et al.*, 2015; Naderi *et al.*, 2016; Noguchi, Homma and Matsubara, 2017; Rol *et al.*, 2020). Freeze-dried fibres (1.00 g) were re-dispersed in de-ionized water to 1 wt%. Samples were then impregnated with ammonium dihydrogen phosphate (0.850 g) and urea (7.25 g) for 30 min under continuous stirring. The impregnation step was conducted at room temperature (25 °C). Three molar ratios of anhydroglucose units (AGU) to reagents were used, assuming cellulose to be the main components of the pulp fibres. Phosphorous salt and urea were added according to the ratios (1) 1:1.2:4.9, (2) 1:1.2:9.8 and (3) 1:1.2:19.6 as AGU : Salt : Urea.

After the impregnation step, fibres were dried in an oven at 105 °C overnight and then cured at 150 °C for 30 min. Some studies include a filtration step between impregnation and drying but the study by Rol *et al.* (2020) found that no filtration is better as the filtration step was found to eliminate most phosphate salt which can still react with fibres during the curing stage. Therefore, the step was omitted, and fibres were directly placed in the oven after impregnation. After curing, fibres were cooled to room temperature, re-dispersed to 2 wt% in DI water and thoroughly rinsed using vacuum filtration with boiling water and cold DI water to remove excess reagents.

3.3.2.2 Film production

After pre-treatment of fibres by phosphorylation, the washed fibres are once again re-dispersed (with DI water), this time to 0.33 wt%. The dilute fibre suspension was then mechanically treated by using a 900 W Nutribullet. Samples were blended for intervals of 30 sec for a total of 5 min, placing the suspension in a cold-water bath between runs to bring the temperature down. The aim was to determine if gel-like nanofiber suspension could be obtained after a total blending time of 5 min.

Samples that produced nanocellulose (NFC) gels were used for film production. A simple film producing method, similar to the one reported by Ankerfors (2012), was used. Briefly, gel suspensions were further diluted to approximately 0.2 wt% with DI water. The gel-suspensions were then poured into a 90 × 90 mm^2 polystyrene petri dish (purchased from Kimix Chemicals and Lab Supplies) and stirred using a magnetic stirrer for approximately 8 hours under ambient conditions. To further ensure

no trapped air bubbles remain, the NFC suspension in the petri dish was vacuum sealed in a vacuum sealable bag. The petri dish was then placed in an incubator at 45 °C and a relative humidity of 50% for 24 h.

3.4 Characterization and analytical procedures

3.4.1 Fourier Transform Infrared Spectroscopy (FTIR)

FTIR was used to identify functional groups present and determine differences in fibers at different stages in the process. The IR absorption spectra were recorded using a Bruker Alpha-P ATR-IR instrument with an analysis range of 400 to 4000 cm^{-1}. A background measurement was performed before each experimental spectrum was recorded. The peaks of spectra were compared with literature to assist in peak assignments.

3.4.2 Scanning Electron Microscopy (SEM)

SEM analyses were completed at the Central Analytical Facility of Stellenbosch University. Images of biocomposites films were captured at magnifications of 100, 50, 20, 10 and 2 μm using a Zeiss Merlin Field Emission Scanning Electron Microscope. Films were prepped for analysis prior to taking images by coating films with dimensions 1.5 cm × 1.5 cm with gold and sticking the film on a stub with double sided tape. A voltage of 3 kV was implemented under vacuum conditions.

3.4.3 Thermogravimetric Analysis (TGA)

The thermal stability of films was determined using a Mettler Toledo TGA500 analyzer. This was done by the Analytical Facility of the Process Engineering Department, Stellenbosch University. Samples were systematically heated from 25 to 800 °C with a temperature ramp of 10 °C/min and a nitrogen flowrate of 30 mL/min. An inert environment with nitrogen is used to prevent thermo-oxidative degradation.

3.4.4 X-Ray Diffraction (XRD) and Crystallinity Index (CI)

XRD was performed using a Bruker D2 Phaser X-ray Diffractometer with a monochromatic Cu$K\alpha$ radiation source (λ = 1.52184 Å, 30 kV, 10 mA) with a 2θ angle ranging from 3.99° to 40.0° (1°/min). The crystallinity index (CI) was calculated using the Segal method (Chen *et al.*, 2011) which is an empirical relationship as shown in equation 30 where $I_{2\,0\,0}$ refers to the peak intesity at 2θ = 22.5 ° and I_{am} the peak intensity at 2θ = 18°.

$$CI\ (\%) = \frac{I_{2\,0\,0} - I_{am}}{I_{2\,0\,0}} \cdot 100 \qquad [30]$$

3.4.5 Particle size and surface charge

NFC gel suspensions were diluted to <0.01 wt% and analyzed with a Malvern Nano-ZS90 Zetasizer® instrument to determine particle size, polydispersity index and the zeta potential. The particle diameters are analyzed by dynamic light scattering, measuring multi-angle particle size up to 5 μm (Malvern Instruments Ltd., 2013). Measurements were obtained at a scattering angle of 90° at a

temperature of 25 °C. Particles with a size greater than 5 μm were analyzed with a Saturn DigiSizer® II which can analyze particle within a size range of 40 nm to 2500 μm. The instrument also employs a light scattering technique and further processes data using data reduction based on Mie theory (Micromeritics Instrument Corporation, 2016).

The Zetasizer® software was used to determine the size distributions of the particles. The software also reports the polydispersity index, which is a dimensionless number ranging from 0 to 1, that is calculated form the cumulant distribution of the sample analyzed. The number gives an indication to what extent the sample is mono- or polydisperse. Samples with an index <0.08 are said to be very monodispersed whereas an index >0.7 can be said to have a broad size distribution. Zeta potential is also determined by this instrument which gives an indication to particles tendency to repel each other and thus there is no tendency to flocculate. In general, stable suspensions have a zeta potential of above 30 mV or below -30 mV.

3.4.6 Chemical composition analyses

The composition of samples was determined by using the National Renewable Energy Laboratory (NREL) Laboratory Analytical Procedure (LAP) methods for biomass. Samples were prepared according to the NREL/TP-510-42620 procedure (Hames *et al.*, 2008). The structural carbohydrates and lignin contents were determined according to the NREL/TP-510-42618 procedure (Sluiter *et al.*, 2011). Analyses were performed in duplicates.

The process consists of a two-step acid hydrolysis to fractionate the biomass into forms that can be quantified. A sample of 3.000 ± 10.0 mg is measured and transferred to a pressure tube. The weight is recorded to the nearest 0.1 mg. Next 3.00 ± 0.01 mL of 72% sulphuric acid is added to each pressure tube. Samples are then incubated for 60 minutes in a water bath set at a temperature of 30 ± 3 °C, stirring every 5 minutes. Lignin is fractionated into acid soluble and acid insoluble material. Upon completion of the incubation period the samples are removed and diluted with 84.00 ± 0.04 mL DI water. The diluted samples are sealed and autoclaved for 60 min at 121 °C and then left to cool to near romm temperature (25 °C).

Acid insoluble lignin is measured by gravimetric analysis. The acid insoluble is determined by vacuum filtering the autoclaved solution through previously weighed filter paper (medium porosity). The filter paper and residue are dried in an oven at 105 ± 3 °C until a constant weight is achieved. Equation 31 was then used to determine the amount of acid insoluble lignin. This is a simplified equation from the NREL method, since the samples in this case do not contain protein and not a significant amount of ash (concluded from the Daily Drain reports from the mill which recorded ash content far below 1%) according to the NREL/TP-510-42620 procedure. The ODW_{sample} term, oven dry weight, which corrects for moisture in samples in this case is also negligible because the samples used have been freeze-dried to remove all moisture.

$$AIL = \frac{Weight_{crucible\ plus\ residue} - Weight_{crucible}}{ODW_{sample}} \cdot 100 \qquad [31]$$

The filtrate from vacuum filtration (approximately 50 mL) of the autoclaved hydrolysis is captured and used to determine the amount of acid soluble lignin. Half of the sample is used for determination of acid soluble lignin while the other half is used to analyze the sample for structural carbohydrates. The acid soluble lignin is measured by UV-Vis spectroscopy. Equation 32 was used to determine the amount of acid soluble lignin, where $UVabs$ equals the average UV-Vis absorbance for the sample at the appropriate wavelength as specified by the NREL/TP-510-42618 procedure, $Volume_{filtrate}$ was set to a value of 86.73 mL according to the procedure followed, $Dilution$ represents the dilution factor as shown in equation 33, ε is biomass absorptivity and $Pathway$ is the pathlength of the UV-vis cell in cm.

$$ASL = \frac{UV_{abs} \cdot Volume_{filtrate} \cdot Dilution}{\varepsilon \cdot Pathlength} \cdot 100 \quad [32]$$

$$Dilution = \frac{Volume_{sample} + Volume_{diluting\ solvent}}{Volume_{sample}} \quad [33]$$

During hydrolysis polymeric carbohydrates are hydrolyzed to their monomeric forms which can be measured by HPLC. Half of the filtrate as mentioned in the preceding paragraph is used for analysis by HPLC. Prior to analyzing samples by HPLC the samples are neutralized using calcium carbonate to a pH of between 5 and 6. Samples are then decanted through a 0.2 μm filter into an autosampler vial. The cellulose content was determined by equation 34, using the glucose concentration as measured by HPLC. In the equation C_{HPLC} is the concentration of sugar in mg/mL and $\%R_{sugar}$ is the sugar recovery standard value determined by dividing the concentration detected by HPLC by the known concentration of the sugar before hydrolysis. The sugar cellulose percentage is then calculated using equation 35. The HPLC chromatograms need to be checked for the presence of cellobiose and oligomeric sugars as a concentration greater than 3 mg/mL indicates incomplete hydrolysis. In the event that the concentration of cellobiose exceeds 3 mg/mL fresh samples need to be hydrolyzed and analyzed.

$$Cellulose\ content\ \left[\frac{mg}{mL}\right] = 0.9 \cdot \left(\frac{C_{HPLC}}{\frac{\%R_{sugar}}{100}}\right) \quad [34]$$

$$\%\ Cellulose = Cellulose\ content\ \left[\frac{mg}{L}\right] \cdot \frac{Volume_{filtrate} \cdot \frac{1g}{1000mg}}{ODW_{sample}} \cdot 100 \quad [35]$$

3.4.7 Gravimetric yield

Dilute NFC suspensions with a solid content of around 0.1 wt% was centrifuged at 6000 rpm for 30 min to separate the nanofibrillated material from the non-fibrillated of partially fibrillated fractions. The nanofibrillated fibres are collected in the supernatant and placed in crucibles to be oven-dried at 105 °C for 2 to 3 hours. The gravimetric yield was defined as given in equation 36 (Noguchi, Homma and Matsubara, 2017).

$$Gravimetric\ yield\ (\%) = \frac{[supernatant\ solution\ (wt\%)]}{0.1} \cdot 100 \qquad [36]$$

3.4.8 Solubility tests

Solubility tests were done with 95% ethanol to give an indication as to the solubility of films in alcohol. This was done by cutting the film in strips with dimensions 2 cm × 2 cm and adding 30 mL of 95% ethanol in a plastic falcon tube. The weight of the film is measured before placing it in the tube. The tubes are then placed in a shaking water bath set at 25 °C for 24 hours. Afterward, samples are oven-dried at 40 °C for a day. The final weight of films is recorded. Solubility is calculated as a percentage of the film that dissolves in the solvent. The ability or inability of film solubility in alcohol influences their potential application in certain products like drug delivery (Section 6.5).

3.4.9 Film thickness

Film thickness was measured using a model 456CFSS elcometer, which is an electronic coating thickness gauge that uses the electromagnetic induction principle to measure film thickness. Before measuring the thickness of films, certified foils together with zero test plates are used to ensure the accuracy of the coating thickness gauge. At least 50 measurements were made per film to determine the average film thickness.

4 RELEVANT AND CHARACTERISTICS OF WASTE STREAMS FOR FIBRE RECOVERY FROM KRAFT PULP AND PAPER MILL

4.1 Abstract

Three sources for fibre recovery were identified from Kraft pulp and paper mill (PPM) namely (1) paper machine (PM41), (2) Alkaline and (3) Acid Effluent. The fibre reporting to PM41 Effluent resulted from a portion of white water left untreated by the mill save-all device as well as regular overflows from the paper machine broke system. These overflows occurred due to the inadequate volume of the broke system which was not large enough to contain all fibre lost from grade changes, paper machine breakdown periods and off-spec product. The fibre reporting to Alkaline and Acid Effluent resulted from "spills" or overflows in the bleaching plant as well as fibre lost during washing stages. It was theorized that these sources of waste could be categorized either into (1) continuous and (2) batch losses or (1) effluent, (2) sludge and (3) dry samples. Two batches of PM41, Alkaline and Acid Effluent samples were collected from Kraft PPM and had average size distributions of 93 ± 3.1, 72 ± 3.9 and $93\pm5.3\ \mu m$. The pH, conductivity, temperature and TSS concentration of these streams were recorded as well. The average pH concentration for PM41, Alkaline and Acid Effluent was 6.38, 10.6 and 2.23 respectively whereas the conductivity was 1276, 7010 and 7680 $\mu S/cm$ respectively. The TSS concentration of samples collected varied between the first and second batch. PM41 Effluent had TSS concentrations of 2187 and 1764 ppm, Alkaline Effluent had concentrations of 589 and 409 ppm and Acid Effluent concentrations of 257 and 227 ppm for the first and second batch respectively. It was important to determine characteristics like pH, conductivity, temperature and TSS concentrations as these variables influence colloidal gas aphron (CGA) stability and thus recovery rates during flotation. It should be noted that although the pH, conductivity and TSS concentrations are reported in this chapter, the effect these variables had on recovery rates is discussed in Chapter 5.

4.2 Introduction

On average pulp and paper mills (PPMs) lose about 1 to 3% of fiber to waste effluent streams (Boniface and Redding, 1974). A more recent literature publication by Simão *et al.* (2018) states that Kraft mills producing bleached paper generate 40 to 50 kg of sludge per ton of virgin paper product produced. The publication further states that about 70% of this sludge consists of primary sludge (i.e. a total of 28 to 35 kg of sludge per ton of product) which as discussed in Section 2.2.1 consists mostly of cellulose fibre and fillers. The loss is substantial considering that large-scale mills produce about 1.4 million ton of product per annum according to Simão *et al.* (2018) this amounts to about 39 200 ton of fiber going to waste per year if the mill produces 28 kg of sludge per ton of product. According to this ratio, Kraft PPM which produced 403790 ton of bleached pulp in a year should have produced 11306 ton of sludge. According to the fibre mass balance only 3289 ton of sludge was produced which makes the ratio 8.15 kg of sludge produced per ton of product. This is more than three times less than the amount predicted by Simão *et al.* (2018). The percentage of fibre lost according to Boniface and Redding (1974) gives a more accurate representation where if 1% of fibre fed to the mill was lost would amount to

5508 ton of sludge going to waste per annum. The true percentage of fibre lost in the case of Kraft PPM was 0.6%.

Currently, the trend in industry is to treat the biomass in wastewater treatment plants (WWTPs). The sludge from WWTPs is either incinerated or transported to landfills. Disposing the sludge to landfills is not an optimal solution as it is accompanied by many environmental hazards as well as transport and/or Capex investment costs. Furthermore, the industry needs to consider legislation on carbon emission currently being implemented in South Africa , which has stipulated polluter fines of R120 per ton of carbon dioxide emitted (Lekha *et al.*, 2017). According to (Buswell and Mueller, 1952) 1 ton of low-ash sludge theoretically releases about 2.96 ton of carbon dioxide when landfilled. Consider the Kraft PPM that produces 8.15 kg of sludge per ton of product produced, this carbon tax will amount to a fee of around R2 100 000 per annum owed, as shown in equation 37. Except for environmental and economic considerations, it is also a waste of valuable fibers that can be used as a resource for producing a range of alternative high-value products.

$$\frac{0.00815\ ton\ sludge}{ton\ pulp} \cdot \frac{2.96\ ton\ CO_2}{ton\ sludge} \cdot \frac{720\,000\ ton\ pulp}{annum} \cdot \frac{R120}{ton\ CO_2} \approx R2\ 100\ 000/annum \qquad [37]$$

Thus, for environmental, as well as economic reasons, it is essential to minimize the amount of sludge and/or find suitable methods for developing alternative products from sludge that is produced. This chapter describes sources and characteristics of waste in the Kraft mill operation and ways to categorize the various sources. In the end, it is discussed whether it is feasible to combine all the sources into a single waste source for value addition purposes.

4.3 Methodology for identifying the sources of fibre loss in a Kraft pulp and paper mill

The Kraft process consists of a relatively uniform process scheme, which makes it possible to contextualize results from a single mill. In order to gain a better understanding of the Kraft pulping process a mill visit was arranged before starting the project. To further identify and evaluate sources where fibre is lost in the Kraft pulping process, it was necessary to collect certain basic mill data. First accurate diagrams showing the various mill operations of Kraft PPM and flow of materials throughout the mill were obtained. The collection of information needed to identify waste sources entailed much time spent in the tracing of water and stock lines, investigating the details of certain processing equipment (as discussed in Section 2.2) as well as interviewing operating personnel and site engineers. Following the development of process flow diagrams, it was necessary to obtain an accurate sewer layout. For those unfamiliar with PPMs, it should be pointed out that the sewer systems of PPMs are usually quite complex consisting of an intricately branched network of drains (Savage and Koch, 1950). According to Savage and Koch (1950) older mills are especially tedious to investigate as sewer systems here were not designed for investigative purposes. The Kraft PPM that was investigated for this project however did not have this problem and an up-to-date sewer layout was easily obtained.

The next step was to obtain basic mill data. The task involved determining the characteristics and amount of waste containing fibre that is discharged. Samples (2 L from each waste stream) were taken

from the effluent and physical measurements such as conductivity and pH and temperature were made. The conductivity and pH were measured in the lab using standard equipment whereas the temperature was recorded in the field. Measurements were made for two separate batches, taken on different days, when mill operation was considered stable. These batches are referred to as Batch 1 and Batch 2. The results can be found in Section 794.4.1 (**Table 10**). The conductivity of effluent streams was only determined for Batch 1 as the instrument used to measure conductivity was unfortunately unavailable when the second batch was collected. Information about the TSS concentration in the respective waste streams was obtained from the mill's daily drain reports. The information is recorded in **Table 10** for Batch 1 and 2. The mill's daily drain report also contains the field pH measurements of acid and alkaline effluent streams. A year's worth of data was obtained for the TSS and pH values to obtain an average, minimum and maximum which is summarized in Section 794.4.1 (**Table 11**). The TSS values were also used to perform the fibre mass balance as discussed in Section 2.2. The mass balance gives an indication of how much fibre goes to waste annually.

Knowledge of the pulp and papermaking process was also needed to gain a better understanding of the physical and functional properties of the cellulosic fibers. This was done by consulting literature about the Kraft process in general (Section 2.3.3) and studying chemistry involved during delignification and bleaching sequences (Section 2.3.4 and 2.3.5). As discussed in Section 1.3 the mill investigated, Kraft PPM, has a hardwood and softwood line but only the hardwood line is of interest in this project. The process flow diagram of the entire Kraft PPM is shown in **Figure 22** with the route of interest shown in orange text. PM41 refers to the paper machine processing most of the fully bleached hardwood pulp whereas PM42 refers to the paper machine processing unbleached softwood and a portion of the fully bleached hardwood pulp. The ratio of fully bleached hardwood pulp sent between PM41 and PM42 is clearly shown in the mass balance in Appendix A.

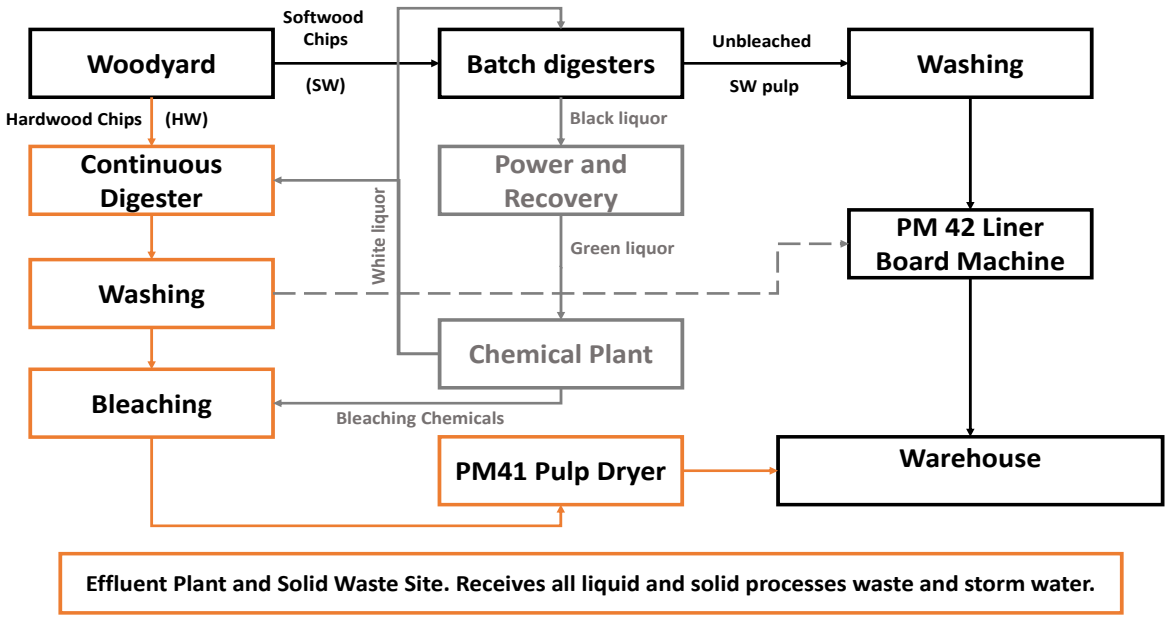

Figure 22: Process Flow Diagram of Kraft pulp and paper mill.

The bleaching sequence used by the mill is a four stage ECF DualD™ process which is a patented chlorine dioxide bleaching process. A summary of the four stages is given in **Table 9**. Like described in Section 2.3.5.4 the process combines a traditional chlorine dioxide bleaching process with a hot acid treatment, usually sulphuric acid, in the first reactors (Dual D stage in **Table 9**). The chlorine dioxide provides the bleaching action while the sulphuric acid treatment attacks HexA groups before being removed in an alkaline extraction step (OP stage in **Table 9**) in the second reactor. The final two stages use chlorine dioxide as a final bleaching stage (D1 and D2 stages in **Table 9**). As described in Section 2.3.3.2, to increase brightness to values of around 90% ISO two further chlorine dioxide stages are needed or alternatively a combination of chlorine dioxide and hydrogen peroxide stages.

Table 9: The four stage ECF DualD™ bleaching sequence used by Kraft pulp and paper mill.

Stage number	Stage name	Description	Chemicals used
1	Dual D[1]	Pre-bleaching with chlorine dioxide	ClO_2 and H_2SO_4
2	OP[2]	Pressurized alkaline extraction	$NaOH$, H_2O_2 and O_2
3	D1[3]	Final bleaching stage with chlorine dioxide	ClO_2
4	D2[4]	Final bleaching stage with chlorine dioxide	ClO_2 or H_2O_2

[1] D-stage bleaching with "dual" action due to addition of H_2SO_4. [2]Combined O-stage and P-stage bleaching. [3]First of two brightening stages with chlorine dioxide (i.e., D-stage). [4]Final brightening stage with chlorine dioxide.

4.4 Results and discussion

The three sources of fibre loss according to literature, as stated in Section 2.2, were confirmed by completion of a fibre mass balance around the hardwood line of Kraft PPM. A simplified version of this mass balance is given in **Figure 23** and demonstrates to what extent fibres were lost in reported effluent streams. The full mass balance is reported in Appendix A. The mass balance was completed by using data extending over the period of a year from the daily mill reports of Kraft PPM from September 2020 to September 2021. **Figure 23** reports that 550867 Adt/year (Adt is the air dry ton of pulp product where the weight of the pulp product is corrected to reflect the weight that the pulp product would be if the pulp were composed of 10% water and 90% fiber) was fed to the digester which produced 403790 Adt/year of product, i.e. fully bleached hardwood pulp from *Eucalyptus globulus*. The amount of fibre was reported as air dry ton of pulp product (Adt) where the weight of the pulp product is corrected to report the weight that the pulp product would be if the pulp were composed of 90% dry solids content and 10% water (Isaksson *et al.*, 2016).

A total of four losses were reported by the mass balance. The loss of 72540 Adt/year from the digester was due to alkaline hydrolysis which leads to the dissolution of lignin and hemicelluloses and partial dissolution of cellulose as stated in Section 1.1. The losses reported in the bleach plant refer to alkaline and acid effluent lines which contained fibre from various bleaching and washing stages. Losses of 585 and 658 t/year (dry weight) were reported. The final loss was the portion of whitewater left untreated by the save-all device from the paper machine. The loss as reported in the mass balance in **Figure 23**

was 2046 t/year. It can thus be seen that the type of losses reported from the mass balance correspond with those identified from literature.

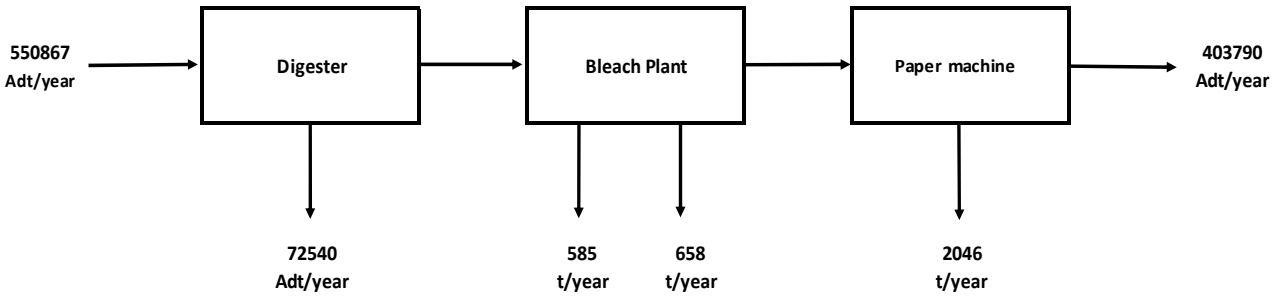

Figure 23: Kraft pulp and paper mill hardwood line fibre mass balance.

The amount of fibre from PM41 was almost double the amount lost in Alkaline and Acid drains together. The reason for this major difference was determined by interviewing operating personnel and site engineers and was related to various events occurring from the paper machine including (1) grade changes, (2) breakdowns and (3) off-spec product. A grade change, discussed in detail in Section 1.1, refers to a quality change on a paper machine. A paper machine breakdown refers to an unplanned shutdown and off-spec product to product that fails to meet the applicable quality specifications. These events occur often as the paper machine delivers the final product and quality control at this stage of the process is severe. When these three events occur, fibre is disposed of by washing or "dumping" it into the broke system situated below the paper machine (Section 1.1). The problem lies in the capacity or volume of the broke system according to the site engineers interviewed. When too many of these events occur and the broke system reaches its maximum capacity, white water containing much of the fibre from the broke system starts to overflow into PM41 drains. The broke system also does not cover the entire area of the paper machine and some of the product flows directly into PM41 Effluent. This overflow from the broke system was consequently the reason for most of the reported fibre present in PM41 drains. A smaller, but still considerable, amount of fibre is lost from the portion of white water left untreated by the save-all device which is installed to clarify white water for re-use in the process as discussed in Section 2.2. The treated white water is re-used in the process while the untreated portion is disposed of in PM41 effluent. As mentioned in Section 2.2, save-all devices usually have an efficiency between 33 to 90% (Khan et al., 2017). The efficiency could be improved by installing another save-all device in series with the current device although a cost-benefit analysis would need to be done to determine if such an investment would be worthwhile.

According to the site engineers of Kraft PPM, grade changes occur often and significantly contribute to PM41 fibre loss. This reported loss agrees with literature as, according to Viljamaa et al., 2001, nowadays paper machines have at least one grade change per day. On average these paper machines may produce up to 300 000 ton of paper per year (Viljamaa, Peltonen and Koivo, 2001). According to Yeo *et al.* (2005) a grade change takes approximately 15 min. Grade changes are completed in as short a time as possible to minimize machine downtime. Assuming a paper machine that produces this

amount of product (i.e., 300 000 ton of paper per year) this amounts to around 571 kg of paper being produced per minute. Assuming a grade change that takes 15 min, occurs once a day for 365 days, this adds up to 8562 kg of product lost during a grade change per day.

From inspection of the mill during the visit referred to in Section4.3, the losses reported in the Alkaline and Acid Effluent (585 and 658 ton per year) resulted from "spills". These spills can be seen in various locations of the mill as shown in **Figure 24**.

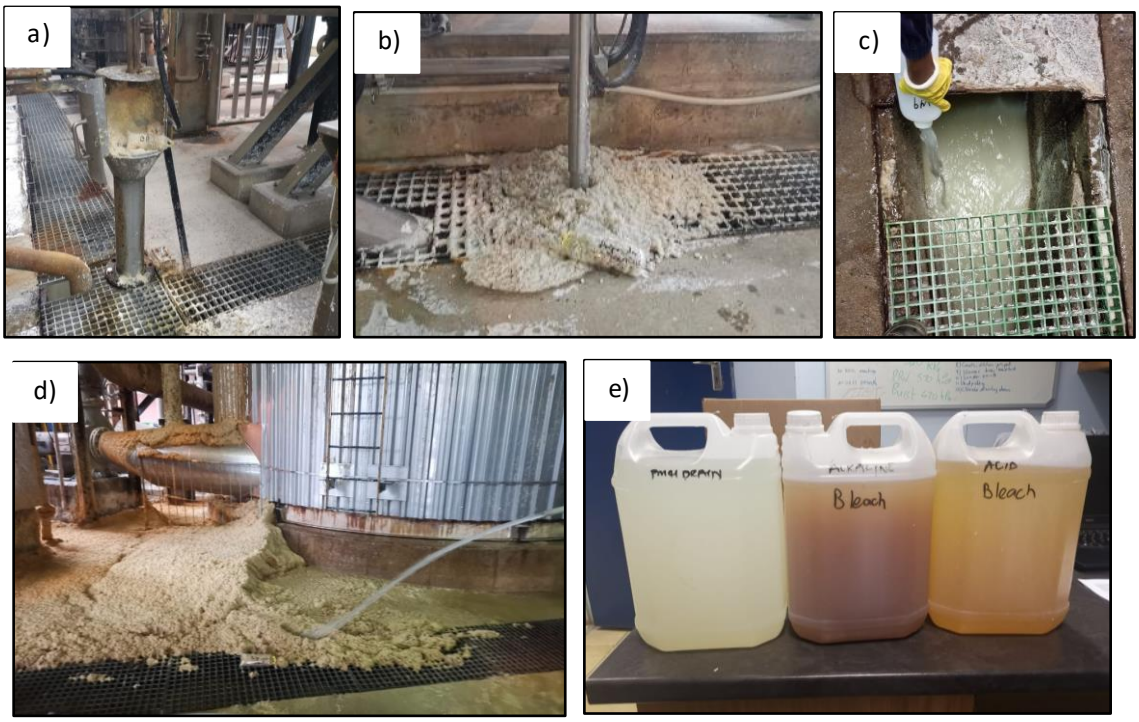

Figure 24: Sources of fibre waste from a Kraft pulp and paper mill a) sampling point spill, b) spill from drain valve or corroded pipe leak c) paper machine drain containing 'white water', d) tank overflow and e) collected samples from drains (left to right: PM41, Alkaline and Acid Effluent).

The first image (**Figure 24** a) shows a sampling point from which pulp is collected and taken to the lab to be analyzed. These sampling points are located throughout the mill, notably after the washing stage of each bleaching stage. Other spills occur between stages from either drain valves that have been opened or leaking pipes (**Figure 24** b). Drain valves are situated along the pipe network in the event of a process upset in which case the product needs to be drained. Pulp can also cause plugging or clogging in pipes and in the event of this happening drain valves are used to unclog pipes resulting in fibre loss as shown in **Figure 24** b. Pipe leaks occur due to corrosion which is not an uncommon problem in the pulp and paper industry as the piping is exposed to extreme corrosive environments in almost all applications (Moskal, 2018). These leaks can more accurately be referred to as gasket leaks. A gasket is a mechanical component that provides a tight seal between surfaces thus preventing leakage from the joined sections of piping. Corrosion damages the gasket over time resulting in the same source of fibre loss as events in which drain valves are opened (**Figure 24** b).

Figure 24 c) shows white water from the PM41 drain which is where the PM41 Effluent samples were collected as discussed in Section 3.2.1.1. **Figure 24** d) shows an event related spill where, in this case, the breakdown of a pump led to the overflow of a tank upstream. Tank overflows can also be caused by other operational issues like e.g., faulty, or offline tank level sensors. The resultant spills are sprayed into Alkaline or Acid Effluent drains depending on the location of the spill. It is possible to minimize fibre loss from spills by ensuring proper maintenance of pumps and that every working pump has a back-pump in working condition. Spills can further be minimized by improving process control around the process. **Figure 24** d) shows the effluent that was collected where the container on the left contains PM41 Effluent, the middle container Alkaline Effluent and the container on the right Acid Effluent.

According to literature, as stated in Section 1.1, fibre losses occur during screening and washing stages (Brogdon, 2015). This source of fibre loss also occurred in the Kraft PPM, especially during the bleaching sequence where each stage is followed by a washing stage (Section 2.3.3.2). It was however difficult to quantify exactly how much fibre was lost as the efficiencies of the screening and washing equipment were unknown and thus contributed an unknown amount of fibre to the total 585 and 658 ton of fibre per year for Alkaline and Acid Effluent.

It is possible to predict the efficiency of washing stages using equations like those developed by Kumar, Kumar and Singh (2010), Dahl (2011), and Potůček and Rahman (2019). These equations assume that pulp washing is a solid-liquid extraction process (Section 2.2) and according to this assumption the equations are described in terms of a displacement ratio and a Norden efficiency factor (Kumar, Kumar and Singh, 2010; Dahl, 2011). The equation predicting efficiency is derived from a model where each stage in pulp washing is treated as a black box. The model is based on a material balance and expresses the efficiency of a washing stage in terms of performance parameters such as the equivalent displacement ratio and Norden efficiency factor. The study by Potůček and Rahman (2019) developed a more complex equation to investigate the influence of wash liquid temperature on displacement washing. An axially dispersed plug flow model including one dimensionless criterion, the Péclet number, was used to determine the wash yield. Studies like the one by Potůček and Rahman (2019) show that it is possible to improve the efficiency of washing stages by controlling the wash liquid temperature. The calculation and improvement of washing yields however fall outside the scope of this project and were thus not considered further.

It was possible to collect the fibres losses described in this section from PM41, Alkaline and Acid Effluent drains before these fibres were sent to the WWTP of the Kraft PPM where sludge would normally have been dewatered and transported to landfill or incinerated. For this study the effluent was collected separately from PM41, Alkaline and Acid Effluent drains. In the case of Kraft PPM these effluent streams do not merge into a combined sources or a single combined waste stream. The possibility of combining these three waste streams is discussed in Chapter 7. The sources of waste described in this section were categorized (Section 4.4.1) and characterized according to particle size distribution (Section 4.4.2), composition (Section 4.4.3) and functional groups (Section 4.4.4). The particle size distribution was determined using a Saturn DigiSizer® instrument as described in Section

3.4.5. The composition of fibres was determined according to the NREL method as summarized in Section 3.4.6 and the functional groups were determined using FTIR as described in Section 3.4.1.

4.4.1 Categorization of waste sources

A summary of waste sources identified in Section 4.4 and their location in the Kraft PPM is given in **Figure 25**. All samples were collected from either the bleaching or the paper machine section of the mill which is why only these stages are shown in **Figure 25** which represents part of the process flow diagram presented in **Figure 22**. According to the waste sources identified in Section 4.4 it was theorized that fiber losses can be divided into two categories, namely continuous and batch losses. The former consists of (1) spills from sampling points (**Figure 24** a), (2) fibre loss from screening and washing stages (3) the portion of white water not treated by save-all devices which reports directly to the PM41 drain (**Figure 24** c), and (4) paper machine trimmings. The latter consists of (1) broke system overflow which are caused by grade changes, paper machine breakdown and off-spec product as described in Section 4.4, (2) event related spills leading to tank overflows (**Figure 24** d) and (3) spills from drain valve openings or leaking pipes (**Figure 24** b).

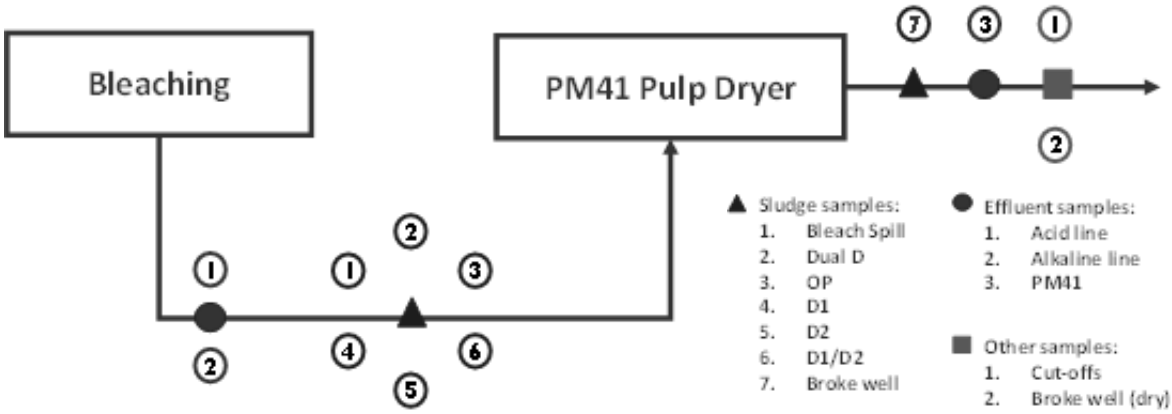

Figure 25: Summary of waste sources identified and categorized as effluent, sludge and dry samples.

Another way fiber loss can be categorized is according to the water content samples contained. There were effluent samples which are very dilute streams, sludge samples that are dewatered to an extent and dry samples. It was easier to refer to samples in this manner when referring to the types of samples collected from Kraft PPM and subsequently this categorization system was used in this document. Sample locations as shown in **Figure 25** were grouped according to this categorization system (effluent, sludge and dry samples). The three effluent streams were referred to as PM41, Alkaline and Acid Effluent and their location in the mill is indicated by a circle symbol in **Figure 25**. PM41 includes fibre loss from the portion of whitewater not treated by save-all devices (referred to as a continuous loss previously) and the broke system overflow caused by too many occurrences of grade changes, paper machine breakdown and off-spec product (previously referred to as a batch loss). The sludge samples, as indicated by a triangle symbol in **Figure 25**, were collected from what is referred to as Bleach Spill, Dual D, OP, D1, D2, D1/D2 and Broke well. The dry samples are referred to

as Cut-offs and Broke Dry samples and their location in the mill is indicated by a square symbol in **Figure 25**.

The sludge samples listed in **Figure 25** are mostly from sample point spills in the bleaching plant (**Figure 24** a). Exceptions are Bleach Spill samples which came from the oxygen delignification plant and Broke Well samples which came from the paper machine broke system as the name implies. The sample names Dual D, OP, D1 and D2 are given according to respective bleaching stage acronyms as stated in **Table 9**. The bleaching sequence progresses in this order i.e., Dual D, OP, D1 and D2 as discussed in Section 4.3. The change in color of samples as the bleaching process progresses is shown **Figure 26** except for the first sample on the left which is from the broke system (Broke Well samples). From left to right the samples are Broke Well, Bleach Spill, Dual D, OP, D1, D1/D2 and D2.

Figure 26: Freeze-dried fibre showing the difference (from left to right) in pulp color as bleaching progresses. From left to right: Broke Well, Bleach Spill, Dual D, OP, D1, D1/D2 and D2.

Sample D1/D2 was located on a deck between the two stages D1 and D2 as the name. The loss of fibre was due to a process upset and consequently a drain valve was opened to drain the product (**Figure 24** b). The Bleach Spill sample occurred from an overflowing tank prior to the start of the bleaching sequence due to a defoamer pump not working (**Figure 24** d). The sample referred to as Broke Well is from the wet-end paper machine section that ended up in the broke system. All sludge samples from the bleaching plant i.e., Bleach Spill, Dual D, OP, D1, D1/D2 and D2 end up in either Alkaline or Acid sewers. The composition of Alkaline and Acid Effluent was thus a mixture of these sources of fibre loss as well as an unknown amount from washing stages depending on the efficiency as discussed in Section 4.4. Accordingly, the composition and amount will vary from day to day depending on mill operation and the process control exercised to prevent fibre losses like overflows and spills.

The dry samples listed in **Figure 25** collected from the Kraft PPM are referred to in this document as Cut-offs and Broke Dry. The samples referred to as Cut-offs were collected from the paper machine trimmings (location shown in **Figure 25**). In the final stage when pulp blocks are cut, the edges are discarded. These trimmings or cut-offs are normally washed off into PM41 sewers but for the purpose of this project the samples were recovered in their dry form to determine if the characteristics of nanocellulose produced from Cut-offs differ compared to the results of nanocellulose material obtained from D2 which is the sludge equivalent of Cut-offs before being subjected to drying in the final stages of the paper machine section. This is of interest because, as mentioned in Section 2.4.4,

according to Desmaisons *et al.* (2017), the quality of NFC produced from never-dried pulp is around 10% higher than that of dried sample forms.

The sample referred to as Broke Dry (location shown in **Figure 25**) is from the dry end of the paper machine section that ended up in the broke system. As for Cut-offs and D2, it was of interest to compare the difference in the properties of nanocellulose produced from Broke Well sludge and the equivalent dried form Broke Dry. The broke system, as explained in detail in Section 1.1, 2.2 and 4.4, refers to the partly or fully manufactured paper or board that is discarded. A broke pit or well is situated below the paper machine into which broke or semi-manufactured product is disposed from the machine floor (Vector Solutions, 2021b). This section of the broke system, (i.e., the broke well) extends to a dry end re-pulper where fully manufactured (i.e., dry fibre) is deposited into.

4.4.2 Particle size distribution of fibres from waste streams

The particle size range for effluent sources (i.e., PM41, Alkaline and Acid Effluent) is shown in **Figure 27**. As mentioned in Section 4.4.1 PM41 Effluent was a mixture of fibre loss from the portion of white water left untreated by save-all devices and overflows from the broke system. Alkaline and Acid Effluent on the other hand comprised of a varying mixture of sludge samples referred to as Bleach Spill, Dual D, OP, D1, D1/D2 and D2 as well as fibre lost during washing stages between each bleaching stage. More than 60% of particle diameters fall in the range of 0 to 100 μm (**Figure 27**). The size distribution observed makes flotation an ideal recovery method as the process most effectively removes particles between 10 to 200 μm according to (Wakeman, 2011) and more than 90% of particles fall within this range for all three effluent types. The mean particle size for PM41, Alkaline and Acid Effluent is 93 $\pm$ 3.1, 72$\pm$ 3.9, and 93 $\pm$ 5.3 μm respectively.

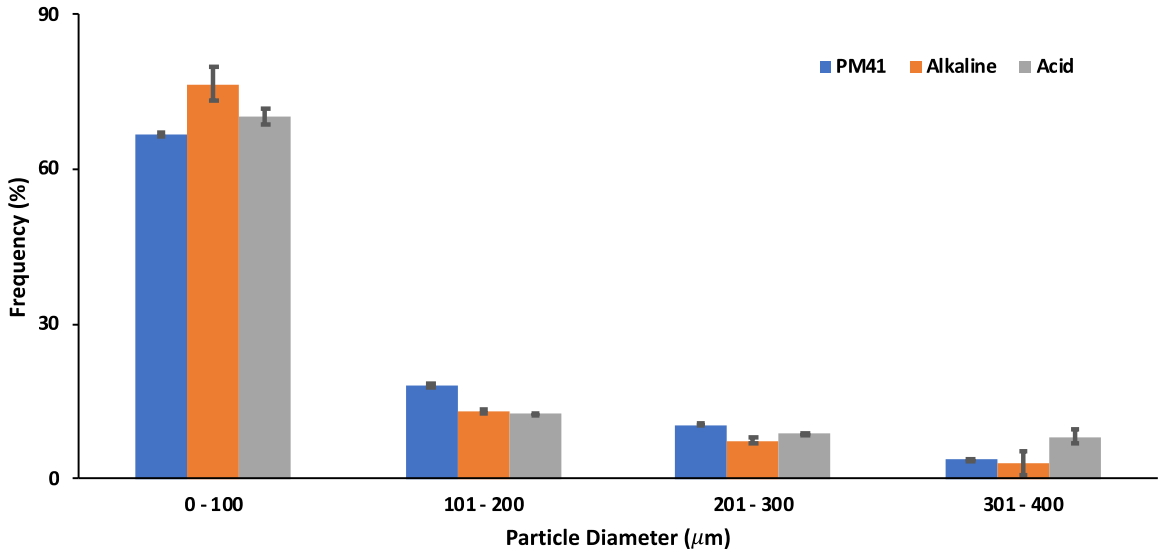

Figure 27: Particle size classes for pulp and paper mill effluent samples from Kraft pulp and paper mill. Error bars represent the standard deviation with a 95% confidence interval.

According to Boniface and Redding (1974) a major portion of the fibres lost in waste streams are short fibres with an average length shorter than 0.1 mm, which confirms the results shown in **Figure 27**

which indicate that more than 60% of fibres are shorter than 0.1 mm or 100 µm. The largest fibres from PM41, Alkaline and Acid Effluent are reported in the class size of 301 to 400 µm and thus according to Wolfer et al. (1997) these fibres are not suitable for re-use in the papermaking process. According to Wolfer et al. (1997) these fibres are not re-used in the process because short fibres with a length of less than 1 mm will not be retained by the Fourdrinier wires of a paper-making machine. Short fibres are also undesirable for re-use in the process as they give a slow draining characteristic to the paper machine furnish and this negatively affects the speed and capacity of the paper machine (Boniface and Redding, 1974). Even though these fibres are not suitable for re-use in the process they are suitable for other application like functionalization to nanocellulose.

4.4.3 Composition of fibres from waste streams

The composition of the effluent streams (PM41, Alkaline and Acid Effluent) differs quite substantially in terms of pH, conductivity, temperature and TSS concentration as can be seen in **Table 10**. The average, minimum and maximum values for pH and TSS, determined from a years' worth of data from the mill's daily drain reports as explained in Section 4.3, are summarized in **Table 11**.

When observing the pH values in these tables, it can be seen that the variation between samples PM41, Alkaline and Acid differs substantially with the average pH for PM41, Alkaline and Acid Effluent being 6.38, 10.6 and 2.23 (note that this is the average pH of samples collected from Batch 1 and Batch 2 in **Table 10** and not **Table 11**). The variation between the batches of samples collected i.e., Batch 1 and Batch 2 however does not differ substantially, with the pH for PM41 being 6.34 and 6.42 for Batch 1 and Batch 2 respectively (**Table 10**). Likewise, the pH for Alkaline was 10.88 and 10.37 for Batch 1 and 2 compared to Acid Effluent with pH values of 2.11 and 2.35 for Batch 1 and 2 respectively. Regarding conductivity, PM41 Effluent had the lowest conductivity at 1276 $\mu S/cm$ while the other two effluent streams have high conductivities around 7000 $\mu S/cm$ (**Table 10**). The pH and conductivity values of the waste streams were important to record as these variables influence colloidal gas aphron (CGA) stability during flotation (Jauregi, Gilmour and Varley, 1997; Feng, Singhal and Swift, 2009; Zhao *et al.*, 2018; Akhlaghi and Riahi, 2019). This is discussed in more detail in Section 5.5.4.

The temperatures of PM41, Alkaline and Acid Effluent were all above 40 °C (**Table 10**). This is important information to report because as discussed in Section 2.2.3.2.2 the stability of CGAs is temperature dependent and temperatures of below 40 °C are necessary ensure these microbubbles remain stable. Thus, when considering the required conditions for flotation with CGAs on industrial scale it would be important to ensure that the effluent streams are cooled to temperatures below 40 °C before recovery by flotation. For experimental purposes the temperature was kept a constant factor as mentioned in the Research Design and Methodology (Section 3.2.1.1) with samples being allowed to reach room temperature before being used.

From **Table 10**, the TSS concentrations between Batch 1 and Batch 2 differs considerably for Alkaline Effluent (589 and 409 ppm) only slightly for PM41 Effluent (2187 and 1764 ppm), and not significantly for Acid Effluent (257 and 227 ppm). The deviation between samples is 30.6, 19.3 and 11.7% for each of the effluent streams respectively. The efficiency of flotation was determined in terms of TSS

(Section 5.3). Although this efficiency was determined in terms of the TSS concentration of the concentrate and tailings, it was still useful to have a reference point and it was found that the initial TSS concentration in the feed played an important role in recovery of fibre by flotation with CGAs. This is discussed in more detail in Section 5.5.4.

From **Table 11**, the average values for Acid and Alkaline Effluent is 3.34 and 9.90 respectively. According to the data received from the mill there are days when the Acid Effluent pH reaches 12.9 and the Alkaline Effluent a pH of 4.10. These values were verified by the mill operators who reported that there are cases where sludge spills (as specified in Section 4.4.1) are washed in the opposing drain (i.e. alkaline spills washed into Acid Effluent drains and vice versa) depending on the location of the spill and the closest drain.

Table 10: Process drain effluent characterization of samples ordered from Kraft pulp and paper mill according to pH, conductivity, temperature, and total suspended solids (TSS).

	Sample	pH	Cond (μS/cm)	Temp ($^{\circ}C$)	TSS (ppm)
Batch 1	**Acid Effluent**	2.11	7680	71	257
	Alkaline Effluent	10.88	7010	46	589
	PM41 Effluent	6.34	1276	49	2187
Batch 2	**Acid Effluent**	2.35	-	65	227
	Alkaline Effluent	10.37	-	50	409
	PM41 Effluent	6.42	-	40	1764

Table 11: Average process drain effluent characterization of waste streams from Kraft pulp and paper mill according to pH and total suspended solids (TSS).

Sample	pH			TSS (ppm)		
	Average	Min	Max	Average	Min	Max
Acid Effluent	3.34	1.13	12.9	52.6	3.67	890
Alkaline Effluent	9.90	4.10	11.8	93.8	3.00	627
PM41 Effluent	-	-	-	868	12.5	4466

The chemical composition of recovered fibres was determined according to the NREL method described in Section 3.4.6. The results are summarized in **Table 12**. None of the samples contained cellobiose concentrations greater than 3 mg/mL which indicates there was complete hydrolysis (Sluiter *et al.*, 2011). **Table 12** shows that the cellulose content remains relatively constant throughout the bleaching sequence, which indicates that the cellulose is not severely degraded during the bleaching sequence.

Table 12: Chemical composition of pulp and paper mill sludge samples. Reported on a dry weight basis.

	Broke Dry	Broke Well	Bleach Spill	Dual D	OP	D1	D1/D2	D2	Cut-offs
Cellulose (% w/w)	54.2	61.5	55.7	58.2	63.2	57.6	63.9	65.3	64.7
AIL (% w/w)	12.4	16.4	5.50	6.00	1.70	2.80	2.90	3.50	1.44
ASL (% w/w)	3.03	2.86	2.34	2.31	2.28	2.43	2.56	2.52	2.78
Total lignin (% w/w)	15.43	19.26	7.84	8.31	3.98	5.23	5.46	6.02	4.22

The values obtained for cellulose and lignin concentrations are similar to other studies that analyzed virgin pulp samples according to the NREL method. A study by Bester (2018) found that virgin pulp samples obtained cellulose and lignin concentrations of 61.2% and 15.3% respectively while a study by Chimphango (2020) obtained values 47.2% and 18.5% respectively. In **Table 12**, the acid insoluble lignin (AIL) values generally decrease as the bleaching sequence progresses, but that acid soluble lignin (ASL) remains relatively constant with an average of 2.57%. The results indicate that ASL is not removed by further bleaching of samples but that only the remaining AIL is subsequently removed as the bleaching sequence progresses.

Xylose and arabinose sugars were not detected by HPLC, which shows that at this stage of the process, most of these sugars have been degraded and removed along with lignin during the cooking stage in the digester and further during delignification using oxygen before the bleaching stages. It was expected that arabinose sugars would not be present in samples as literature values report that conventional Kraft cooking results in a loss of around 80% of this sugar and consequently concentrations of around 0.1 to 0.3% w/w are left after pulping (Zanão *et al.*, 2019). It was however expected that xylan concentrations would be around 8 to 13% w/w which are average values reported from literature (Santiago and Neto, 2008; Zanão *et al.*, 2019). The study by Santiago and Neto (2008) reported that Eucalyptus globulus wood before being processed had a xylose concentration of 15% w/w. The final concentration of xylose reported after conventional Kraft cooking was 8.8% w/w. Similarly a xylose loss of 40.2% was reported by Zanão *et al.* (2019) for standard Kraft pulping which resulted in the concentration of xylose being 13.3% after pulping. This is an anomaly that should be investigated further. Ash and extractives were not determined.

4.4.4 Functional groups and structure of fibres from waste streams

Figure 28 shows FTIR analysis of all sludge samples. As expected, the functional groups present are the same for all samples but to varying degrees. A summary of IR spectra assignment is given in Appendix D. The IR spectra of lignin has a strong wide band between 3200 to 3650 cm^{-1}. These bands are assigned to O-H stretching vibrations caused by the presence of alcoholic and phenolic hydroxyl groups involved in hydrogen bonds. Peaks that appear between 2835 and 2938 cm^{-1} are also associated with lignin and represent aromatic methoxy groups and methylene side chains in lignin molecules. Other narrow peaks associated with lignin include peaks present between 1640 and 1650 cm^{-1} as well as between 1422 and 1430 cm^{-1} which are assigned to water present in lignin and C-H

asymmetric deformation in lignin respectively. However, peaks present between 1420 and 1442 cm^{-1} can also represent the crystalline structure of cellulose, specifically CH CH_2 and OCH bending vibrations.

The IR bands in **Figure 28** showed that the peak heights between 1200 and 3650 cm^{-1}, which are assigned to lignin, decreased clearly between samples in the following order: Broke Dry, Broke Well, Bleach Spill, Dual D, OP, D1, D1/D2, D2 and Cut-offs. This is expected as this is the order in which samples are located as the bleaching sequence progresses, from Bleach Spill to D2 and then the final product Cut-offs. Broke Dry contains the most lignin and Broke Well the second most which makes sense because these samples were discarded early in the process. In the same way the crystalline structure of cellulose indicated by the peak at 1430 cm^{-1} decreases.

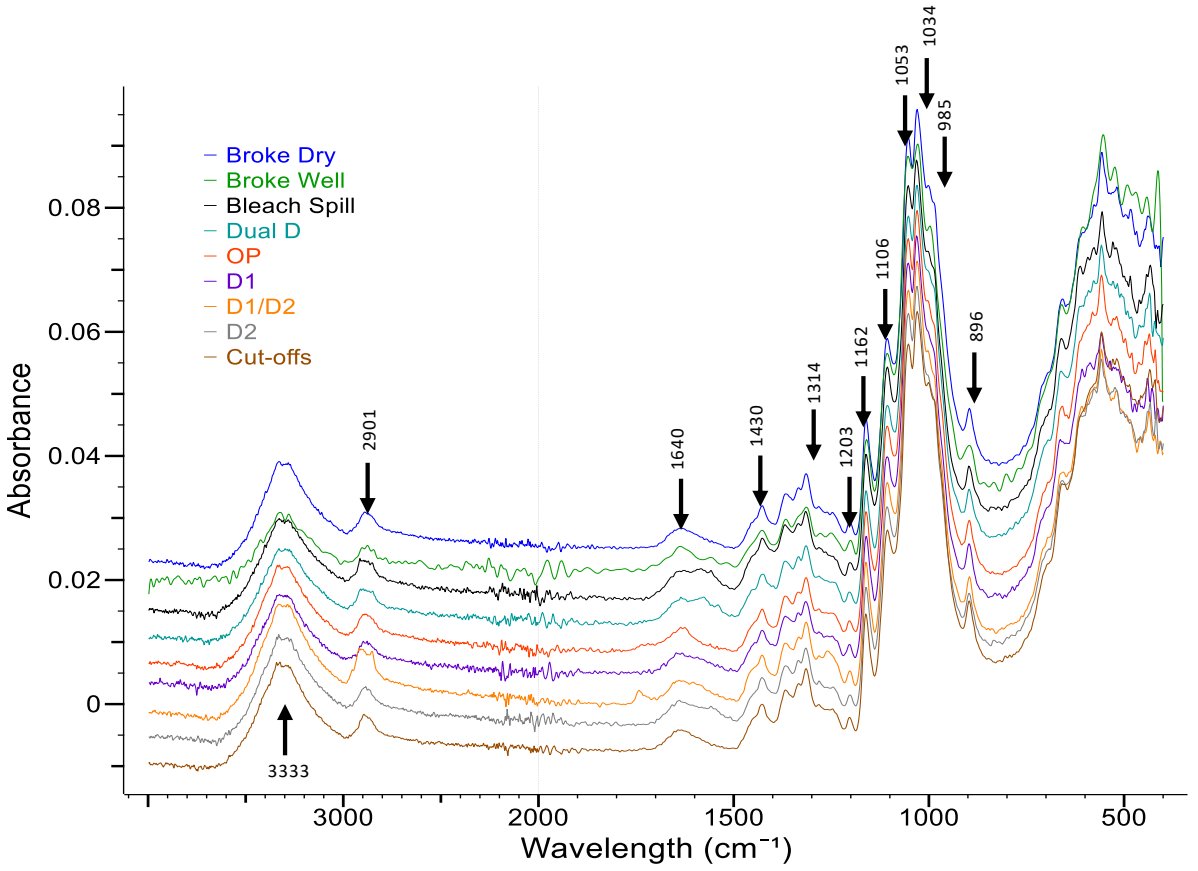

Figure 28: FTIR analysis to determine functional groups of sludge samples from Kraft pulp and paper mill before treatment by phosphorylation.

The IR spectra further confirmed the presence of characteristic bands of cellulose, like peaks between 1120 and 1165 cm^{-1} which are characteristic bands of cellulose chains, specifically C – O – C groups from glycosidic units or from β-(1→ 4) glycosidic bonds (Ghanadpour *et al.*, 2015). A peak at 985 cm^{-1} represents arabinose side chains in hemicellulose. Xylan is represented at peak 1034 cm^{-1}. The height between peaks between 900 to 1200 cm^{-1} does not differ significantly, showing that the bleaching sequence applied does not lead to significant dissolution of cellulose and hemicellulose. This proves chlorine dioxide is a selective delignification agent, leaving cellulose chains virtually intact.

The peak at 896 cm^{-1} represents the β-glycosidic linkages of hemicelluloses. The presence of these peaks indicates the presence of sugar units of hemicelluloses within the lignin extracts. It can be seen from the IR spectra in **Figure 28** that the peak height between samples decreases in the same order as lignin, thus being consistent with the order of bleaching and process sequence.

Figure 29 shows FTIR analysis of all effluent samples. Comparing **Figure 29** with **Figure 28** shows that the effluent samples display the same peaks as sludge samples. The peaks associated with lignin (between 1200 and 3650 cm^{-1}) are highest for PM41 Effluent. The results were contrary to what was expected considering that the PM41 samples are fully bleached fibers. However, the characteristic peaks between 3200 and 3650 cm^{-1} which can be associated with lignin (Carrillo *et al.*, 2004; Bouafif *et al.*, 2008) can also be associated with cellulose and hemicellulose and are assigned to hydroxyl stretching vibration between 3200 and 3345 cm^{-1} (Buranov and Mazza, 2010; Rosa *et al.*, 2010; El Halal *et al.*, 2015).

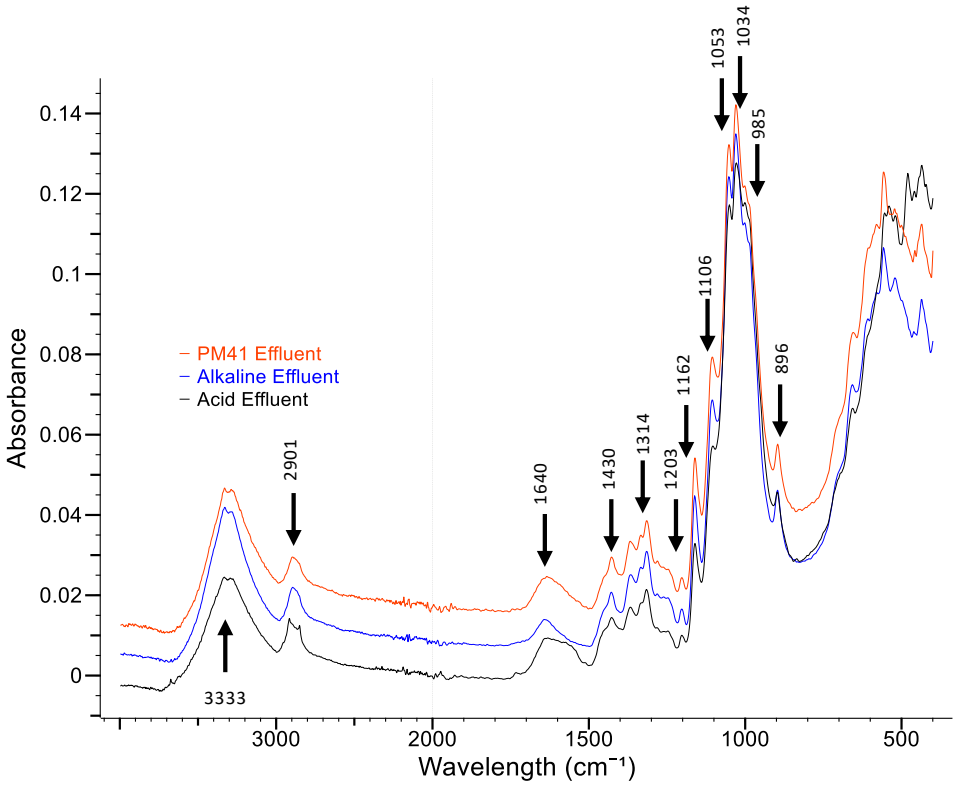

Figure 29: FTIR analysis to determine functional groups of effluent samples from Kraft pulp and paper mill.

Peaks at 2901 cm^{-1} could also represent CH_2 stretching in cellulose (Yuan *et al.*, 2010). This could explain why the peak for PM41 Effluent samples is higher than Alkaline and Acid Effluent samples. The Alkaline Effluent has the second highest peaks in this region, which makes sense because this waste stream will contain the lignin and cellulose extracted during by the sodium hydroxide and hydrogen peroxide stages during the bleaching sequence. Acid Effluent contains the lowest amount of cellulose and lignin. PM41 also contains a much higher content of hemicelluloses as indicated by peak at 896 cm^{-1} and the slightly higher peaks at 985 cm^{-1} and 1034 cm^{-1}.

4.4.5 Characteristics of other pulping methods compared to Kraft pulping and their influence on recovery and functionalization

In Section 1.1 it was mentioned that any papermaking process will have the same losses as those reported for PM41 Effluent including the portion of white water not treated by save-all devices and potential overflows from broke systems depending on the design and volume of the system. This source of fibre loss is relevant for mechanical, thermo-mechanical (TMP) and chemical thermo-mechanical pulping (CTMP) pulping processes (Section 2.3.2). In cases where a mill does not have a save-all device or broke system the loss of fibre to this effluent stream will be much greater. CTMP as mentioned in Section 2.3.2.3 consists of partial chemical digestion which is followed by screening and washing stages where some additional loss of fibre will occur. Looking at the process, the same will be true for any chemical pulp mill (Kraft or sulphite) producing unbleached pulps and some fibre loss will occur during screening and washing stages after cooking (Riley, 2012). Chemical pulping mills that produce bleached pulp will have additional losses in the bleaching plant similar to those reported for Alkaline and Acid Effluent. Tank overflows, drainage of product through drain valves and pipe leaks due to corrosion will be a universal possibility in any pulping plant. The frequency of such events depends on process control as well as the condition and maintenance of piping and equipment such as pumps.

Regarding the composition of waste streams, fibre from mechanical or TMP pulps will have much higher lignin and hemicellulose content as the process does not remove lignin or any other impurities (Section 2.3.2.1). Fibre from CTMP pulps will contain slightly less lignin and hemicellulose as these pulps are subjected to partial degradation during a semi-chemical process either by Kraft or sulphite pulping methods. The presence of lignin thus results in reduced transparency in nanocellulose films which is a limiting for some applications where high transparency is a desired property (Qing *et al.*, 2013; Noguchi, Homma and Matsubara, 2017). The presence of hemicellulose is advantageous however with regard to functionalization of fibre to nanocellulose, as hemicellulose is known to aid delamination of the cell wall during fibrillation (Page, 1989).

With reference to Section 4.4.3, the pH and conductivity are important factors that influence recovery rate during flotation with CGAs. The pH of mechanical and TMP will be near neutral as no chemicals are used in the process. CTMP will have neutral as well as either alkaline or acid effluent streams depending on the chemical pulping process used (Kraft or sulphite). The pulp will be washed after cooking and thus effluent generated after this stage will be near-neutral. Regarding conductivity, chemical pulping processes will have the highest conductivity followed by CTMP processes due to the pulping and bleaching chemicals used which are a great source of ions. This is confirmed from literature where Xu (2017) reported the typical estimated conductivity levels for some of the major grades of paper and board. Uncoated Free Sheets had the lowest conductivity < 1000 $\mu S/cm$ while Coated Free Sheets had slightly higher conductivity just over 1000 $\mu S/cm$. Newsprint grades (usually produced by mechanical pulping as mentioned in Section 2.3.2.1.) have a conductivity between 1800 and 2900 $\mu S/cm$. Linerboard on the other hand (produce by Kraft pulping) has conductivity of up to

5000 $\mu S/cm$. The amount of ion carryover is determined by the efficiency of washing processes (Xu, Pruszynski and Hart, 2017).

4.5 Conclusion

The greatest source of fibre loss was reported for PM41 Effluent. The second greatest loss was reported for Acid Effluent followed closely by Alkaline Effluent. Fibre losses of 2046, 658 and 585 ton per year were reported from Kraft PPM for these three streams respectively. Many of the fibre losses reported can be minimized to an extent by, for example, improving the efficiency of washing stages or by improving the broke system situated below paper machines. The former can be done by controlling the wash water temperature while the latter can be accomplished by increasing the volume or capacity of the system or by better process control strategies. Another strategy to reduce fibre loss is by ensuring the occurrence of tank overflows is minimized. This can be accomplished by regular maintenance of working pumps and installation of back-up pumps in the event that a working pump fails. Cost-benefit analyses are needed before implementing any of the suggested improvements. These improvements will not solve the problem of fibre loss entirely and there will therefore always be a need for treatment methods to remove these fibres from effluents.

The fibres in the waste streams (PM41, Alkaline and Acid Effluent) have fibre lengths of less than 1 mm which makes their re-use in the papermaking process undesirable. However, even though these fibres are not suitable for re-use in the papermaking process they are suitable for a wide range of other applications like nanocellulose, fish feed, building materials or biofuel. Before fibres can be functionalized, the fibres need to be recovered from the dilute effluent streams (PM41, Alkaline and Acid Effluent). Factors that influence fibre recovery by flotation with colloidal gas aphrons include the pH and conductivity. In Kraft PPMs the pH varies substantially between different waste streams and the reported values for PM41, Alkaline and Acid Effluent were 6.38, 10.6 and 2.23 respectively. The conductivity for PM41 Effluent was lower than for Alkaline and Acid Effluent with a value of 1276 $\mu S/cm$ reported for PM41 Effluent while the other two effluent streams have high conductivities around 7000 $\mu S/cm$. The differences in pH and conductivity between waste streams is attributed to the highly acidic and alkaline chemicals used during pulping and bleaching which are great sources of ions.

The characteristics of waste streams from mechanical, thermo-mechanical (TMP) and chemical thermo-mechanical pulping (CTMP) will be similar to Kraft mill waste streams. All waste streams from mechanical and TMP mills will have a neutral pH and low conductivity. CTMP mills will have either an alkaline or acid effluent stream depending on the type of chemical process used for cooking (Kraft or sulphite) as well as a near-neutral effluent stream once the pulp has been screened and washed after cooking. The conductivity of CTMP mills will be higher than for mechanical and TMP mills due to pulping and bleaching chemicals used but will be less than for chemical pulping mills as less chemicals are used for CTMP pulping. The amount of fibre lost from TMP and CTMP mills will most likely be less than the amount lost in Kraft PPMs that produce bleached paper grades as the mill will have more bleaching and washing stages which are sources of fibre loss.

5 WASTE STREAM FIBRE RECOVERY BY FLOTATION WITH COLLOIDAL GAS APHRONS (CGAS)

5.1 Abstract

The application of colloidal gas aphrons (CGAs) in recovery of cellulosic fibres from pulp and paper mill waste streams is an inexpensive method of separation. On average a volume of between 50.0% and 78.0% solid material which would normally require further disposal was recovered. A flotation column with a diameter of 0.05 m and a height of 0.5 m was used and surfactants were generated using a homogenizer with a speed setting of 10 000 rpm. A central composite design experiment was conducted to find the optimal CGA sparging rate and wastewater flowrate. All experiments thereafter were done using the optimized parameters which were found to be 1.13 mL/s and 1.80 mL/s for CGA sparging rate and wastewater flowrate respectively. The alternative surfactant investigated, N-Dodecyl β-D-maltoside (DDM), proved a promising green alternative to Triton X-100 obtaining similar recoveries only marginally less than those of the synthetic surfactant. The highest recovery obtained was 77.8% and 73.7% for Triton X-100 and DDM respectively. Efficiency is a complex function of fibre condition, column height, CGA stability in adverse conditions as well as the TSS concentration. Overall, Triton X-100 obtained the highest recoveries for PM41 Effluent whereas DDM obtained the highest recoveries for Alkaline Effluent. Acid Effluent generally contains lower concentrations of TSS which likely contributes to its lower efficiency compared to the other effluent streams.

5.2 Introduction

For a pulp mill waste stream fibre recovery method to be efficient, the composition of the effluent needs to be considered. From mill data acquired and summarized in Section 4.4.2 the average concentration of TSS for PM41, Alkaline and Acid Effluent varies between around 200 to 3000 ppm which is 0.02 to 0.3% respectively. Due to the streams being very dilute, flotation is a better recovery method compared to screening technology where low concentrations are associated with higher energy demands. The average particle size is also less than 200 μm according to analysed samples from the mill (Section 4.4.2), and is therefore an ideal size for efficiently recovering particles by flotation according to (Wakeman, 2011).

Considering all the methods previously explored for recovery of fibres from pulp and paper mill waste stream as outlined in Section 2.2.1.2, dissolved air flotation (DAF) and flotation aided by colloidal gas aphrons (CGAs) were the most promising. Froth flotation was ruled out mainly because of the inferior recovery rates compared to those of DAF and flotation aided by CGAs. The study by Redlinger-Pohn et al. (2016) found that for all cases investigated the recovery per length class in one unit was always below 40%. The recovery of smaller fibres was even lower. The washing of the froth led to depletion of fibres and in the end only 7% of the largest fibres were recovered from the suspension. These recovery rates were much lower than those obtained by Mukherjee et al. (2015) where recovery rates of between 60 to 76% were reported using a natural surfactant saponin extracted from soapnut plant. The other synthetic surfactants used in the study obtained lower recovery rates of between 30 to 50%. SEM micrographs of the recovered fibres showed they were of good quality and could potentially be reused in the paper making process.

The main objective of the study by Miranda et al. (2013) was not to recover fibres but to reduce the dissolved solid concentration. Consequently, the study only reports the total solids recovered (which consists of suspended solids and dissolved solids). However, it has been reported that DAF can remove between 80 to 99% of suspended solids (Ben *et al.*, 2003; Basta *et al.*, 2004). Even though higher recoveries are obtainable by DAF according to literature, the method is quite common and very well documented in as the method is used extensively in the mining and wastewater treatment industries (Edzwald, 2010). Flotation using CGAs in comparison is not so well documented and there are fewer articles available in literature. Thus, it was decided to study flotation with CGAs as the value of information and data gathered regarding this topic will be greater to the research community.

5.3 Materials and methods

The materials and methods relevant to this section of the project are detailed in Section 3.2. Briefly, two non-ionic surfactants namely Triton X-100 and Dodecyl β-D-maltoside (DDM) were used to recover fibres from Kraft PPM effluent as outlined in Section 3.2.1. The characteristics of these streams are summarized in **Table 10** and **Table 11** (measured variables including conductivity, pH etc.), **Figure 28** and **Figure 29** (functional groups as determined by FTIR) and **Figure 27** (particle size distribution). The flotation column dimensions and experimental setup to generate CGAs is given in Section 3.2.2. CGAs were characterized by determining the air hold-up and half-life as outlined in Section 3.2.3. A central composite design was considered to determine the optimal operating conditions (CGA sparging rate and wastewater flowrate) as outlined in Section 3.2.4 after which experiments with the alternative surfactant DDM was conducted as outlined in Section 3.2.5. The efficiency of the flotation process was calculated in terms of total suspended solids (TSS) using a simple equation as shown in equation 38. TSS was calculated based on Method 2540 D of *Standard Methods for the Examination of Water and Wastewater*, 23rd edition (Baird, Eaton and Rice, 2017). The method is suitable for all natural waters in raw, municipal and industrial, process and treated agricultural waters. Shortly, a known volume of well-mixed sample was filtered, collecting the solid residue on the filter paper. The residue was evaporated to a constant weight at a temperature of 103 to 105 °C. The concentration of TSS was then calculated using the equation 39 where m_{final} is the weight of the filter plus the dried residue and $m_{initial}$ is the weight of the unused filter.

$$\eta = \frac{TSS_{foamate}}{TSS_{foamate} + TSS_{tailings}} \quad [38]$$

$$TSS = \frac{m_{final}(mg) - m_{initial}(mg)}{sample\ volume\ (L)} \quad [39]$$

5.4 Motivation for recovery method chosen

As mentioned in the introduction (Section 5.2), part of the reason why flotation using colloidal gas aphrons (CGAs) was explored as a recovery method instead of dissolved air flotation (DAF) was because it was deemed that the contribution to literature would be greater. However, this was not the only reason and methods were evaluated according to the objectives as outlined in Section 1.2 considering industrialization, economic feasibility, and environmental awareness. Regarding

industrialisation, even though froth flotation is commonly used in processing operations to remove fine particles which do not have practical settling rates under gravity, foam is difficult to pump as it loses its characteristics due to its rheology (Mukherjee *et al.*, 2015). Compared to CGAs and air bubbles in saturated air/water which can easily be pumped this is a major drawback. Consequently, considering the poor fibre recovery rate and difficulties regarding pumping of foam, this method was ruled out. The other two methods are further compared by considering ease of industrialization, environmental impact of the method and economic feasibility.

Both DAF and flotation aided by CGAs can be industrialised. DAF has been used in Scandinavia for drinking water treatment since the 1960's (Edzwald, 2010). The method has been used for removing low density particles from water as an alternative clarification method to sedimentation. Conventional DAF processes have hydraulic loadings of 5 to 15 m/h but more recent DAF processes have been developed with loading rates of 15 to 30 m/h and even higher. The industrial application of CGAs is less common and usually restricted to smaller scale operations due to the high cost of surfactants. However, owing to their high interfacial area and rheological properties which makes them easy to pump and provides increased froth stability, this method of recovery has been used on a large scale in batch and continuous mode using flotation column set-up (Jauregi and Dermiki, 2010).

From an economic perspective, the most expensive equipment cost for CGA separation is a diafiltrating system for the removal of the surfactant; if this step is removed the equipment cost would be lower than for most other flotation methods. This can potentially be accomplished when using green-based instead of synthetic surfactants, especially in the case where xylan surfactants are used in the method. As mentioned in Section 2.4.2 hemicelluloses are known to facilitate delamination and would thus be advantageous in downstream processing to produce nanocellulose. Regarding the operational cost of CGA separation, although surfactants are very expensive, low concentrations are required to generate CGAs (Jauregi and Varley, 1999). According to Jauregi and Varley (1999) the cost of utilities, which includes the cost of electricity, is high for CGA extraction but is most likely not higher than the energy input required for compression of water in DAF. A detailed cost analysis is needed to confirm this which is not part of this study.

Flotation aided by CGAs will be a more cost-effective method if the diafiltrating step can be removed. In the event that this step can be removed the most expensive operational cost for flotation with CGAs is the surfactant required as a foaming agent. DAF also requires surfactants which act as flocculants or coagulants to improve fiber recovery. An economic assessment is necessary to determine which of these two methods would be more attractive from an operational point of view. According to the decision-making tree in Figure 1, there is potential in reducing the cost of flotation aided by CGAs if the diafiltrating step can be replaced or removed. Both flotation methods are thus considered and the next criteria is whether the chemicals (i.e. surfactants) are green-based, non-toxic and non-hazardous.

Both methods (flotation using CGAs and DAF) are environmentally friendly separation processes, excluding the synthetic surfactant used to compare results to the study of Mukherjee et al. (2015). Usually, one of the drawbacks of using CGA separation is the toxicity of surfactants used. For some

applications non-ionic green-based surfactants can replace toxic ionic surfactants, which is the case in the study conducted by Mukherjee et al. (2015). The use of a plant origin surfactant which achieves such high recovery rates is very promising. Not only is it a green method promoting a biodegradable and non-toxic surfactant, but it also obtained higher recovery rates than those of synthetic surfactants. The only drawback is that natural surfactants are usually much more expensive than synthetic surfactants. The expense can however be justified by their much lower concentrations needed according to Mukherjee et al. (2015) and the fact that in most cases these natural surfactants do not need to be separated from the bioproducts by membrane filtration or diafiltration systems.

According to the decision-making tool developed (Figure 1) both DAF and flotation aided by CGAs are good recovery methods to consider up to the last two criteria where it should be considered which of these two methods contributes toward research gaps in literature and toward the biorefinery concept. DAF has been extensively researched and implemented in PPM wastewater treatment plants and will thus not really contribute toward literature (Edzwald, 2010). With flotation aided by CGAs however, there is a gap in researching alternative bio-based surfactants that can replace synthetic surfactants. In this study the potential use of Dodecyl β-D-maltoside (DDM) as a sugar-based non-ionic surfactant was explored.

5.5 Results and discussion

5.5.1 Technical aspects and considerations

The height of a flotation column was an important factor to consider in order to ensure the required separation is achieved. The study by Mukherjee *et al.* (2015) used a column with a height of 1 m. However, a study by Hashim and Sen Gupta (1998), which also focused on recovery of fine cellulosic fibres from pulp and paper mill wastewater, studied the effect of column height on efficiency rates and concluded that up to 70% flotation efficiency could be achieved within a short column height of 0.3 to 0.35 m. Other aspects considered when choosing dimensions for the flotation column setup include pipe dimensions. A study by Zhao, Pillai and Pilon (2009) and Larmignat *et al.* (2008) however found that pipe shape and hydraulic diameter do not affect CGA rheology.

When considering which parameters to measure during flotation experiments and which equations to use to determine the efficiency of fibre removal, it was important to first determine by which mechanism the particles would be recovered. Particles in flotation are either removed by what is referred to as true flotation which is when particles attach to air bubbles or by entrainment which is when particles are captured in spaces or voids between bubbles and “trapped” in the froth layer moving upward through the column. In most cases these are the two main mechanisms that need to be considered (Savassi, 2005).

The kinetics around adhesion of bubbles to particle surfaces is referred to as the three-phase contact (TPC) formation and is significantly influenced by the type of surfactant, charge, pH and additives such as salt. TPC formation is completely different for hydrophobic and hydrophilic solid surfaces. When considering nonionic surfactants on hydrophilic surfaces like cellulosic fibres, the TPC line dynamics

are electrostatically driven which means bubble attachment is determined by charge and/or polar interaction (Tadros, 2014). However, for the bubble to attach to a negatively charged surface the natural negative charge at the bubble surface needs to be reversed to positive which is only possible for cationic surface solutions (Kosior *et al.*, 2015). This means that the sole mechanism by which particles will be recovered using a nonionic surfactant for removal of cellulosic fibres from waste streams will be by entrainment.

When considering a flotation process and modeling approaches thereof, a column is divided into three regions namely the collection, quiescent and froth region as shown schematically in **Figure 30**. The quiescent zone represents the transition to a less turbulent zone which is essential for stability of the pulp-froth interface. At this interface air bubbles cause water and suspended particles to become entrained. In the figure symbols C, F and T refer to the flowrates of the concentrate, feed and tailing respectively and subscripts wat and sus refer to water and suspended particles. The symbol IN refers to influx to the froth.

According to a modeling approach by Savassi (2005) the degree of entrainment is expressed as a ratio between the recovery of entrained particles to the concentrate divided by the recovery of water to the concentrate, defined mathematically in equation 40 where $ENTFEED$ is the entrainment in the feed. The symbol R refers to the recovery of either water or suspended particles as indicated by subscripts wat and sus respectively. Recovery is defined as the flowrate of either suspended particles or water recovered in the concentrate (C_{sus},C_{wat}) divided by the flowrate of the suspended particles or water initially (F_{sus}, F_{wat}).

A more rigorous approach to determining entrainment is to determine the influx of suspended particles to the froth zone as expressed in equation 41 where the superscript FR indicates the froth region. In the equation F_{sus} and F_{wat} from equation 40 are replaced by IN_{sus} and IN_{wat}. It is important to note that subscript sus when applied to the froth indicates suspended particles that crossed the pulp-froth interface by entrainment, whether or not these particles remain suspended in water (where pulp in this case refers to the incoming feed) by entrainment.

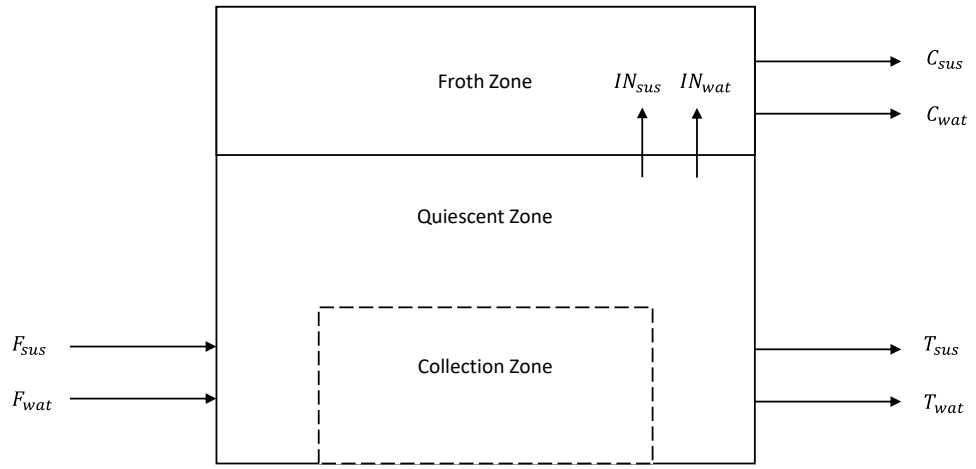

Figure 30: The collection, quiescent and froth zone in a conventional flotation cell. (Savassi, 2005)

$$ENTFEED = \frac{R_{sus}}{R_{wat}} = \frac{C_{sus}/F_{sus}}{C_{wat}/F_{wat}} \quad [40]$$

$$ENT = \frac{R_{sus}^{FR}}{R_{wat}^{FR}} = \frac{C_{sus}/IN_{sus}}{C_{wat}/IN_{wat}} \quad [41]$$

Where for equation 40 and 41:

$ENTFEED = entrainment\ in\ the\ feed$

$R_{sus} = recovery\ of\ suspended\ particles$

$R_{wat} = recovery\ of\ water$

$C_{sus} = flowrate\ of\ suspended\ particles\ to\ the\ concentrate$

$C_{wat} = flowrate\ of\ water\ to\ the\ concentrate$

$F_{sus} = flowrate\ of\ suspended\ particles\ to\ the\ feed$

$F_{wat} = flowrate\ of\ water\ to\ the\ feed$

$IN_{sus} = flowrate\ of\ suspended\ particles\ to\ the\ froth\ zone$

$IN_{wat} = flowrate\ of\ water\ to\ the\ froth\ zone$

$ENT = entrainment\ in\ the\ froth\ region$

$FR = froth\ region$

The concentration of pulp in the feed, concentrate and tailings is further expressed as shown in equation 42 where the symbol ω refers to the respective concentration of either suspended particles or water indicated by subscripts sus and wat. Concentration is defined for the concentrate, feed and tailings as indicated by superscripts $conc$, $feed$, and $tail$. According to a theory known as the bubble swarm theory, proposed by (Smith and Warren, 1989), the entrainment mechanism causes suspended particle and water to enter the froth region in the same ratio as they exist in the quiescent zone which means an expression ω_{sus}^{QZ} can also be defined as shown in equation 43 where QZ refers to the quiescent zone.

$$\omega_{sus}^{conc} = \frac{C_{sus}}{C_{wat}};\ \omega_{sus}^{feed} = \frac{F_{sus}}{F_{wat}};\ \omega_{sus}^{tail} = \frac{T_{sus}}{T_{wat}} \quad [42]$$

$$\omega_{sus}^{QZ} = IN_{sus}/IN_{wat} \quad [43]$$

Where for equation 42 and 43:

$\omega_{sus}^{conc} = concentration\ of\ suspended\ particles\ in\ the\ concentrate$

$\omega_{sus}^{feed} = concentration\ of\ suspended\ particles\ in\ the\ feed$

$\omega_{sus}^{tail} = concentration\ of\ suspended\ particles\ in\ the\ tailings$

$\omega_{sus}^{QZ} = concentration\ of\ suspended\ particles\ in\ the\ quiescent\ zone$

$C_{sus} = flowrate\ of\ suspended\ particles\ to\ the\ concentrate$

$C_{wat} = flowrate\ of\ water\ to\ the\ concentrate$

$F_{sus} = flowrate\ of\ suspended\ particles\ to\ the\ feed$

$F_{wat} = flowrate\ of\ water\ to\ the\ feed$

$IN_{sus} = flowrate\ of\ suspended\ particles\ to\ the\ froth\ zone$

$IN_{wat} = flowrate\ of\ water\ to\ the\ froth\ zone$

$T_{sus} = flowrate\ of\ suspended\ particles\ to\ the\ feed$

$T_{wat} = flowrate\ of\ water\ to\ the\ feed$

By combining all the equations, $ENTFEED$ and ENT can be redefined as expressed in equation 44. This equation shows it is unnecessary to establish the influx of suspended particles to the froth zone. Instead it is only necessary to determine the concentration of suspended particles in the concentrate, feed and quiescent as indicated by symbols ω_{sus}^{conc}, ω_{sus}^{feed} and ω_{sus}^{QZ}. These equations can be combined to obtain a relationship between $ENTFEED$ and ENT. Further, equation 40 can be used to eliminate $ENTFEED$, resulting in equation 45.

$$ENTFEED = \frac{\omega_{sus}^{conc}}{\omega_{sus}^{feed}};\ ENT = \frac{\omega_{sus}^{conc}}{\omega_{sus}^{QZ}} \qquad [44]$$

$$R_{sus} = \frac{\omega_{sus}^{QZ}}{\omega_{sus}^{feed}} \cdot ENT \cdot R_{wat} \qquad [45]$$

Where for equation 44 and 45:

$ENTFEED = entrainment\ in\ the\ feed$

$ENT = entrainment\ in\ the\ froth\ region$

$R_{sus} = recovery\ of\ suspended\ particles$

$R_{wat} = recovery\ of\ water$

$\omega_{sus}^{conc} = concentration\ of\ suspended\ particles\ in\ the\ concentrate$

$\omega_{sus}^{feed} = concentration\ of\ suspended\ particles\ in\ the\ feed$

$\omega_{sus}^{QZ} = concentration\ of\ suspended\ particles\ in\ the\ quiescent\ zone$

The use of equation 45 still requires operating conditions about the concentration of suspended particles beneath the pulp-froth interface, which is a measurement that is hardly available. A study by Johnson (1972) however found that for fine suspended particles in water, perfect mixing can be assumed, which means that the concentration of fine suspended particles should be the same at every point of the pulp region. Thus, the concentration of suspended particles in the quiescent zone and tailings (ω_{sus}^{QZ} and ω_{sus}^{tail}) can be assumed to be equal as stated in equation 46. Combining this equation with equation 45 gives the final equation 47 where recovery of suspended particles can be calculated by determining the concentration of suspended solids in the feed and tailings (ω_{sus}^{feed} and ω_{sus}^{tail}) as

well as R_{wat} which is equal to the ratio of the water flowrate in the concentrate (C_{wat}) divided by the feed flowrate (F_{wat}).

$$\omega_{sus}^{QZ} = \omega_{sus}^{tail} \quad [46]$$

$$R_{sus} = \frac{\omega_{sus}^{tail}}{\omega_{sus}^{feed}} \cdot ENT \cdot R_{wat} \quad [47]$$

Where for equation 46 and 47:

$\omega_{sus}^{feed} = concentration\ of\ suspended\ particles\ in\ the\ feed$

$\omega_{sus}^{tail} = concentration\ of\ suspended\ particles\ in\ the\ tailings$

$\omega_{sus}^{QZ} = concentration\ of\ suspended\ particles\ in\ the\ quiescent\ zone$

$ENT = entrainment\ in\ the\ froth\ region$

$R_{sus} = recovery\ of\ suspended\ particles$

$R_{wat} = recovery\ of\ water$

5.5.2 Colloidal gas aphron (CGA) characterization

In this study, the half-life and air hold-up of colloidal gas aphrons (CGAs) from both Triton X-100 and DDM was determined as outlined in Section 3.2.2 to confirm that the surfactants are suitable to use for flotation. The half-life of Triton X-100 at a concentration of 1.9 mM was found to be $\pm$120 s which is very comparable to the study by Mukherjee where a solution of 2 mM had a half-life of 145 s. The air hold-up was calculated to be 31.3% which is much better than Mukherjee's study which had an air hold-up between 14-21%. The half-life and air hold-up of DDM was found to be $\pm$135 s and 22.1% and therefore DDM was deemed a suitable alternative surfactant to investigate.

It is known that not all surfactants can generate CGAs, although the reason for this has not been investigated up to date (Molaei and Waters, 2015). From literature it is known that Triton X-100 is able to form stable CGAs but it was unsure whether DDM would do the same. DDM is however known to be used as a foam stabilizer in diverse harsh conditions like high temperatures, high salinity and in the presence of strong acids or alkalis (Stubenrauch *et al.*, 2009; Zhao *et al.*, 2018). Results from the study by Zhao *et al.* (2018) showed that DDM was able to maintain high half-life values even in the mediums of 0.5 $M\ HCl$ or $NaOH$, and 320 000 ppm salinity. Liquid drainage was also measured and showed that foam remains stable for quite a long period after being generated. The half-life and air hold-up results from this study proved that this is indeed the case and DDM has similar properties to Triton X 100.

5.5.3 Optimal operating conditions determined by central composite design (CCD)

The efficiency results obtained for the screening and CCD experiment with Triton X-100 are summarized in **Table E1** and **Table E2** in Appendix E. The highest efficiency achieved was 77.5%. The

ANOVA results are summarized in Appendix E in **Table E3** and **Table E4**, respectively. From the ANOVA results for the screening experiments, the CGA sparging rate and wastewater flowrate both have significant effects on the efficiencies achieved ($P < 0.05$). The interaction between these two variables was also significant with $P = 0.008$. Seeing as both parameters have an effect on efficiency according to the screening results, a CCD was done to determine the optimal flotation parameters. This was done with PM41 wastewater and Triton X-100.

From the ANOVA results of the CCD experiment (**Table E4**), the linear and quadratic effects for CGA sparging rate are significant ($P < 0.05$). For the wastewater flowrate only, the linear effects were significant. The interaction between these two variables was found to be insignificant. The regression model used as expressed in equation **Error! Reference source not found.** is highly significant for TSS r emoval in the concentrate, with a predicted R^2 and MS residual value of 84.4% and 47.0 respectively. The R^2 value is a measure of the accuracy of the model.

Figure 31 shows the fitted surface for the regression model used. From Figure 28, there is an optimum in the direction of increasing CGA sparging rate and wastewater flowrate as can be seen from the contour that reaches a maximum at 1.80 mL/s, beyond which, the concentration of fibre in the concentrate decreases. These observations are in agreement with a study by Hashim and Sen Gupta (1998) which found that separation efficiency improved with increasing CGA flowrate and after a flowrate of $3.0\times10^{-7}\ m^3/s$ the separation efficiency declined. The operating conditions in terms of CGA sparging rate and wastewater flowrate (**Table 7**) were the maximum operating parameters of the peristaltic pumps used as outlined in the experimental schematic (**Figure 26**) and thus it was not possible to adjust the flowrate beyond the sparging rates and flowrates specified.

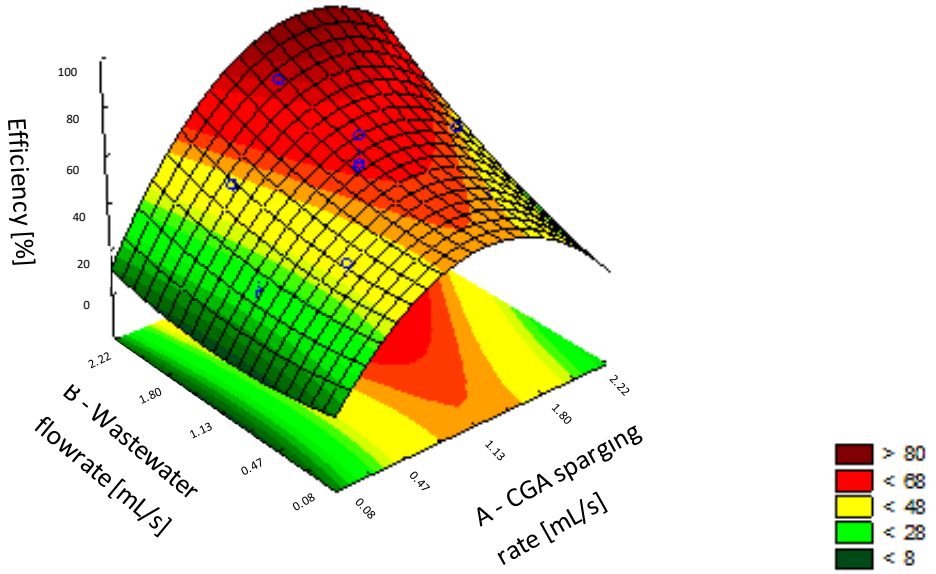

Figure 31: Fitted surface plot of central composite design experiment with Triton X-100.

The Pareto chart (**Figure 32**) shows the standardized effects of factors A (CGA sparging rate) and B (wastewater flowrate), which visually summarize the significance of linear, quadratic and interaction

effects between factors A and B on the efficiency. Finally, **Figure 33** shows the predicted vs observed values of the model and results. The closer the points (i.e. the results or observed values) are to the 45° line, the more accurate the model is. For the model to be sufficient, a difference of no more than 0.20 between the predicted R^2 value and adjusted R^2 value is allowable. In this case the adjusted R^2 value is 73.3% which gives a difference of 0.111. The two values are thus in sufficient agreement. The data points in the figure are closely and evenly distributed along a 45° line which confirms that the predicted values are close to the actual values and that the data is a good fit.

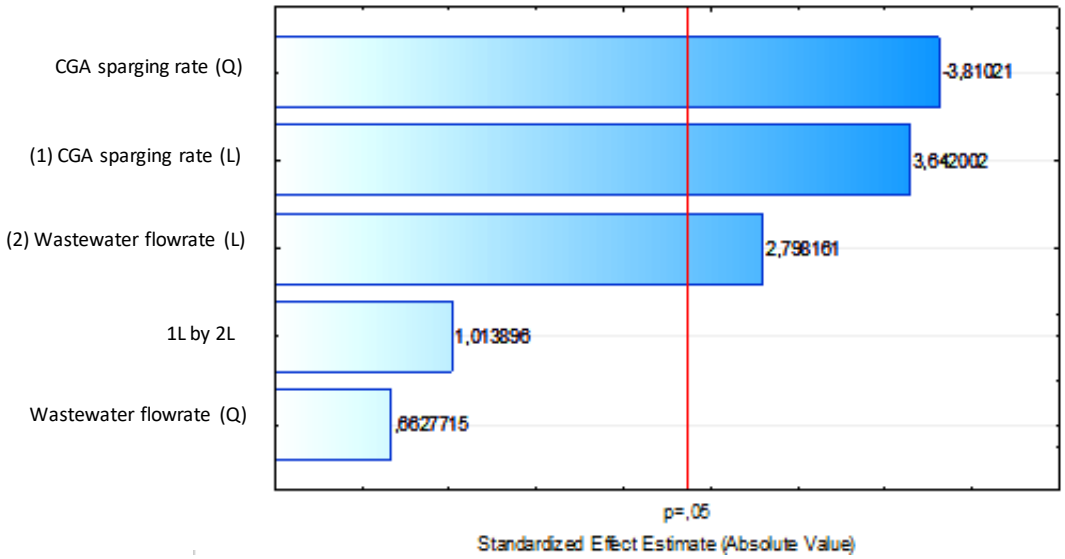

Figure 32: Pareto chart of standardized effects of central composite design experiment with Triton X-100 where factor A is the CGA sparging rate and factor B the wastewater flowrate.

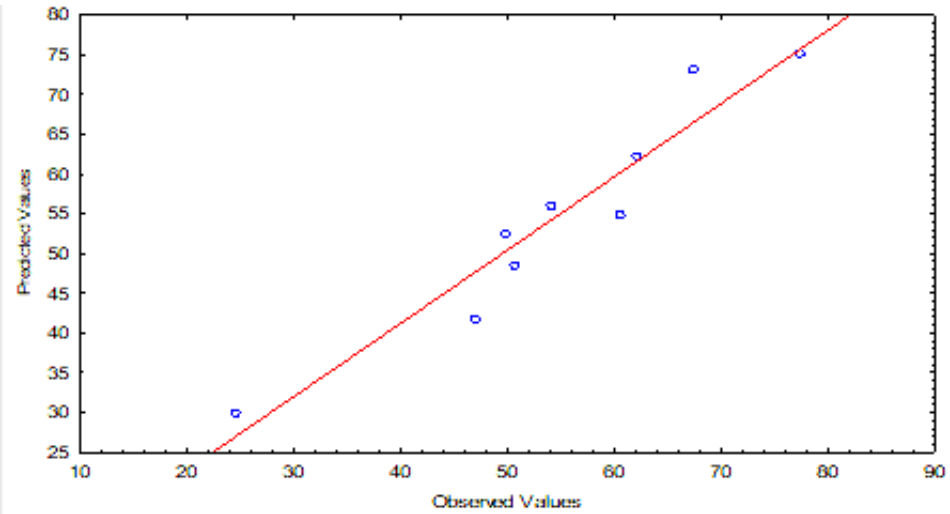

Figure 33: Observed vs. predicted values central composite experiment with Triton X-100.

From visual observation of flotation experiments, the results obtained make sense. In cases where the CGA sparging rate was low, dead zones of fibre in the bottom of the column were observed. This observation is in agreement with a study by Hashim and Sen Gupta (1998) which found that efficiency improved with increasing flowrate of CGAs. Even though CGAs are fairly stable dispersions (with a volumetric gas fraction (quality) of at most 0.74), they will slowly "cream" and separate into a clear liquid region and a froth layer which is what likely happens at a very early height in the flotation column when the flowrate is so low (Longe, 1989). This leads to CGAs being more closely packed leaving smaller voids for particles to become entrained. On the other hand, when the sparging rate is too high, the recovery efficiency of fibres decreased as seen in the fitted surface plot (**Figure 31**). The effect could be due to a viscous drag that becomes dominant, causing fibres to detach and become part of tailings Mukherjee *et al.* (2015). This explains the quadratic relationship between sparging rate and efficiencies achieved during flotation.

Regarding the wastewater flowrate, when the flowrate was very slow (below 0.47 mL/s) the height of foam in the column was lower and the recovered fibre concentration was less. This can be explained by interbubble gas diffusion as explained in the literature review section. As time progresses small bubbles tend to disappear due to greater internal gas pressure. As illustrated in **Figure 6** a driving force for mass transfer exists from smaller bubbles to larger bubbles which causes gas to diffuse from small bubbles. As explained in Section 2.2.3.1.2, when gas diffusion between two bubbles occurs the internal area across which the gas molecules are transferred is reduced thereby slowing the diffusion rate which is expressed mathematically by Fick's law. As a result, the voids between bubbles also becomes smaller which makes recovery by entrainment less effective. This explains the linear relationship between increasing efficiency with an increasing wastewater flowrate.

5.5.4 Potential in substituting synthetic surfactant Triton X-100 with biosurfactant

The highest recoveries obtained was 77.8% and 73.7% for Triton X-100 and DDM respectively. From the CCD experiment with Triton X-100 and PM41 Effluent it was concluded that the optimal experimental operating conditions are when a CGA sparging rate of 1.13 mL/s and wastewater flowrate of 2.22 mL/s are used. Values beyond those reported in **Table 8** could not be used as these were the limits of the peristaltic pumps used. Experiments with the alternative surfactant were performed and the efficiencies were compared to that of Triton X-100 as summarized in **Figure 34** where the highest *average* (not maximum) efficiencies were reported for Triton X-100 (73.2%) and DDM Batch 1 (68.4%) for recovery of fibre from PM41 and Alkaline Effluent respectively. The data of **Figure 34** including repeat experiments are presented in Appendix E (Table E5). The *average* value is thus the average of the triplicate set of data as presented in **Figure 34**.

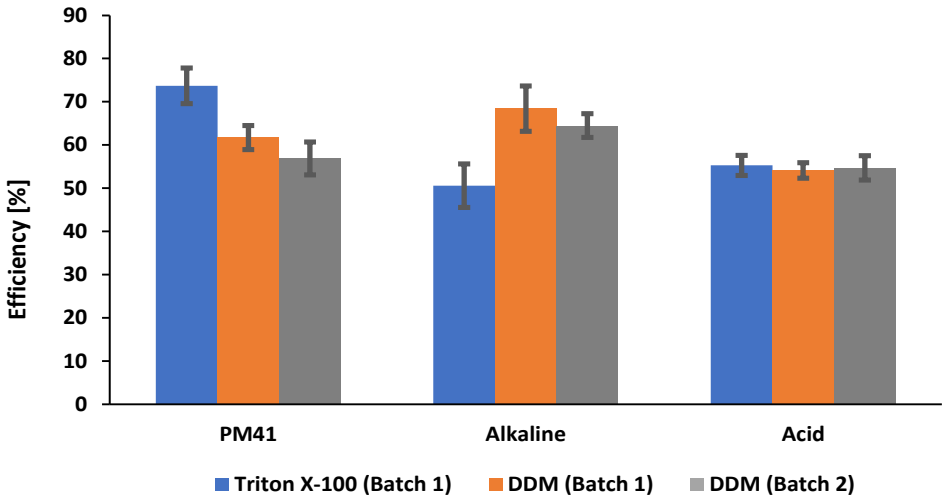

Figure 34: Flotation efficiencies achieved with alternative surfactant DDM. Error bars represent the standard deviation between runs.

Even though the recovery rates using DDM as surfactant were less than the highest recovery achieved using Triton X-100, the recovery rates are still relatively high compared to the recovery rates achieved by other flotation methods like the screening device invented by Gardner (1965) . The screen designed and used in the study by Gardner (1965) reported recoveries of at least 55% and often 75% or more using a single screen. There is thus also quite a lot of variation when using this method of recovery. When a second screen was placed in series with the first recoveries of between 90 and 95% could be achieved. The fibres recovered were predominantly Southern Pine with an average length of 3 mm. Notably, no recovery or efficiency rates were reported by other authors (Boniface and Redding, 1974; Wolfer *et al.*, 1997; McDonald, 2003).

The highest efficiency rates reported in flotation studies by authors such as Hashim and Sen Gupta (1998 and Mukherjee *et al.* (2015) was 70% with a column height of 0.35 m and 76% with a column height of 1 m respectively. The study by Hashim and Sen Gupta (1998) used commercial cellulosic pulp dried in an oven at 70°C for 24 h. The column was filled with a dilute feed slurry of 0.5 kg/m^3 or 500 ppm and sodium dodecyl sulphate (SDS) was used as a cationic surfactant. The study by Mukherjee *et al.* (2015) also used synthetic wastewater but at a concentration of 200 ppm. The efficiencies achieved for the variety of surfactants used in the study, namely soapnut, CTAB, SDS and Triton X-100, were 60, 50, 37 and 30% respectively. These efficiencies were achieved with flowrates for CGA and wastewater of 0.267 mL/s. What makes the current study different, is that true effluent was used instead of making synthetic feed slurries. It is thus debatable how comparable the results of this study are with these previous studies from literature as it is known that the behavior of fibres after being dried and re-dispersed is quite different. At the lowest flowrates in this study (0.08 mL/s) the efficiency achieved with Triton X-100 was 47% compared to the 30% achieved in the study by Mukherjee *et al.* (2015) with higher flowrates of 0.267 mL/s. This difference could also be due to the difference in column height, surfactant concentration used (2 mM), TSS concentration, and retention time of froth in the column

before being removed in the concentrate. In each case however the optimized parameters obtained efficiencies of around 70 to 76%.

Figure 34 shows that the efficiencies of fibre recovery from Acid Effluent remained relatively constant at around 55% in all cases (using Triton X-100 and DDM in Batch 1 and 2) which could be explained by observing the pH and TSS values between Batch 1 and 2 in **Table 10**. The values did not vary significantly between batches. From **Table 10** the pH values were 2.11 and 2.35 and the TSS values were 257 and 227 ppm for Batch 1 and 2 respectively. From the efficiencies observed it seems that the stability of Triton X-100 and DDM CGAs in acidic mediums with high conductivities are similar.

For Triton X-100 the lower efficiencies achieved for Alkaline Effluent (50.6%) and Acid Effluent (55.3%) compared to PM41 Effluent (73.2%), as shown in **Figure 34**, are attributed to the high conductivity of Alkaline and Acid Effluent. As mentioned in Section 3.2.1.2 the CMC range for Triton X-100 is between 0.2 to 0.9 mM. A study by Akhlaghi and Riahi (2019) found that increasing the salt concentration leads to lower CMC values (in the lower spectrum of the range between 0.2 and 0.9 mM) of Triton X-100. As mentioned in Section 2.2.2.1.1 CMC is the concentration at which molecules organize themselves into spheres called micelles. Lower CMC values (i.e., closer to 0.2 than 0.9 mM) mean that lower concentrations (w/v) of the surfactant are needed to form these micelles. Above this concentration the interface of micelles does not change, and excess surfactant molecules just end up in the bulk fluid. However, even though increased salinity leads to lower CMC values, a study by Feng, Singhal and Swift (2009) found that stability of CGAs decreases with increasing pH and salt concentration. This is in agreement with a study by Jauregi, Gilmour and Varley (1997) which found an increase in surfactant concentration increases stability whereas the addition of salt leads to the opposite effect. Gas hold-up depends on salt concentration as well as surfactant concentration. This explains why in general the efficiency in fibre recovery of PM41 Effluents, which contain much lower levels of salt, are higher than for Acid Effluents.

The lowest efficiency (50.6%) was obtained for fibre recovery from Alkaline Effluent using Triton X-100. The reason for this is attributed to the high conductivity of the effluent like for Acid Effluent and the fact that the pH is so much higher which as explained in the preceding paragraph negatively affects the stability of CGAs according to Feng, Singhal and Swift (2009). This caused the efficiency to be even lower than for Acid Effluent. Another plausible reason is that the hydroxyl groups negatively affect the performance of Triton X-100, as a study by Saien and Akbari (2010) found that the interfacial tension of Triton is significantly weakened by hydroxyl ions.

DDM is an exception to the response normally observed regarding pH and salts. As mentioned earlier in Section 5.5.2, DDM is used as a foam stabilizer in many cases which means it is stable in alkaline as well as acidic solutions (Zhao *et al.*, 2018). The study by Zhao *et al.* (2018) found that the half-life of DDM was higher in acidic and alkaline mediums compared to a neutral solution and that in 0.5 M HCl the half-life was higher than in a solution of 0.5 M $NaOH$. This potentially explains why the efficiency for Alkaline Effluents (68.4% and 64.5%) is higher than for PM41 Effluents (61.7% and 56.9%) but it does not explain why the Acid Effluent is lower (54.1% and 54.7%) than both Alkaline and PM41

Effluent, as it would be expected to be higher when considering that the half-life is the highest. However, it could be attributed to the slightly higher conductivity and lower TSS concentration of Acid Effluent compared to Alkaline Effluent (**Table 10**). This observation is theoretical and should be investigated further by conducting experiments with fixed TSS and conductivity values.

When the TSS concentration is higher, it can be observed that the efficiency in recovering fibres in effluent is also higher. This is theoretically possible by observing the efficiencies obtained for fibre recovery from PM41 Effluent from Batch 1 and 2 using DDM. The TSS concentration is 2187 ppm versus 1764 ppm for Batch 1 and 2 respectively, which led to fibre efficiencies of 61.7% and 56.9% respectively. Likewise, for Alkaline Effluent the TSS concentrations were 589 and 409 ppm which led to efficiencies of 68.4% and 64.5%. TSS likely plays an important role in fibre recovery, as when more fibres are present a sort of "network" with overlapping fibres will exist. When there are less fibres, there is enough space in the column for negatively charged particles to repel other particles resulting in fibres being more widely separated from another. It is easier to entrain a network of fibres compared to individual fibres which explains why TSS concentration effects fibre recovery. Further investigation and experiments are necessary to validate this observation.

5.6 Conclusion

Flotation using CGAs proved to be a feasible method for recovering cellulosic fibre from pulp and paper mill waste streams with efficiency values comparing well with other methods as well as similar studies to the one in this case. The CCD experiment to optimize flotation parameters showed that both the CGA sparging rate and wastewater flowrate have an effect on efficiencies achieved and that the interaction between these is also important. The quadratic model used to describe the behavior of the system had a good fit with an R^2 value of 84.4%. Furthermore, DDM obtained similar half-life and air hold-up values to Triton X-100 which resulted in similar recoveries. This proves that DDM can potentially be used as an alternative to non-ionic surfactants like Triton X-100.

6 FUNCTIONALIZATION OF RECOVERED FIBRES TO NANOCELLULOSE

6.1 Abstract

Phosphorylation has proved to be a successful pre-treatment method for treating cellulosic fiber prior to mechanical treatment to reduce the energy consumption normally required to mechanically delaminate fibres to nanoscale range. In this study an AGU : Salt : Urea ratio of 1 : 1.2 : 19.6 was used. The amount of urea used was around four times the amount used in previous studies and resulted in fibres being fibrillated to gel-like suspensions within 5 min using a 900 W high-speed blender. The suspensions obtained were highly heterogenous with a polydispersity index of ≈ 1 for all samples. Successful phosphorylation was confirmed by FTIR and SEM-EDX. Films had an average thickness of between 5.5 and 10 μm. The variation is due to the solvent casting method chosen to produce films combined with a vacuum filtration step to remove entrapped air bubbles prior to drying. Films were confirmed to be thermally stable with a final residue of 41% at 800 °C. The solubility of films was low which indicates the films are more hydrophobically orientated. The nanosized fractions for samples ranged from 20.0 to 92.3%. In general, the best results were obtained with Bleach Spill, Dual D, D2 and Cut-offs samples.

6.2 Introduction

Nanocellulose is a material that is (1) bio-based, (2) biodegradable and (3) biocompatible (Rol *et al.*, 2019). There are various definitions for these terms. The term bio-based according to CEN, the European Committee for Standardization (EN 16575) refers to products wholly or even only partially derived from biomass such as plants, trees, and animals. A material can still be bio-based after being treated chemically or biologically. Standard tests like EN 16640 can be used to measure the amount of bio-based carbon along with EN 16785-1 and 16785-2. The former accounts for other bio-based elements in polymers through elemental analysis while the latter accounts for other is a material balancing method to determine the renewable content of a bio-based product. (European Bioplastics, 2019)The term biodegradation refers to a chemical process in which materials are metabolized into water, carbon dioxide and biomass with the help of microorganisms. For a material to be classified as biodegradable it must be able to decompose under ambient conditions within a certain timeframe. This is regulated by applicable standards such as EN 13432 which requires that the material achieves at least 90% disintegration after 12 weeks and 90% biodegradation in six months. The test also requires tests on ecotoxicity and heavy metal content. This procedure is specified for packaging materials. Standards like EN 14995 or ISO 18606 describe the same requirements as tests EN 13432 but can be applied to plastics as well as packaging in general. (European Bioplastics, 2019)

The final term used to describe nanocellulose is biocompatibility. This term is most often used when describing materials for medical devices such as implants or other medical devices that come in contact with skin, blood, tissue or bone. A formal definition often used describes biocompatibility as ‘the ability of a material to perform with an appropriate host response in a specific application’ (Williams, 1987). Tests like ISO 10993 can be used to determine a materials biocompatibility, although it is difficult to standardize such a test as biocompatibility strongly depends on the type of the

application. As a minimum requirement the material must not induce any unwanted responses such as toxic reactions in the area where the material is placed.

Nanocellulose materials also present with good barrier and mechanical properties. One limiting factor for some applications though is the materials hydrophilicity. Modification methods exist to improve hydrophobicity if it is required. These methods are mostly easy, inexpensive, and eco-friendly physical adsorption processes to modify surface properties. A study by Lozhechnikova *et al.* (2014) for example used amphiphilic galactoglucomannan (GGM) derivatives to impart a hydrophobic character to nanofibrils which increased hydrophobicity and achieved a water contact angle of 60°. With all these promising properties it is not surprising that nanocellulose is the second-ranked priority of the European bioeconomy (Rol *et al.*, 2019).

Except for the advantageous properties of nanocellulose materials already discussed, nanofibers that have been treated by phosphorylation have the additional benefit of being flame-retardant (Ghanadpour *et al.*, 2015). Flame-retardant materials are needed in industries such as transport, military, and furniture upholstery materials. These materials are blended into polymers which then have the benefit of not igniting and decomposing easily when heated. Normally flame-retardant materials are based on halogens instead of phosphorous as these compounds are the most cost-effective but at the same time pose a serious risk to humans, animals, and the environment. Halogen-based materials release toxic gases when combusted whereas phosphorous-based materials favor the formation of char instead. Char is a multilamellar carbonous material with thermal insulation properties which can surround and protect polymers from further decomposition (Ghanadpour *et al.*, 2015).

6.3 Materials and methods

The materials and methods relevant to this section of the project are detailed in Section 3.3. Briefly, the materials used include sludge samples collected from various locations, mostly along the bleaching sequence, in Kraft PPM as outlined in Section 3.3.1.1. **Figure 25** shows the exact location of where in the mill sludge samples were collected. Other chemicals used include urea and ammonium dihydrogen phosphate as outlined in Section 3.3.1.2. The method to pre-treatment fibres by phosphorylation is outlined in Section 3.3.2.1. After pre-treatment samples were mechanically treated using a 900 W high-speed blender to produce unfunctionalized nanocellulose which was used to produce films as outlined in Section 3.3.2.2.

6.4 Motivation for functionalization method chosen

As shown in **Figure 17** the phosphorylation has great potential regarding industrialization and produces an extremely good quality of nanocellulose (scoring 8 out of 10 according to **Figure 17**). The quality of nanocellulose as indicated by a score out of 10 in **Figure 17** was determined from mechanical properties, turbidity, nanosized fraction and size of remaining fibres in nanocellulose suspensions. Other methods that can be considered for industrialization include the enzymatic route and carboxymethylation. Carboxymethylation however produces a very low quality of nanocellulose,

scoring a 5 out of 10 according to **Figure 17** and was thus not considered a good method to investigate. Pre-treatment with enzymes was a promising alternative to phosphorylation as it is an environmentally friendly process that can very easily be industrialized and produces relatively good quality NFC, scoring 6 out of 10. Enzymes are however expensive and require exact conditions whereas the chemicals required for phosphorylation are much more cost-effective and it is a more 'robust' method.

The other method that was considered as it is a very popular topic in literature is TEMPO-oxidization (Qing *et al.*, 2013; Boufi and Chaker, 2016; Isogai and Zhou, 2019). This method scores 3 out of 5 for industrialization and 7 out of 10 for quality of NFC produced according to **Figure 17**. The method uses non-eco-friendly components like $NaClO$ and $NaClO_2$ which is one of the reasons why enzymatic NFCs are the most widely produced today (Li *et al.*, 2013). The method is also very time consuming and pH dependent (Rol *et al.*, 2019). Many literature topics focus on simplifying the multi-step procedure or finding ways to limit the amount of non-eco-friendly components used (Balea et al., 2017; Hiraoki et al., 2015; Isogai & Zhou, 2019; Masruchin et al., 2020). Despite these efforts, phosphorylation remains a cost-efficient, non-toxic, and easy method to implement making it the overall best method compared to enzymatic and TEMPO-oxidation pre-treatment (Rol et al., 2019).

Phosphorylation also addresses the biggest concern for producing nanocellulose on industrial scale: energy consumption. Like TEMPO-oxidation and carboxymethylation, anionic phosphate groups introduce charged groups onto pulp fibres which enhances delamination of fibre walls by increasing the osmotic pressure inside the fibre wall and hence the fibres swelling. For this study it was decided that pre-treated fibres would be mechanically treated by blending with a 900 W high-speed blender (NutriBullet 900 series) purchased from Nutribullet, Takealot Online (Pty) Ltd. The aim is to produce gel-like nanocellulose suspensions by blending after 5 min. Although there are many other possible mechanical treatment methods, it was decided that blending is sufficient for lab-scale experiments and no other alternatives were investigated. When considering a mechanical treatment method for industrial-scale production, economy of scale would need to be considered.

One disadvantage of phosphorylation, and for most methods to utilize sludge, is the waste produced which cannot be treated in existing Kraft Mill WWTPs without adjustments or sometimes in a separate treatment plant. In the case of phosphorylation, the waste is not toxic but needs to be processed as urea and phosphorous are responsible for an environmental condition known as eutrophication, which is when a lake or other water body contains excessive richness of nutrients leading to excessive plant and algal growth (Yeoman *et al.*, 1988). Urea is most often removed from wastewater streams by (1) biological treatment, (2) electrochemical oxidation, (3) enzymes or (4) adsorption and hydrolysis using thermal treatment (Zaher and Shehata, 2021). Phosphorous is removed from wastewater by either chemical precipitation reactions with addition of calcium, iron or aluminum salts or by biological treatments such as aerobic or anaerobic digestion (Yeoman *et al.*, 1988). Sometimes a combination of both is used to remove phosphates from activated sludge.

It is possible that if these chemicals can be recovered, they can be further utilized in fertilizer products. A study by Machdar *et al.* (2018) found that treating wastewater from a fertilizer plant with $MgCl_2$, KH_2PO_4 and KOH resulted in added-worth where the urea in wastewater is treated and a slow-release fertilizer is produced. The highest removal efficiency of ammonium achieved by this method was 94.7%. Other studies by authors such as (Uysal, Yilmazel and Demirer, 2010; Muster *et al.*, 2013; Szymańska *et al.*, 2019) involve formation of struvite ($MgNH_4PO_4$) which is a precipitation product obtained from a liquid fraction of anaerobic digestion. The formation of struvite can lead to scaling and thus operational problems, but controlled struvite formation would provide an opportunity to recover nutrients with significant commercial value.

Referring to Section 6.2, another advantageous property of phosphorylated nanocellulose is that these materials are thermally stable and flame-retardant (Ghanadpour *et al.*, 2015). This means that the material does not ignite and decompose easily when being heated. According to Ghanadpour *et al.* (2015) these phosphorous-based materials favor the formation of char instead of decomposing into volatile species. Due to this property phosphorylated nanocellulose makes excellent films, nanopaper, foams and aerogels for industries such as transport and the military.

6.5 Results and discussion

It was found that by increasing the amount of urea to about four times the amount used in previous studies (Ghanadpour *et al.*, 2015; Noguchi, Homma and Matsubara, 2017; Rol *et al.*, 2020) made it possible to successfully obtain gel-like nanocellulose suspensions by mechanically treating fibres for 5 min using a 900 W blender. It is known that the degree of substitution (DS) by phosphorous depends on (1) the molar ratio of phosphorylating agent and AGU units, (2) time of curing and (3) temperature of reaction (Ghanadpour *et al.*, 2015). Different molar ratios have been used in previous studies, and in general it has been found that salt adsorption increases with an increase in phosphorylating agent (Rol *et al.*, 2020). However, more of interest in this study was changing the molar ratio of urea used. Excess amounts of urea are used as a catalyst and to prevent degradation of cellulose which occurs during the curing stage due to the release of sulfuric acid as product of the reaction (Ghanadpour *et al.*, 2015). Normally, about 4 mol of urea is used per mole of phosphorous salt. A study by Yurkshtovich *et al.* (2007) showed however that a urea concentration of up to 3.33 M results in much higher charge content leading to easier fibrillation. This is about 4 times higher than the urea concentration reported in previous articles. Hence, the ratios chosen for this study.

It was observed that for experiments with a molar ratio of urea less than 19.6, no gel-like suspensions were obtained within 5 minutes of blending with a 900 W high-speed blender. These samples, as well as Broke Dry with a ratio of 1 : 1.2 : 19.6, did produced films with a 'paper-like' instead of 'plastic' texture. The Broke Dry and Broke Dry (+2 min) samples were further analyzed along with other gel-like suspensions, but other samples were discarded. Gel-like suspensions with varying thickness as summarized in **Table 13** were obtained for all samples with an AGU : Salt : Urea ratio of 1 : 1.2 : 19.6, with the exception of Broke Dry which did not obtain a gel-like texture even after 2 min of additional blending. The sample will be referred to as Broke Dry (+2 min). The use of such high urea levels indicate

a trade-off between the energy requirements and chemical usage to produce nanocellulose suspensions.

Table 13: Properties of gel-like suspensions and films produced from sludge samples.

Sample	Ratio	Gel-like consistency	Crystallinity (%)	Solubility (%)	Gravimetric yield (%)	Zeta potential (mV)	Film thickness (µm)
D2	N/A	No	N/A	N/A	10 ± 3.2	-13.5 ± 10.4	N/A
Broke Dry	1:1.2:19.6	No	26.7	63.0	20.0 ± 5.06	-30.9 ± 7.60	14.5 ± 2.84
Broke Well	1:1.2:19.6	Thin to moderate	18.4	78.2	44.7 ± 2.90	-52.8 ± 4.59	9.25 ± 4.22
Bleach Spill	1:1.2:19.6	Thick	14.9	97.5	87.8 ± 4.50	-58.4 ± 5.56	6.53 ± 1.67
Dual D	1:1.2:19.6	Very thick	15.4	99.1	67.7 ± 3.70	-60.4 ± 4.87	5.74 ± 1.76
OP	1:1.2:19.6	Thin	15.2	88.4	35.4 ± 2.30	-37.1 ± 11.2	6.00 ± 2.15
D1	1:1.2:19.6	Moderate	22.2	96.7	58.1 ± 3.40	-38.7 ± 5.62	7.51 ± 1.70
D1/D2	1:1.2:19.6	Thin to moderate	23.7	86.3	53.5 ± 5.10	-40.5 ± 5.61	8.90 ± 1.62
D2	1:1.2:19.6	Moderate to thick	21.6	99.0	66.4 ± 4.67	-50.3 ± 3.45	9.95 ± 2.03
Cut-offs	1:1.2:19.6	Very thick	12.5	97.8	92.3 ± 2.60	-40.5 ± 6.49	9.17 ± 1.84

Table 13 summarizes some of the analyses results, including a qualitative description of the thickness of films obtained, the crystallinity index, gravimetric yield, zeta potential and film thickness. The crystallinity index, gravimetric yield and zeta potential are discussed in subsections. The consistency of gel suspensions varies quite considerably for samples as can be seen in **Table 13**. The best consistencies were achieved with Dual D and Cut-offs samples. The thickness of suspensions is referred to as 'very thick'. Bleach Spill samples obtained similar consistencies although always slightly less viscous than the former samples and thus the consistency is described as only 'thick'.

Other samples did not achieve the same (thick) viscosity as these three samples. Some samples are described as having a "moderate" viscosity and other samples had a "thin" viscosity (**Table 13**). Broke Dry was the only sample to not form a gel-like suspension under these conditions, with OP being second to last with a gel suspension that was just obtained after 5 min of mechanical treatment. The average film thickness, excluding Broke Dry, had film thicknesses between 5.5 and 10 μm. Broke Dry had an average thickness of 14.5 μm. The variation in film thickness is likely due to the vacuum filtration that is applied to remove entrapped air bubbles before placing films in the incubator.

Another property reported in **Table 13** is the solubility of films. The films retain between 87 and 99% of their weight (**Table 13**), i.e., lost only between 1 to 13% of their weight, when placed in 95% ethanol indicating that these films are alcohol insoluble. As mentioned in Section 3.4.8, the ability or inability of a film to dissolve in alcohol influences the application for which they can be used. Films that are alcohol insoluble are desirable for used in drug delivery as most drugs on the market today are either weakly basic or weakly acidic and it has been found that their undesired drug release kinetics poses a high risk of dose dumping and drug toxicity in certain cases like when alcohol is co-ingested with drugs

like opioids (Han and Chang, 2018). This has led to studies, like the one by Han and Chang (2018), where the objective was to produce alcohol-insoluble nanoparticle suspensions and design a coating for drug delivery that prevents alcohol-induced dose dumping.

The color of gel-like suspensions was the same as the pulp samples shown in **Figure 26** with sample transparency increasing as the bleaching sequence progressed (i.e., Bleach Spill, Dual D, OP, D1 and D2). Even though the transparency of the gel-like suspensions differed, the films produced were too thin to observe a difference in transparency. **Figure 35** shows the initial freeze-dried pulp samples and the final product obtained, which is a transparent NFC film.

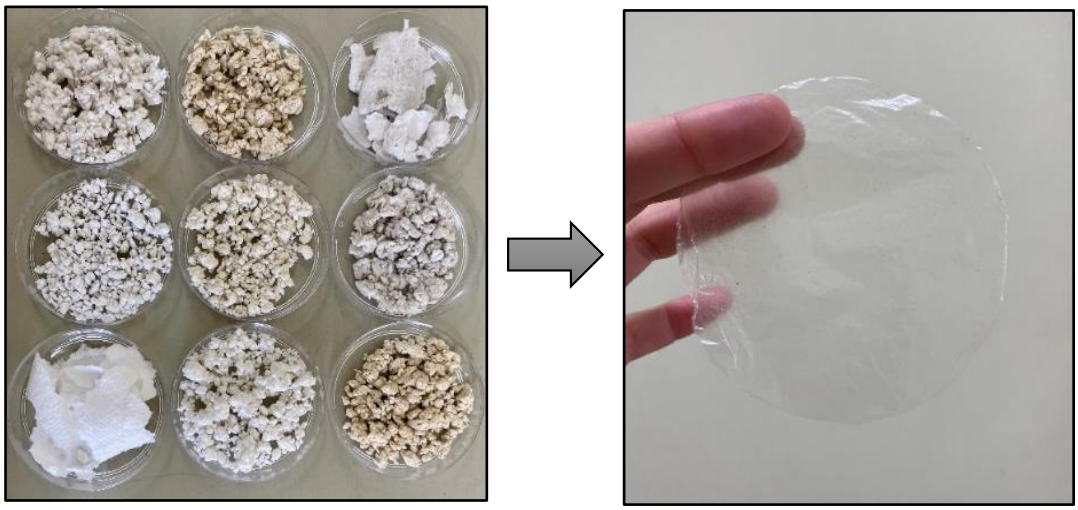

Figure 35: Transparent microfibrillated cellulose (NFC) film made from phosphorylated fibres.

6.5.1 Functional groups and structure of fibres after phosphorylation

The IR spectra in **Figure 36** and **Figure 37** confirms that phosphorylation was successful. **Figure 36** displays the IR spectra of all sludge samples that were treated by phosphorylation, which when compared to the IR spectra of untreated samples in **Figure 28**, shows the same general trends. Once again peak intensity in the region between 3200 and 3650 cm^{-1} decreases as bleaching progresses, i.e., from Bleach Spill to Cut-offs. The discarded samples from Broke Dry and Broke Well have the highest peak intensity overall. The difference in peak intensity is not as noteworthy in the region between 900 and 1200 cm^{-1} although peak height is a bit more pronounced for spectra in **Figure 36** than **Figure 28**. New peaks indicating that phosphorylation was successful appear at 832, 910, 1230 and 1710 cm^{-1}. This can better be seen by comparing treated and untreated samples as shown in **Figure 37**.

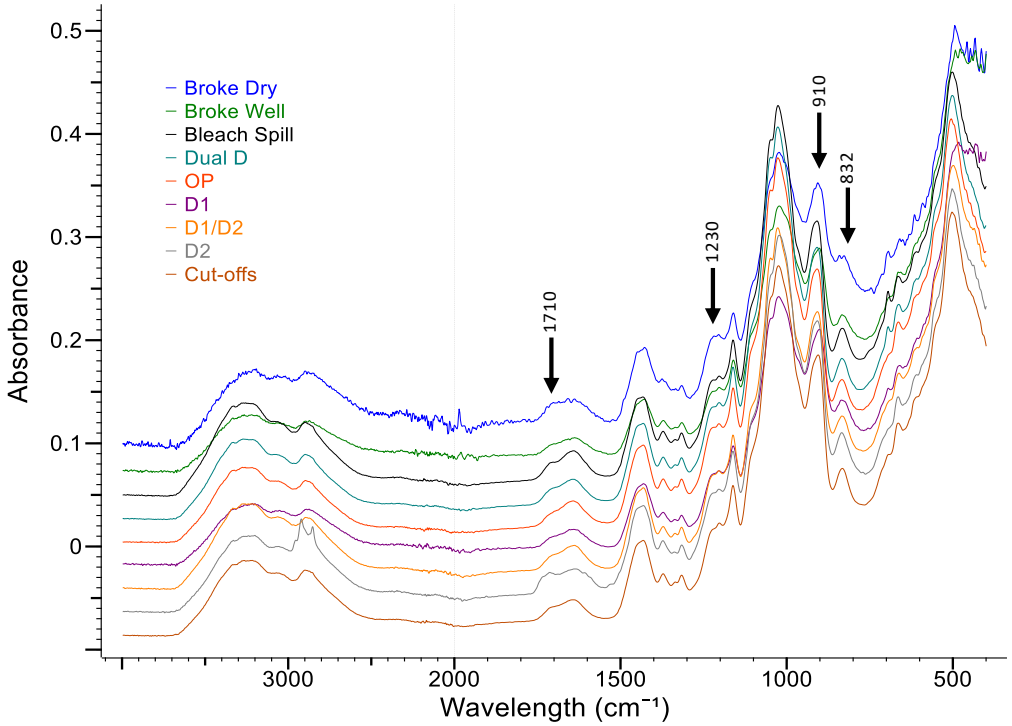

Figure 36: FTIR analysis to determine functional groups of sludge samples from Kraft pulp and paper mill after treatment by phosphorylation.

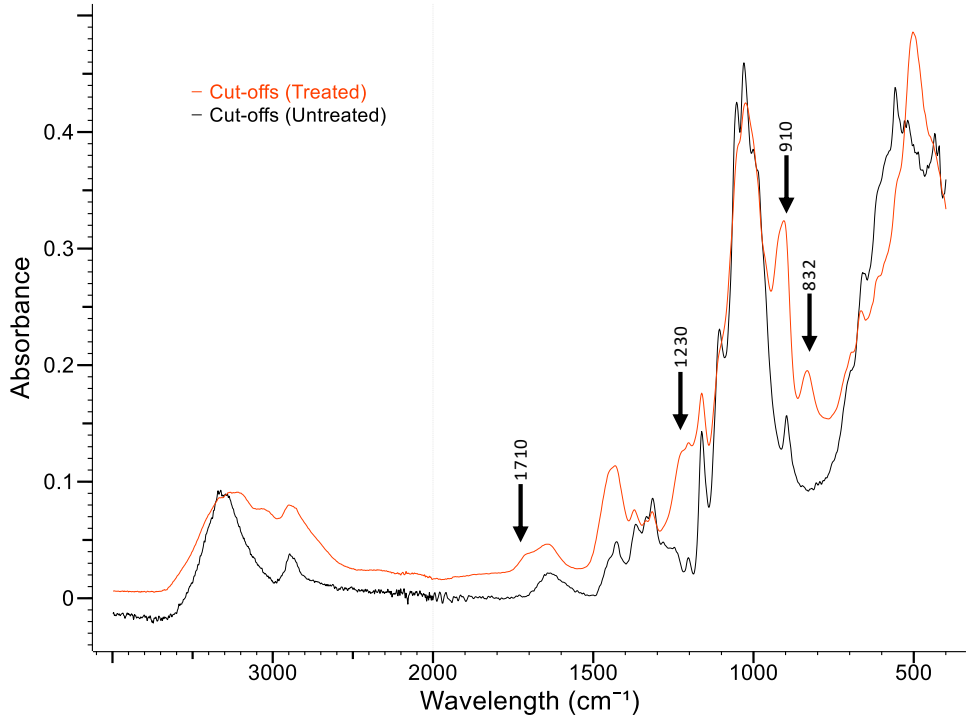

Figure 37: FTIR analysis of Cut-offs comparing functional groups of untreated and treated fibres by phosphorylation.

Figure 37 shows the IR spectra of Cut-offs, comparing the untreated and treated spectra. New peaks are present at 1710, 1230, between 900 and 940 and at 832 cm^{-1}. The new band at 1710 cm^{-1} corresponds to the C = O stretching mode (Aoki and Nishio, 2010). This occurrence supports the

hypothesis that oxidation occurs during the reaction when fibres are cured. The study by Ghanadpour *et al.* (2015) found that oxidation increases with curing time. The bands at 1230 cm^{-1} and 910 cm^{-1} further support phosphorylation with the peaks corresponding to the P = O stretching mode (Suflet, Chitanu and Popa, 2006; Coleman *et al.*, 2011; Božič *et al.*, 2014) and P – OH stretching mode (Suflet, Chitanu and Popa, 2006; Coleman *et al.*, 2011). The final new band at 832 cm^{-1} corresponds to the P – O – C aliphatic bond (Suflet, Chitanu and Popa, 2006).

The IR spectra of untreated versus treated spectra for all other sludge samples can be found in **Figure F1** in Appendix F. The spectra of these samples follow the same general trends as the IR spectra for Cut-offs described previously. The only difference is that for some samples the peak at 1030 cm^{-1} which represents C-O valence vibration related to cellulose, specifically C(3)-O(3)H, according to Lehtonen *et al.*, (2020) is lower and less pronounced. This is specifically the case for Broke Dry, Broke Well and D1. This could be an indication that cellulose degradation occurs to an extent in these samples but not other samples.

6.5.2 Presence of phosphorous after pre-treatment and metal components

In initial experiments SEM-EDX was used to determine if phosphorylation was successful. This was done by phosphorylating sludge samples obtained from the WWTP of Kraft PPM after dewatering. After phosphorylation the samples were repeatedly washed with DI water in a vacuum filtration setup to ensure all excess phosphorous salt and urea is removed from samples. The photos taken are shown in **Figure 38**. The number displayed at the top of the figure corresponds to resultant spectrums that are attached in Appendix G. The presence of heavy metals can potentially limit the application for which these fibres can be used, for example, in food packaging where certain metals can be harmful to human health if digested (Conti, 2008). Heavy metals like cadmium (Cd), barium (Ba) and copper (Cu) are known to accumulate in leachate wastewater from PPM wastewater (Aprianti *et al.*, 2018).

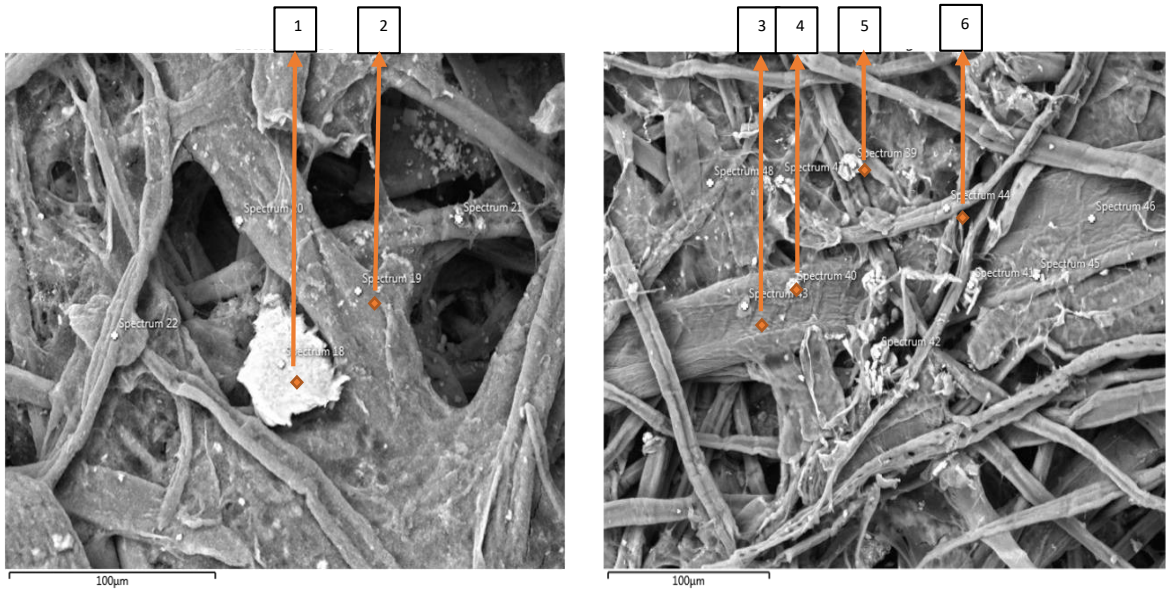

Figure 38: SEM-EDX images of sludge obtained from Kraft pulp and paper mill to confirm phosphorylation and presence of contaminants.

Spectrum 1 in this case indicates the presence of aluminum in samples. Spectrum 2 captures information about the fibre and has a strong phosphorus peak (11.0 cps/eV), indicating that phosphorylation was successful. Spectrum 3 indicates the presence of calcium in samples. Spectrum 4 shows minor peaks of sodium and potassium (< 2.00 cps/eV) as well as a major peak indicating silicon (16.0 cps/eV) present in samples. Spectrum 5 does not necessarily confirm phosphorylation, although a major peak of phosphorous is present (12.2 cps/eV). This peak is most likely a precipitated phosphate salt by the presence of calcium. It is possible that the presence of these salt still help to decrease energy consumption when producing MFC as this is the case with carboxymethyl cellulose adsorption (Rol *et al.*, 2019).The same is true for Spectrum 6 which confirms phosphorylation with a peak of 21.5 cps/eV and indicates the presence of some metals and silica (< 2 cps/eV). Silica is usually used in papermaking as a chemical compound in paper coating and is known to improve brightness and opacity of paper (Lourenço *et al.*, 2015).

The presence of metals is not uncommon for pulp and paper mill sludge. These metal salts contribute to the conductivity of effluent streams. Calcium is likely from the incoming fresh water. A high presence of calcium is possible especially if the water is hard (Xu, Pruszynski and Hart, 2017). Additives will also contribute to ion presence as most additives are designed in a salt form for good water solubility. Examples include Rosin soap which give Na^{+} or K^{+} and alum or poly-aluminum-chloride (PAC) which introduced Al^{+3}(Xu, Pruszynski and Hart, 2017). The acid and caustic soda added to the process for pH adjustments will add additional ions. Magnesium ions (Mg^{+2}) are likely present from the wood itself depending on the growing environment (Xu, Pruszynski and Hart, 2017).

The presence of these metals increases the conductivity of effluent streams which influences the performance of surfactants in recovery by flotation as discussed in Section 5.5.3. None of the metals listed are however heavy metals like Cd, Ba or Cu that pose a risk to human health or endanger the environment and will thus not implicate or limit the potential application of unfunctionalized nanocellulose from these fibres.

6.5.3 Macroscale and nanoscale range of fibres in nanocellulose (NFC) suspensions

The apparent heterogeneity of samples is confirmed by PdI values which is ≈1 for all samples. Fibres in suspension also tend to agglomerate, which makes it very difficult to capture an accurate size distribution. For this reason, gel-like suspensions were diluted and analyzed using a ZetaSizer® to capture information about the agglomerate dimensions and a gravimetric method described earlier was used to determine the nanosized fraction to quantify the amount of nanomaterial present in samples. The gravimetric results are previously summarized in **Table 13**. The ZetaSizer results are summarized in **Table 14** and visually shown in **Figure 39** which further confirms the heterogeneity in samples.

Table 14: Summary of nanocellulose (NFC) particle size diameters determined using a ZetaSizer®.

Sample	Peak 1		Peak 2	
	Size (nm)	Intensity (%)	Size (nm)	Intensity (%)
Broke Dry	198.7 ± 25.56	50.4	1523 ± 265.8	49.6
Broke Well	222.8 ± 23.59	45.8	1719 ± 287.4	54.2
Bleach Spill	559.8 ± 74.59	100		
Dual D	500.8 ± 43.16	100		
OP	51.06 ± 8.751	7.20	622.0 ± 231.6	92.8
D1	135.2 ± 12.71	48.7	882.4 ± 114.0	51.3
D1/D2	228.3 ± 20.91	100		
D2	582.3 ± 50.99	100		
Cut-offs	205.7 ± 24.34	63.6	1209 ± 165.8	36.4

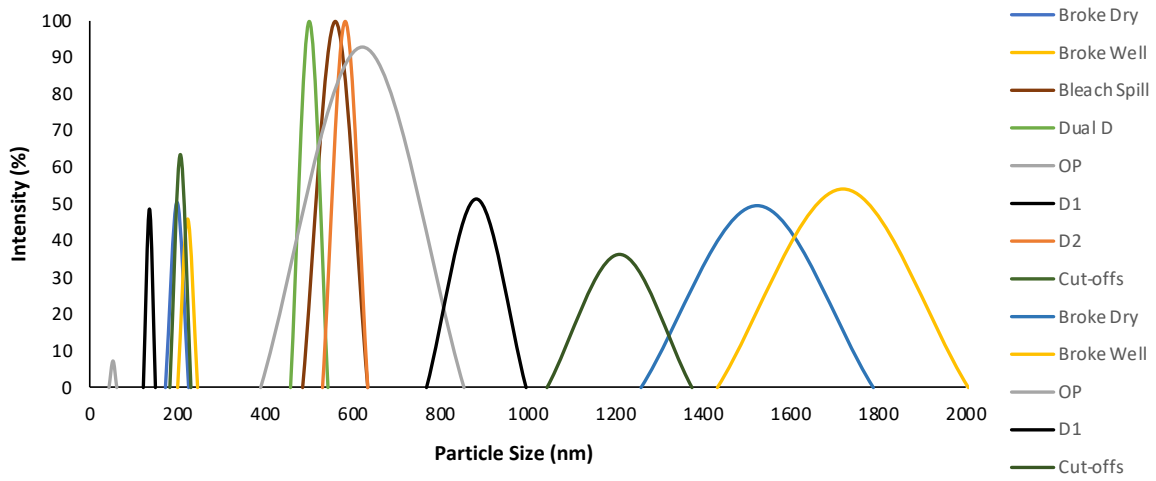

Figure 39: Visual distribution of nanocellulose (NFC) particle size diameters determined using a ZetaSizer®.

According to **Table 14** and **Figure 39** Broke Dry samples contain some nanoclusters in the nanoscale range (198.7 ± 25.56 nm) although these clusters could not be seen in FE-SEM images. Broke Well displays a similar particle size distribution with almost 50% of particles being in a class range of 222.8 ± 23.59 nm and the rest being in a class range of 1719 ± 287.4 nm which is actually in the micrometer range. It can be seen from FE-SEM images that phosphorylation seems more successful for Broke Well than Broke Dry as the fibres are separated compared to the denser fibre network of Broke Dry. Individual fibres and clusters show that the degree of substitution is higher, leading to fibres repelling one another which subsequently leads to a "swelling" effect. This behavior is mimicked by the zeta potential values which is higher for Broke Well compared to Broke Dry with values being -52.8 and -30.9 respectively.

Like Broke Dry and Broke Well, Bleach Spill, Dual D and D2 samples have similar size distributions. These samples have only one peak according to Zetasizer results with size distributions of 559.8 ± 74.59, 500.8 ± 43.16 and 582.3 ± 50.99 nm. Nanoclusters and individual fibres can clearly be seen

from FE-SEM images at magnifications of 10, 20, 50 and 100 μm. OP samples have two size classes with around 7.20% being in the nanoscale range of 51.06 $\pm$ 8.751, which is also the smallest size class reported from Zetasizer results, and 622.0 $\pm$ 231.6 nm. The larger size class has a very large variance and thus more particles closer to the microscale range than Bleach Spill, Dual D and D2 samples. From the FE-SEM images some of these very small nanoclusters can be seen although they are few and widely dispersed in the sample. The same can be said for D1 samples which follow a similar trend although with larger particle size distributions of 135.2 $\pm$ 12.71 nm and 882.4 $\pm$ 114.0 nm. According to Zetasizer results D1/D2 and Cut-offs samples have the smallest high-intensity peaks of 100% at 228.3 $\pm$ 20.91 and 205.7 $\pm$ 24.34 nm respectively. The FE-SEM image of Cut-offs does not really show and fibres in the image taken at a magnification of 100 μm and the fibres in the image appear much flatter, likely due to the fact that the fibres were dried before being re-dispersed and pre-treated prior to mechanical treatment.

The Zeta potential and gel-consistency seem to be positively correlated when looking at data from **Table 13**. Zeta potential gives an indication to the degree of substitution of phosphorous salts to fibres, with higher zeta potential indicating higher degree of substitution. In general, thin to moderate gel consistencies like OP, D1 and D1/D2 have lower zeta potential values compared to thick gel suspensions like Bleach Spill and Dual D. Dried samples Broke Dry and Cut-offs have much weaker potentials than their counterparts Broke Well and D2, which once again confirms the irreversible changes in morphology of dried fibres. During drying, the removal of water brings adjacent fibres in close contact which leads to hydrogen bonds forming between them (Garcia *et al.*, 2002). The result is a loss in fibre conformability and swelling capacity which impedes the bonding potential of these fibres. These changes will influence defibrillation process as well as pre-treatments prior to mechanical treatment. According to the quality index developed by (Desmaisons *et al.*, 2017) the quality of never-dried NFC is around 10% higher. Samples containing more lignin, i.e., samples earlier in the bleaching process like Bleach Spill and Dual D, have higher zeta potential values (-58.4 and -60.4 mV) than samples further along in the bleaching sequence.

This observation is in disagreement with a study by Balea *et al.* (2017) who reported that NFC from unbleached pulp had lower zeta potential values compared to bleach pulp NFC. The fibres were pre-treated by TEMPO-oxidation and resulted in zeta potential values of between -20 and -60 mV. According to the author this is because the cellulose of bleached pulp is completely available for TEMPO-mediated oxidation and thus the zeta potential for bleached pulp is entirely due to the anionic charge of NFC whereas sample with higher lignin concentration consumes $NaClO$ to release part of lignin. This reduces the efficiency of TEMPO-oxidation and NFC zeta potential. Released impurities with anionic charge counterbalance the charge and increase the zeta potential. In the case of phosphorylation, the urea and phosphorous salt do not attack or degrade lignin which could explain why this does not occur with phosphorylated NFC. Lignin is naturally hydrophobic and group addition is known to influence both the hydrophobicity and negative charge of lignin (Wu *et al.*, 2020). This is a potential reason for the higher zeta potential values of Bleach Spill and Dual D.

The highest gravimetric yields were obtained for Cut-offs followed by Bleach Spill, Dual D and D2 which achieved yields of 92.3, 87.8, 67.7 and 66.4% which indicates these samples have the highest nanofraction. This is more or less in agreement with the Zetasizer results. Cut-offs have a class size with an average of 205.7 $\pm$ 24.34 nm whereas the peaks for the other three samples are double or more in size. Cut-offs do however have fibre sizes in the microscale range with a peak at 1209 nm. The intensity of this peak is around 36.4%. All other samples have gravimetric yields of less than 60.0%. Broke Dry samples have the lowest yield of 20.0% whereas Broke Well has a gravimetric yield of 44.7% which is strange when compared to the Zetasizer results but could potentially be due to agglomerates that formed causing the Zetasizer to determine the peak intensities of these clusters more than individual fibres.

6.5.4 Crystallinity index (CI) of nanocellulose pre-treated by phosphorylation

The reported crystallinity indices for phosphorylated NFC in this study, as summarized in **Table 13**, is much lower than for other reported studies. Values range from 12.5 for Cut-offs to 26.7% for Broke Dry. The plots generated from XRD to determine the crystallinity indices can be found in Appendix I. The study by Noguchi, Homma and Matsubara (2017) obtained crystallinities of between 84 and 86%. The author also pre-treated fibres by phosphorylation, following more or less the same method. Noteworthy differences in methodology include lower curing time which in this case was a maximum time of 10 min and a lower concentration of urea was used (12 g urea for every 10 g of pulp).

Other phosphorylation studies did not report crystallinity index values. The difference in this case is thus attributed to the difference in curing time as longer curing times lead to greater oxidation or the higher quantity of urea used in this study. High concentrations of urea can lead to a side reaction creating carbamate (Rol *et al.*, 2020). From a nanofibrillation point of view this is not a problem as the formation of carbamate also weakens H-O bonds between cellulose nanofibrils. The high possibility of this reaction occurring would explain the lower crystallinity index values as the cellulose I crystal structure groups are degraded. Lower crystallinities are also an indication of complete separation of crystalline cellulose microfibril bundles into individual nanofibers (Isogai and Zhou, 2019).

6.5.5 Morphology of nanocellulose (NFC) films

Electron microscopy images of dried films are shown in **Figure 40** for Broke Dry and Bleach Spill at a magnification of 100 μm. Images of the other samples at magnifications of 10, 20, 50 and 100 μm are attached in Appendix G. The NFC suspensions are a multiscale and complex material with fibre dimensions in the millimeter, micrometer, and nanometer range, images were captured at these various magnifications to obtain information about the microfibre as well as nanofibre dimensions.

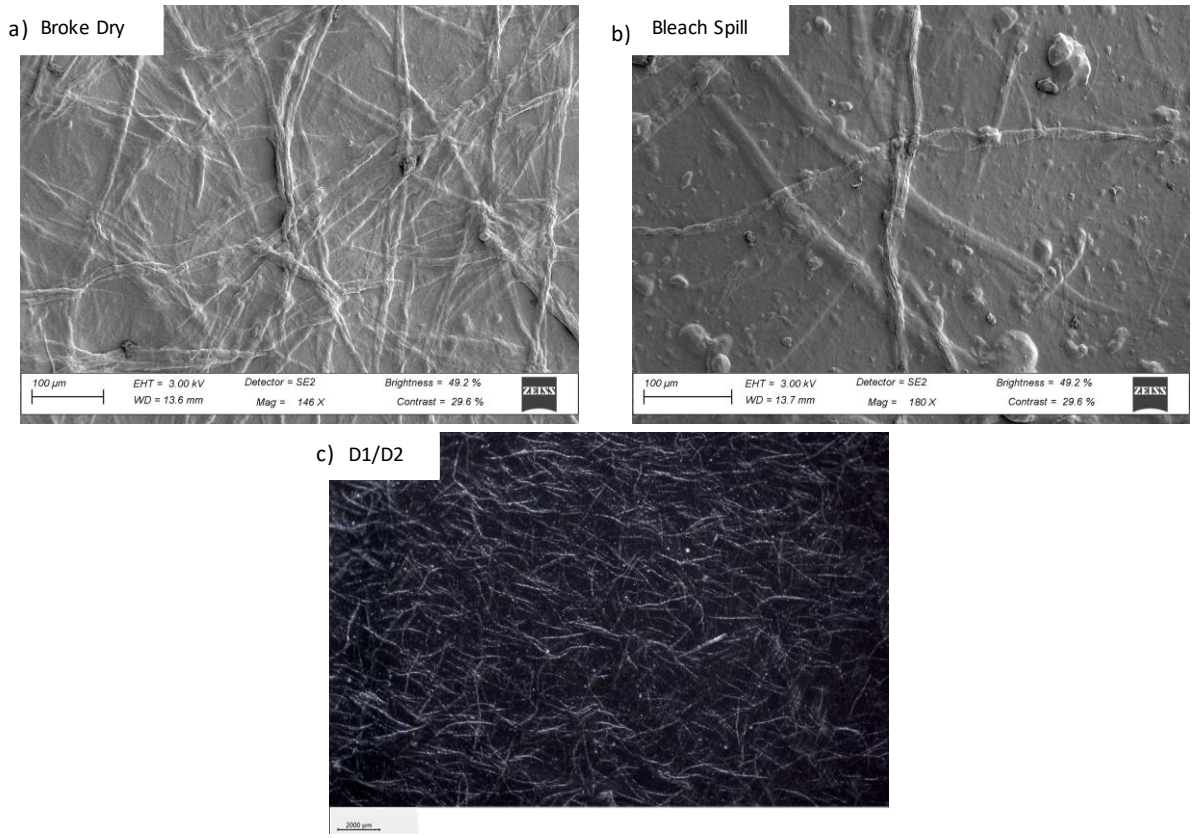

Figure 40: FE-SEM images of a) Broke Dry (100 μm magnification) and b) Bleach Spill dry films (100 μm magnification). Absence of micro air bubbles is confirmed with optical microscopy as shown in c) at 2000 μm magnification.

The Broke Dry films were different from Bleach Spill films (**Figure 40** a and b, respectively) in the sense that Broke Dry films showed an entangled fibre network with no clusters present whereas Bleach Spill films (**Figure 40** b) had small nanoclusters. The Broke Dry films are the only film samples that did not show any clear nanoclusters, all the other samples appear to contain varying quantities of short, rod-like particles (shown in Appendix G) compared to the larger more networked fibrils as in the Broke Dry films. The presence of these nanoclusters is an indication of how effectively fibres could be fibrillated or delaminated after being pre-treated by phosphorylation. According to Isogai and Zhou (2019) the efficient repulsion between anionic nanofibers in water leads to the randomly orientated, closely packed nanofiber clusters seen in these images. The negatively charged groups generate strong repulsive forces, which result in the separated individual fibres seen in SEM images.

Enzyme pre-treated fibres from a study by Qing *et al* (2013) had similar morphologies to those in this study. The study by Qing *et al* (2013) reported that the pre-treated films contained large portion of short, rod-like particles while samples that were only mechanically treated using a Super Mass Collider grinder, formed larger and more networked structures similar to Broke Dry samples. The same study reports that some mechanical treatments are able to create more uniform nanomaterials, but usually these technologies are not as easily scalable and thus not preferred for industrial scale (Qing *et al.*, 2013). Multi-staged or optimized process conditions like solids content and disk gap could possibly

result in more uniform fibres resulting in more homogenous materials but these additional steps and cost might not be necessary depending on the application and desired properties of the material.

The absence of micro bubbles was confirmed for all sample with optical microscopy. **Figure 40** (c) shows the result for D1/D2 films. The absence of air bubbles is attributed to the combination of stirring samples for 8 h at ambient temperature followed by vacuum filtration before being placed in the incubator to be dried. It was found that only stirring was not sufficient to remove all entrapped air. Samples are diluted to more easily remove entrapped bubbled from the gel-like suspensions.

6.5.6 Thermal stability of films produces from nanocellulose (NFC) suspensions

TGA analyses was performed to determine the thermal stability of films produced. The curves displayed in these figures were used to determine the onset temperature ($T_{onset10\%}$), the temperature at maximum rate of weight loss (T_{max}) and the residue at 800 °C. The onset temperature is the temperature at which 10% of weight loss has occurred. It was expected that all films would display the same trend, which was confirmed by analyses. The resultant curve is shown in **Figure 41**. The orange curve represents the typical behavior of thermal degradation of cellulose (untreated by phosphorylation) in a nitrogen environment and is redrawn based on results from the study by Ghanadpour *et al.* (2015) which used the same feedstock material for producing nanocellulose as in this study. It would have been more accurate to compare the results to an untreated sample of this study and can be considered a recommendation for future research. The black curve presents the results from films treated by phosphorylation in this study. Values for $T_{onset10\%}$ and T_{max} are 200 and 248 °C respectively. The final residue at the end of the test was 41%.

These values compare well to literature findings. The study by Ghanadpour *et al.* (2015) produced phosphorylated films with temperatures 258 and 283 °C for $T_{onset10\%}$ and T_{max} respectively. Typical results for nanofilms prepared via other or no pretreatment methods typically results in TGA curves similar to the blue curve displayed in **Figure 41**. A study by Chen *et al.* (2011) which pre-treated fibres with sodium chlorite and potassium hydroxide prior to mechanical treatment reported a $T_{onset10\%}$ of 335 °C and T_{max} of around 370 °C. Final residue at only 600 °C was already at a low 20%. The completely unmodified pulp fibres from the study by Ghanadpour *et al.* (2015) reported a $T_{onset10\%}$ and T_{max} of 315 and 358 °C respectively and obtained a final residue of around 20% at 800 °C.

The presence of phosphorous in films causes an earlier dehydration reaction toward char formation as can be seen in **Figure 41**. The maximum rate of weight loss is however reached much faster, after which the film weight decomposes at a much slower rate. The final residue at 800 °C is higher for films prepared from phosphorylated fibres compared to untreated fibres by 20% or more. The improved weight retention could be purely due to the presence of non-volatile phosphorous compounds. In a nitrogen environment the phosphorylated films displayed higher stability above temperatures of 330 °C. For certain applications of nanocellulose this property of films is extremely valuable especially in industries such as transport and the military as discussed in Section 6.4.

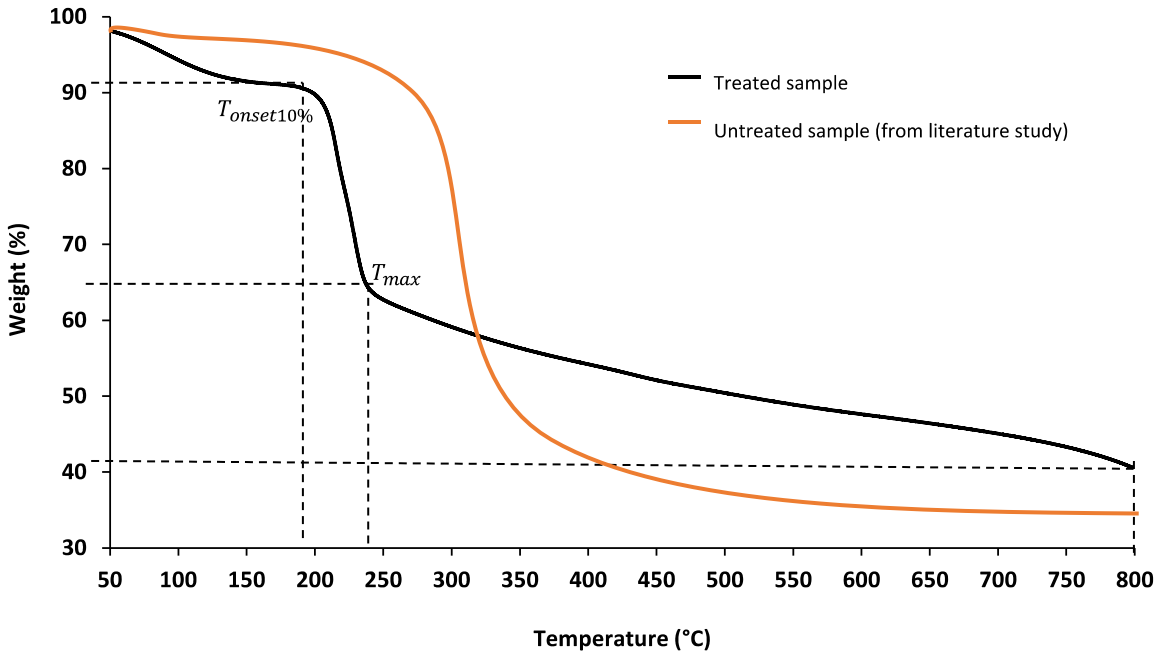

Figure 41: Thermogravimetric Analysis (TGA) curve of phosphorylated cellulose fibre films to determine the thermal stability of films.

6.6 Conclusion

The films produced from nanocellulose suspensions were thermally stable and alcohol insoluble. The former property makes films appropriate for applications like films, nanopaper, foams and aerogels in transport and military industries. The latter property holds great potential for drug delivery applications where the objective is to produce coatings that prevent alcohol-induced dose dumping. One potential downside of the materials produced is its multiscale dimensions, with all samples tested having a polydispersity index of ≈1. Depending on the desired application, this can be a limiting factor. The transparency of films can also be a limiting factor for some applications. If that is the case samples from the broke system as well as Bleach Spill, Dual D and OP samples need to be kept separate from other samples and used for alternative applications.

The overall best quality nanocellulose was difficult to determine, but in general Bleach Spill, Dual D, D2 and Cut-offs samples produced better quality nanocellulose with thicker gel-like consistencies, higher gravimetric yields, higher (negative) zeta potential values and smaller particle size distributions. The crystallinity indices for all samples were between 12.5 and 26.7% which is very low compared to previous studies, although it was difficult to compare due to few studies reporting these values. However, the lower values are attributed to longer curing time and the much higher concentration of urea used which leads to a side reaction forming carbamate that consequently weakens h-o bonds between cellulose.

7 THE POTENTIAL TO COMBINE WASTE STREAMS AND THE USE OF SOFT SENSORS TO PREDICT FIBRE'S AND FILM'S QUALITY

The identified potential sources of fibre waste sources have the potential to be combined into a single waste source. However, there is need to consider how the fibre waste should be transported to the intended plant for recovery and functionalization. There are many possible solutions and considerations to be taken into account including the sewer layout. However, these considerations are Kraft PPM specific because it is difficult to contextualize a solution presented to other Kraft mills as the feedstock, products produced, layout and equipment varies for each. Note that the discussion in this chapter is presented as a guideline for future research efforts.

An important factor to consider when the goal is to functionalize waste fibres to nanocellulose or even other products like biofuels, biopolymers, building materials or fish feed include the amount of sludge produced and sludge uniformity. The amount of sludge produced according to (Scott and Smith, 1995) as mentioned earlier would amount to around 41760 ton of sludge produced per annum for a mill the size of Kraft PPM. From the mass balance it was seen that the amount of effluent going into drains is 12716 ton fibre per year. A more accurate estimation is 1 to 3% of fibre going waste. For Kraft PPM 2.5% of their production ended up going to waste.

Collecting fibers at a common point like just before a WWTP is not the best option as there is a lot of other contaminants washed down effluent lines that will collect with fibers at this point like sand, grit, and bits of bark and potentially small rocks. Effluent sent to WWTP has a concentration of non-fibrous solid material that is ordinarily several times the amount of fibrous material, usually 1 to 10% more by weight (Gardner, 1965). It is possible to separate contaminants from fiber using a screen but then there is always the potential of clogging and moving screens require regular maintenance and are energy intensive. It would thus be better to devise a solution that collects these fibres before all drains combine.

An example solution would be recovering fibers from PM41 by flotation, then transporting the concentrated product to a functionalization plant. Sludge samples could be sprayed down into Acid and Alkaline effluent lines, as normally done, and then be collected at the point where these two effluent lines are combined. This will likely be beneficial as combination of these streams will neutralize the pH to some extent making functionalization easier if a neutral pH is required. The combined effluent is then transported to a functionalization plant. The streams will likely be very dilute which would make flotation or alternative dewatering or concentrating method necessary for most functionalization applications. By collecting these at an earlier stage of the process like described would result in a smaller volume of effluent to be treated in WWTPs which is likely to be cost beneficial to the process.

Nanocellulose suspensions from PM41 contain fully bleached fibres and thus the result is a clear gel compared to fibres from earlier in the bleaching sequence. The presence of chromophores in samples like Bleach Spill and Dual D result in decreased light transmittance and thus resultant films are not as clear compared to fully bleached samples. Combining different waste streams would thus also depend

on the application and whether high transparency is desired. If it does not matter then potentially all effluent streams, PM41, Acid and Alkaline Effluent, could be combined to recover fibres.

When combining different effluent streams the quality of nanocellulose will vary depending on the amount of fibre from each source. This is where soft sensor development has a lot of potential to help predict the quality of the nanocellulose produced. Essentially the model uses near-infrared spectroscopy (NIR) data combined with lab data to create calibration curves. An example of such a graph is given in **Figure 42** where the online Kappa number is used to predict the lab Kappa number. It can be seen that in this case the linear model is a good fit for the data with an R^2 value of 94.8%. The equation displayed is then used to predict the online Kappa number based on lab values. These values are used to validate the model and can essentially be compared to a memo to test the accuracy of the model. It can be seen from **Figure 42** that there are some outliers in the data. As time progresses and more data is added the accuracy of predictions will improve.

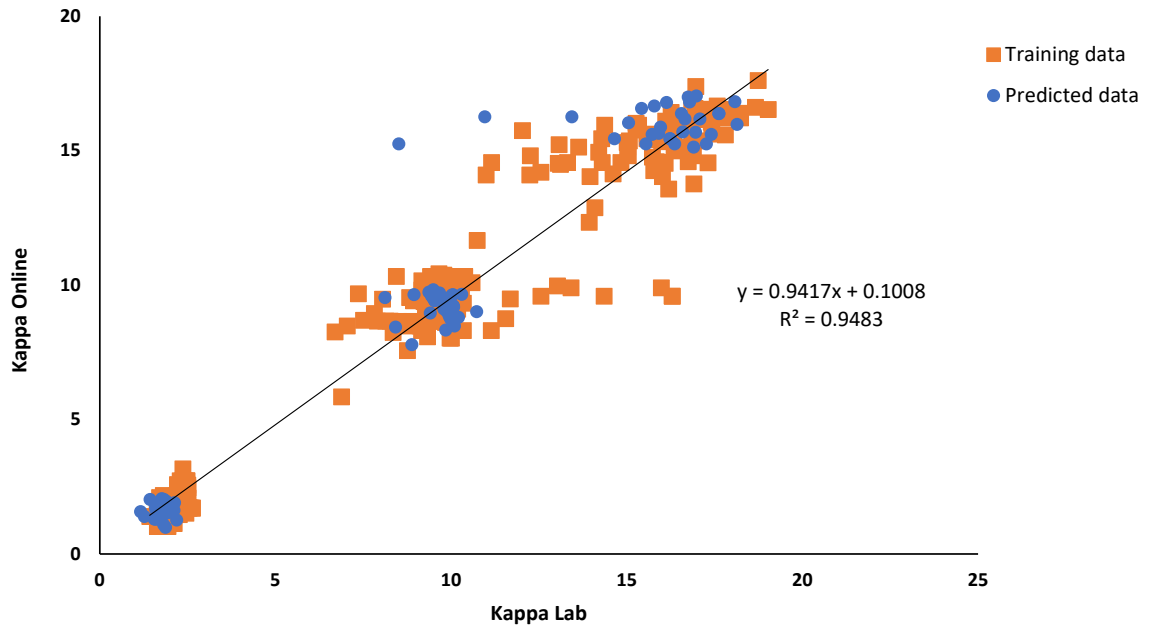

Figure 42: Soft sensor development calibration curve to predict the Kappa number.

Many other predictions like the one in **Figure 42** are possible. Authors such as (Daraei, 2016) used NIR spectra of raw wood chips to predict the amount of acid insoluble lignin, moisture content and yield as well as the Kappa number. Regression models were developed relating spectra of NIR to known amounts of lignin and moisture in the wood which were determined by standard methods in the lab. The models had R^2 values of 92%, 89%, 85% and 99% indicated a good fit for the data. In a similar manner to predicting the Kappa number, moisture content in wood chips, acid insoluble lignin and yield the quality of nanocellulose can be predicted using quality indexes (QI) like the one suggested by (Desmaisons *et al.*, 2017). The NIR values are associated with QI values and can be used to generate a similar calibration curve to the one in **Figure 42** where the y-axis in this case would read "QI Online" and the x-axis "QI Lab".

8 CONCLUSIONS AND RECOMMENDATIONS

8.1 Conclusions

This study found that it is possible to recover a reasonable amount of cellulosic fibre from Kraft pulp and paper mills. For Kraft PPM, around 0.6% of fibre in the feed was lost to effluent streams which resulted in 3289 ton of valuable fibre going to waste through landfilling and incineration in a year. This amounts to an average of 8.15 kg of sludge produced per ton of pulp. The biggest source of fibre loss is from the portion of paper machine whitewater left untreated by the save-all device which resulted in a loss of 2046 ton of fibre lost in a year. Other waste streams identified include Alkaline and Acid Effluent from the Kraft bleaching plant which resulted in fibre losses of 658 and 585 ton in a year.

This study further found that recovery by flotation using colloidal gas aphrons was a suitable method for recovering these fibres with high recovery rates of up to 77.8%. Recovery by flotation can easily be integrated into Kraft pulp and paper mills as a kidney technology to support existing WWTPs and reduce the amount of effluent that needs to be treated. Depending on the mill sewer layout, it is possible to combine and recover these fibres from a single waste stream.

Recovered fibre was functionalized to nanocellulose and phosphorylation was found to be an effective pre-treatment method that produced thermally stable films. This study along with previous studies showed that phosphorylation has immense potential as a pre-treatment method. The method is simple, easy to industrialize and does not require any toxic chemicals. Hence, pre-treating recovered fibre by phosphorylation should be easy to integrate into a Kraft mill system. The method has the added benefit of requiring a low solid content of around 1 wt% and thus minimal de-watering is needed before pre-treating fibres by this method. There is also the potential of further utilizing the excess urea and phosphorous salts from this pre-treatment method to fertilizer products.

Overall, flotation using CGAs and pre-treatment by phosphorylation proved to be promising methods for fibre recovery and functionalization at industrial level. Finally, this study found that near-infrared spectroscopy (NIR) combined with properties like chip moisture and lignin content has a lot of potential to be used in developing soft sensors. These properties are used to generate calibration curves that predict future values thereby reducing the need to rely only on time-consuming lab tests that can lead to hours of off-spec product. Soft sensors can potentially further be used to predict the quality of nanocellulose being produced from recovered fibres.

8.2 Recommendations and future work

Pilot-scale flotation studies and a detailed cost analysis are needed before recovery methods such as the one proposed in this study can be successfully industrialized. Furthermore, there are many other green-based surfactants that can be studied for generation of colloidal gas aphrons (CGAs). It is known that not all surfactants can form CGAs, although the reason for this is not known. A study to determine the reason for this would be worthwhile as it would make finding suitable, green-based alternatives to synthetic surfactants easier.

The potential of specifically using xylan as an alternative surfactant is especially promising as xylan is a valuable component of cellulosic fibre that is normally lost during the cooking stage of Kraft pulping. Using xylan to generate CGAs which would likely help to further reduce energy requirements for producing nanocellulose and also contribute toward the biorefinery concept within a Kraft mill. There are many articles and publications about methods that have been investigated to recover this component prior to cooking in Kraft pulping and functionalizing it to products like surfactants. Questions that have not yet been addressed or adequately investigated include (1) the cost of producing xylan surfactants, (2) whether xylan surfactants can be used to produce CGAs and (3) whether a diafiltrating system is necessary to remove the surfactant prior to functionalizing recovered fibres to nanocellulose.

Regarding phosphorylation as a pre-treatment method, a detailed cost analysis as well as a review of all the different methods to recover and utilize excess phosphorous salts and urea in wastewater generated by this method is needed before industrialization can be considered. Finally, the potential of using soft sensors to predict nanocellulose quality can be further explored. A combination of NIR and lab data can be used to train partial-least square (PLS) or principal component regression (PCR) models which can then be used to predict the response (in this case the quality of nanocellulose) using the calibrated model. A large set of data considering many different processing conditions will be needed to create a calibration curve that can accurately predict the quality of nanocellulose.

9 REFERENCES

Akhlaghi, N. and Riahi, S. (2019) 'Salinity Effect on the Surfactant Critical Micelle Concentration through Surface Tension Measurement', *Petroleum Engineering Iranian Journal of Oil & Gas Science and Technology*, 8(4), pp. 50–63.

Amazouz, M., Platon, R. and Champagne, M. (2005) 'The application of soft sensors in the pulp and paper and cement manufacturing sectors for process and energy performance improvement: Opportunity analysis and technology assessment', *Canmet Energy Technology Centre*, (July), p. 77. doi: 10.13140/RG.2.1.2312.9442.

Ankerfors, M. (2012) *Microfibrillated cellulose: Energy-efficient preparation techniques and key properties*. KTH Royal Institute of Technology.

Antes, R. and Joutsimo, O. P. (2015) 'Fiber Surface and Paper Technical Properties of Eucalyptus globulus and Eucalyptus nitens Pulps after Modified Cooking and Bleaching', *BioResources*, 1, pp. 1599–1616.

Aoki, D. and Nishio, Y. (2010) 'Phosphorylated cellulose propionate derivatives as thermoplastic flame resistant/retardant materials: influence of regioselective phosphorylation on their thermal degradation behaviour', *Cellulose*, 17(5), pp. 963–976.

Aprianti, T. *et al.* (2018) 'Heavy metal ions adsorption from pulp and paper industry wastewater using zeolite/activated carbon-ceramic composite adsorbent', *AIP Conference Proceedings*, 2014. doi: 10.1063/1.5054531.

Arthur, J. C. (1989) 'Chemical Modification of Cellulose and its Derivatives', *Comprehensive Polymer Science and Supplements*. Edited by G. Allen and J. C. B. T.-C. P. S. and S. Bevington, 6, pp. 49–80. doi: https://doi.org/10.1016/B978-0-08-096701-1.00182-8.

Backlund, B. (2009) 'Towards increased closure and energy efficiency', *Pulping Chemistry and Technology*, pp. 363–390. doi: 10.1515/9783110213423.

Bäckström, M., Kolar, M.-C. and Htun, M. (2008) 'Characterisation of fines from unbleached kraft pulps and their impact on sheet properties', *Holzforschung*, 62(5).

Baird, R. B., Eaton, A. D. and Rice, E. W. (2017) *Standard Methods for the Examination of Water and Wastewater*. 23rd edn. American Public Health Association. American Water Works Association. Water Environment Federation.

Bajpai, P. (2015) 'Generation of waste in pulp and paper mills', in *Management of Pulp and Paper Mill Waste*. Springer, pp. 9–17.

Bajpai, P. (2018) 'Pulping Fundamentals', in *Biermann's Handbook of Pulp and Paper*. 3rd edn. Elsevier, pp. 295–351. doi: https://doi.org/10.1016/B978-0-12-814240-0.00012-4.

Balasubramanian, S., Gupta, M. K. and Singh, K. K. (2012) 'Cryogenics and its Application with Reference to Spice Grinding: A Review', *Critical Reviews in Food Science and Nutrition*, 52(9), pp. 781–794. doi: 10.1080/10408398.2010.509552.

Balea, A. *et al.* (2017) 'Assessing the influence of refining, bleaching and TEMPO-mediated oxidation on the production of more sustainable cellulose nanofibers and their application as paper additives', *Industrial crops and products*, 97, pp. 374–387.

Basta, A. H. *et al.* (2004) 'Cleaning efficiency of process water in newsprint mill', *Progress in Paper Recycling*, 13, pp. 13–22.

Ben, Y. *et al.* (2003) 'Contaminant removal from deinking process water, Part I: Mill benchmarking: DAF units are very efficient in removing large suspended solids', *Pulp & Paper Canada*, 104(1), pp. 42–48.

Bester, L. M. (2018) *Development and optimisation of a process for cellulose nanoparticle production from waste paper sludge with enzymatic hydrolysis as an integral part*. Stellenbosch University.

Bian, H. *et al.* (2018) 'Contribution of lignin to the surface structure and physical performance of cellulose nanofibrils film', *Cellulose*, 25(2), pp. 1309–1318. doi: 10.1007/s10570-018-1658-x.

Bird, M. and Talberth, J. (2008) *Waste stream reduction and re-use in the pulp and paper sector*. Santa Fe, New Mexico.

Bonhivers, J.-C. and Stuart, P. R. (2013) 'Applications of Process Integration Methodologies in the Pulp and Paper Industry', in Klemeš, J. (ed.) *Woodhead Publishing Series in Energy*. Woodhead Publishing, pp. 765–798. doi: https://doi.org/10.1533/9780857097255.5.765.

Boniface, A. and Redding, W. (1974) 'System for recovery of fiber from paper mill effluent, including a sieve bend screen'. United States Patent.

Bouafif, H. *et al.* (2008) 'Analysis of among-species variability in wood fiber surface using DRIFTS and XPS: Effects on esterification efficiency', *Journal of Wood Chemistry and Technology*, 28(4), pp. 296–315.

Boufi, S. and Chaker, A. (2016) 'Easy production of cellulose nanofibrils from corn stalk by a conventional high speed blender', *Industrial Crops and Products*, 93, pp. 39–47. doi: 10.1016/j.indcrop.2016.05.030.

Bousios, S. and Worrell, E. (2017) 'Towards a Multiple Input-Multiple Output paper mill: Opportunities for alternative raw materials and sidestream valorisation in the paper and board industry', *Resources, Conservation and Recycling*, 125(February), pp. 218–232. doi: 10.1016/j.resconrec.2017.06.020.

Božič, M. *et al.* (2014) 'Enzymatic phosphorylation of cellulose nanofibers to new highly-ions adsorbing, flame-retardant and hydroxyapatite-growth induced natural nanoparticles', *Cellulose*, 21(4), pp. 2713–2726.

Brännvall, E. (2018) 'Increasing pulp yield in kraft cooking of softwoods by high initial effective alkali concentration (HIEAC) during impregnation leading to decreasing secondary peeling of cellulose', *Holzforschung*, 72(10), pp. 819–827. doi: doi:10.1515/hf-2018-0011.

Briggs, D. G. (1994) 'Chapter 8: Pulp and Paper', in *Forest product measurements and conversion factors: with special emphasis on the U.S. Pacific Northwest*, pp. 96–100.

Brogdon, B. (2015) 'Some Factors that Impact Pulp Yields During Kraft Pulping and Bleaching', in *TAPPI Peers Conference*. Atlanta, pp. 2339–2347.

Buranov, A. U. and Mazza, G. (2010) 'Extraction and characterization of hemicelluloses from flax shives by different methods', *Carbohydrate polymers*, 79(1), pp. 17–25.

Buswell, A. M. and Mueller, H. F. (1952) 'Mechanism of Methane Fermentation', *Industrial & Engineering Chemistry*, 44(3), pp. 550–552. doi: 10.1021/ie50507a033.

Carnö, B. and Hartler, N. (1976) *Kraft pulping to low kappa numbers*, *Sweden Pulp and Paper Research Institute (STFI) -Report B*.

Carrillo, F. *et al.* (2004) 'Structural FTIR analysis and thermal characterisation of lyocell and viscose-type fibres', *European Polymer Journal*, 40(9), pp. 2229–2234.

Chen, W. *et al.* (2011) 'Individualization of cellulose nanofibers from wood using high-intensity ultrasonication combined with chemical pretreatments', *Carbohydrate Polymers*, 83(4), pp. 1804–1811. doi: 10.1016/j.carbpol.2010.10.040.

Chiang, W. K., Zhang, D. and Zhou, L. (2006) 'Predicting and explaining patronage behavior toward web and traditional stores using neural networks: a comparative analysis with logistic regression', *Decision Support Systems*, 41(2), pp. 514–531. doi: https://doi.org/10.1016/j.dss.2004.08.016.

Chimphango, A. (2020) *The valorisation of paper sludge for green composite material*. Stellenbosch University.

Chinga-Carrasco, G. (2013) 'Optical methods for the quantification of the fibrillation degree of bleached MFC materials', *Micron*, 48, pp. 42–48.

Chun, S.-J. *et al.* (2011) 'Preparation of ultrastrength nanopapers using cellulose nanofibrils', *Journal of Industrial and Engineering Chemistry*, 17(3), pp. 521–526.

CNBM Anyang Machinery (no date) *Disc filter - important equipment of paper washing process*. Available at: http://www.paperpulpingmachine.com/disc-filter/ (Accessed: 4 March 2021).

Coleman, R. J. *et al.* (2011) 'Phosphorylation of alginate: synthesis, characterization, and evaluation of in vitro mineralization capacity', *Biomacromolecules*, 12(4), pp. 889–897.

Conti, M. E. (2008) 'Heavy metals in food packagings, The state of the art', *Intergovernmental Forum on Chemical Safety*, p. 10. doi: 10.1201/9781420003987.ch9.

Dahl, O. (2011) 'Brown Stock Washing Efficiency-Past, Today and Future', in *Clean Technologies Research Group*. Stockholm, Finland: Aalto University.

Dai, Z. *et al.* (2019) 'A brief review of nanocellulose based hybrid membranes for CO2 separation', *Fibers*, 7(5), pp. 1–18. doi: 10.3390/FIB7050040.

Daraei, M. (2016) *Evaluation and Prediction of Wood Properties in Pulp and Paper Production*. Mälardalen University.

Desmaisons, J. *et al.* (2017) 'A new quality index for benchmarking of different cellulose nanofibrils', *Carbohydrate Polymers*, 174, pp. 318–329. doi: 10.1016/j.carbpol.2017.06.032.

Eastoe, J. (2010) 'Surfactant Aggregation and Adsorption at Interfaces', in Cosgrove, T. (ed.) *Colloid Science: Principles, methods and applications*. Second, pp. 61–89. doi: 10.1016/j.solener.2019.02.027.

Edwards, P. J. *et al.* (1999) 'The application of neural networks to the papermaking industry', *IEEE Transactions on Neural Networks*, 10(6), pp. 1456–1464. doi: 10.1109/72.809090.

Edzwald, J. K. (2010) 'Dissolved air flotation and me', *Water Research*, 44(7), pp. 2077–2106. doi: 10.1016/j.watres.2009.12.040.

Eikelboom, M. *et al.* (2018) 'A multi-criteria decision analysis of management alternatives for anaerobically digested kraft pulp mill sludge', *PLoS one*, 13(1). doi: 10.1371/JOURNAL.PONE.0188732.

Ek, M., Gellerstedt, G. and Henriksson, G. (2009) *Pulp and Paper Chemistry and Technology - Pulping Chemistry and Technology, Volume 2*. De Gruyter. Available at: https://app.knovel.com/hotlink/toc/id:kpPPCTPC03/pulp-paper-chemistry/pulp-paper-chemistry.

Ekland, D. (1991) *Paper chemistry: an introduction*. Edited by T. Lindstrom. Kauniainen, Finland: DT Paper Science.

European Bioplastics (2019) *Fact Sheet Bioplastics – Industry standards & labels*. Berlin, Germany.

Fang, Z. *et al.* (2020) 'Critical Role of Degree of Polymerization of Cellulose in Super-Strong Nanocellulose Films', *Matter*, 2. doi: 10.1016/j.matt.2020.01.016.

Faryar, R. (2019) *Conversion of xylan into value-added products*. Lund University.

Feng, W., Singhal, N. and Swift, S. (2009) 'Drainage mechanism of microbubble dispersion and factors influencing its stability', *Journal of colloid and interface science*, 337(2), pp. 548–554.

Fengel, D. and Wegener, G. (1989) *Wood: chemistry, ultrastructure, reactions*. De Gruyter.

Fischer, W. J. *et al.* (2017) 'Pulp fines-characterization, sheet formation, and comparison to microfibrillated cellulose', *Polymers*, 9(8). doi: 10.3390/polym9080366.

Fortuna, L., Graziani, S. and Xibilia, M. G. (2005) 'Soft sensors for product quality monitoring in debutanizer distillation columns', *Control Engineering Practice*, 13(4), pp. 499–508. doi: 10.1016/j.conengprac.2004.04.013.

Garcia, O. *et al.* (2002) 'Effect of cellulase-assisted refining on the properties of dried and never-dried eucalyptus pulp', *Cellulose*, 9(2), pp. 115–125.

Gardner, A. T. (1965) 'Vibrating treatment for fiber recovery from waste effluent'. United States Patent.

Ghanadpour, M. *et al.* (2015) 'Phosphorylated Cellulose Nanofibrils: A Renewable Nanomaterial for the Preparation of Intrinsically Flame-Retardant Materials', *Biomacromolecules*, 16(10), pp. 3399–3410. doi: 10.1021/acs.biomac.5b01117.

Ghasemi Naghdi, F. and Schenk, P. M. (2016) 'Dissolved air flotation and centrifugation as methods for oil recovery from ruptured microalgal cells', *Bioresource Technology*, 218, pp. 428–435. doi: https://doi.org/10.1016/j.biortech.2016.06.093.

Glasser, W. G. (1980) 'Pulp and Paper - Chemistry and Chemical Technology', in Casey, J. P. (ed.). New York: Wiley.

GreenCape (2020) *2020: Market Intelligence Report: Waste*, *Waste*. Available at: https://www.greencape.co.za/assets/WASTE_MIR_20200331.pdf.

El Halal, S. L. M. *et al.* (2015) 'Structure, morphology and functionality of acetylated and oxidised barley starches', *Food chemistry*, 168, pp. 247–256.

Hames, B. *et al.* (2008) *Preparation of Samples for Compositional Analysis: Laboratory Analytical Procedure (LAP)*. Available at: www.nrel.gov (Accessed: 14 June 2021).

Hamm, U. and Schabel, S. (2007) 'Effluent-free papermaking: Industrial experiences and latest developments in the German paper industry', *Water Science and Technology*, 55(6), pp. 205–211. doi: 10.2166/wst.2007.230.

Han, H. and Chang, R. (2018) *Design and Optimization of Nanoparticulate Permeability-Modifiers for pH-independent Drug Release and Alcohol-resistant Dosage Forms*. University of Toronto.

Hashim, M. A. and Sen Gupta, B. (1998) 'The application of colloidal gas aphrons in the recovery of fine cellulose fibres from paper mill wastewater', *Bioresource Technology*, 64(3), pp. 199–204. doi: 10.1016/S0960-8524(97)00169-7.

Henriksson, M. *et al.* (2008) 'Cellulose nanopaper structures of high toughness', *Biomacromolecules*, 9(6), pp. 1579–1585.

Hielscher Ultrasonics (2020) *Probe-Type Sonication vs. Ultrasonic Bath: An Efficiency Comparison*. Available at: https://www.hielscher.com/probe-type-sonication-vs-ultrasonic-bath-an-efficiency-comparison.htm (Accessed: 10 April 2020).

Hinze, J. O. (1955) 'Fundamentals of the hydrodynamic mechanism of splitting in dispersion processes', *AIChE Journal*, 1(3), pp. 289–295.

Hiraoki, R. *et al.* (2015) 'Molecular Mass and Molecular-Mass Distribution of TEMPO-Oxidized Celluloses and TEMPO-Oxidized Cellulose Nanofibrils', *Biomacromolecules*, 16(2), pp. 675–681. doi: 10.1021/bm501857c.

Horvath, A. E., Lindström, T. and Laine, J. (2006) 'On the indirect polyelectrolyte titration of cellulosic fibers. Conditions for charge stoichiometry and comparison with ESCA', *Langmuir*, 22(2), pp. 824–830.

Horvath, E. (2003) *Appropriate conditions for polyelectrolyte titration to determine the charge of cellulosic fibers*. KTH Royal Institute of Technology.

Hostachy, J. C. *et al.* (2012) 'Pulp bleaching with ozone industrial achievements & perspectives', *Paper Asia*, 28(2), pp. 34–44.

Howe, K. J. *et al.* (2012) *Principles of water treatment*. John Wiley & Sons.

Hughes, R. (2010) 'An Introduction to Colloids', in Cosgrove, T. (ed.) *Colloid Science - Principles, Methods and Applications*. Second. John Wiley & Sons, pp. 1–10.

Ince, B. K., Cetecioglu, Z. and Ince, O. (2011) 'Pollution prevention in the pulp and paper industries', *Environmental Management in Practice*, pp. 224–246.

Isaksson, J. *et al.* (2016) 'Transportation fuel production from gasified biomass integrated with a pulp and paper mill–Part A: Heat integration and system performance', *Energy*, 103, pp. 557–571.

Isogai, A. and Zhou, Y. (2019) 'Diverse nanocelluloses prepared from TEMPO-oxidized wood cellulose fibers: Nanonetworks, nanofibers, and nanocrystals', *Current Opinion in Solid State and Materials Science*, 23(2), pp. 101–106. doi: 10.1016/j.cossms.2019.01.001.

Iwasawa, Y., Oyama, N. and Kunieda, H. (2001) *Proceedings of the International Conference on Colloid and Surface Science*. Elsevier.

Jauregi, P. and Dermiki, M. (2010) 'Separation of value-added bioproducts by colloidal gas aphrons (CGA) flotation and applications in the recovery of value-added food products', *Separation, Extraction and Concentration Processes in the Food, Beverage and Nutraceutical Industries*, pp. 284–313. doi: 10.1533/9780857090751.1.284.

Jauregi, P., Gilmour, S. and Varley, J. (1997) 'Characterisation of colloidal gas aphrons for subsequent use for protein recovery', *Chemical Engineering Journal*, 65(1), pp. 1–11. doi: https://doi.org/10.1016/S1385-8947(96)03154-3.

Jauregi, P. and Varley, J. (1999) 'Colloidal gas aphrons: Potential applications in biotechnology', *Trends in Biotechnology*, 17(10), pp. 389–395. doi: 10.1016/S0167-7799(99)01363-3.

Jiang, C. and Ma, J. (2000) 'De-inking of waste paper: flotation', *Enzymatic Deinking Technologies*, pp. 1–2.

Johansson, B. *et al.* (1984) 'Modified continuous kraft pulping-a way to decrease lignin content and improve pulp quality', *Svenska Traeforskningsinst.*

Johnson, N. W. (1972) 'The flotation behaviour of some chalcopyrite ores'.

Kangas, H. *et al.* (2014) 'Characterization of fibrillated celluloses. A short review and evaluation of characteristics with a combination of methods', *Nordic Pulp & Paper Research Journal*, 29(1), pp. 129–143.

Khan, T., Rehman, A. and Nasir Jamal, M. (2017) 'To Investigate the Performance of Disc Filter in Retaining Clay and Sand Particles', *International Journal of Scientific Engineering and Applied Sciences*, 4.

Klemm, D. *et al.* (2011) 'Nanocelluloses: A new family of nature-based materials', *Angewandte Chemie - International Edition*, 50(24), pp. 5438–5466. doi: 10.1002/anie.201001273.

Kosior, D. *et al.* (2015) 'Influence of non-ionic and ionic surfactants on kinetics of the bubble attachment to hydrophilic and hydrophobic solids', *Colloids and Surfaces A: Physicochemical and Engineering Aspects*, 470, pp. 333–341.

Krüger, H., Kuzel, P. and Schwab, H. (1975) 'Einsatz von wasserstoffperoxid und seinen derivaten in bleichprozessen, zur desinfektion und im umweltschutz', *Chemischer Informationsdienst*, 6(29), p. no-no.

Kumar, D., Kumar, V. and Singh, V. P. (2010) 'Mathematical modeling of brown stock washing

problems and their numerical solution using MATLAB', *Computers & Chemical Engineering*, 34(1), pp. 9–16. doi: https://doi.org/10.1016/j.compchemeng.2009.08.005.

Kumar, V. *et al.* (2014) 'Comparison of nano- and microfibrillated cellulose films', *Cellulose*, 21(5), pp. 3443–3456. doi: 10.1007/s10570-014-0357-5.

Kyrklund, B. and Strandell, G. (1969) 'Applicability of chlorine number for evaluation of lignin content of pulp', *Paperi ja puu*, 51(4 A), p. 299.

Larmignat, S. *et al.* (2008) 'Rheology of colloidal gas aphrons (microfoams)', *Colloids and Surfaces A: Physicochemical and Engineering Aspects*, 322(1–3), pp. 199–210.

Lauren, S. (2018) 'What are surfactants and how do they work?', *Biolin Scientific*, June.

Lehtonen, J. *et al.* (2020) 'Phosphorylated cellulose nanofibers exhibit exceptional capacity for uranium capture', *Cellulose*, 27(18), pp. 10719–10732. doi: 10.1007/s10570-020-02971-8.

Lekha, P. *et al.* (2017) 'Pulp and paper mill sludge: A potential resource for producing high-value products', *Journal for the Technical Association of the Pulp and Paper Industry of South Africa (TAPPSA)*, (Quarter 1), pp. 16–18.

Lemlich, R. (1972) *Adsorptive Bubble Seperation Techniques*. London: Academic Press. doi: 10.1002/cite.330450427.

Li, Q. *et al.* (2013) 'Nanocellulose Life Cycle Assessment', *ACS Sustainable Chemistry & Engineering*, pp. 31–53. doi: 10.1002/9781118489451.ch3.

Liu, H.-B., Li, X.-Y. and Yang, C. (2018) 'Soft Sensor Modeling of Papermaking Waste Water Treatment Process Using PCA Dimensional Reduction Models', *Zhongguo Zaozhi Xuebao/Transactions of China Pulp and Paper*, 33, pp. 50–57. doi: 10.11981/j.issn.1000-6842.2018.04.50.

Longe, T. A. (1989) *Colloidal gas aphrons: Generation, flow characterization and application in soil and groundwater decontamination*. Virginia Polytechnic Institute and State University.

Loras, V. (1980) 'Bleaching in Pulp and Paper Chemistry and Chemical Technology third edit by James P', *Casey, Willey Interscience John Willey and Sons*.

Lourenço, A. F. *et al.* (2015) 'Improving paper mechanical properties using silica-modified ground calcium carbonate as filler', *BioResources*, 10(4), pp. 8312–8324. doi: 10.15376/biores.10.4.8312-8324.

Lozhechnikova, A. *et al.* (2014) 'Modification of nanofibrillated cellulose using amphiphilic block-structured galactoglucomannans', *Carbohydrate Polymers*, 110, pp. 163–172. doi: https://doi.org/10.1016/j.carbpol.2014.03.087.

Luukko, K. (1999) 'Fines quantity and quality in controlling pulp and paper quality', in *International Mechanical Pulping Conference*. Houston, Texas: TAPPI Press, pp. 67–75.

Machdar, I. *et al.* (2018) 'Ammonium Nitrogen Removal from Urea Fertilizer Plant Wastewater via Struvite Crystal Production', *IOP Conference Series: Materials Science and Engineering*, 358(1). doi: 10.1088/1757-899X/358/1/012026.

Madden, D. R. and Safferling, M. (2007) 'Macromolecular Crystallography Protocols', in *Methods in Molecular Biology*, p. 52.

Mahmood, T. and Elliott, A. (2006) 'A review of secondary sludge reduction technologies for the pulp and paper industry', *Water research*, 40(11), pp. 2093–2112.

Malvern Instruments Ltd. (2013) 'Size theory', *Zetasizer Nano User Manual*, MAN0485(11), p. 250.

Matsumura, S. *et al.* (1998) 'Surface Activity, Antimicrobial Properties and Biodegradability of n-Alkyl Xylosides, Xylobiosides, and Xylotriosides', *Journal of Japan Oil Chemists' Society*, 47(3), pp. 247-

255,291. doi: 10.5650/jos1996.47.247.

McDonald, J. P. (2003) 'System for recovering and recycling usable fibers from white water in a papermaking process'. United States Patent.

Micromeritics Instrument Corporation (2016) 'Saturn DigiSizer II | Micromeritics'. Available at: http://www.micromeritics.de/Produktübersicht/Saturn-DigiSizer-II.aspx.

Miranda, R. *et al.* (2013) 'Efficiency of chitosans for the treatment of papermaking process water by dissolved air flotation', *Chemical Engineering Journal*, 231, pp. 304–313. doi: 10.1016/j.cej.2013.07.033.

Mladenov, M. and Pelovski, Y. (2010) 'Utilization of wastes from pulp and paper industry', *Journal of the University of Chemical Technology and Metallurgy*, 45(1), pp. 33–38.

Molaei, A. and Waters, K. E. (2015) 'Aphron applications - A review of recent and current research', *Advances in Colloid and Interface Science*, 216, pp. 36–54. doi: 10.1016/j.cis.2014.12.001.

Moskal, M. (2018) 'A hundred years of corrosion in the pulp and paper industry', *TAPPI Journal*, 17, pp. 253–258. doi: 10.32964/TJ17.05.253.

Mukherjee, S. *et al.* (2015) 'Optimization of pulp fibre removal by flotation using colloidal gas aphrons generated from a natural surfactant', *Journal of the Taiwan Institute of Chemical Engineers*, 53, pp. 15–21. doi: 10.1016/j.jtice.2015.02.037.

Muster, T. H. *et al.* (2013) 'Towards effective phosphorus recycling from wastewater: Quantity and quality', *Chemosphere*, 91(5), pp. 676–684. doi: 10.1016/j.chemosphere.2013.01.057.

Naderi, A. *et al.* (2016) 'Phosphorylated nanofibrillated cellulose: production and properties', *Nordic Pulp & Paper Research Journal*, 31(1), pp. 20–29. doi: doi:10.3183/npprj-2016-31-01-p020-029.

Naderi, A., Lindström, T. and Sundström, J. (2015) 'Repeated homogenization, a route for decreasing the energy consumption in the manufacturing process of carboxymethylated nanofibrillated cellulose?', *Cellulose*, 22(2), pp. 1147–1157.

Nakama, Y. (2017) 'Surfactants', *Cosmetic Science and Technology*. Edited by K. Sakamoto et al., pp. 231–244. doi: https://doi.org/10.1016/B978-0-12-802005-0.00015-X.

Nechyporchuk, O. and Belgacem, M. N. (2016) 'Production of cellulose nanofibrils: A review of recent advances', *Industrial Crops and Products*, 93, pp. 2–25. doi: 10.1016/J.INDCROP.2016.02.016.

Nogi, M. *et al.* (2009) 'Optically transparent nanofiber paper', *Advanced materials*, 21(16), pp. 1595–1598.

Noguchi, Y., Homma, I. and Matsubara, Y. (2017) 'Complete nanofibrillation of cellulose prepared by phosphorylation', *Cellulose*, 24(3), pp. 1295–1305. doi: 10.1007/s10570-017-1191-3.

Norden, S. and Teder, A. (1979) 'Modified kraft processes for softwood bleached-grade pulp'.

Odabas, N. *et al.* (2016) 'Cellulosic fines: Properties and effects', *Progress in Materials Science*, 83(July), pp. 574–594. doi: 10.1016/j.pmatsci.2016.07.006.

Oksman, K., Mathew, A. P. and Sain, M. (2009) 'Novel bionanocomposites: processing, properties and potential applications', *Plastics, rubber and composites*, 38(9–10), pp. 396–405.

Österberg, M. (2000) *On the interactions in cellulose systems: Surface forces and adsorption*, *Helsinki University of Technology*. KTH Royal Institute of Technology.

Page, D. (1989) 'Fundamentals of papermaking fibers: transactions of the symposium held at Cambridge', *UK, September*, pp. 17–22.

Paquet, M., Chang, J. and Rutkowski, J. (2016) 'Cellulose specifications : Summary of the 2009 proposed up-grades and improvements and new possibilities for future revisions', in *International*

Nitrocellulose Symposium. Montreal: General Dynamics Ordance and Tactical Systems.

PCC Group (no date) *Surfactant Manufacturers*. Available at: https://www.products.pcc.eu/en/surfactant-manufacturers/ (Accessed: 28 April 2020).

Perrin, J. *et al.* (2014) 'Formation of carbonyl and carboxyl groups on cellulosic pulps: Effect on alkali resistance', *BioResources*, 9(4), pp. 7299–7310. doi: 10.15376/biores.9.4.7299-7310.

Potůček, F. and Rahman, M. (2019) 'Displacement Washing of Kraft Pulp at Various Wash Water Temperature', *Acta Facultatis Xylologiae Zvolen, volume 61, issue: 2*.

Qing, Y. *et al.* (2013) 'A comparative study of cellulose nanofibrils disintegrated via multiple processing approaches', *Carbohydrate Polymers*, 97(1), pp. 226–234. doi: 10.1016/j.carbpol.2013.04.086.

Raffaele, D. and Ondruch, T. (2020) *Data-driven soft sensor for continuous production monitoring: an application to paper strength*. doi: 10.1109/ETFA46521.2020.9212113.

Ravikumar, M. (2017) 'Ultrasonication: An Advanced Technology for Food Preservation', *International Journal of Pure & Applied Bioscience*, 5(6), pp. 363–371. doi: 10.18782/2320-7051.5481.

Redlinger-Pohn, J. D. *et al.* (2016) 'Separation of cellulose fibres from pulp suspension by froth flotation fractionation', *Separation and Purification Technology*, 169, pp. 304–313. doi: 10.1016/j.seppur.2016.06.004.

Riley, A. (2012) 'Paper and paperboard packaging', *Packaging Technology*, pp. 178–239. doi: 10.1533/9780857095701.2.178.

Ritter, G. J. and Kurth, E. F. (1933) 'Holocellulose, total carbohydrate fraction of extractive-free maple wood', *Industrial & Engineering Chemistry*, 25(11), pp. 1250–1253.

Rodriguez, M. H. (2015) *Preparation and Characterization of Nanocellulose Films and Coatings from Industrial Bio-Residues*. Lulea University of Technology.

Rojo, E. *et al.* (2015) 'Comprehensive elucidation of the effect of residual lignin on the physical, barrier, mechanical and surface properties of nanocellulose films', *Green Chemistry*, 17(3), pp. 1853–1866. doi: 10.1039/c4gc02398f.

Rol, F. *et al.* (2019) 'Recent advances in surface-modified cellulose nanofibrils', *Progress in Polymer Science*, 88, pp. 241–264. doi: 10.1016/j.progpolymsci.2018.09.002.

Rol, F. *et al.* (2020) 'Cellulose phosphorylation comparison and analysis of phosphorate position on cellulose fibers', *Carbohydrate Polymers*, 229(July 2019), p. 115294. doi: 10.1016/j.carbpol.2019.115294.

Rosa, M. F. *et al.* (2010) 'Cellulose nanowhiskers from coconut husk fibers: Effect of preparation conditions on their thermal and morphological behavior', *Carbohydrate polymers*, 81(1), pp. 83–92.

Rydholm, S. A. (1965) 'Pulping processes.'

Saien, J. and Akbari, S. (2010) 'Interfacial Tension of Hydrocarbon + Different pH Aqueous phase Systems in the Presence of Triton X-100', *Industrial & Engineering Chemistry Research*, 49(7), pp. 3228–3235. doi: 10.1021/ie900402u.

Saito, T. *et al.* (2006) 'Homogeneous suspensions of individualized microfibrils from TEMPO-catalyzed oxidation of native cellulose', *Biomacromolecules*, 7(6), pp. 1687–1691.

Santiago, A. S. and Neto, C. P. (2008) 'Impact of Kraft Process Modifications on Eucalyptus globulus Pulping Performance and Polysaccharide Retention', *Industrial & Engineering Chemistry Research*, 47(19), pp. 7433–7440. doi: 10.1021/ie071488g.

Santucci, B. S. *et al.* (2016) 'Evaluation of the effects of chemical composition and refining treatments on the properties of nanofibrillated cellulose films from sugarcane bagasse', *Industrial Crops and*

Products, 91, pp. 238–248. doi: 10.1016/J.INDCROP.2016.07.017.

Savage, R. H. and Koch, H. C. (1950) 'Evaluation of Wastes Disposal Problems in the Pulp and Paper Industry', *Sewage and Industrial Wastes*, pp. 1567–1572.

Savassi, O. N. (2005) 'A compartment model for the mass transfer inside a conventional flotation cell', *International Journal of Mineral Processing*, 77(2), pp. 65–79. doi: 10.1016/j.minpro.2005.02.003.

Schaum, C. and Lux, J. (2010) 'Sewage sludge dewatering and drying', in Thome-Kozmiensky, K. J. and Pelloni, L. (eds) *Waste Management*. Berlin, Germany: Rhombos-Verlag, pp. 727–737.

Schmitt, U., Koch, G. and Lehnen, R. (2013) 'Wood', *Ullmann's Encyclopedia of Industrial Chemistry*. Wiley-VCH Verlag GmbH & Co. doi: 10.1002/14356007.a28_305.pub2.

Scott, G. M. and Smith, A. (1995) 'Sludge characteristics and disposal alternatives for the pulp and paper industry', *TAPPI Proceedings - International Environmental Conference*, 1, pp. 269–279.

Sebba, F. (1971) 'Microfoams—an unexploited colloid system', *Journal of Colloid and Interface Science*, 35(4), pp. 643–646.

Sebba, F. (1987) *Foams and biliquid foams, aphrons*. Wiley.

Sehaqui, H. *et al.* (2010) 'Fast preparation procedure for large, flat cellulose and cellulose/inorganic nanopaper structures', *Biomacromolecules*, 11(9), pp. 2195–2198.

Sekine, M. *et al.* (2013) 'The direct and one-pot transformation of xylan into the biodegradable surfactants, alkyl xylosides, is aided by an ionic liquid', *RSC Advances*, 3(43), pp. 19756–19759. doi: 10.1039/c3ra42680g.

Shaw, D. J. (1992) 'Introduction to Colloid and Surface Chemistry, 4th edn., Butter worth Heinemann'. Oxford.

Simão, L. *et al.* (2018) 'Wastes from pulp and paper mills - A review of generation and recycling alternatives', *Ceramica*, 64(371), pp. 443–453. doi: 10.1590/0366-69132018643712414.

Sjostrom, E. (1981) *Wood chemistry: fundamentals and applications.* New York: Academic Press.

Sluiter, A. *et al.* (2011) *Determination of Structural Carbohydrates and Lignin in Biomass: Laboratory Analytical Procedure (LAP)*. Available at: http://www.nrel.gov/biomass/analytical_procedures.html (Accessed: 14 March 2021).

Smith, P. G. and Warren, L. J. (1989) 'Entrainment of particles into flotation froths', *Mineral Procesing and Extractive Metallurgy Review*, 5(1–4), pp. 123–145.

Soares, S. *et al.* (2011) *Design and Application of Soft Sensor in the Paper Pulp Industry Using Small Datasets*. University of Coimbra.

De Souza, A. G. *et al.* (2017) 'Cellulose nanostructures obtained from waste paper industry: A comparison of acid and mechanical isolation methods', *Materials Research*, 20, pp. 209–214. doi: 10.1590/1980-5373-mr-2016-0863.

Stevenson, P. (2010) 'Inter-bubble gas diffusion in liquid foam', *Current Opinion in Colloid & Interface Science*, 15(5), pp. 374–381. doi: https://doi.org/10.1016/j.cocis.2010.05.010.

Stubenrauch, C. *et al.* (2009) 'Aqueous foams stabilized by n-dodecyl-β-d-maltoside, hexaethyleneglycol monododecyl ether, and their 1: 1 mixture', *Soft Matter*, 5(16), pp. 3070–3080. doi: 10.1039/b903125a.

Suflet, D. M., Chitanu, G. C. and Popa, V. I. (2006) 'Phosphorylation of polysaccharides: new results on synthesis and characterisation of phosphorylated cellulose', *Reactive and Functional Polymers*, 66(11), pp. 1240–1249.

Szymańska, M. *et al.* (2019) 'Struvite—an innovative fertilizer from anaerobic digestate produced in a

bio-refinery', *Energies*, 12(2), p. 296.

Tadros, T. F. (2014) *An introduction to surfactants*. de Gruyter.

Teder, A. and Olm, J. (1981) 'Extended delignification by combination of modified kraft pulping and oxygen bleaching'.

Tovar, R. G. *et al.* (2015) 'White Water Recirculation Method as a Means to Evaluate the Influence of Fines on the Properties of Handsheets', *BioResources*, 10(4), pp. 7242–7251.

Turbak, A. F., Snyder, F. W. and Sandberg, K. R. (1983) 'Microfibrillated cellulose, a new cellulose product: properties, uses, and commercial potential', in. United States. Available at: https://www.osti.gov/servlets/purl/5062478.

Uysal, A., Yilmazel, Y. D. and Demirer, G. N. (2010) 'The determination of fertilizer quality of the formed struvite from effluent of a sewage sludge anaerobic digester', *Journal of Hazardous Materials*, 181(1–3), pp. 248–254.

Vector Solutions (2021a) *Broke System Inventory Management*. Available at: https://www.vectorsolutions.com/course-details/broke-system-inventory-management/fe92ce9a-9583-e811-a985-02ec32550f44/ (Accessed: 29 October 2020).

Vector Solutions (2021b) *Broke System Purpose and Operation*. Available at: https://www.vectorsolutions.com/course-details/broke-system-purpose-and-operation/56a9ce9a-9583-e811-a985-02ec32550f44/ (Accessed: 29 October 2020).

Velaga, S. P., Nikjoo, D. and Vuddanda, P. R. (2018) 'Experimental Studies and Modeling of the Drying Kinetics of Multicomponent Polymer Films', *AAPS PharmSciTech*, 19(1), pp. 425–435. doi: 10.1208/s12249-017-0836-8.

Viljamaa, P., Peltonen, H. and Koivo, H. N. (2001) 'Estimation of Target Values for Grade Changes in Paper Machine', in Leiviskä, K. (ed.) *Industrial Applications of Soft Computing: Paper, Mineral and Metal Processing Industries*. Heidelberg: Physica-Verlag HD, pp. 211–221. doi: 10.1007/978-3-7908-1822-2_14.

Visanko, M. (2015) *Functionalized nanocelluloses and their use in barrier and membrane thin films*. University of Oulu. doi: 10.13140/RG.2.1.4859.9769.

Wakeman, R. J. (2011) 'Flotation', in *A-to-Z Guide to Thermodynamics, Heat and Mass Transfer, and Fluids Engineering*. Begellhouse. doi: 10.1615/AtoZ.f.flotation.

Williams, D. F. (1987) 'Advanced applications for materials implanted within the human body', *Materials science and technology*, 3(10), pp. 797–806.

Wills, B. A. and Finch, J. A. (2016) 'Dewatering', in *Will's Mineral Processing Technology*. Eighth. Boston: Butterworth-Heinemann, pp. 417–438. doi: https://doi.org/10.1016/B978-0-08-097053-0.00015-7.

Wolfer, E. P. *et al.* (1997) 'Method for recovering fiber from effluent streams'. United States Patent.

Wu, J. *et al.* (2020) 'Enhancing Enzyme-Mediated Cellulose Hydrolysis by Incorporating Acid Groups Onto the Lignin During Biomass Pretreatment', *Frontiers in Bioengineering and Biotechnology*, 8, p. 1325. doi: 10.3389/fbioe.2020.608835.

Xiang, W. *et al.* (2019) 'Measuring the interfacial behavior of sugar-based surfactants to link molecular structure and uses', in *Biobased Surfactants*. Elsevier, pp. 387–412.

Xu, L., Pruszynski, P. E. and Hart, P. W. (2017) 'Effect of conductivity on paper and board machine performance a review and new experiences', *Tappi Journal*, 16(10), pp. 567–579. doi: 10.32964/tj16.10.567.

Yang, Z. *et al.* (2010) 'A Novel Process to Isolate Fibrils from Cellulose Fibers by High-Intensity Ultrasonication, Part 1: Process Optimization', *Journal of Applied Polymer Science*, 116(5), pp. 2658–2667. doi: 10.1002/app.

Yeo, Y. K. *et al.* (2005) 'Model Algorithmic Control of grade change operations in paper mills', *Korean Journal of Chemical Engineering*, 22(3), pp. 339–344. doi: 10.1007/BF02719408.

Yeoman, S. *et al.* (1988) 'The removal of phosphorus during wastewater treatment: A review', *Environmental Pollution*, 49(3), pp. 183–233. doi: 10.1016/0269-7491(88)90209-6.

Yuan, T.-Q. *et al.* (2010) 'Structural and physico-chemical characterization of hemicelluloses from ultrasound-assisted extractions of partially delignified fast-growing poplar wood through organic solvent and alkaline solutions', *Biotechnology advances*, 28(5), pp. 583–593.

Yurkshtovich, N. K. *et al.* (2007) 'Esterification of viscose fibres with orthophosphoric acid and study of their physicochemical and mechanical properties', *Fibre Chemistry*, 39(1), pp. 31–36. doi: 10.1007/s10692-007-0007-x.

Zaher, A. and Shehata, N. (2021) 'Recent advances and challenges in management of urea wastewater: A mini review', *IOP Conference Series: Materials Science and Engineering*, 1046(1), p. 012021. doi: 10.1088/1757-899x/1046/1/012021.

Zanão, M. *et al.* (2019) 'Evaluation of Kraft-PS Cooking for Eucalypt and Pine Wood Chip Mixtures', *Journal of Wood Chemistry and Technology*, 39(3), pp. 149–165. doi: 10.1080/02773813.2018.1533979.

Zarko, B. A. *et al.* (2019) 'OPTIX™ Applied Intelligence-The Only Real-time Quality Measurement for Finished Product Real-time Quality Measurement'.

Zhao, H. *et al.* (2018) 'Understanding of the foam capability of sugar-based nonionic surfactant from molecular level', *Colloids and Surfaces A: Physicochemical and Engineering Aspects*, 551(March), pp. 165–173. doi: 10.1016/j.colsurfa.2018.05.010.

Zhao, J., Pillai, S. and Pilon, L. (2009) 'Rheology of colloidal gas aphrons (microfoams) made from different surfactants', *Colloids and Surfaces A: Physicochemical and Engineering Aspects*, 348(1–3), pp. 93–99.

APPENDIX A – FIBRE MASS BALANCE

NOTE: Adt/d means an air dry tonne of pulp product where the weight of the pulp product is corrected to reflect the weight that the pulp product would be if the pulp were composed of 10% water and 90% fibre;

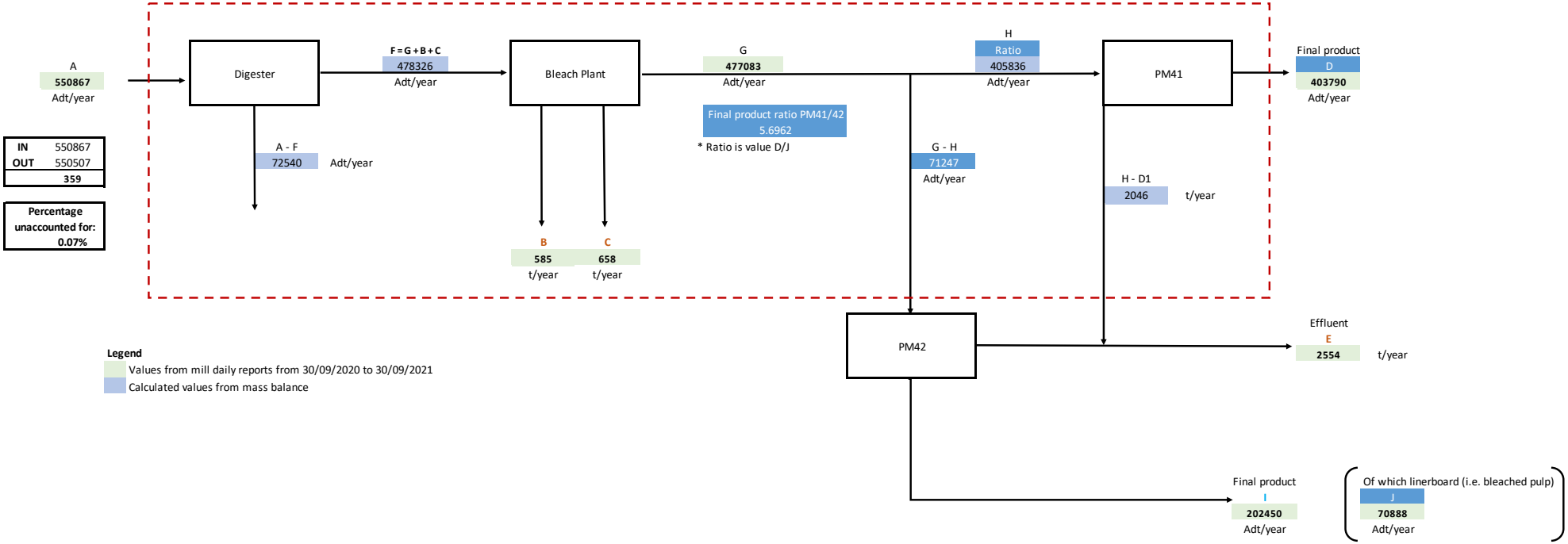

APPENDIX B – BLEACHING NOMENCLATURE AND COMMON BLEACHING SEQUENCES

Table B1: Bleaching nomenclature. (Loras, 1980)

Stages	Chemicals	Symbols
Chlorination	Cl_2	C
Alkaline extraction	$NaOH$	E
Hypochlorite	$NaOCl + NaOH$	H
Chlorine dioxide	ClO_2	D
Peroxide	$Na_2O_2 + NaOH$	P or
	$H_2O_2 + NaOH$	P/E
Oxygen	$O_2 + NaOH$	O
Chlorination with small amounts ClO_2	$Cl_2 + ClO_2$	C_D
Sequential bleaching without intermediate washing	ClO_2/Cl_2	D/C
	$Cl_2/NaOCl + NaOH$	C/H
	$Cl_2/NaOCl + NaOH$	D/H
Bleaching with mixture Cl_2 and ClO_2	$Cl_2 + ClO_2$	C + D
Chlorination at low concentration	Cl_2	(C)
Gas-phase-bleaching	Cl_2	C_g
	ClO_2	D_g
Ozone	O_3	Z
Acid	e.g. CH_3CO_3H	A

Table B2: Common Kraft industrial bleaching sequences. (Rydholm, 1965; Krüger, Kuzel and Schwab, 1975; Loras, 1980)

Number of stages	Sequence
Three (semi– bleached)	C – E – H
	D/C – O – D
Four (partly semi– bleached)	C – E – H – D
	C – E – H – P
	C – E – H – H
	C – H – E –H
	C – D – E – D
	O – C – E – H
	O – C – E – D
	O – D – O – D
Five	C – E – H – P – D
	C – E – H – D – P
	C – E – H – E – H
	C – E – D – E – D
	C – E – D – P – D
Six	C – H – E – D – E – D
	C – E – H – D – E – D
	O – C – E – D – E – D
	O – C + D – E – D – E – D
	O – C – D – E – H – D

APPENDIX C – FLOTATION WITH COLLOIDAL GAS APHRONS EXPERIMENTAL SETUP

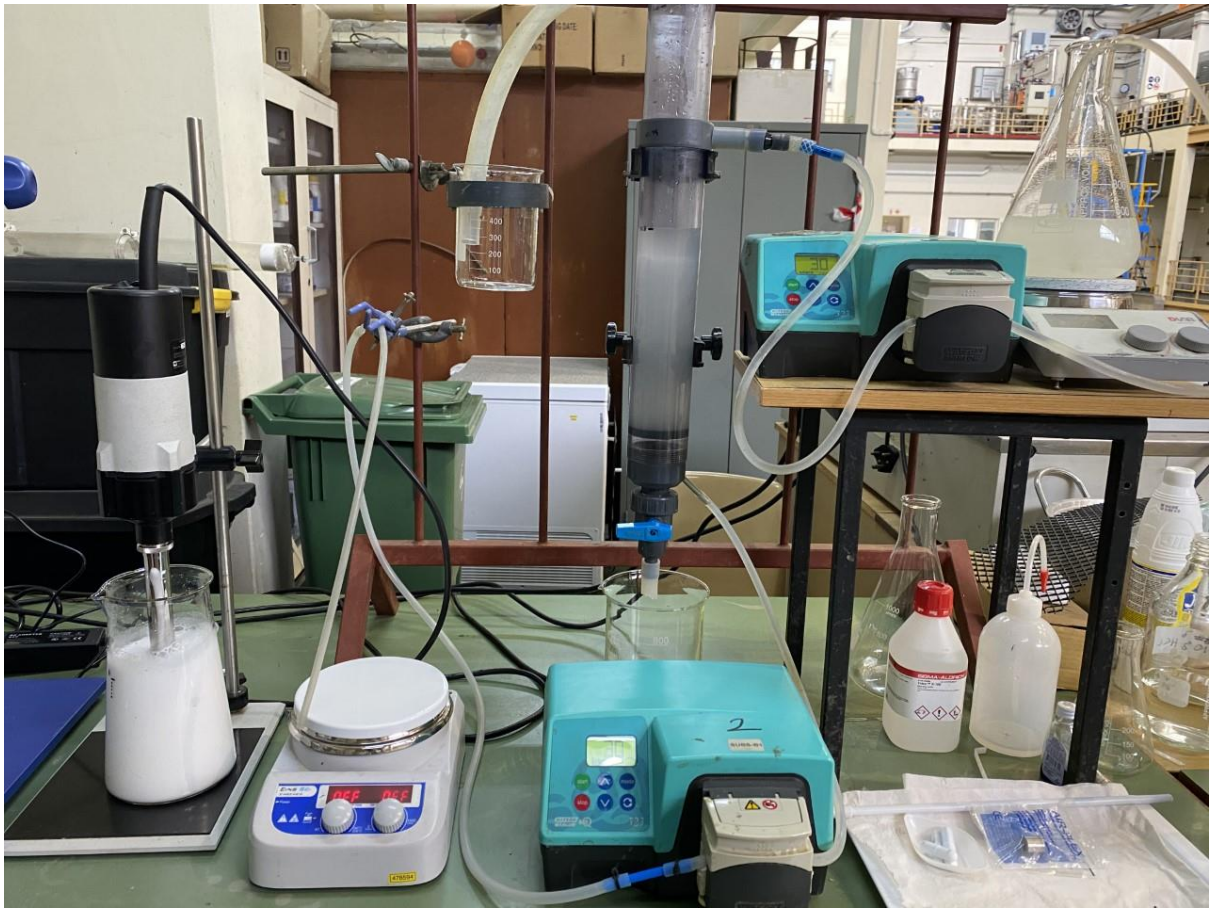

APPENDIX D – FOURIER TRANSFORM INFRARED (FTIR) BAND ASSIGNMENTS

Wavelength (cm-1)	Interpretation/Assignment	Component Identification	Reference
3200 - 3650	O-H groups including absorbed water, aliphatic alcohols in carbohydrates and lignin, aromatic alcohols in lignin and extractives.	Lignin	(Carrillo *et al.*, 2004; Bouafif *et al.*, 2008)
3200 - 3345	Hydroxyl stretching vibration of cellulose and hemicellulose	Cellulose, hemicellulose	(Buranov and Mazza, 2010; Rosa *et al.*, 2010; El Halal *et al.*, 2015);
2901	CH2 stretching in cellulose	Cellulose	(Yuan *et al.*, 2010)
2835 - 2938	C-H (symmtric or asymmetric). Aromatic methoxyl groups and methylene side chains.	Lignin	(Carrillo *et al.*, 2004; Popescu *et al.*, 2007)
1710	C=O stretching mode in cellulose	Cellulose	(Aoki and Nishio, 2010)
1640 - 1650	Water in lignin or cellulose.	Lignin	(Carrillo *et al.*, 2004; Popescu *et al.*, 2007)
1422 - 1430	C-H (aromatic) asymmetric deformation in lignin	Lignin	(Carrillo *et al.*, 2004; Yang *et al.*, 2010; Shi, Xing and Lia, 2012; Yang, Wang and Huang, 2015)
1420 - 1442	Crystalline structures of cellulose representing the CH, CH2 and OCH bending vibrations	Cellulose	(Ciolacu, Ciolacu and Popa, 2011; Poletto, Pistor and Zattera, 2013)
1230	P=O stretching mode	Phosphor	(Suflet, Chitanu and Popa, 2006; Coleman *et al.*, 2011; Božič *et al.*, 2014)

1200 - 1205	O-H in-plane deformation in carbohydrates	Cellulose, hemicellulose	(Carrillo *et al.*, 2004; Popescu *et al.*, 2007)
1125 - 1162	C-O-C bonds in cellulose or asymmetric stretching found in cellulose and hemicellulose	Cellulose, hemicellulose	(Carrillo *et al.*, 2004; Popescu *et al.*, 2007; Yang, Wang and Huang, 2015)
1120 - 1165	C-O-C groups from glycosidic units	Cellulose	(Ghanadpour *et al.*, 2015)
1060 - 1128	C-O-C , C=C, and C-C-O stretching in cellulose, hemicellulose and lignin	Cellulose, hemicellulose, lignin	(Carrillo *et al.*, 2004; Yang, Wang and Huang, 2015)
	C-O stretches in cellulose, hemicellulose and lignin		(Carrillo *et al.*, 2004; Shi, Xing and Lia, 2012)
1034	Xylan peak of hemicellulose	Hemicellulose	(Buranov and Mazza, 2010)
985	Arabinose side chains in hemicellulose	Hemicellulose	(Sun *et al.*, 2005)
900 - 940	P-OH stretching mode	Phosphor	(Suflet, Chitanu and Popa, 2006; Coleman *et al.*, 2011)
896	Beta-glycosidic linkages of hemicelluloses. Presence indicates the presence of sugar units of hemicelluloses within lignin extracts	Hemicellulose, lignin	(Sabiha-Hanim and Aziatul-Akma, 2016)
832	P-O-C aliphatic bond	Phosphor	(Suflet, Chitanu and Popa, 2006)

APPENDIX E – SCREENING AND CENTRAL COMPOSITE DESIGN (CCD) RESULTS AND ANOVA TABLES

Table E1: Flotation screening experiment with Triton X-100 coded values and results.

Factor A	Factor B	Efficiency [%] Run 1	Efficiency [%] Run 2
1	-1	49.9	42.8
-1	1	50.7	51.4
-1	-1	47.0	48.0
1	1	67.5	68.7

Table E2: Flotation CCD experiment with Triton X-100 coded values and results

Factor A	Factor B	Efficiency [%]
-1	-1	47.0
-1	1	50.7
1	-1	49.9
1	1	67.5
-1.414	0	24.6
1.414	0	60.6
0	-1.414	54.2
0	1.414	77.5
0	0	73.6
0	0	55.0
0	0	60.8
0	0	59.8
0	0	61.7

Table E3: Flotation screening experiment with Triton X-100 ANOVA results.

	SS	DOF	MS	F	P
Intercept	22684.50	1	22684.50	1147.885	0.000000
CGA flowrate	300.13	1	300.13	15.187	0.011443
Wastewater flowrate	239.81	1	239.81	12.135	0.017593
Interaction	84.50	1	84.50	23.620	0.008279
Error	98.81	5	19.76		

Table E4: Flotation CCD experiment with Triton X-100 ANOVA results.

	SS	df	MS	F	p
(1)A (L)	623.251	1	623.2513	13.26418	0.008265
A (Q)	682.153	1	682.1531	14.51774	0.006626
(2) B (L)	367.899	1	367.8988	7.82971	0.026594
B (Q)	20.640	1	20.6400	0.43927	0.528689
1L by 2L	48.303	1	48.3025	1.02798	0.344388
Error	328.913	7	46.9876		
Total SS	2114.812	12			

Table E5: Flotation with colloidal gas aphrons experimental data

		Flotation Efficiency (%)		
	Run	**Triton X-100**	**DDM (Batch 1)**	**DDM (Batch 2)**
PM41	1	77.8	58.7	56.7
	2	69.7	64.5	53.2
	3	73.6	61.8	60.9
	Average	**73.7 ± 4.1**	**61.7 ± 2.9**	**56.9 ± 3.9**
Alkaline	1	44.9	68.1	67.5
	2	52.3	63.4	63.6
	3	54.5	73.7	62.3
	Average	**50.6 ± 5.0**	**68.4 ± 5.2**	**64.5 ± 2.7**
Acid	1	54.4	55.8	57.9
	2	57.9	54.1	52.3
	3	53.5	52.4	53.9
	Average	**55.3 ± 2.3**	**54.1 ± 1.7**	**54.7 ± 2.9**

APPENDIX F – FOURIER TRANSFORM INFRARED (FTIR) OF PHOSPHORYLATED VERSUS UNTREATED SAMPLES

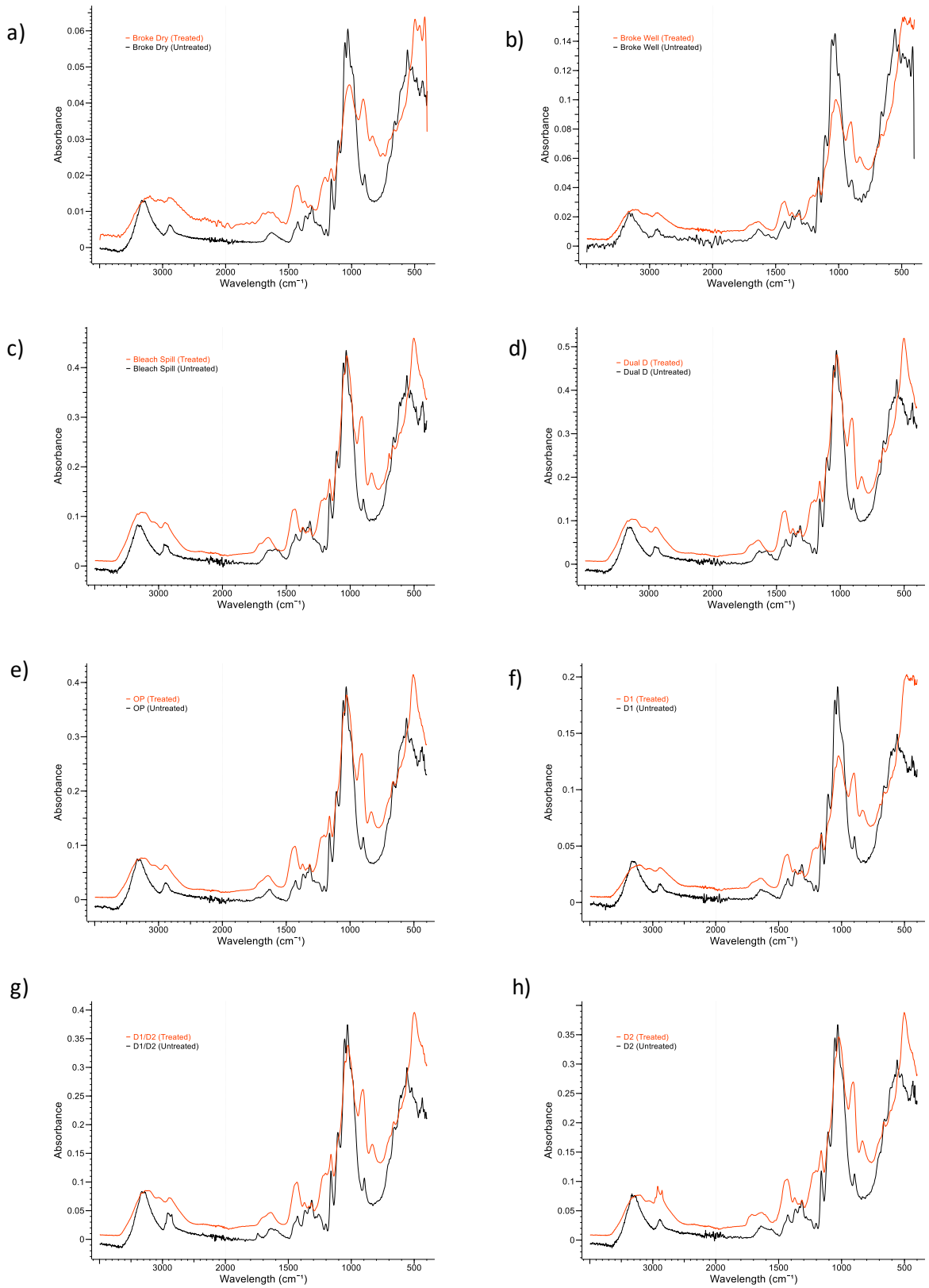

Figure F1: FTIR spectra of a) Broke Dry, b) Broke Well, c) Bleach Spill, d) Dual D, e) OP, f) D1, g) D1/D2 and h) D2 samples

APPENDIX G – SCANNING ELECTRON MICROSCOPY (SEM-EDX) SPECTRUMS

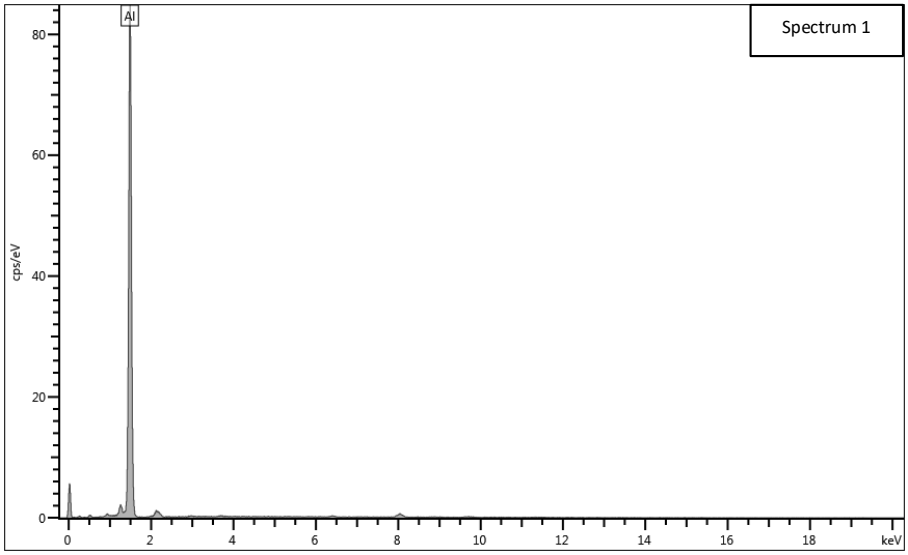

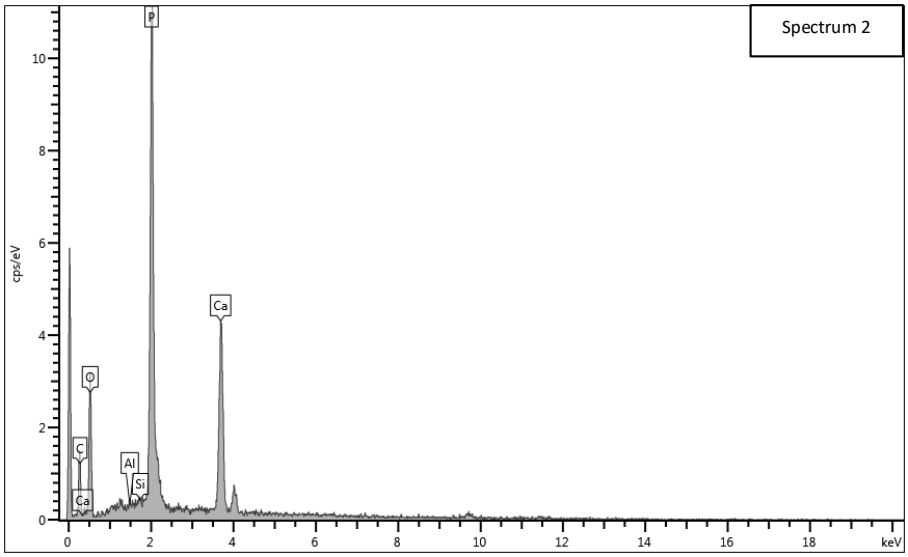

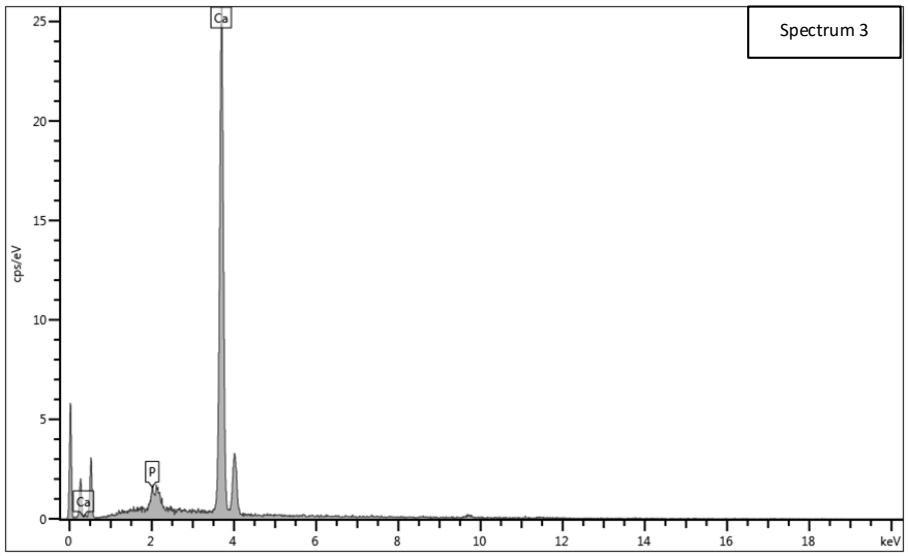

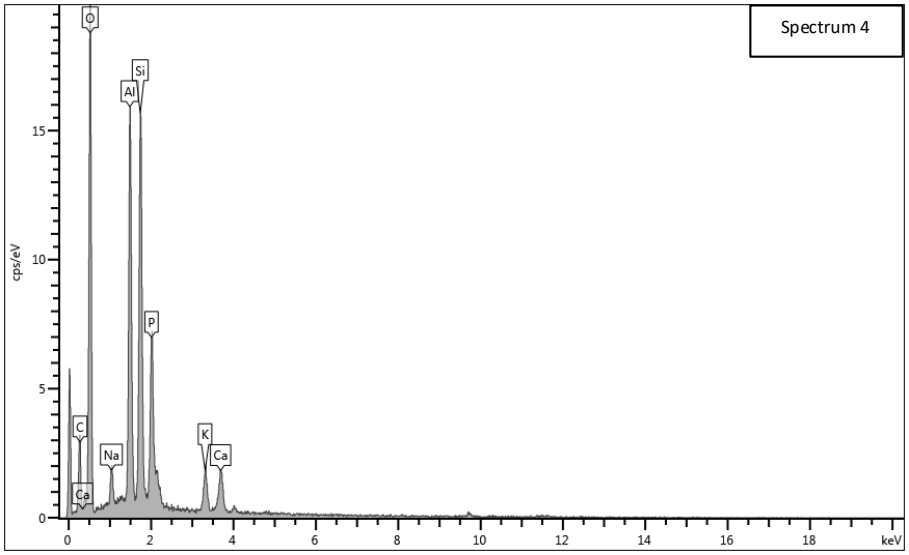

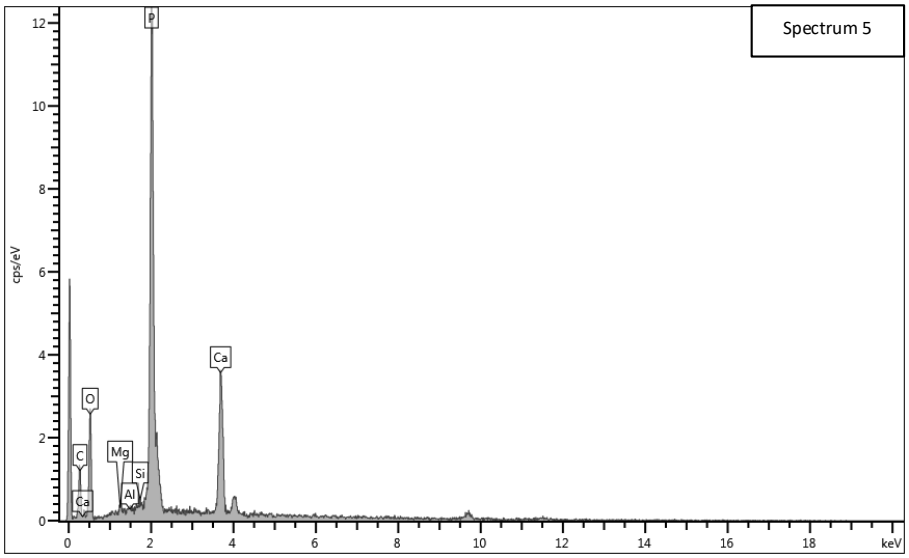

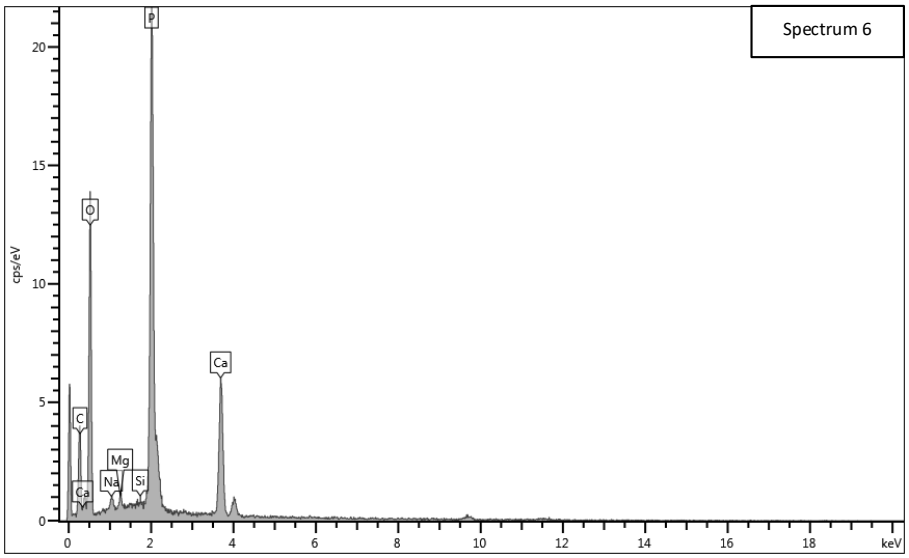

APPENDIX H – SCANNING ELECTRON MICROSCOPY (FE-SEM) IMAGES OF FILMS

BROKE DRY

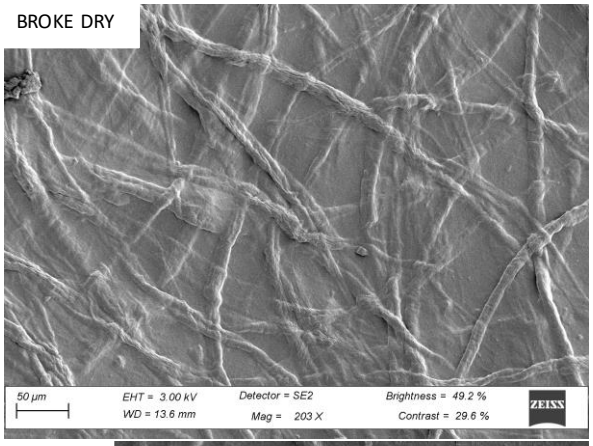

BROKE WELL

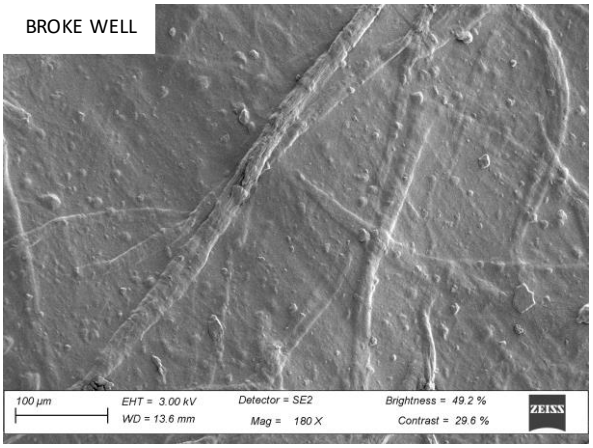

DUAL D

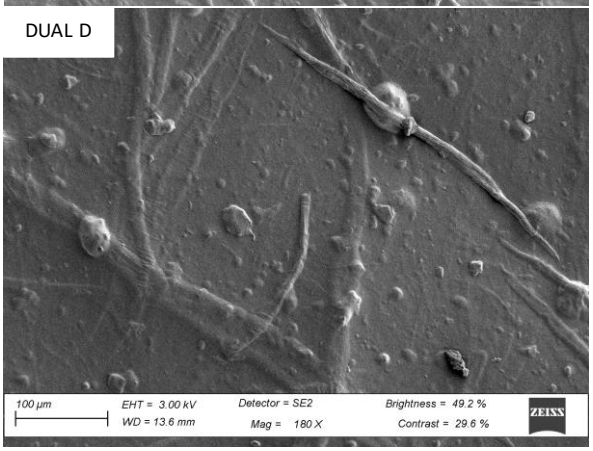

OP

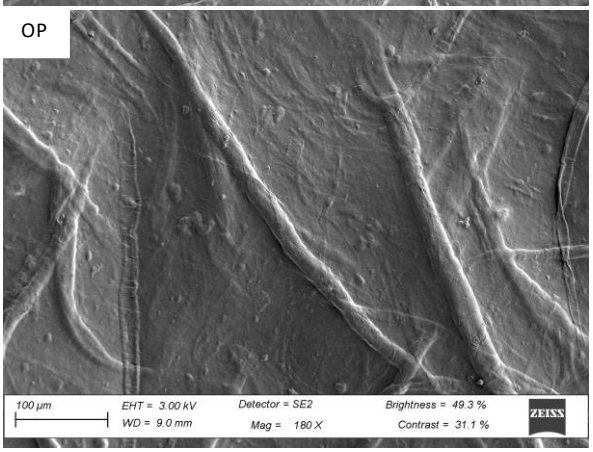

D1

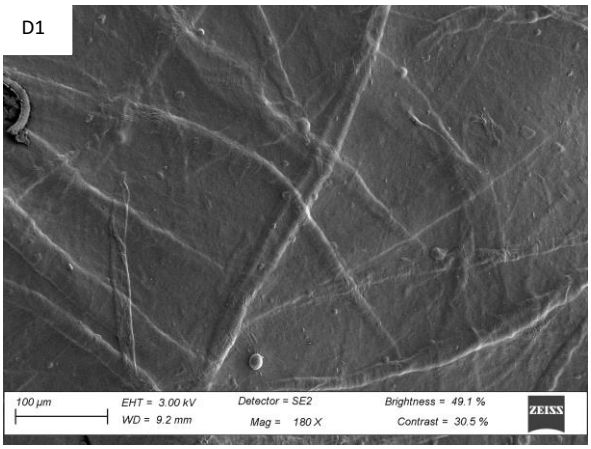

D2

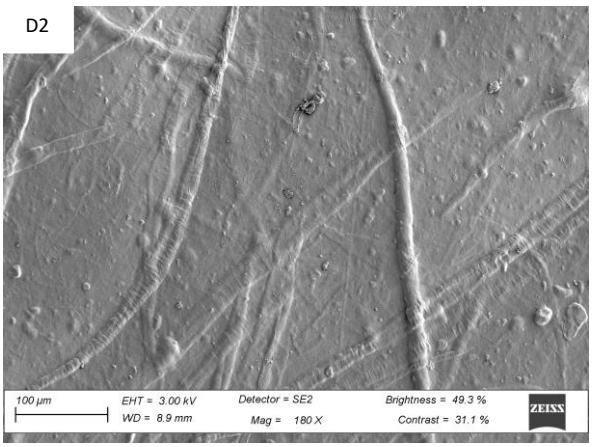

D2

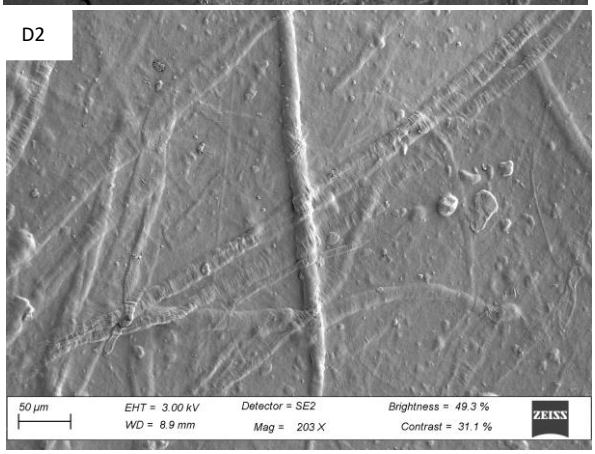

CUT-OFFS

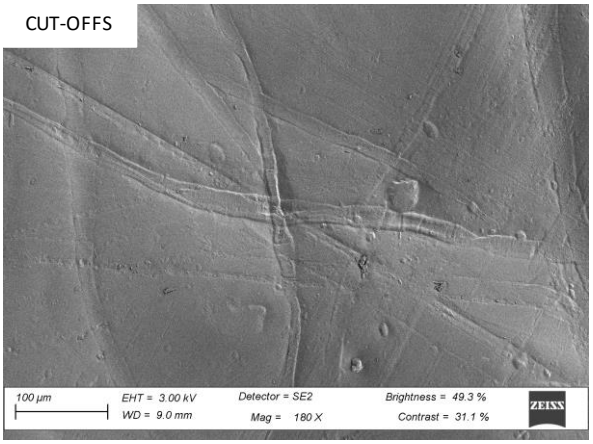

BLEACH SPILL

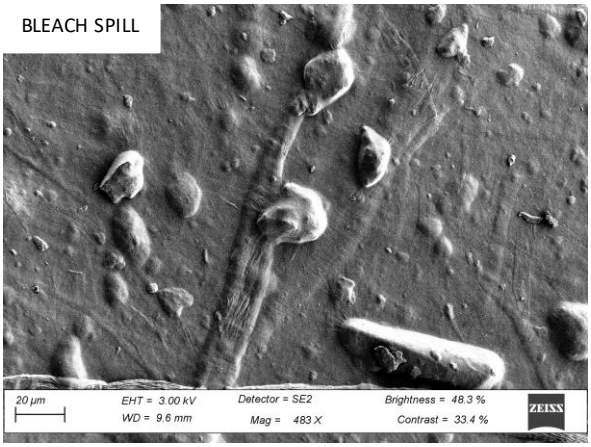

BLEACH SPILL

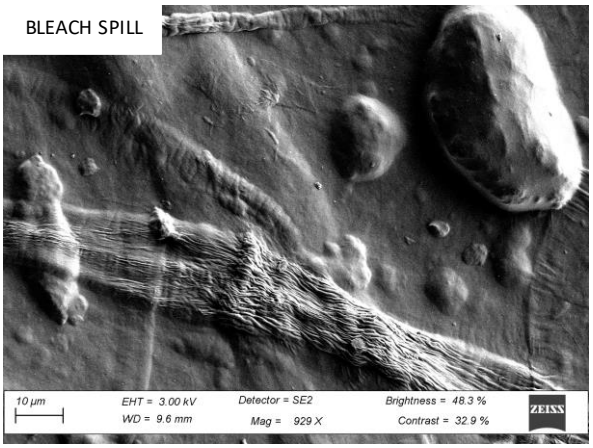

DUAL D

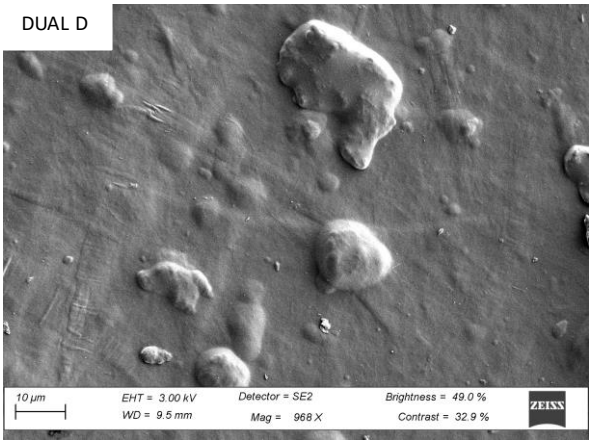

D2

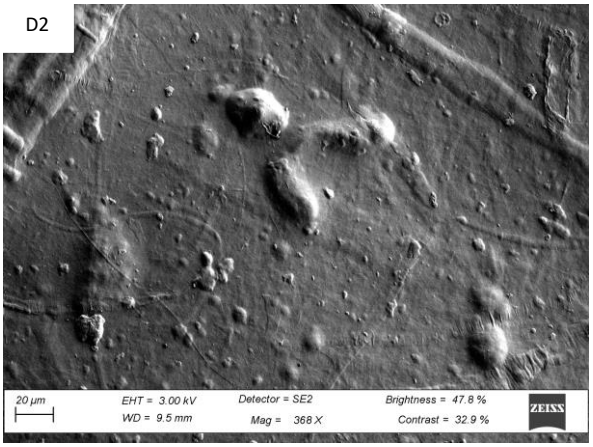

D2

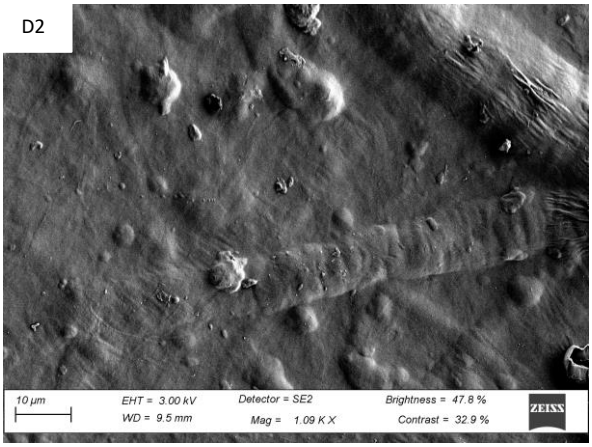

APPENDIX I – X-RAY DIFFRACTION (XRD) AND CRYSTALLINITY INDEX (CI) RESULTS